Sedimentary Facies, Organic Facies, and Hydrocarbon Generation in Evaporite Sediments of the Mulhouse Basin, France

Peter Michael Hofmann

A dissertation submitted to the Graduate Faculty in Earth and Environmental Sciences in partial fulfilment of the requirements for the degree of Doctor of Philosophy, The City University of New York.

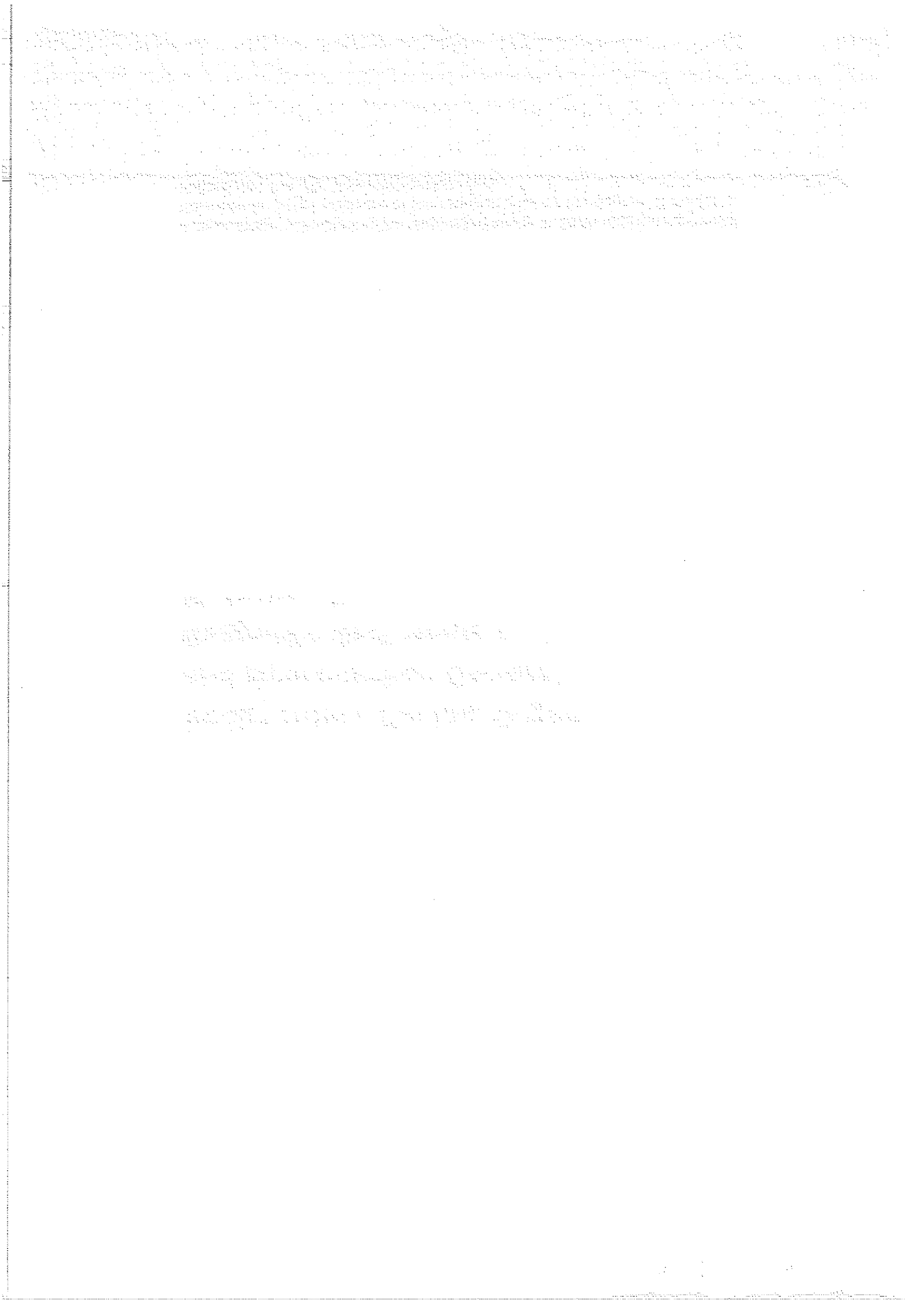

Abstract

SEDIMENTARY FACIES, ORGANIC FACIES, AND HYDROCARBON GENERATION IN EVAPORITE SEDIMENTS OF THE MULHOUSE BASIN, FRANCE

by

Peter Michael Hofmann

Advisor: Prof. B. Charlotte Schreiber

The sediments of the S unit (lower Oligocene) of the Mulhouse Basin, France, display lithofacies characteristic for the deposition in a perennial evaporitic lake that received frequent marine influx. The sediments of the S unit consist of marls, anhydrites (deposited as gypsum), and halite.

The organic content of these sediments stems from algal and most likely bacterial sources. Terrigenous, plant-derived organic matter comprises on average less than 10% of the total organic matter. The mass of the organic matter is concentrated in the marl lithofacies (up to 4.5% TOC), which display a varve-like lamination. The anhydrite and halite lithofacies contain only minor amounts of organic matter (on average less than 0.5% TOC). Based on the maceral content and the molecular composition of the extractable organic matter, two organic facies have

been identified (A and B). The organic facies correlate with distinct lithofacies. It therefore appears that the deposition of sediments and their organic content was governed by the physical conditions of the lake.

The accumulation of organic matter-rich sediments in the S unit of the Mulhouse Basin is thought to have been favored by a high paleoproductivity and good to excellent preservation conditions. Low sedimentation rates in conjunction with elevated salinities led to the accumulation of marls rich in organic matter.

The kerogens of the S unit can be classified as type II. The organic matter from the sites Amelie II and Berrwiller is immature and corresponds to a maturity level of 0.35 and 0.45% vitrinite reflectance, respectively. Petroleum formation resulted in significantly higher amounts of bitumen as expected from shale source rocks of this maturity level. The bitumens are dominated by asphaltenes and NSO-compounds and contain less than 50% hydrocarbons.

In the maturity interval from 0.35-0.45% R_o, hydrocarbon generation took place in all lithofacies of the S unit. Hydrocarbons formed via kerogen conversion in the marl-dominated sediments and via asphaltene/NSO-compound conversion in anhydrite-dominated lithofacies.

The massive anhydrites of the S unit have already expelled hydrocarbons. The naphthalene patterns of this lithofacies show fractionation effects that resulted from water washing during the phase transition from gypsum to anhydrite.

To my wife Kay

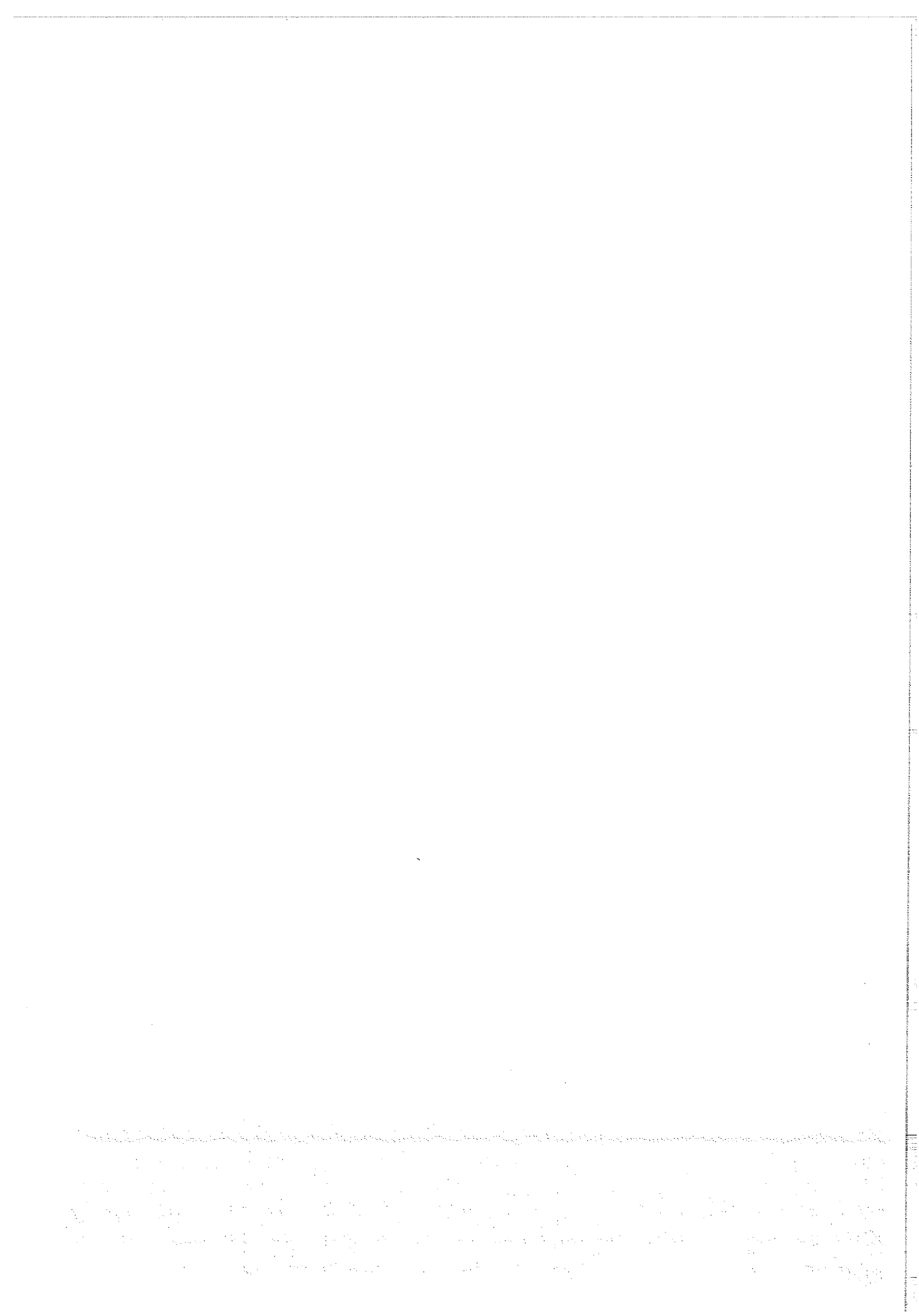

ACKNOWLEDGEMENTS

It is virtually impossible to adequately thank and acknowledge everyone who contributed to the completion of this dissertation. I want to thank Professor D. Leythaeuser for suggesting the topic of the dissertation and for his and Professor Charlotte Schrieber's invaluable help during its completion.

This work was performed under the auspices of the E.N.O.G. (European Network of Organic Geochemistry) and has benefited from scientific discussion within the group. E.N.O.G. comprises Laboratoire de Géochemie, I.F.P., Rueil Malmaison, France; Institute of Petroleum and Organic Geochemistry, K.F.A., Jülich, Germany; Laboratoire de Chimie Organique des Substances naturelles associé au C.N.R.S., Université Louis Pasteur, Strasbourg, France; Organic Geochemistry Unit, Delft University of Technology, Netherlands; Organic Geochemistry Unit, University of Bristol, U.K. and receives funding from the European Economic Community under contract No. SCI-0021-C(TT). The logistical support during the sampling trips by the geologists of the Mines de Potassé d'Alsace is kindly acknowledged.

I would like to thank the members of my committee from the City University of New York, Professor David Thurber and

Professor Somdev Bhattacharji, and particularly Professor Anthony Prave for stepping in at the last minute to read this dissertation.

The assistance and support of all the scientists and technicians at KFA were invaluable in the analysis and interpretation of the data.

My friends and colleagues at K.F.A. Jülich and the City University of New York had a great part in the completion of this dissertation. They helped me in times of frustration with their support and example. They never failed to point out the bright side of life.

My parents and family have supported me all the way towards the completion of this thesis. There is no way to adequately express my deep appreciation.

Finally, I want to thank my wife, Kay Stone. This dissertation could not have been completed without her. Besides her excellent knowledge of geology, typing, and patience in guiding me through the problems of the English language, she was always there to give me the support I needed. I want to thank her very much for her love, her caring, and her patience.

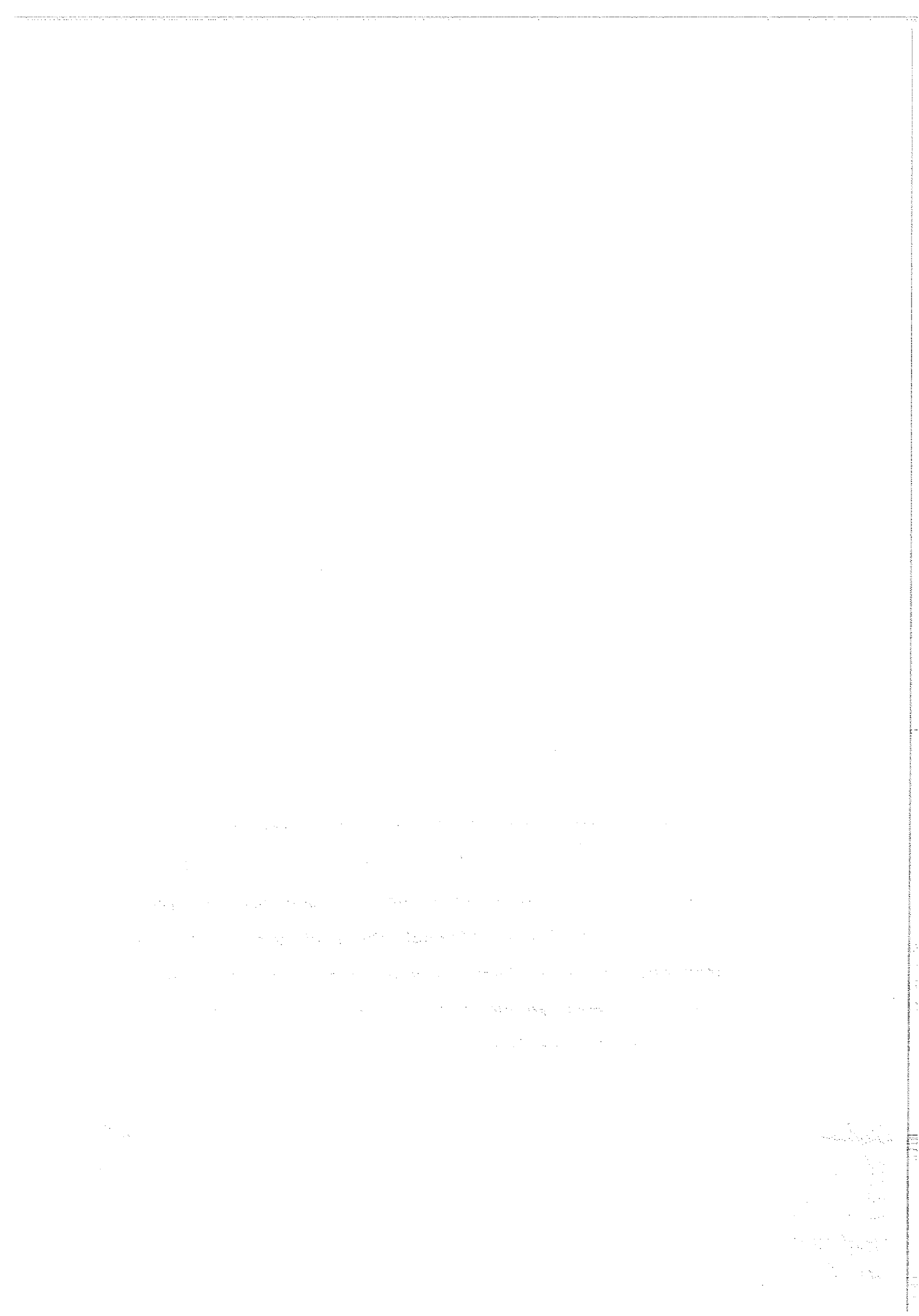

TABLE OF CONTENTS

ABSTRACT iv

ACKNOWLEDGEMENTS viii

LIST OF TABLES xiv

LIST OF ILLUSTRATIONS xvi

1. GENERAL INTRODUCTION 1

2. METHODOLOGY 4

2.1 Sedimentary Petrology 4

2.2 Organic Petrology 7

2.3 Geochemical Analysis 9

3. FACIES RELATIONSHIPS AND DEPOSITIONAL ENVIRONMENTS 11

3.1 Introduction 11

3.2 Geological Overview 13

3.3 Stratigraphy 18

3.4 Facies Description 25

3.4.1 Marl 25

3.4.2 Anhydrite 34

3.4.2.1 Nodular Anhydrite and Lenticular Anhydrite 34

3.4.2.2 Laminated Anhydrite 37

3.4.2.3 Massive Anhydrite 41

3.4.3 Halite 41

3.5 Facies Model 47

3.5.1 General Conditions for Evaporitic Sedimentation 47

3.5.2 Setting 49

3.5.3 Facies Interpretation 50

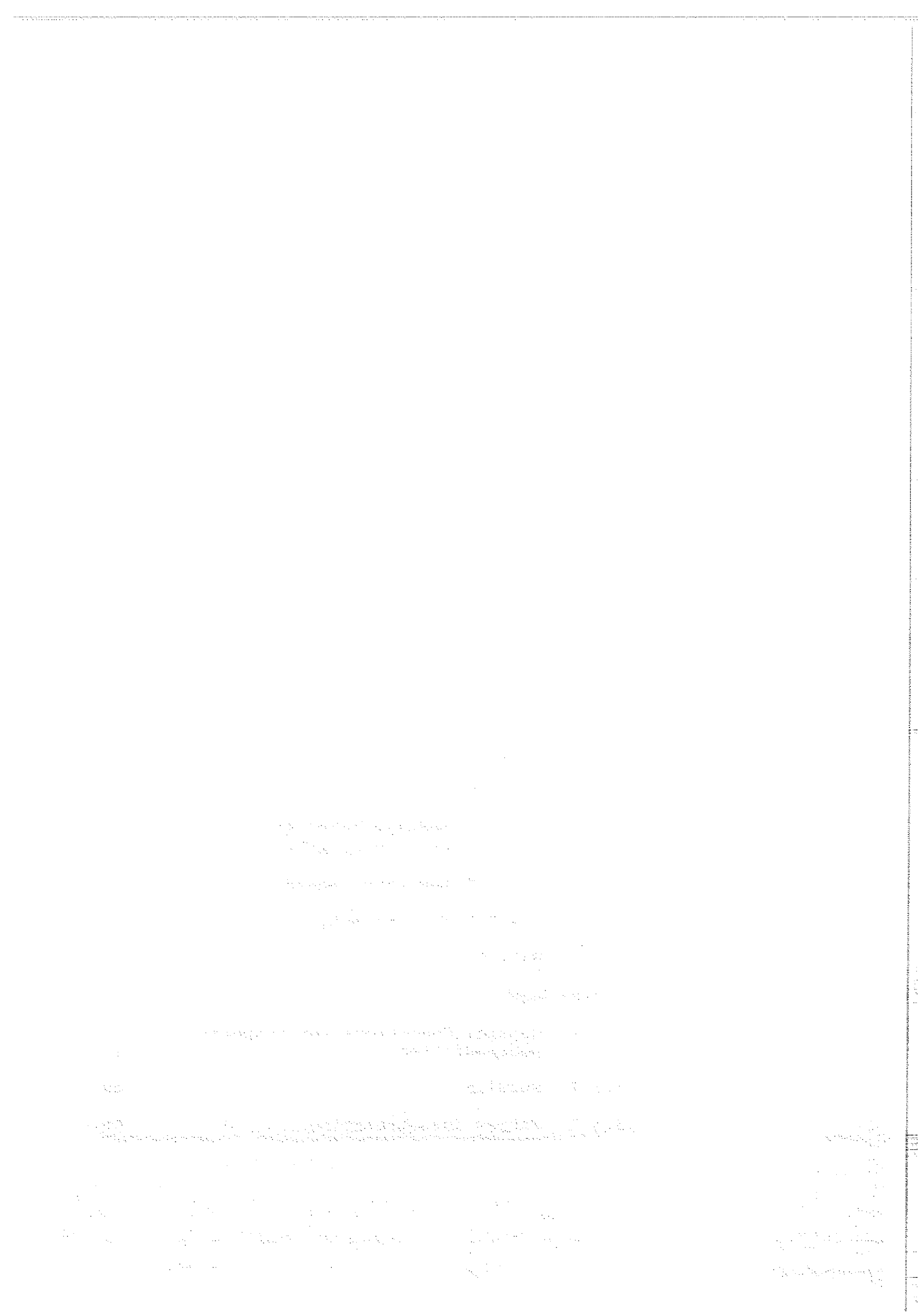

3.5.3.1 Deposition of Marls 50
3.5.3.2 Deposition of Anhydrite 56
3.5.3.3 Halite 59
3.6 Sedimentation Rates 61
3.7 Organic Matter Content of the S-Interval 67
3.7.1 Introduction 67
3.7.2 Abundance and Distribution 68
3.7.3 Quality of Organic Matter 69
3.7.4 Organic Petrology 72
3.7.4.1 Maceral Content 72
3.7.4.2 Marls 73
3.7.4.3 Anhydrites 78
3.5.4.3.1 Lenticular Anhydrites 78
3.7.4.3.2 Laminated Anhydrites 81
3.7.4.3.3 Massive Anhydrites 81
3.7.5 Halite 81
3.8 Organic Facies 85
3.9 Chemical Characterization of the Kerogens 88
3.9.1 Organic Facies 89
3.9.2 Influences on Kerogen Quality 92
3.10 Characterization of the Soluble Organic Matter 97
3.10.1 Aliphatic Hydrocarbons 98
3.10.1.1 N-Alkanes 98
3.10.1.2 Isoprenoid Hydrocarbons 104
3.10.2 Aromatic Hydrocarbons 106
3.10.3 Sulfur Aromatic Hydrocarbons 107
3.11 Rhythmic Organic Carbon Sedimentation 112

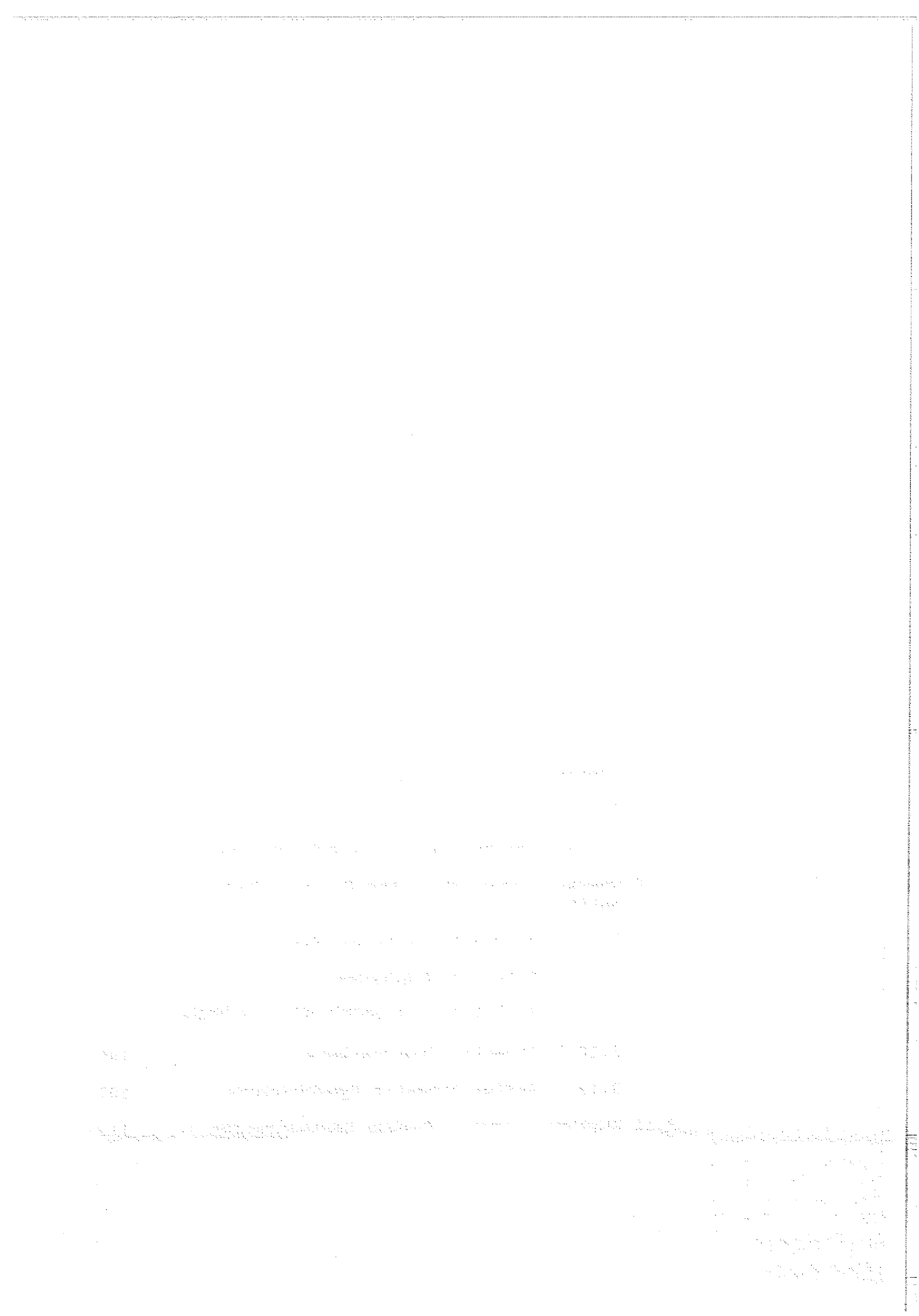

3.12 Organic Carbon Accumulation Rate 117

3.13 Preservation Conditions 119

3.14 Paleoproductivity and Accumulation of Terrestrial Organic Matter 122

3.15 Controlling Factors in the Formation of Organic-Rich Beds in the S Unit 127

3.16 Synthesis: Reconstruction of the Paleodepositional Environment 130

4. FORMATION OF HYDROCARBONS AT LOW MATURITY RANGES 140

4.1 Introduction 140

4.2 Approach 142

4.3 Comparison of the Sampling Sites 145

4.3.1 Paleobasin Morphology 145

4.3.2 Sedimentology 146

4.3.3 Organic Petrography 150

4.3.4 Organic Geochemistry 150

4.3.5 Maturity Assessment 153

4.4 Sample Selection 159

4.5 Methods 163

4.6 Inventory of Chemical Changes of the Lithofacies of the S unit of the Mulhouse Basin over the Maturity Interval 0.35-0.45% R_o 166

4.6.1 Kerogen 166

4.6.2 Total Extracts 172

4.6.3 Aliphatic Hydrocarbons 177

4.6.3.1 Bulk Yields of n-alkanes 179

4.6.3.2 Mass Balance on the Molecular Level 179

4.6.4 Aromatic Hydrocarbons 190

4.6.4.1 Bulk Yields of Naphthalenes 190

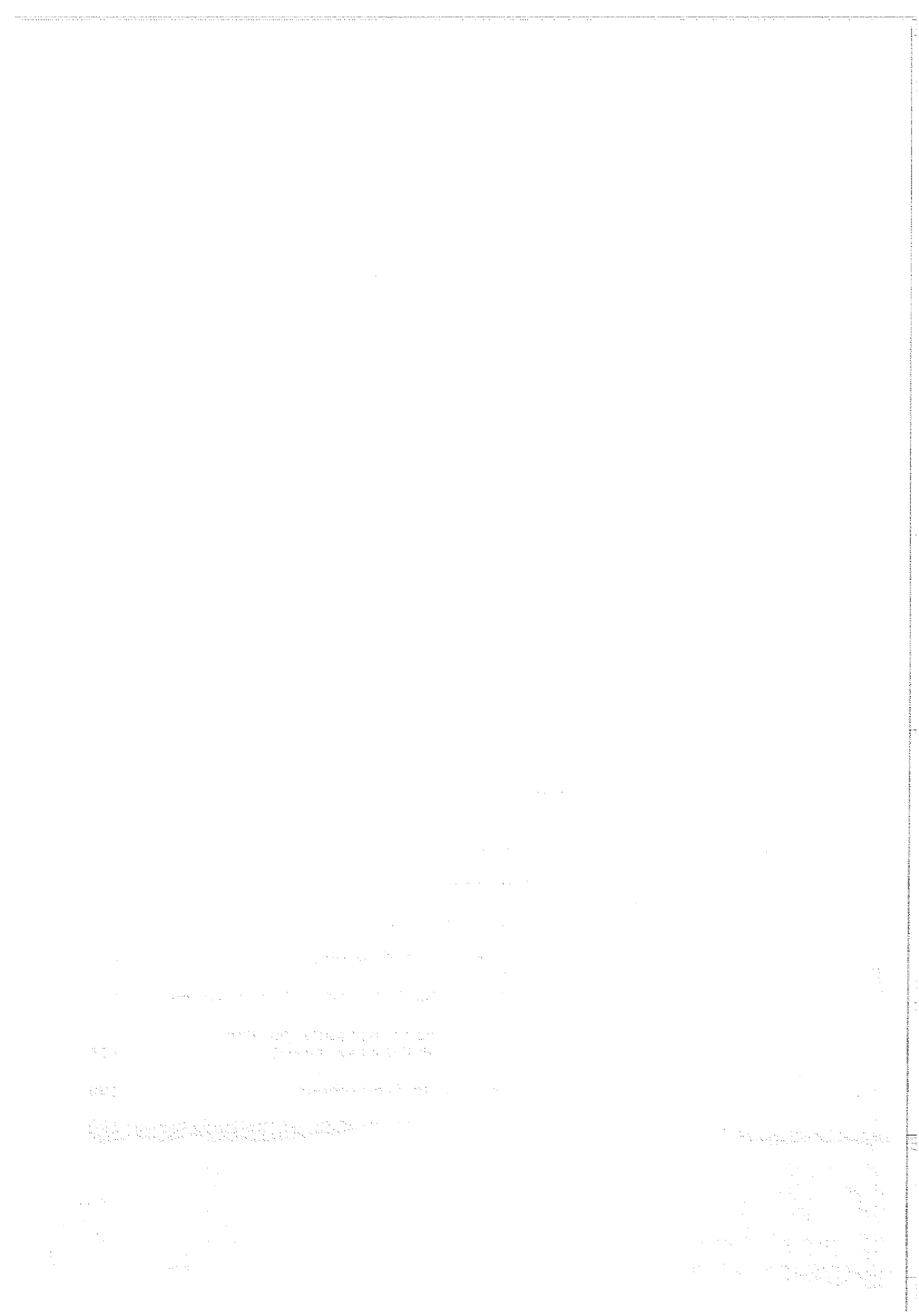

4.6.4.2 Mass Balance on the Molecular Level 193

4.6.5 NSO-Compounds and Asphaltenes 204

4.7 Discussion 209

4.7.1 Petroleum Generation 209

4.7.2 Bitumen Formation 210

4.7.2.1 Bitumens at Maturity Level R_o = 0.35 213

4.7.2.2 Bitumens at Maturity Level 0.45% R_o 217

4.7.3 Molecular Considerations for Hydrocarbon Generation 226

4.7.3.1 Relative Increases in Selected n-alkanes and Naphthalenes 229

4.7.4 Hydrocarbon Migration 236

4.7.4.1 Bitumen Composition of the Massive Anhydrite Lithofacies 237

4.7.4.2 Fractionation of Naphthalenes 241

4.8 Summary and Conclusions 247

5. GENERAL CONCLUSIONS 250

6. APPENDIX 253

7. BIBLIOGRAPHY 269

LIST OF TABLES

Table 1: Estimate of the time span required for the deposition of the S unit at Amelie II. 65

Table 2: Summary of the organic geochemistry parameters of the samples used for the mass-balance calculations in Chapter 4. 162

Table 3: Concentration of the kerogen and extract yields of the lithofacies of the S unit. 167

Table 4: Concentration of the extract yields of the lithofacies of the S unit. 168

Table 5: List of analyzed aromatic and sulfur aromatic compounds. 194

Table 6: Rock-Eval pyrolysis data for marl samples from the site Amelie II. 254

Table 7: Rock-Eval pyrolysis data for marl samples from the site Ungersheim. 255

Table 8: Rock-Eval pyrolysis data for marl samples from the site Berrwiller. 256

Table 9: Total organic carbon and carbonate content of anhydrite and halite samples from the sites Amelie II, Ungersheim, and Berrwiller. 257

Table 10: Organic carbon contents, sedimentation rates and maceral content, and calculated organic accumulation rates of marl samples from site Amelie II. 258

Table 11: N-alkane content of marl samples from Amelie II. 259

Table 12: N-alkane content of anhydrite samples from Amelie II. 260

Table 13: N-alkane content of marl samples from Berrwiller. 261

Table 14: N-alkane content of anhydrite samples from Berrwiller. 262

Table 15: Naphthalene content of marl samples from Amelie II and Berrwiller. 263

Table 16: Naphthalene content of anhydrite samples from Amelie II and Berrwiller. 264

Table 17: Phenanthrene content of selected marl samples from Amelie II and Berrwiller. 265

Table 18: Dibenzothiophene content of selected marl samples from Amelie II and Berrwiller. 266

Table 19: Extract composition of marl samples from Amelie II, Ungersheim and Berrwiller. 267

Table 20: Extract composition of anhydrite and halite samples from Amelie II, Ungersheim and Berrwiller. 268

LIST OF ILLUSTRATIONS

Figure 1: Analysis scheme 5

Figure 2: Position of the Rhine Graben Segment in the Western European Rift System. 14

Figure 3: Location of the evaporite-bearing subbasins of the southern Rhine Graben. 16

Figure 4: Location and stratigraphy of the Mulhouse Basin. 19

Figure 5: Stratigraphic column based on a measured mine section at Traverse 830 at site Amelie II. 20

Figure 6: Isopach map of the S to TS interval in the southern part of the Mulhouse Basin. 21

Figure 7: Lithological column of the S unit at the sites Amelie II, Ungersheim, and Berrwiller. 24

Figure 8: Photomicrograph of a laminated marl sample. 26

Figure 9: Photomicrograph of a foraminifera-rich layer. 28

Figure 10: Photomicrograph of a foraminifera test. 29

Figure 11: Photograph of a sample of marl of type A. 31

Figure 12: Cartoon of a thin section view of alternating laminae of marls of type A and marls of type B. 32

Figure 13: Photography of a sample of marl of type B. 33

Figure 14: Photograph of a polished, lenticular anhydrite sample. 35

Figure 15: Photomicrograph of a lenticular anhydrite sample. 36

Figure 16: Photomicrograph of the laminated anhydrite lithofacies. 38

Figure 17: V-shaped crystal outline of poly-crystalline anhydrite, pseudomorphic after gypsum. 39

Figure 18: Photomicrograph of the laminated anhydrite lithofacies. 40

Figure 19: Photograph of a slab taken from the massive anhydrite lithofacies. 42

Figure 20: Photomicrograph of the massive anhydrite lithofacies. 43

Figure 21: Photograph of a halite layer. 44

Figure 22: Photomicrograph of a hopper crystal. 46

Figure 23: Idealized facies model for the lithofacies of the S unit of the Mulhouse Basin. 51

Figure 24: Interpretation of the laminae of the marls of type A and type B as annual deposits. 54

Figure 25: Sedimentation rates of the marl lithofacies at Amelie II in the stratigraphy interval S1 to CI. 63

Figure 26: Photomicrograph of a marl of type A. 74

Figure 27: Photomicrograph of the fluorescing groundmass of organic facies A. 75

Figure 28: Photomicrograph of marl of type B. 76

Figure 29: Photomicrograph of fluorescing compacted algae. 77

Figure 30: Alginite in the marl matrix between lenticular anhydrite aggregates. 79

Figure 31: Fluorescing organic groundmass in a marl matrix of lenticular anhydrite facies. 80

Figure 32: Disperse algae in marl layer of the laminated anhydrite facies. 82

Figure 33: Single algae in massive anhydrite lithofacies. 83

Figure 34: Average maceral composition of the lithofacies of the S unit. 87

Figure 35: Hydrogen index versus oxygen index diagram for kerogen typing. 90

Figure 36: Discrimination of organic facies A and B of marl samples on the basis of hydrogen and oxygen indices. 91

Figure 37: Variation of the hydrogen index of the marl samples of the S unit with stratigraphic depth at Amelie II. 93

Figure 38: Variation of the hydrogen index of the marl samples with the terrigenous organic matter content. 95

Figure 39: N-alkane distribution pattern I. 99

Figure 40: N-alkane distribution pattern II. 100

Figure 41: Examples of the n-alkane distribution patterns of each lithofacies. 101

Figure 42: Distribution patterns of selected sulfur aromatic compounds. 109

Figure 43: Distribution patterns of selected sulfur aromatic compounds. 110

Figure 44: TOC content of the marl beds at Amelie II. 113

Figure 45: Relationship between sedimentation rate and organic carbon content of the marls at Amelie II. 115

Figure 46: Organic carbon accumulation rate for the marls at Amelie II. 118

Figure 47: Co-variation of pristane and phytane content of the sediments of all lithofacies at Amelie II. 121

Figure 48: Accumulation rates for terrigenous and aquatic organic matter of the marls at Amelie II. 123

Figure 49: Schematic model of the monomict and meromict stages of "Lake Mulhouse." 132

Figure 50: Relationship between sedimentary facies, organic facies and the physical lake conditions during the deposition of the S unit of the Mulhouse Basin. 134

Figure 51: Variation of the total organic carbon content, hydrogen index and carbonate content within the S unit at Amelie II. 147

Figure 52: Variation of the total organic carbon content, hydrogen index and carbonate content at Ungersheim. 148

Figure 53: Variation of the total organic carbon content, hydrogen index and carbonate content at Berrwiller. 149

Figure 54: Example of an n-alkane distribution pattern representative for organic facies A. 151

Figure 55: Example of an n-alkane distribution pattern representative for organic facies B. 152

Figure 56: Maturity level expressed as vitrinite reflectance and present day burial depth of the S unit at Amelie II, Ungersheim and Berrwiller. 155

Figure 57: Variation of the methyldibenzothiophene ratio with kerogen quality. 157

Figure 58: Stratigraphic position of the samples of the lithofacies compared in the mass-balance of Chapter 4 at Amelie II and Berrwiller. 161

Figure 59: Variation of the kerogen concentration of the lithofacies of the S unit with maturity. 171

Figure 60: Extract yields of the lithofacies of the S unit at 0.35 % R_o and 0.45 % R_o. 173

Figure 61: Composition of the extracts of the lithofacies of the S unit at 0.35 R_o and 0.45 R_o. 175

Figure 62: Aliphatic hydrocarbon yields of the lithofacies of the S unit. 178

Figure 63: N-alkane concentrations of the lithofacies of the S unit. 180

Figure 64: N-alkane concentration patterns of marl of type A samples from Amelie II and Berrwiller. 182

Figure 65: N-alkane concentration patterns of marl of type B samples from Amelie II and Berrwiller. 183

Figure 66: Average n-alkane concentration patterns and absolute yield increases of the lithofacies of the S unit. 185

Figure 67: Average n-alkane concentration patterns of samples of the massive anhydrite lithofacies at Amelie II and Berrwiller. 189

Figure 68: Aromatic hydrocarbon yields of the lithofacies of the S unit. 191

Figure 69: Naphthalene concentrations of the lithofacies of the S unit. 191

Figure 70: Naphthalene concentration patterns of marl of type A samples from Amelie II and Berrwiller. 195

Figure 71: Naphthalene concentration patterns of marl of type B samples from Amelie II and Berrwiller. 196

Figure 72: Average naphthalene concentration pattern and absolute yield increase of the lithofacies of the S unit. 198

Figure 73: Phenanthrene concentration patterns of marl of type A samples. 202

Figure 74: Phenanthrene concentration patterns of marl of type B samples 203

Figure 75: Dibenzothiophene concentrations of samples from marls of type A and B. 205

Figure 76: Asphaltene yields of the lithofacies of the S unit. 207

Figure 77: NSO-compound yields of the lithofacies of the S unit. 208

Figure 78: Comparison of the extract yields of the lithofacies of the S unit with other immature source rocks. 212

Figure 79: Comparison of the extract and hydrocarbon yields of the bitumen of the S unit with values for the principal zone of oil formation in the Paris Basin. 214

Figure 80: Net loss and net gains over the maturity interval of 0.35 % R_o - 0.45 % R_o. 219

Figure 81: Generation factors for n-alkanes of the lithofacies of the S unit. 230

Figure 82: Generation factors for naphthalenes of the lithofacies of the S unit. 231

Figure 83: Generation factors for the naphthalenes of the massive anhydrite lithofacies. 233

Figure 84: Mass-balance for the yields of compound classes from extracts of the massive anhydrite lithofacies over the maturity interval 0.35 % R_o - 0.45 % R_o. 238

1. GENERAL INTRODUCTION

Evaporites have received renewed attention over the last few decades. The rising interest was initially generated by sedimentologists (Shearman, 1963; Hardie and Eugster, 1971; Schreiber et al., 1976) who recognized that evaporites cannot only be treated as chemical precipitates, but can also be interpreted as sediments with facies assemblages characteristic of the environment of deposition. The understanding of evaporite sedimentation was greatly advanced by the study of modern evaporite depositional settings such as the sabkhas of the Persian Gulf (Shearman, 1963; Purser, 1985), the continental salt lakes of western North America and eastern Africa (Eugster and Hardie, 1978), the gypsum lakes of southern Australia (Warren, 1989), and modern marine salinas all over the world (Javor, 1989, and references therein). The combined work of sedimentologists and biologists on modern salt works (salinas) emphasized the intricate relationship between the evaporating brine and its organic matter content (Evans and Kirkland, 1988; Gerdes and Krumbein, 1987; Orti Cabo et al., 1984; Cornee, 1988, 1984; Javor, 1989). The evolving knowledge that evaporite depositional environments are, contrary to common belief, not locales of death, but rather are teaming with life and supersede even the most productive oceanic realms with respect to

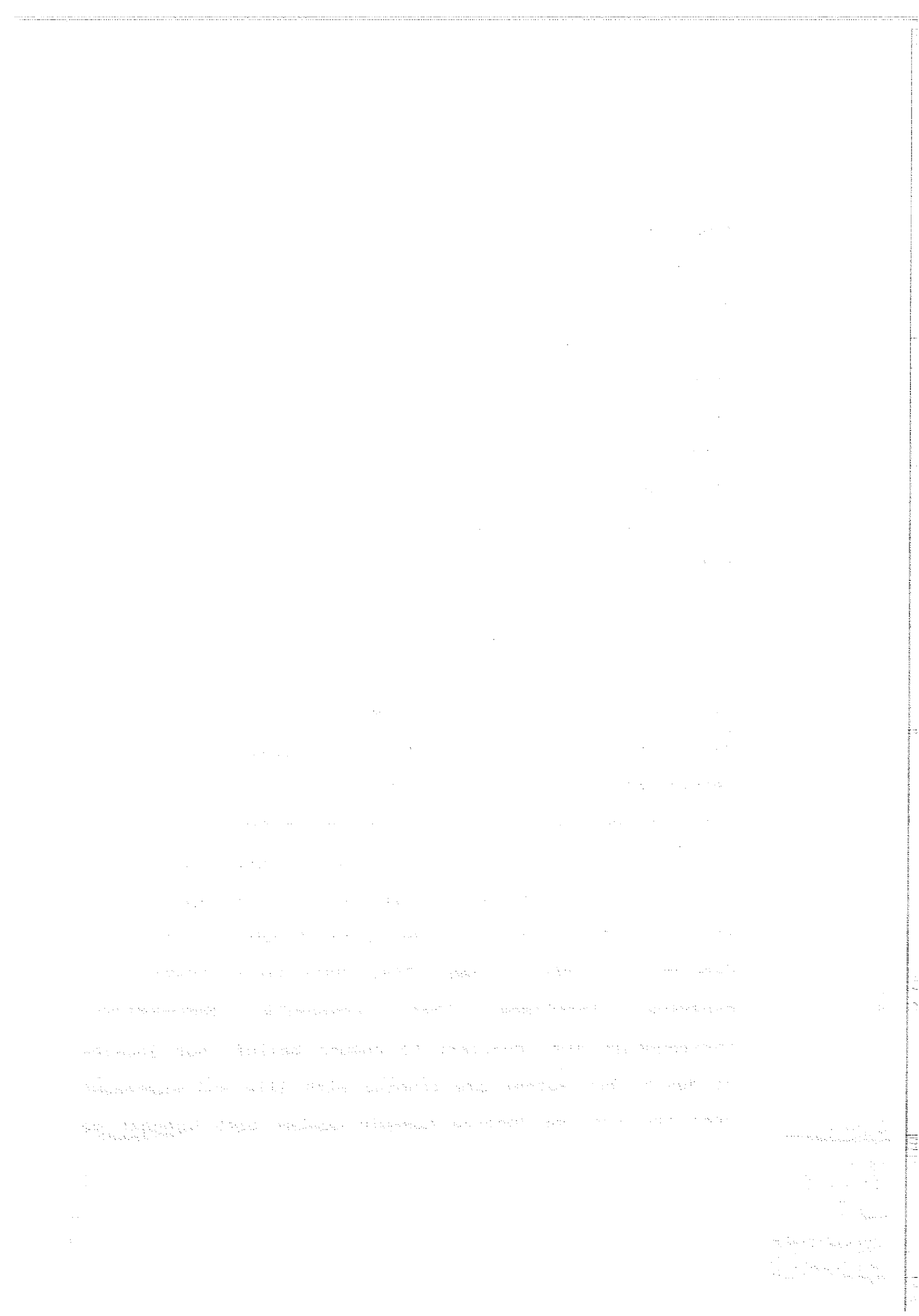

primary bioproductivity led petroleum geologists to propose evaporites as petroleum source rocks (Friedman, 1980; Evans and Kirkland, 1988; Kirkland and Evans, 1981; Eugster, 1985; Warren, 1986). Evidence that carbonate and evaporite source rocks have contributed to some of the world's major oil reserves (Palacas, 1984, and references therein) and the peculiar chemistry of the organic content of many evaporite deposits (Connan et al., 1986; ten Haven et al. 1988, 1985; Sinninghe Damsté et al., 1988, 1986; Mello et al., 1988a, 1988b) have led to intensive research efforts to improve the understanding of evaporite source rock formation and how petroleum is generated from evaporite rocks.

The aim of this dissertation is to understand the processes that lead to the formation of a particular organic matter-rich ancient evaporite deposit and to gain better insight into how petroleum is formed in this deposit at low maturity ranges. For this purpose, a known organic matter-rich interval from the Oligocene evaporites of the Mulhouse Basin in France was selected for detailed investigation.

Part One of this dissertation focuses on the sedimentology and organic matter content of the S unit, a particularly organic matter-rich unit, from the evaporites of the Mulhouse Basin. The paleodepositional environment is

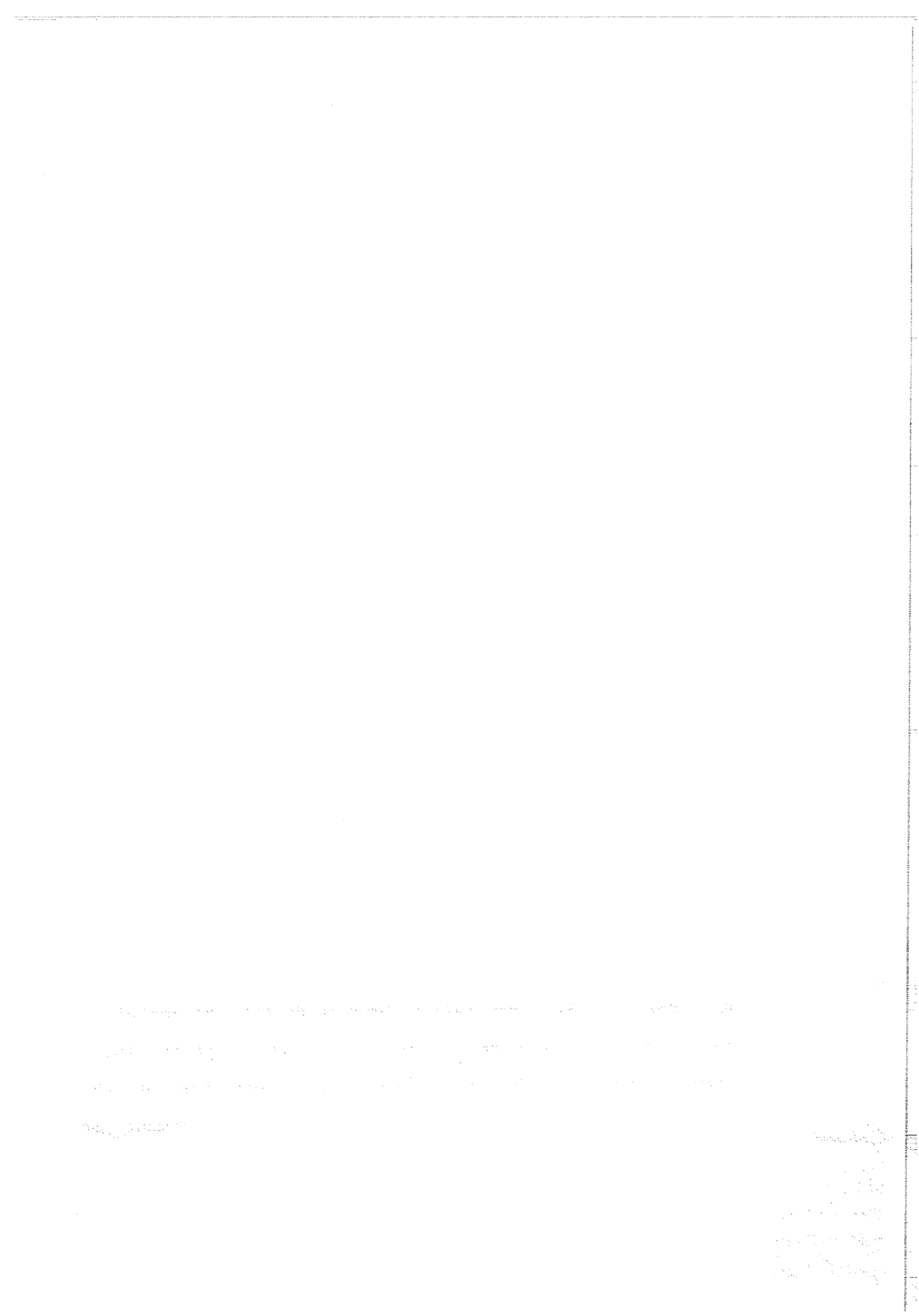

reconstructed and the interaction between organic and anorganic sedimentation is delineated. The second part of this dissertation is concerned with the formation of bitumen and hydrocarbons from the organic matter of the S unit.

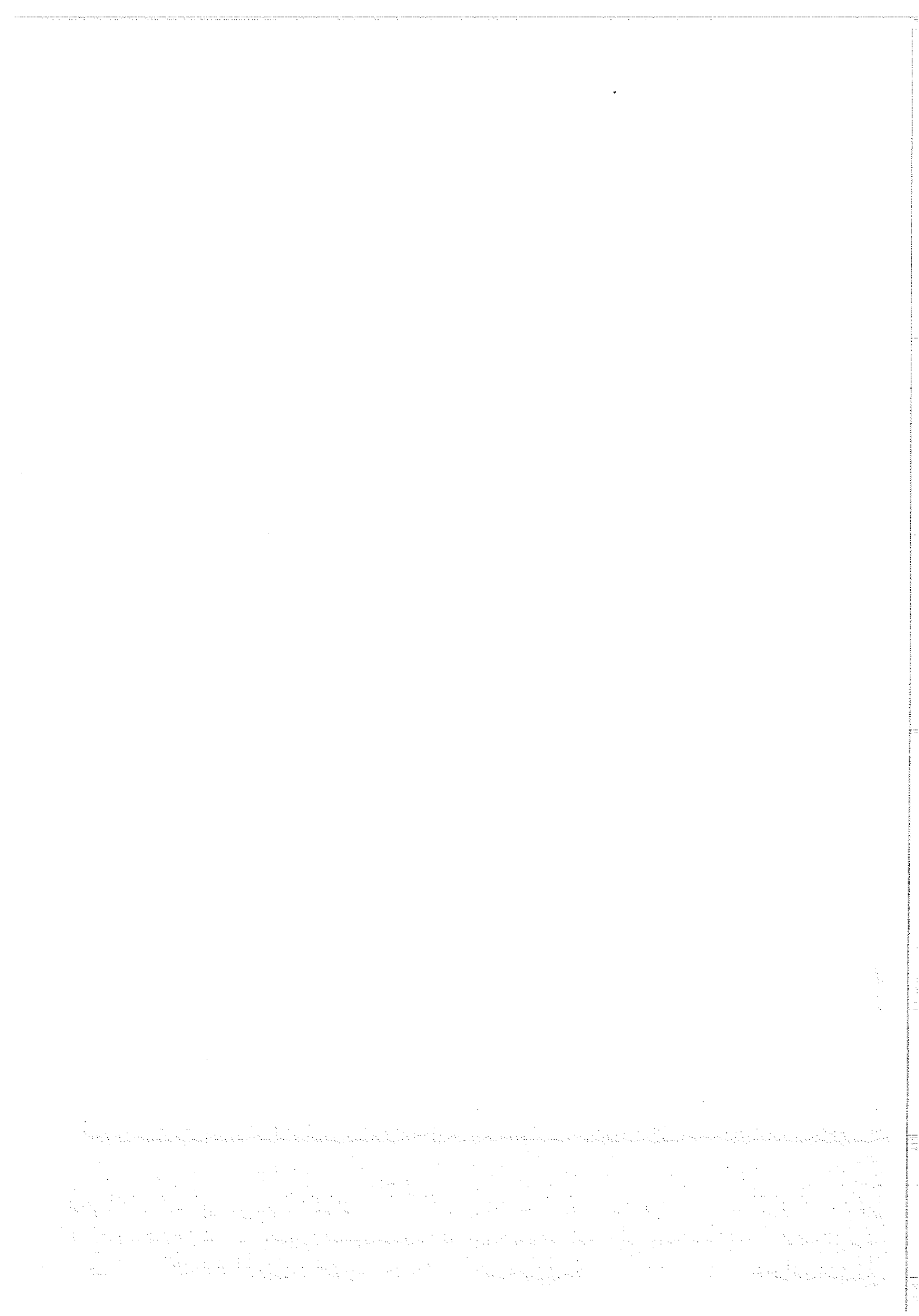

2. METHODOLOGY

The methods applied are depicted in Fig. 1 and described in detail in the following paragraphs. Samples subjected to the analytical techniques listed below were selected to cover the entire stratigraphic interval studied. Special emphasis was placed on the multiple sampling of the sedimentary facies defined in Chapter 3. Between 3 and 22 samples of each sedimentary facies were analyzed for each sampling site.

2.1 Sedimentary Petrology

A detailed petrographic study was performed with the aim of subdividing the stratigraphic section into individual sedimentary facies and to determine the overall depositional environment. Based on these observations, representative examples of each recognized facies were selected for additional, more detailed analysis with techniques listed below.

A thin section of each sample was prepared to determine the mineralogy of each mineral species and to characterize their distribution and morphologies. Additional emphasis was placed on the identification of diagenetic overprints to gain insight into post-depositional changes.

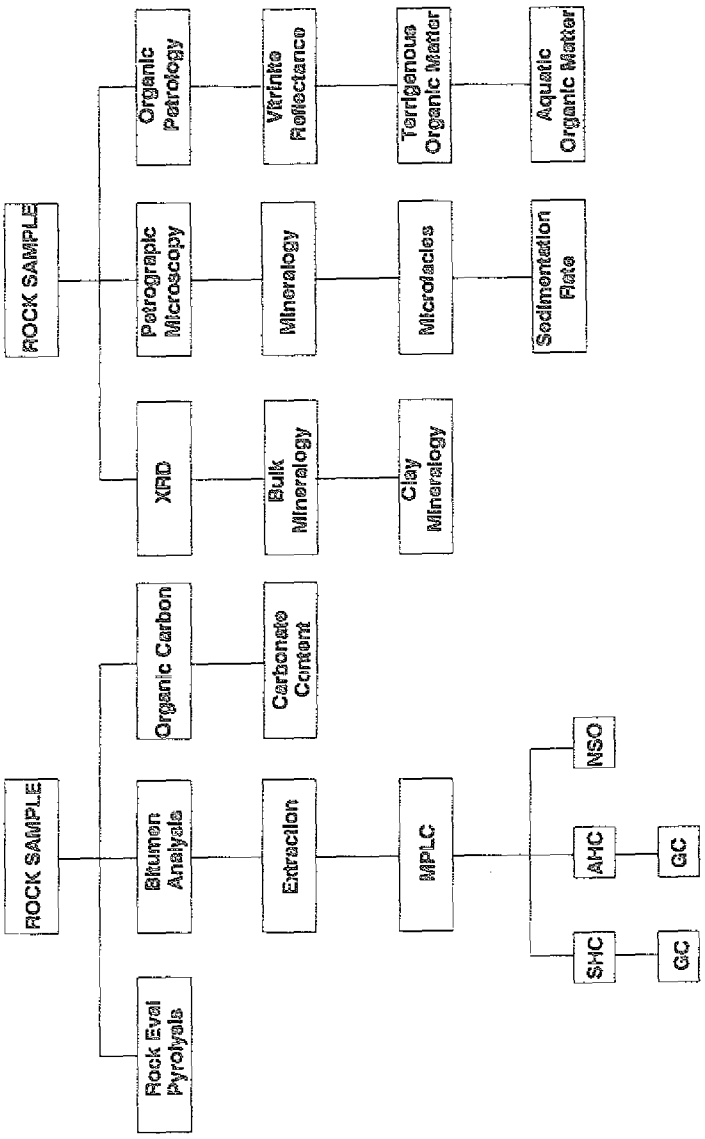

Fig. 1: Analysis scheme
MPLC = Medium Pressure Liquid Chromatography
SHC = Saturated Hydrocarbons
AHC = Aromatic Hydrocarbons
GC = Gas Chromatography
NSO = NSO Compounds
XRD = X-Ray Diffraction

To determine the overall mineralogy of each sample, a number of samples of each sedimentary facies were prepared for x-ray diffractometry. A representative portion of approximately 5 grams was hand ground to a fine powder (<63 μm). Parts of the sample were then loaded into a sample holder following the procedures specified in Brown and Brindley (1980) to prepare an unoriented sample. The powder was analyzed on a PW 1700 Automated Powder Diffractometer System manufactured by Phillips. The analysis conditions were: generator setting 40kV/40mA, Cu k-alpha cathode (2 wave length: 1.54060 Ang., 1.54439 Ang.), step scan (0.050 deg., 20 s/deg.). A monochromator was used. Each run was scanned from 2° theta to 80° theta. A major phase search with the 1983 PDF program was performed on the resulting reflection pattern.

The clay mineralogy of 13 marl samples covering the studied stratigraphic interval was qualitatively determined by x-ray diffractometry using procedures outlined by Moore and Reynolds (1989) and Elsinger and Pevear (1988). Each sample was analyzed in air dried, glycolated, HCl treated, in cation saturated (NH^+, Ca^{2+}) condition and heated to 100°C and 530°C. The final determination of the mineralogic composition was based on a determinative flow chart of Reynolds published in Elsinger and Pevear (1988).

2.2 Organic Petrology

For microscopic studies, 95 samples representing all sedimentary facies were selected. A slab of each sample was embedded in an epoxy resin. One side of the resultant block, oriented perpendicular to bedding, was polished using successively finer abrasives, and then polished with a Wirtz TG 200 polishing machine using 0.05 μm aluminium powder dispersed in an alcohol.

Macerals were classified following Stach et al. (1982) into liptinites (alginites and liptodetrinites), vitrinites, and inertinites by observation in blue light fluorescence and reflected white light, respectively.

The maceral composition was analyzed using a Swift/Prior 7 point counter. Under 600X magnification, first the organic particles identifiable in reflected white light (vitrinite, inertinite) were counted, followed by a second count under blue light excitation, which allows the identification of liptinite particles. A total of 750 points per polished block of thin section was analyzed in each mode. From these counts, volume percentages of the total maceral content were calculated. The percentage of terrigenous versus aquatic organic matter was determined by classifying alginites and liptodetrinites as aquatic

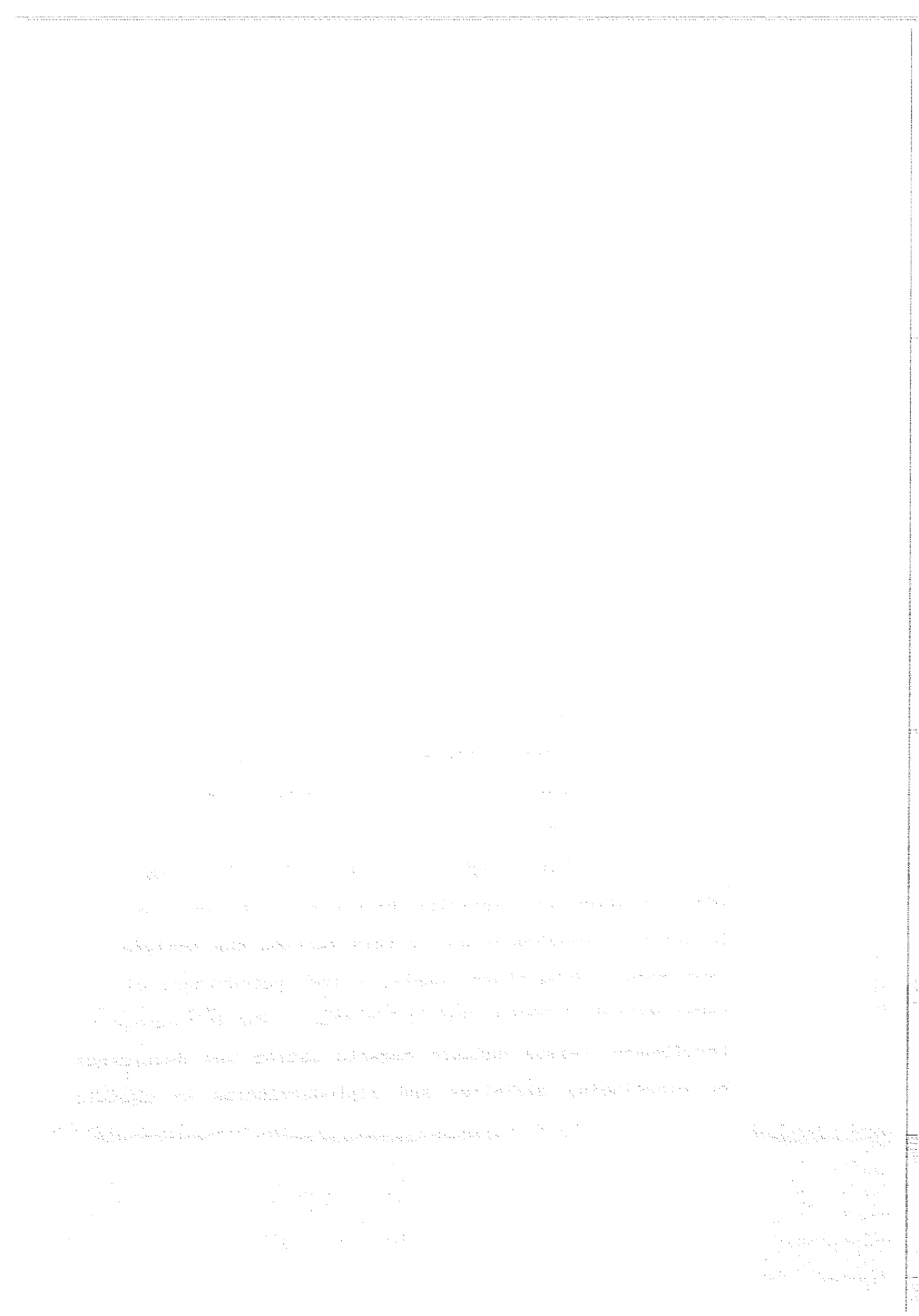

organic matter and vitrinites, sporinites, and inertinites as terrigenous organic matter.

Organic carbon accumulation rates (OCAR) were calculated according to the following equation:

$$OCAR\ (g/cm^2yr) = \text{sedimentation rate (cm/yr)} \times \text{sediment density } (g/cm^3) \times TOC/100$$

where TOC corresponds to total organic carbon content.

Sediment density (SD) was calculated according to the following equation:

$$SD\ (g/cm^3) = (1-(TOC/100)) \times 2.9\ g/cm^3 + (TOC/100) \times 1.2\ g/cm^3$$

where 2.9 g/cm^3 is the density of the organic-carbon-free rock and 1.2 g/cm^3 the density of the organic matter, respectively.

The calculations are adapted version of formulas presented by Stein and Littke (1990) for the same parameters.

Terrigenous and aquatic organic matter accumulation rates (TORCAR and AORCAR, respectively) are determined by

TORCAR = OCAR x percent of terrigenous organic matter

AORCAR = OCAR x percent of aquatic organic matter

Vitrinite reflectance measurements were made with a Zeiss Photomicroscope III in oil immersion at a wave length of 546 nm using a measuring blind of 8 μm diameter. Data were processed by HP 8916S hardware combined with Zeiss Coflex software.

2.3 Geochemical Analysis

Total carbon (TC) determinations were made with a LECO IR-112 carbon analyzer. The same instrument was used for total organic carbon (TOC) measurements after removal of carbonate with hydrochloric acid. Carbonate contents were calculated by difference and expressed as percent $CaCO_3$.

Rock-Eval pyrolysis was performed according to the method described by Espitalié et al. (1977) with a Rock-Eval II-type instrument (GEOCOM).

A modified flow blending technique (Radke et al., 1978) was used to extract the ground sediment samples with a mixture of dichloromethane and methanol (99:1 v/v). Total extracts were separated into saturated hydrocarbons, aromatic hydrocarbons, and heterocomponents by medium pressure liquid chromatography (Radke et al., 1980).

The saturated hydrocarbons were analyzed using a Hewlett-Packard 5710A gas chromatograph equipped with a fused silica capillary column of 25 m length, 0.32 mm internal diameter, coated with poly-(methyl(95%)-phenyl(5%)siloxane) of 0.26 μm film thickness. The oven temperature was programmed to rise from 80°C to 300°C at 4°C/min. Helium was used as the carrier gas. Sample introduction was performed by a programmed-temperature injection system. The split ratio was about 1:100. Selected n-alkanes and isoprenoids were quantified by internal standardization with 5-alpha androstane applied prior to extraction.

The aromatic hydrocarbon fractions were analyzed by a Hewlett-Packard 5731A gas chromatograph equipped with a programmed-temperature injection system (KAS) and a fused silica Ultra #2 capillary column of 50 m length, 0.20 mm internal diameter, coated with cross-linked poly(methyl-(95%)-phenyl(5%)siloxane) of 0.33 μm film thickness. The temperature was programmed to rise from 120°C (hold 2 min.) to 310°C at 3°/min. Helium was used as the carrier gas. Selected naphthalenes and phenanthrenes were quantified by internal standardization with five aromatic standards added prior to extraction. Corrections for evaporation losses were applied.

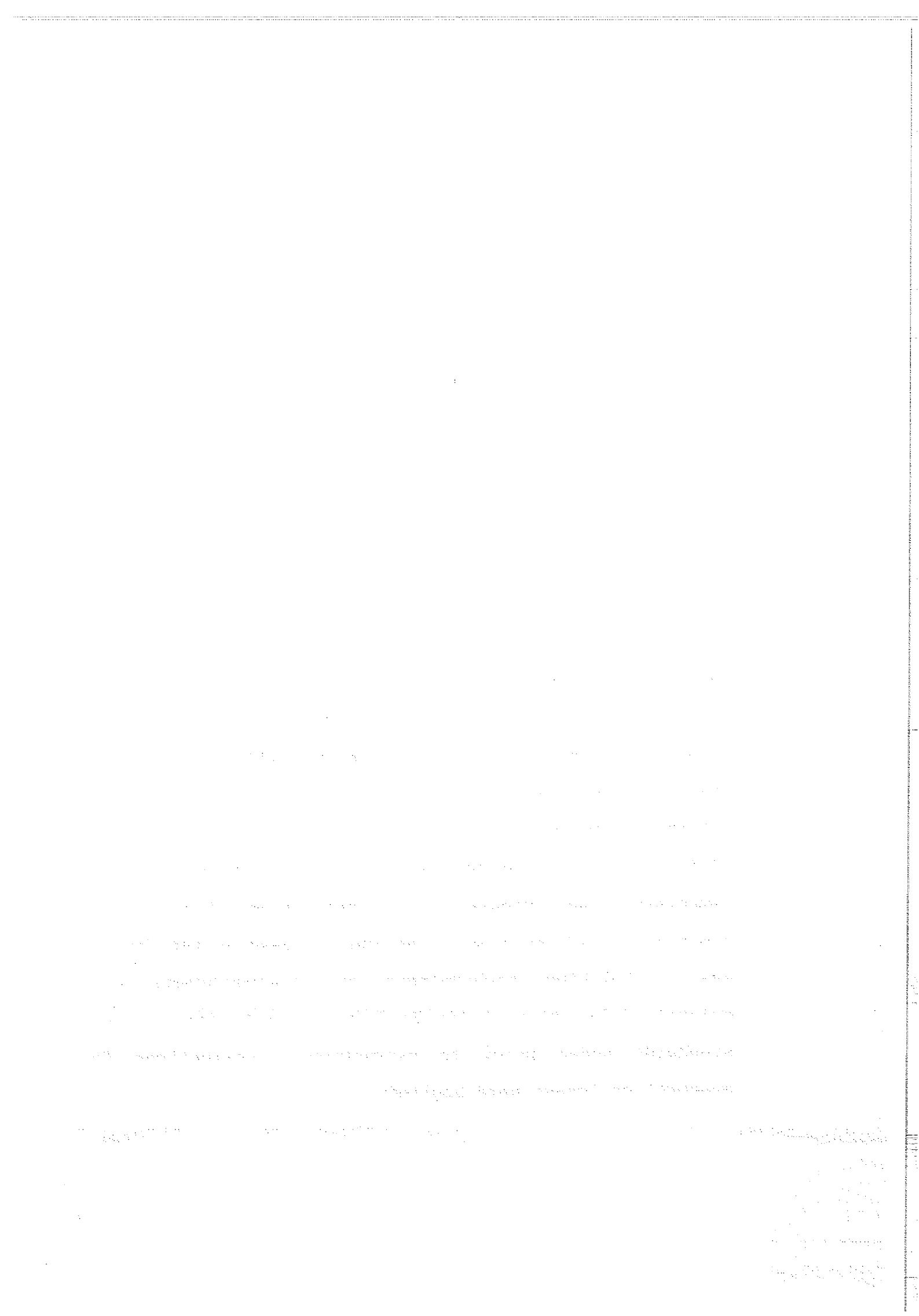

3. FACIES RELATIONSHIPS AND DEPOSITIONAL ENVIRONMENTS

3.1 Introduction

The first part of this dissertation focuses on the sedimentology and characterization of the organic content of the S unit of the Mulhouse Basin. The emphasis of this part of the study was to determine the conditions required for the accumulation and preservation of organic matter in an evaporite depositional environment. Only in recent years have geologists and organic geochemists recognized the source rock potential of some evaporite suites. During the past 20 years, researchers have been able to document that, contrary to common belief, evaporitic environments provide ideal conditions for source rock formation (Kirkland and Evans, 1981; Eugster, 1985; Sonnenfeld, 1985; Warren, 1986; Evans and Kirkland, 1988). This change in opinion stems from the work of biologists and geologists in modern evaporite environments who showed that 1) bioproductivity is very high, even higher than in the most productive zones of the ocean (Warren, 1986; Cornee, 1988), and 2) the preservation potential in the depositional environment is good, because anoxic conditions usually prevail and burrowing and grazing organisms are sparse or absent. Therefore, if the organic matter can be preserved during the diagenesis of the evaporite sequence, organic matter-rich source rocks can

be expected. Evaporites can form in many different environments (e.g. Schreiber, 1986); organic matter production, preservation and destruction are dictated by the physical conditions of each particular setting. Thus far, however, only a few studies (e.g. Connan et al., 1986) have integrated sedimentology and organic geochemistry in order to understand the organic content of an evaporite deposit. In the following chapters, the conditions that lead to the accumulation and preservation of organic matter for one specific evaporite depositional environment are discussed in detail.

3.2 Geological Overview

The Rhine Graben is the central segment of the western European rift system (Fig. 2), which stretches from the Mediterranean Sea to the North Sea. The upper Rhine Graben segment extends from Basel, Switzerland, to Frankfurt am Main, Germany, and is approximately 300 km long and on average 37 km wide. The general strike of the graben as outlined by the graben boundary faults is SSW-NNE (Illies, 1974). Rifting in the Rhine Graben area began in the mid-Eocene (Illies and Greiner, 1978), following a long (beginning in the Cretaceous) period of mantle uplift and surface volcanic eruptions, which were widespread over the future graben and its shoulders (Baranyi et al., 1976; Neugebauer and Temme, 1981). The beginning of rift valley subsidence is indicated by fresh water deposits of mid-Eocene age (Doebl, 1970). Most of the graben subsidence occurred from the middle Eocene to early Miocene as a result of approximately 6 km of crustal extension (Illies, 1972; Villemin et al., 1984). Even though the overall extension is similar throughout the upper Rhine Graben, major differences exist between the northern and southern Rhine Graben. The northern Rhine Graben is characterized by extensional processes that have been active during the last 40 million years, whereas in the south, 10 million years of active extension was

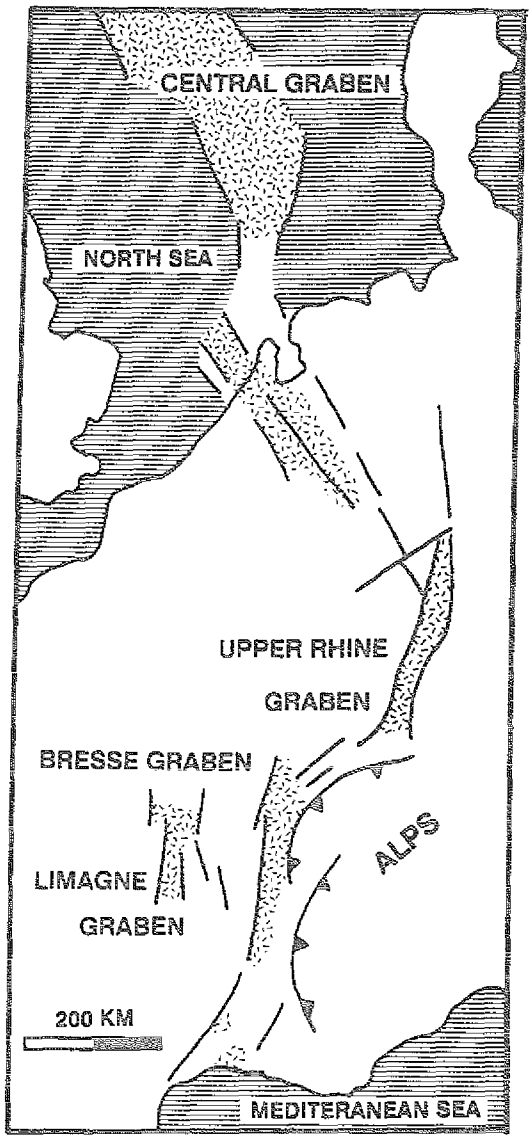

Fig. 2: Position of the Rhine Graben Segment in the Western European Rift System (modified after Pflug, 1982).

followed by a 30 million year period of thermal subsidence (Villemin et al., 1986). The different thermal histories of the northern and southern parts of the graben resulted in a differential subsidence of the graben segments starting in the Eocene (Sittler, 1969; Doebl and Teichmüller, 1979), which led to differentiation of the overall rift valley into a number of subbasins (Fig. 3). In the southern part of the Rhine Graben, four subbasins can be recognized; the Pechelbronn Basin, the Strasbourg Basin, the Selestat Basin and the Mulhouse Basin (Roll, 1979). Each of these subbasins contains evaporite deposits of Eocene to early Oligocene age (Blanc-Valleron, 1991). The paleogeographic situation of the Rhine Graben during the late Eocene to early Oligocene is characterized by an intracontinental rift basin, which at its southern fringe was sporadically connected to the Alpine foredeep through Burgundy via the Bresse Graben (Ziegler, 1988).

The Mulhouse Basin has received attention since the turn of the century, when extensive potash salt deposits were discovered (Förster, 1911). Exploitation of the potash deposits continues today and has led to extensive geological surveys of this subbasin (e.g. Blanc-Valleron, 1991; Martini, 1973; Courtot et al., 1972; Sturmfels, 1943; Maikovsky, 1941). The most recent survey led to the detailed geological mapping of the Upper Salt Formation

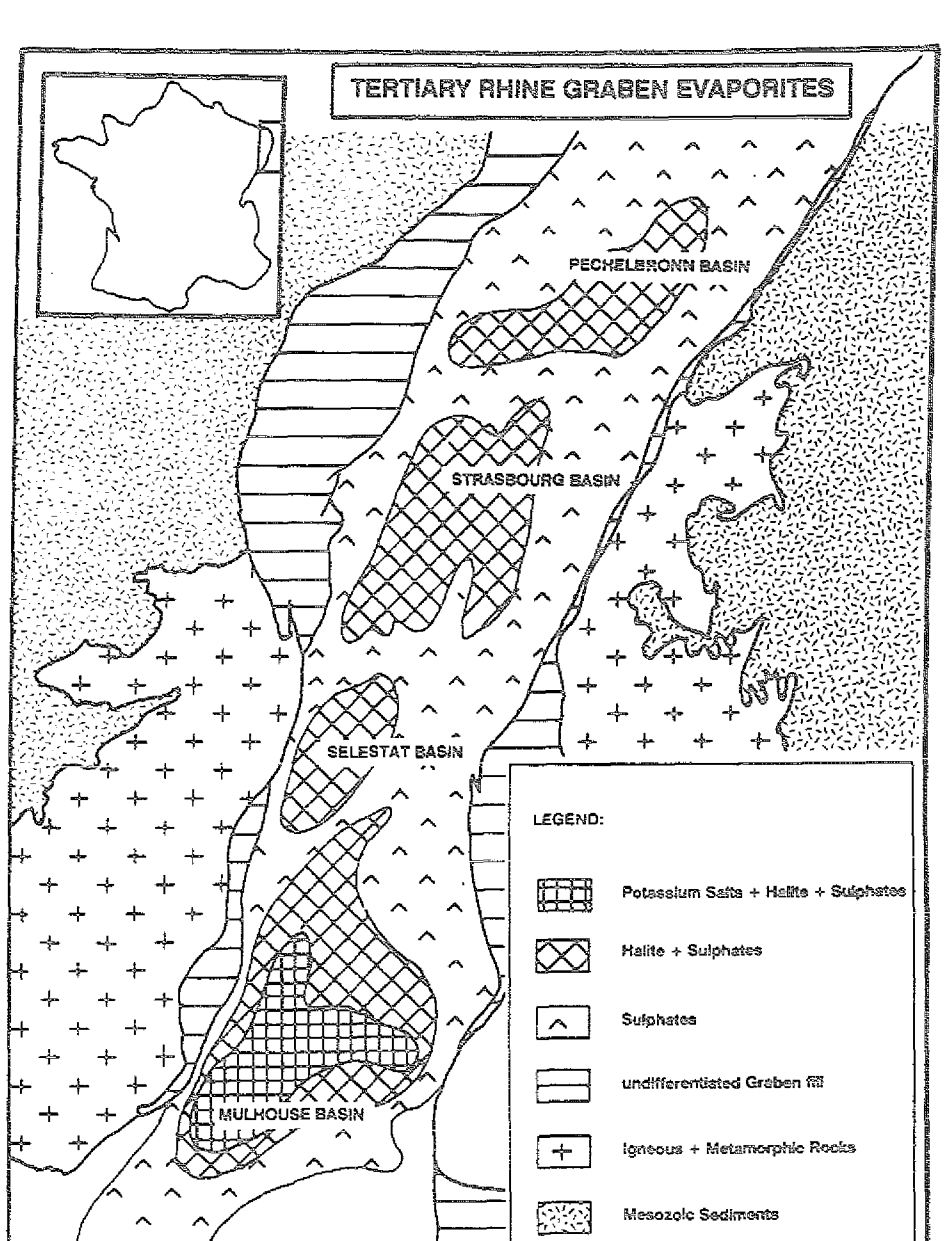

Fig. 3: Location of the evaporite-bearing subbasins of the southern Rhine Graben (modified after Blanc-Valleron, 1991).

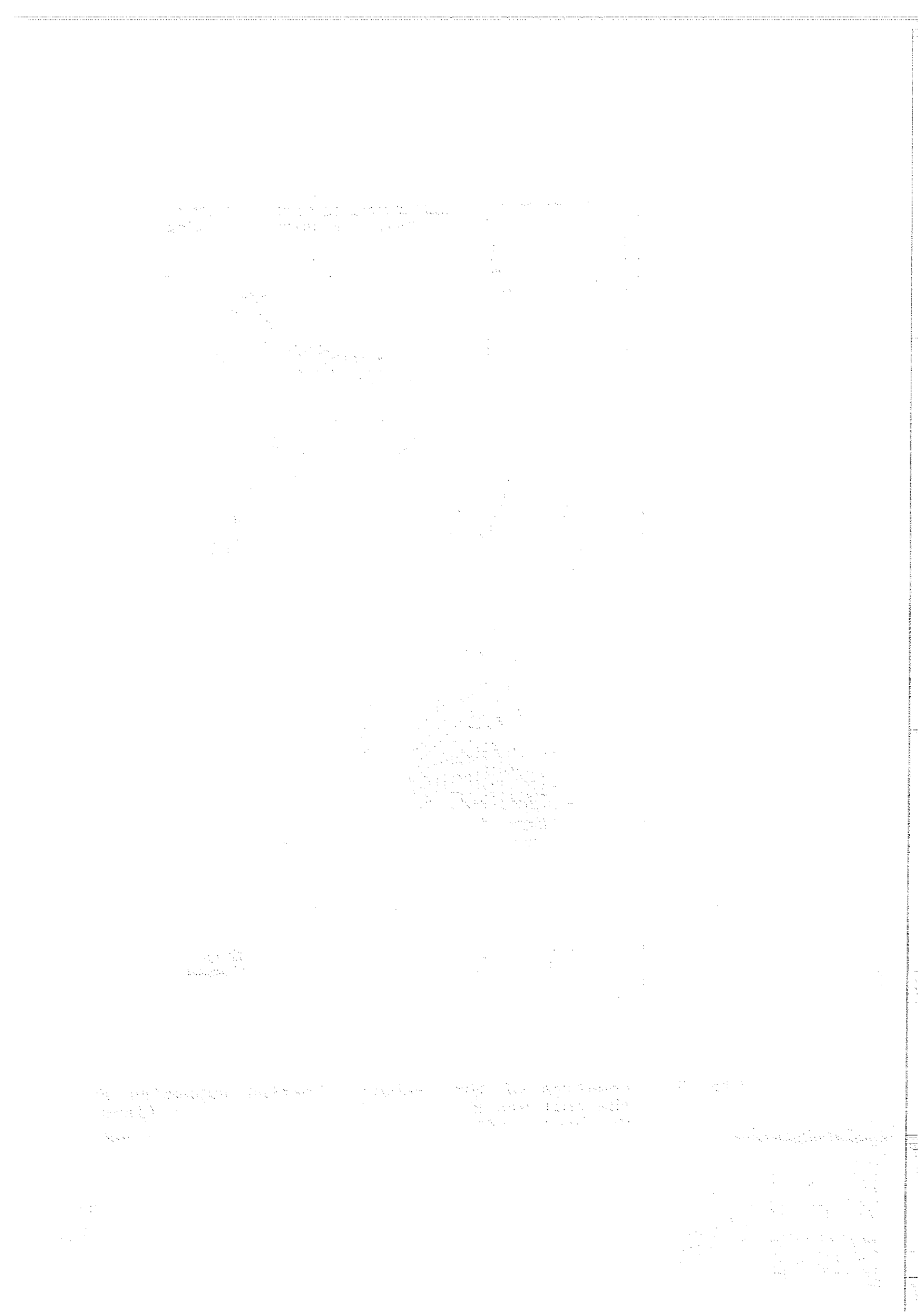

(Blanc-Valleron and Gannat, 1985) and reveals significant insights into the paleobasin morphology. Blanc-Valleron (1986) demonstrated that parts of the lower Oligocene Upper Salt Formation of the Mulhouse Basin are particularly rich in organic matter (up to 7% TOC). Blanc-Valleron et al. (1991, 1989) also noted that the organic and inorganic sedimentation appeared to follow a cyclic sedimentation pattern, which she and her co-workers attributed to climate variations controlled by astronomical phenomena.

The association of organic matter-rich sediments with evaporites in the Upper Salt Formation of the Mulhouse Basin makes this stratigraphic interval highly attractive for the study of the interdependence of evaporite and organic matter sedimentation. Furthermore, the vast amount of information already present in the literature and the good accessibility of this stratigraphic interval in mining outcrops due to the courtesy of Mines de Potassé d'Alsace make this stratigraphic interval an ideal place for the study of organic matter in evaporites.

3.3 Stratigraphy

The stratigraphy of the Mulhouse Basin has been summarized by a number of authors (e.g. Sittler, 1972, 1983, 1985; Courtot et al., 1972; Blanc-Valleron and Gannat, 1985). The emphasis of many of these authors was the correlation of the sedimentary fills of the various subbasins of the upper Rhine Graben. For working purposes, the stratigraphic charts of Blanc-Valleron and Gannat (1985) are the most convenient (Fig. 4) because they contain very detailed lithostratigraphic charts based on the extensive geological database of the Mines de Potassé d'Alsace.

The stratigraphy of the Mulhouse Basin (Fig. 4) shows the presence of several evaporite-dominated salt formations. The Salt IV of the Upper Salt Formation has received the most attention because of the presence of commercially exploitable potash salts (CI and CS units). The salts are located in the lower part of the Salt IV. Blanc-Valleron (1986) recognized the presence of organic matter-rich marls just below and above the potash salts (S1 to T unit), with the highest organic matter concentrated in the S unit (Fig. 4). The commercial exploitation of the potash salts allows easy access to the S1 to CI units. A detailed lithostratigraphic column of this interval measured at the Amelie II mine is depicted in Fig. 5 (see Fig. 6 for location).

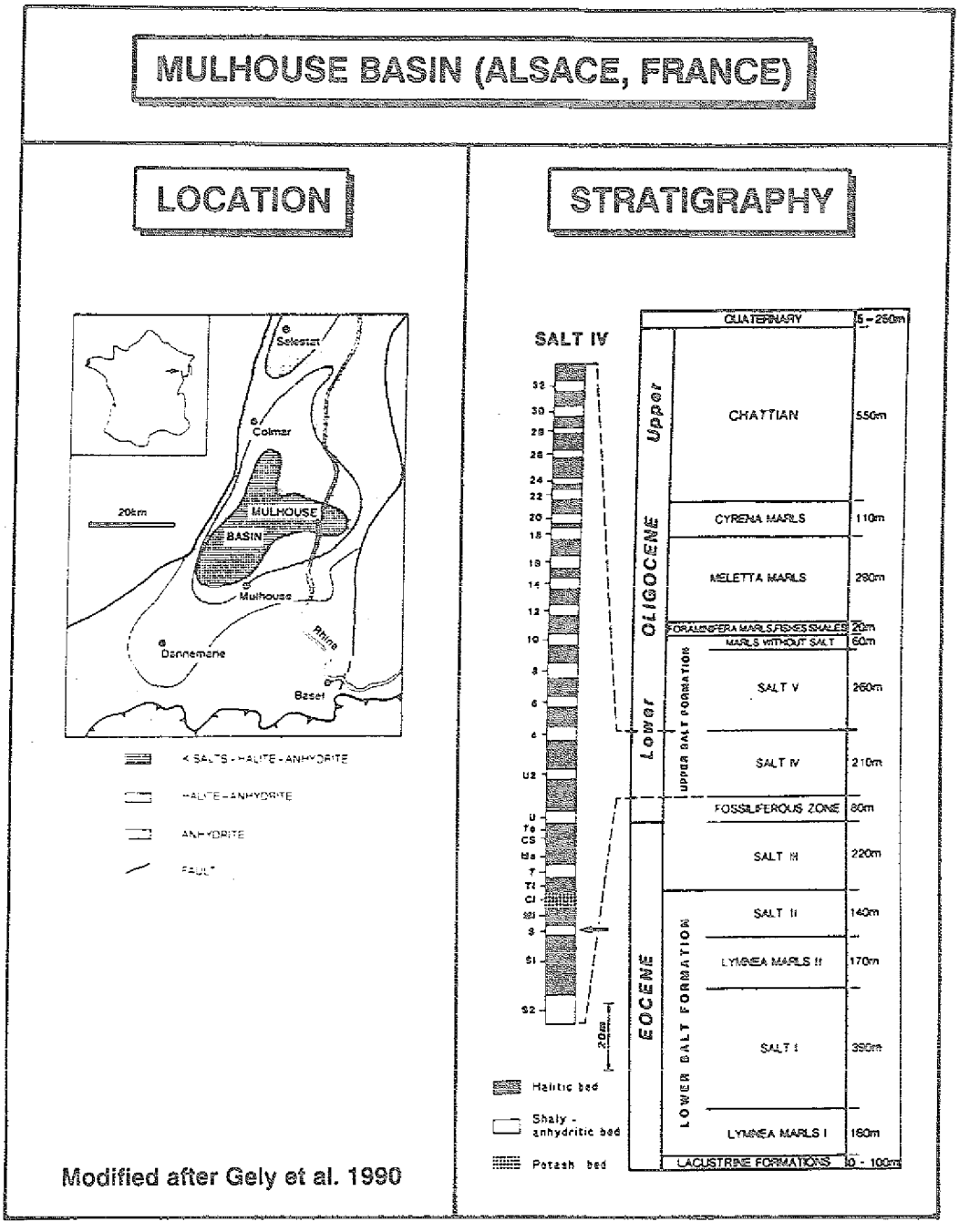

Fig. 4: Location and stratigraphy of the Mulhouse Basin (modified after Gely et al., 1990 and Blanc-Valleron, 1991).

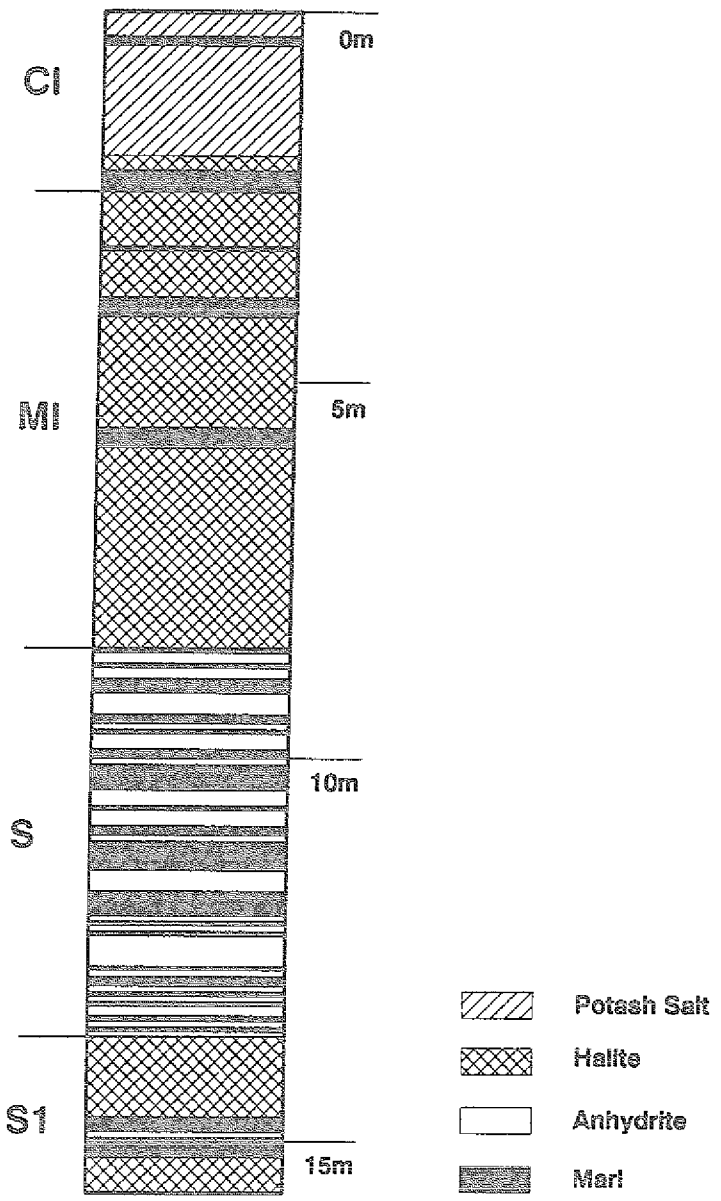

Fig. 5: Stratigraphic column based on a measured mine section at Traverse 830 at site Amelie II.

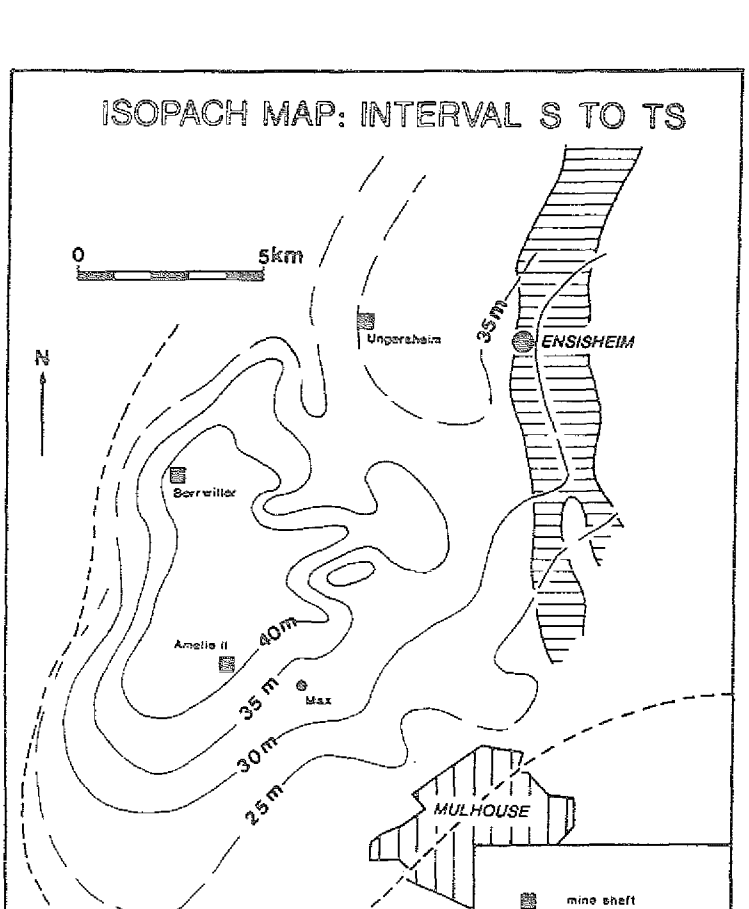

Fig. 6: Isopach map of the S to TS interval in the southern part of the Mulhouse Basin. Sampling locations are indicated (modified after Blanc-Valleron, 1991).

The base of the section consists of the top of the S1 unit. The S1 unit is composed of milky white halite beds (up to several meters thick) separated by thinner intervals (<1 m) of marl and anhydrite. The S1 unit is topped by the S unit. The contact is marked by the presence of anhydrite and marl beds (up to 10 cm thick). The S unit consists of a sequence of marls, anhydrites, and, to a minor extent, halite beds. At traverse 830 at Amelie II the S unit has a thickness of 5.6 m. Above the S unit is the MI unit, which is similar in character to the S1 unit. Several meter-thick, milky-white halite beds are disrupted by three intercalations (up to 50 cm thick) of marl and anhydrite. The boundary of the MI and CI units is a 25 cm thick marl-dominated bed with minor amounts of anhydrite, the "Faux Mur de Marne." It is overlain by several beds of potash salt. The potash salt occurs as a banded salt of alternating halite and sylvite dominated layers. The sylvite layers are colored red by hematite inclusions (Sturmfels, 1943).

The primary target of this dissertation, the S unit, could be sampled in mine outcrops owing to the courtesy of the Mines de Potassé d'Alsace at three locations: Amelie II, Berrwiller, and Ungersheim (Fig. 6). All of these locations were in the central area of the Mulhouse Basin during the deposition of the S to TS units.

The S unit reaches a thickness of 5.60 m at Amelie and 4.25 m at Ungersheim. The total thickness at Berrwiller could not be determined because only the top 2.80 m are exposed at the mine outcrop. At each of the locations, the S unit contains marl and anhydrite beds; halite is exposed only at Amelie II and Ungersheim (Fig. 7). The lithofacies, however, are the same at each of these locations, as is demonstrated in the following sub-chapters.

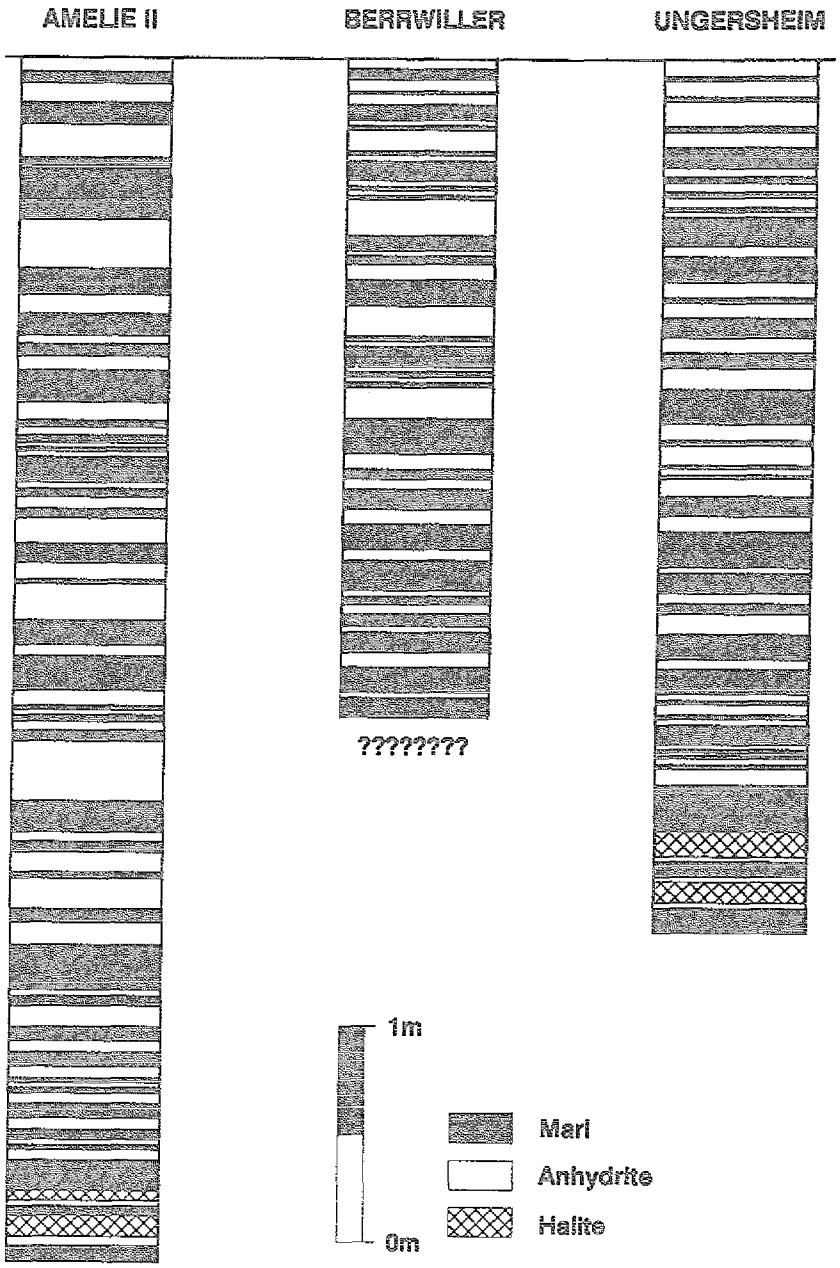

Fig. 7: Lithological column of the S unit at the sites Amelie II, Ungersheim, and Berrwiller. For locations of sites, see Fig. 6.

3.4 Facies Description

As pointed out above, the organic matter content of the S unit is by far the highest in this stratigraphic interval. In order to understand the relationship between organic and inorganic sedimentation, a detailed facies analysis is performed to reconstruct the paleodepositional environment.

3.4.1 Marl

Marls occur in layers varying from 1 cm up to 30 cm in thickness. Each marl layer shows continuous, bedding-parallel laminae. The laminae are defined by color variations from dark brown to light gray. Alternating laminae are composed of either predominantly clay or micritic carbonate (Fig. 8). The clay and carbonate layers form alternating couplets. The clay-rich layers consist predominantly of quartz and illite, with minor amounts of kaolinite. Only two samples also contain traces of chlorite, specifically the "a" layer and the "Faux Mur de Marne" from the section at Amelie II. The carbonate-rich layers are mainly composed of calcite with minor amounts of dolomite and ankerite. Pyrite occurs in each sample in the form of framboids and as subhedral to euhedral cubic crystals, and appears to be enriched in

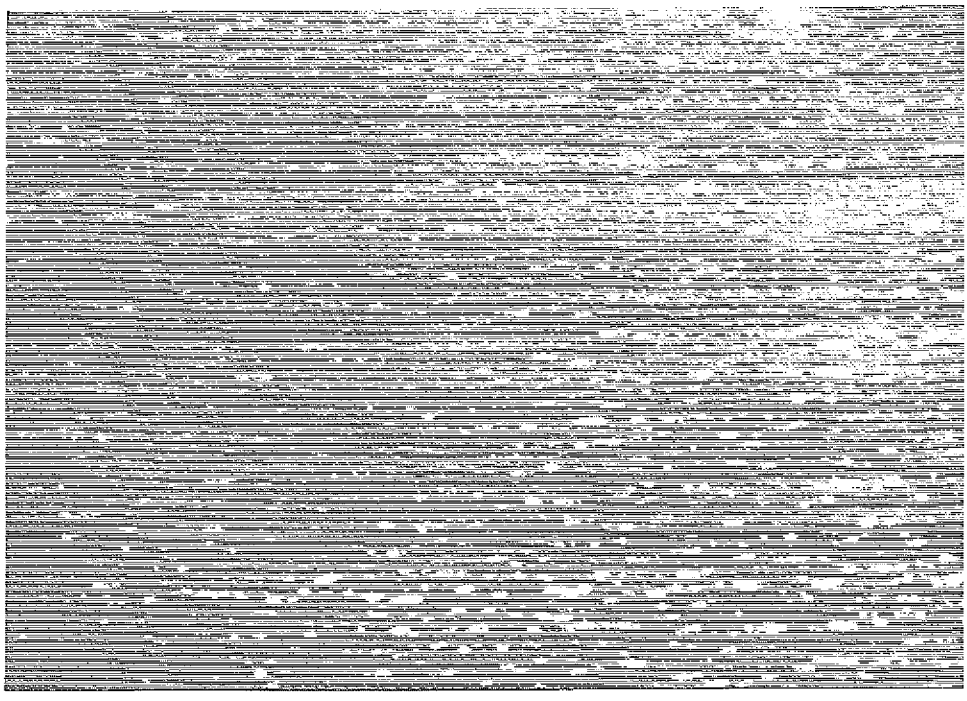

Fig. 8: Photomicrograph of a laminated marl sample. Note alternating clay and carbonate laminae. (Plane-polarized light. Field of view is 8 mm wide).

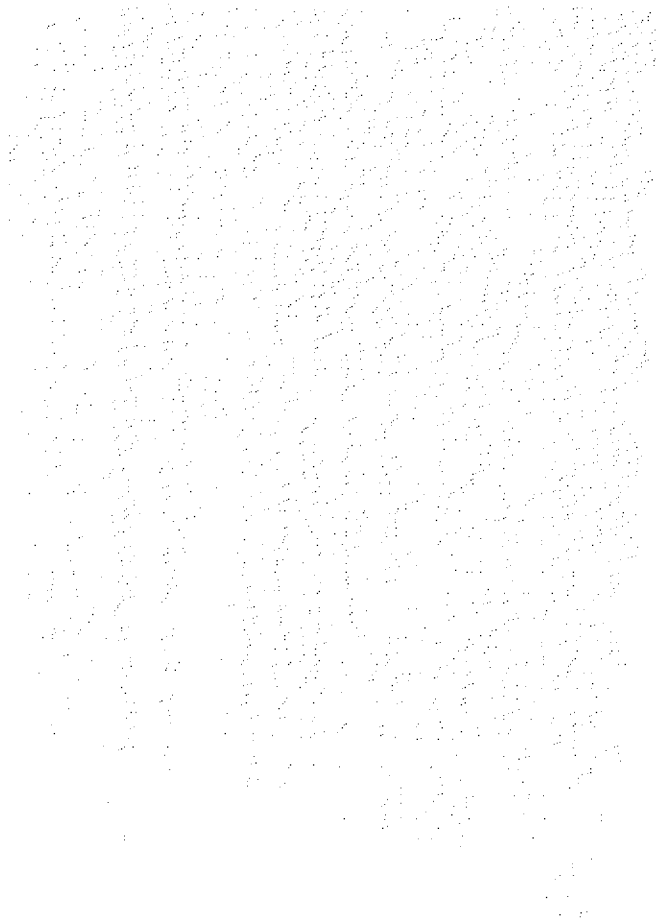

zones that are rich in clay minerals and organic matter. Halite and the sulfate minerals gypsum and anhydrite are also present in some samples, but are restricted to vein and/or microfracture fillings. Halite also occurs as replacive euhedral to subhedral cubes and plates up to 3 cm thick.

Foraminifera-rich layers are present in many marl units (Fig. 9). The layers are up to several tenths of a millimeter thick and composed of foraminifera tests together with detrital minerals. The tests are in most cases well preserved (Fig. 10) and are sometimes partially replaced by framboidal pyrite. The foraminifera-rich layers occur at irregular intervals. The identification of the foraminifera-rich layers was only possible by observation in blue light fluorescence on polished slabs, and were first identified by B.C. Schreiber (personal communication). The occurrence of abundant foraminifera in the marls of the S unit of the Mulhouse Basin was reported for the first time by Hofmann and Leythaeuser (1991). Previous workers (e.g. Blanc-Valleron, 1991; Schuler, 1988) did not recognize the presence of these fossils, most likely because of the destruction of the fossils when standard petrographical and palynological techniques were applied. No attempts were made to identify individual genera of the foraminifera assemblage.

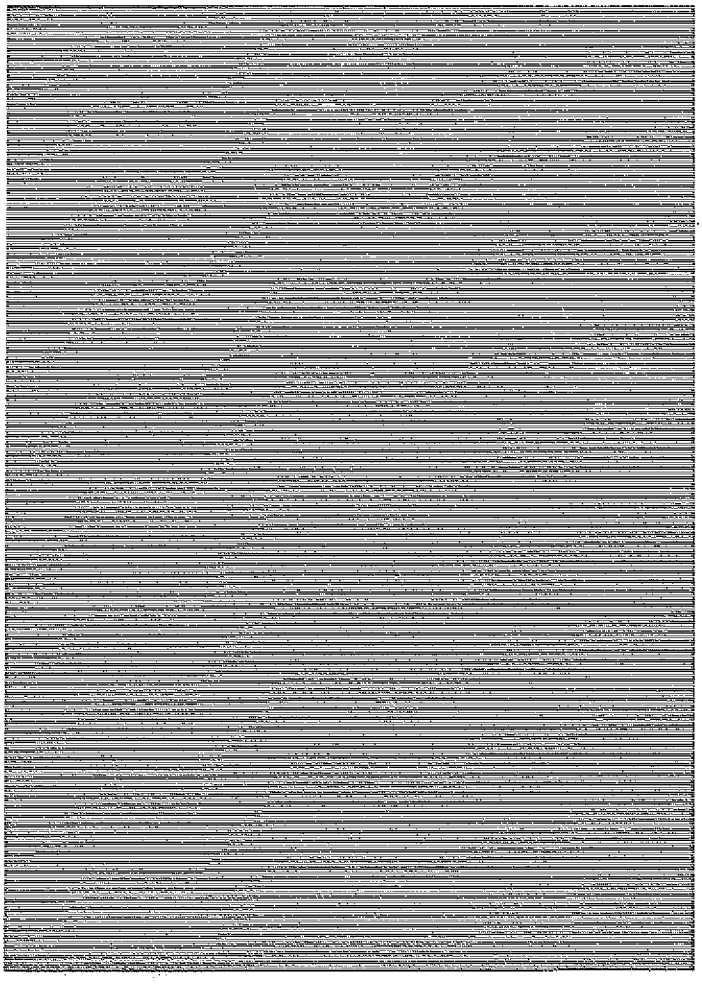

Fig. 9: Photomicrograph of a foraminifera-rich layer. (Blue light. Field of view is 360 μm wide).

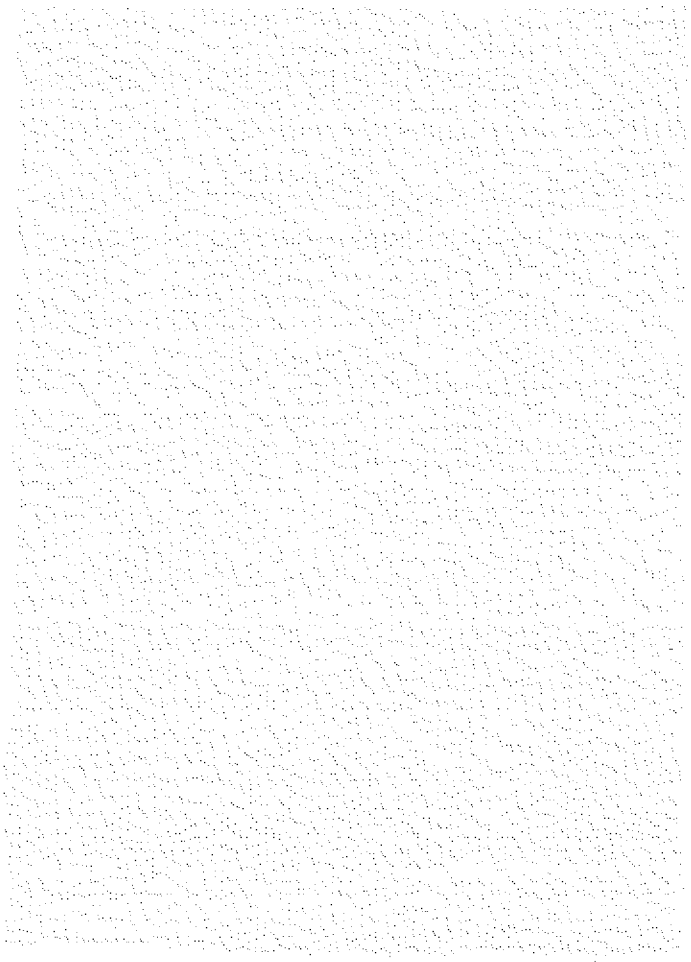

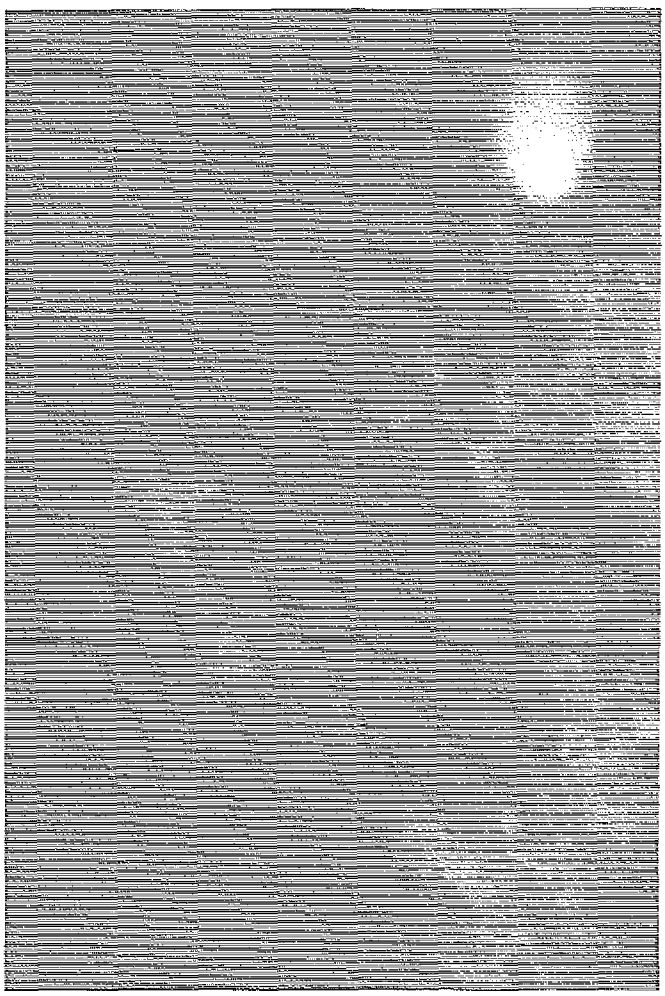

Fig. 10: Photomicrograph of a foraminifera test. The test has been replaced by pyrite. (Blue light. Field of view is 200 μm wide).

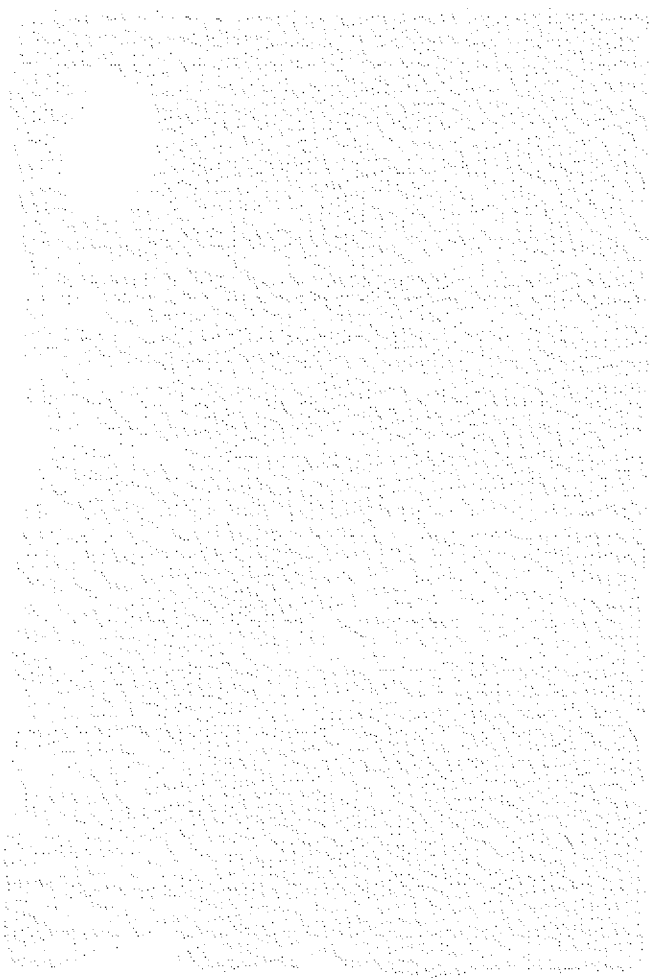

However, most species seem to be of marine planktonic origin; benthic foraminifera appear to be sparse or absent (B.C. Schreiber, personal communication).

The marls can be further subdivided into two distinct facies, type A and type B. Marls of type A are usually light brown to dark brown (Fig. 11). This facies is characterized by well developed submillimeter thick clay/carbonate couplets. The clay-rich laminae of marls of type A contain algal detritus and closely stacked layers of organic matter (Fig. 12). Layers composed of tests of planktonic foraminifera up to several tenths of a millimeter in thickness are common.

Marls of type B are a light gray to steel gray color (Fig. 13). Marls of type B display, on the average, thicker carbonate/clay couplets than do marls of type A. Clay-rich laminae containing stacked layers of amorphous organic matter are absent in the marls of type B (Fig. 12; see also Organic Petrography Section), and foraminifera-rich layers occur less commonly compared to marls of type A.

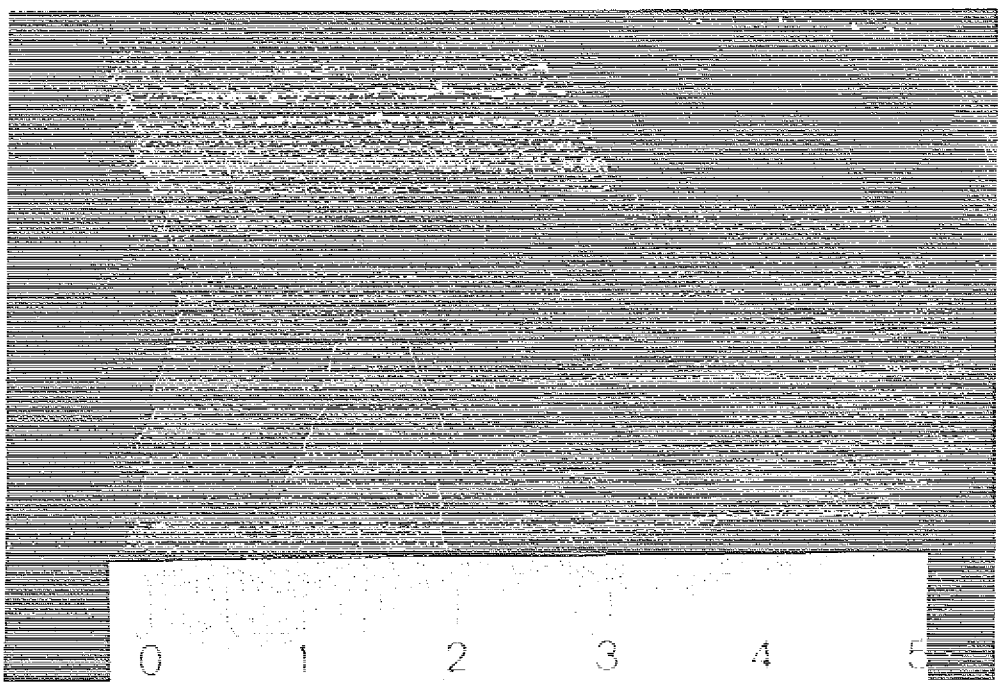

Fig. 11: Photograph of a sample of marl of type A. Note well-developed and well-preserved lamination. (Scale is in cm).

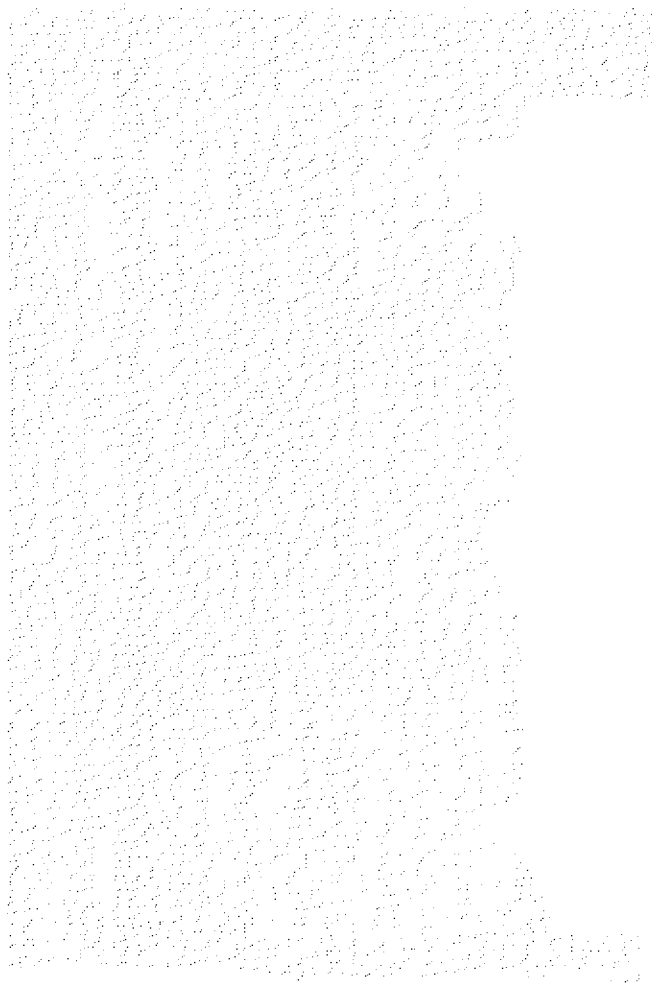

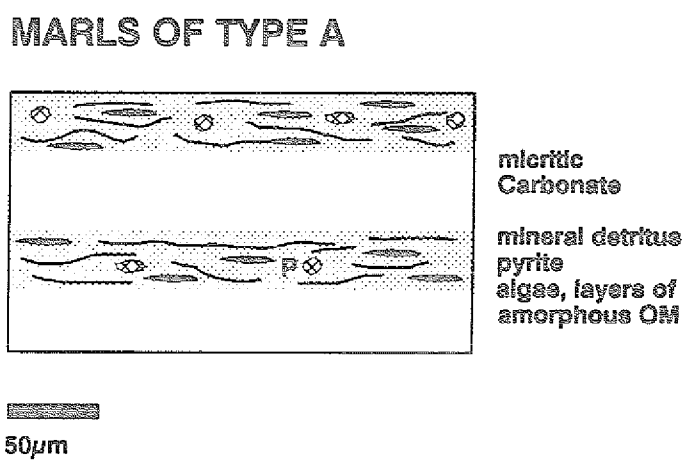

Fig. 12: Cartoon of a thin section view of alternating laminae of marls of type A and marls of type B (P = pyrite).

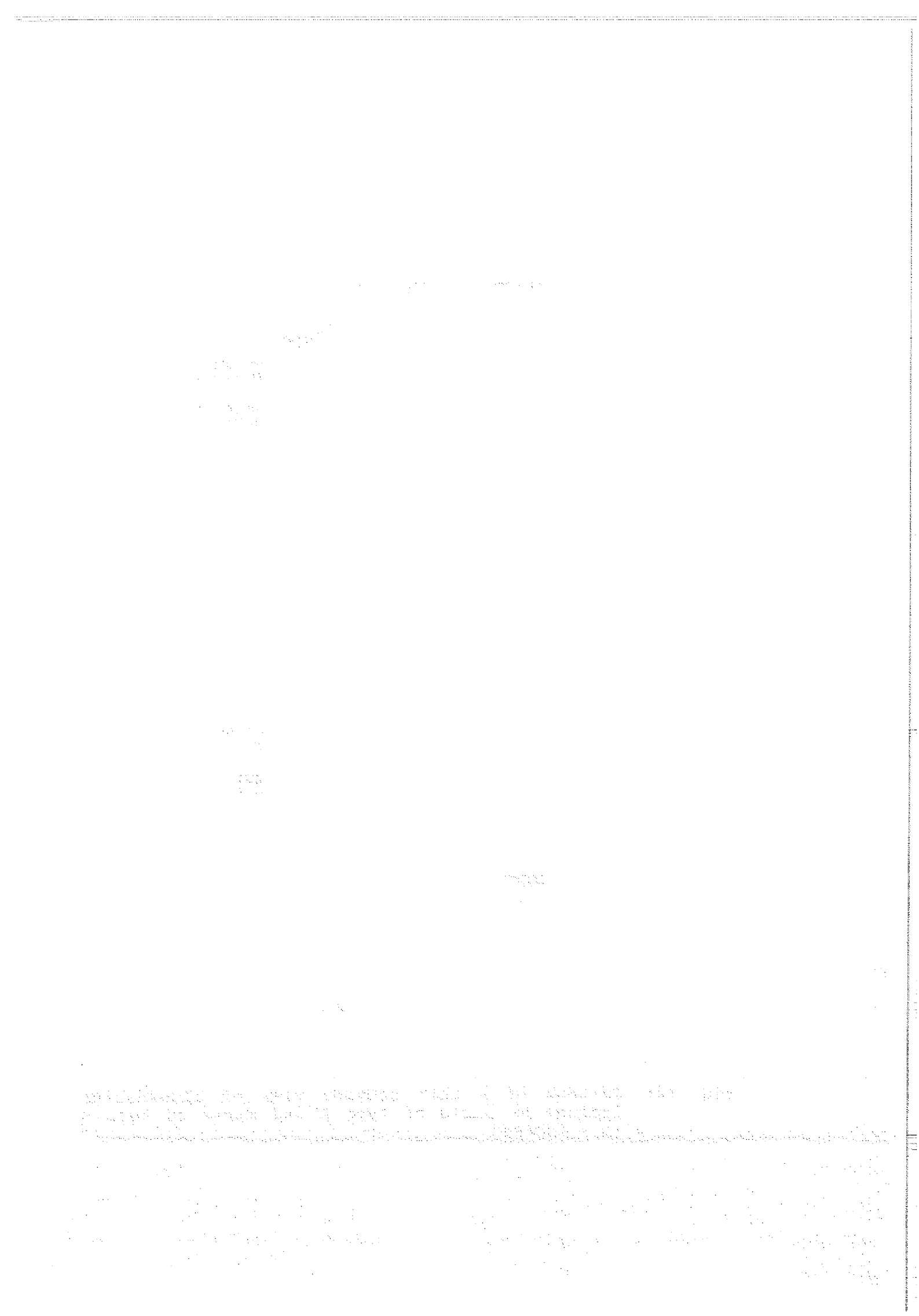

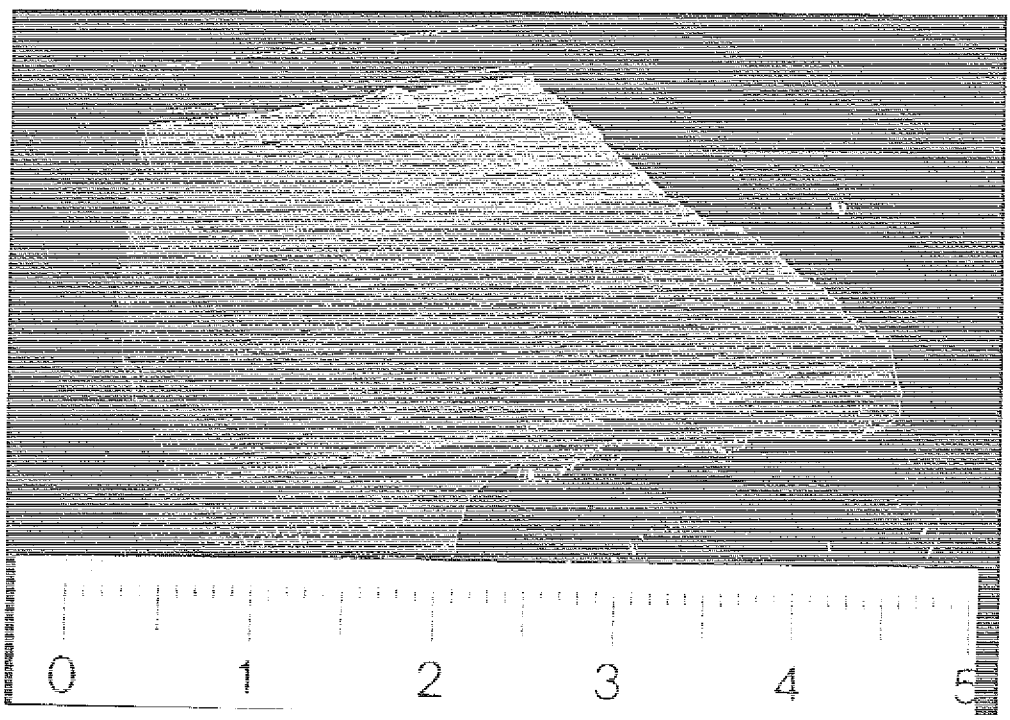

Fig. 13: Photography of a sample of marl of type B. Note perfectly preserved lamination. (Scale is in cm).

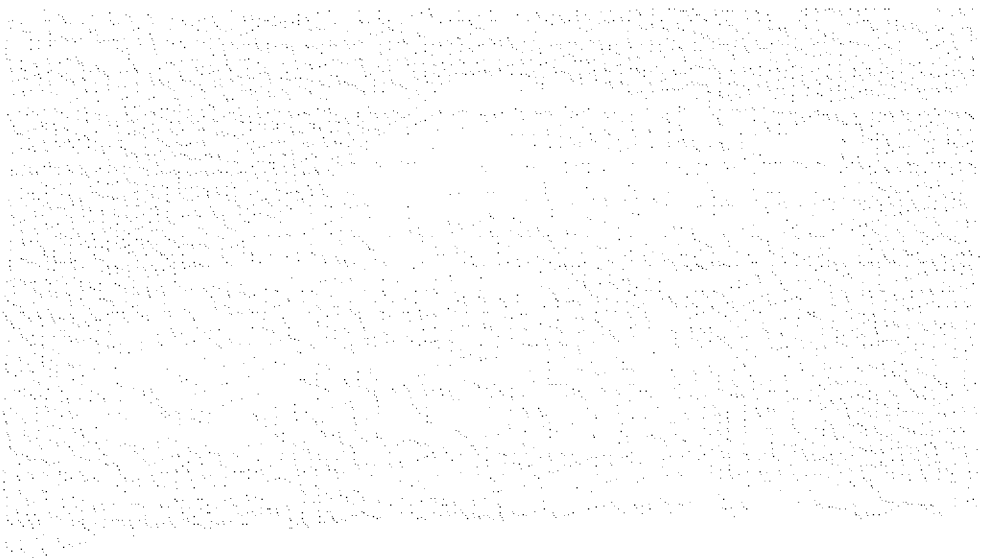

3.4.2 Anhydrite

3.4.2.1 Nodular Anhydrite and Lenticular Anhydrite

Nodular anhydrite occurs in 0.5 - 1.5 cm thick layers in a marl matrix. The nodules occur either as discrete, semicircular aggregates up to 5 mm thick or form layers of aggregates that have fused together. The nodules appear to have grown displacively in the marl matrix and deform the surrounding sediment. The nodules consist either of anhedral anhydrite crystals or are formed by aggregates of lenticular anhydrite. A lenticular anhydrite aggregate is composed of anhedral anhydrite crystals that may have incorporated pyrite. Nodular anhydrite occurs exclusively in a matrix of marls of type A.

Layers composed of lenticular anhydrite are up to 2 cm thick (Fig. 14). The lenticular-shaped aggregates grew displacively in a marl matrix (Fig. 15), which was as a consequence compacted and deformed. The aggregates are composed of anhedral anhydrite crystals that in some cases have incorporated pyrite. Pyrite seems to be especially common in this facies, where it occurs as framboids and as euhedral to subhedral crystals (up to 2 mm in size). The boundary of each lenticular sulfate aggregate is not sharp, but rather shows slight off-sets. Layers of

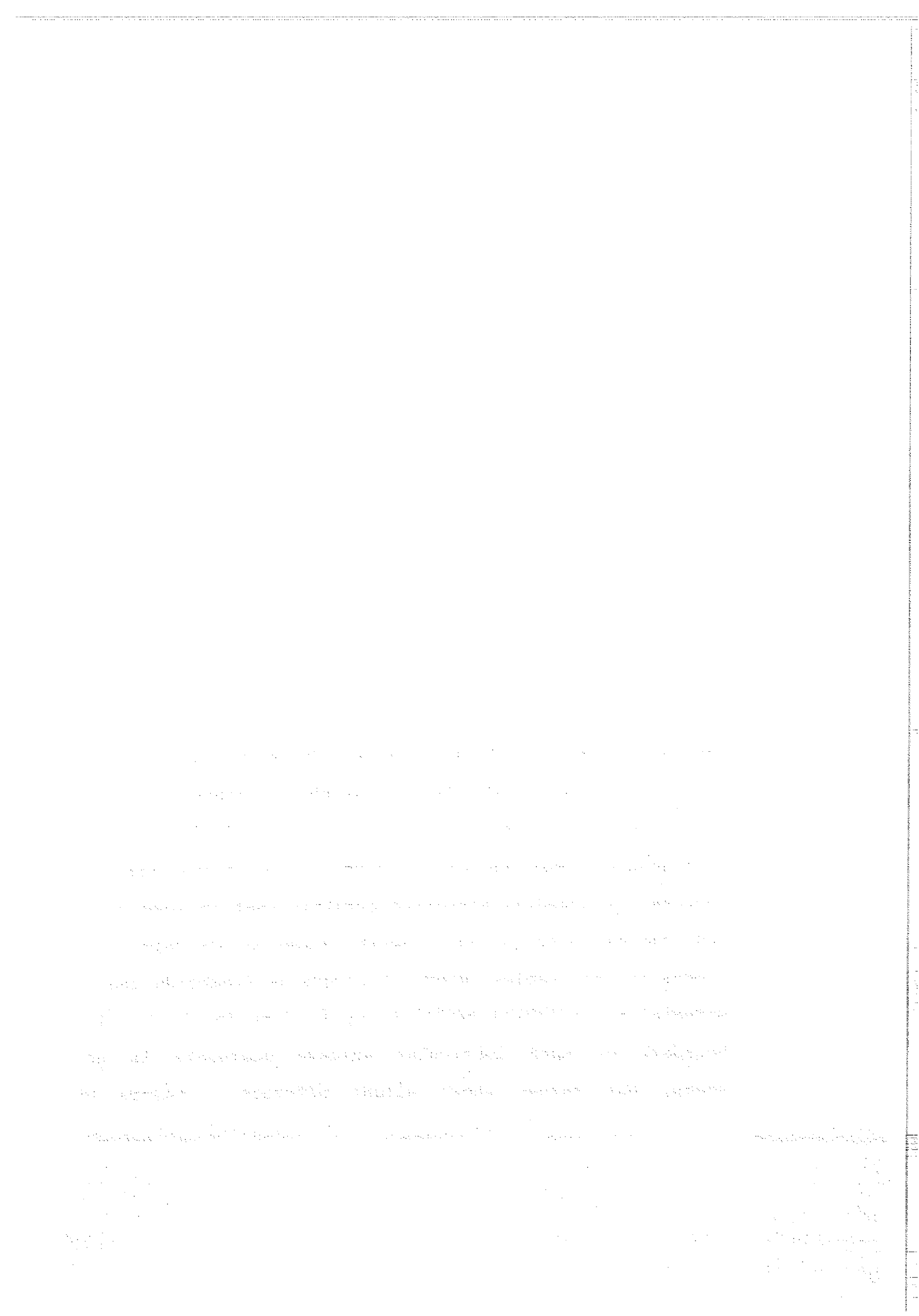

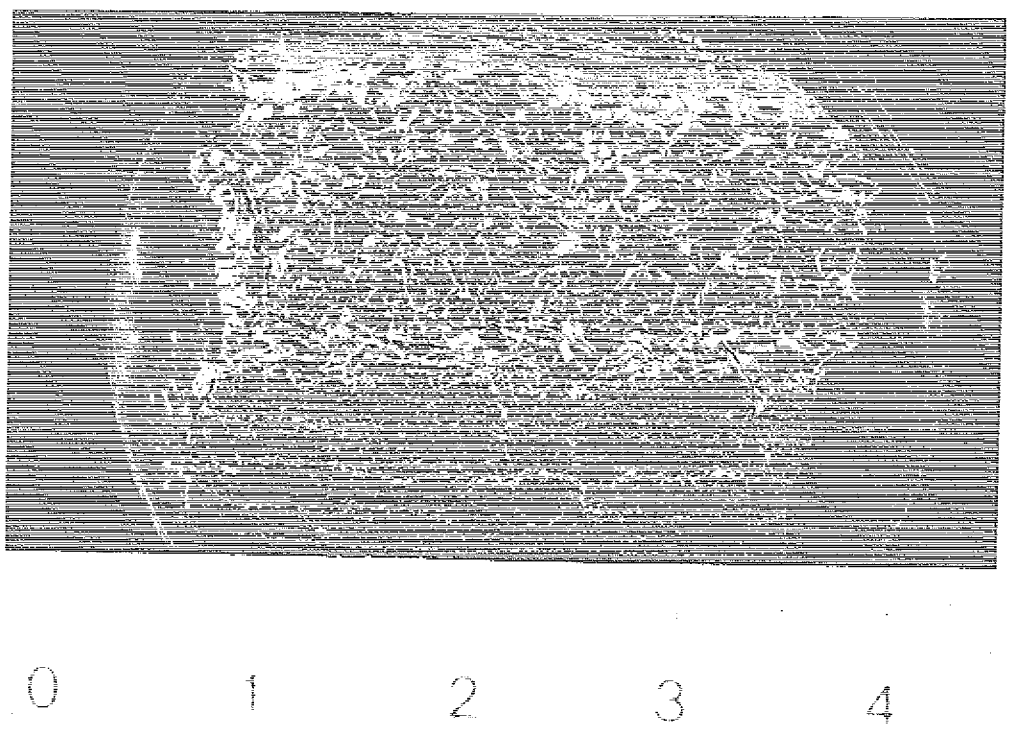

Fig. 14: Photograph of a polished, lenticular anhydrite sample. (Scale is in cm).

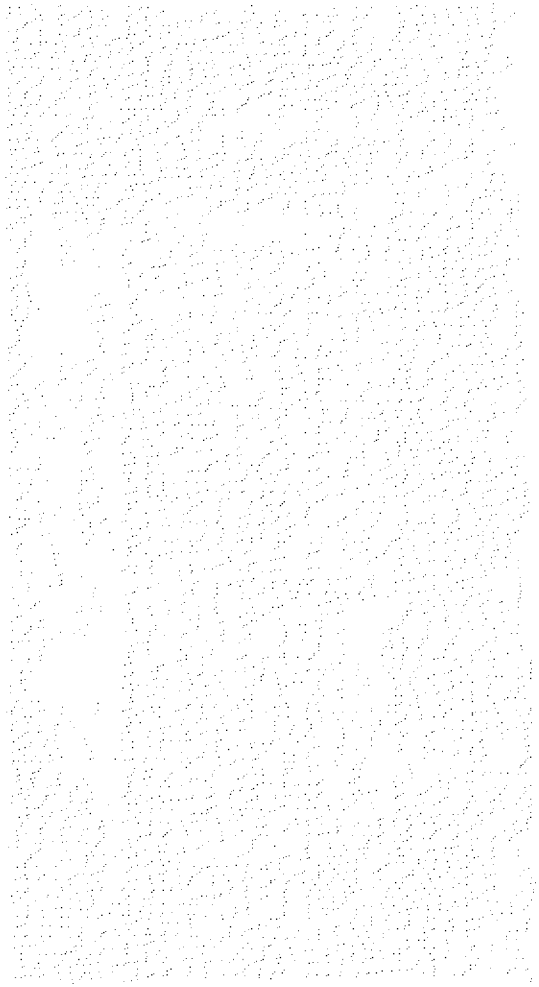

Fig. 15: Photomicrograph of a lenticular anhydrite sample. Note the deformed marl matrix. (Field of view is 5.7 mm wide).

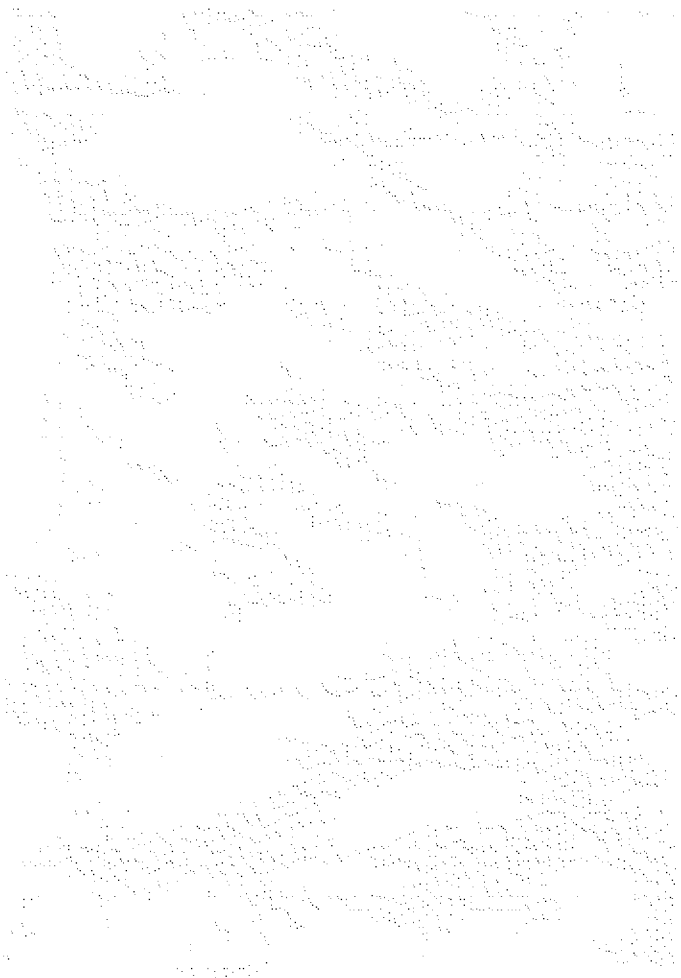

lenticular anhydrite are especially common in marls of type A, particularly within zones enriched in organic matter.

3.4.2.2 Laminated Anhydrite

Laminated anhydrite consists of layers of anhydrite (up to 2 cm thick) alternating with marl layers (up to 0.5 cm thick) that contain sparse foraminifera (Fig. 16). The anhydrite layers are composed of crystals with various morphologies. Some layers are rich in V-shaped crystal outlines composed of polycrystalline anhydrite (Fig. 17); others also contain prismatic and lenticular crystal outlines or larger patches that are made up of anhedral anhydrite. The pore space between the anhydrite crystals is filled either with clear halite cement (Fig. 18) or euhedral to subhedral carbonate rhombs. Halite-filled pores have in some cases maintained an overall cubic shape, which could indicate that halite was already present during sediment deposition. The interbedded clay-rich seams follow the contours of the top of each anhydrite layer, and in some samples, foraminifera tests have been observed in these seams. Large, V-shaped, polycrystalline anhydrite crystal outlines are often located on top of deformed clay-rich seams.

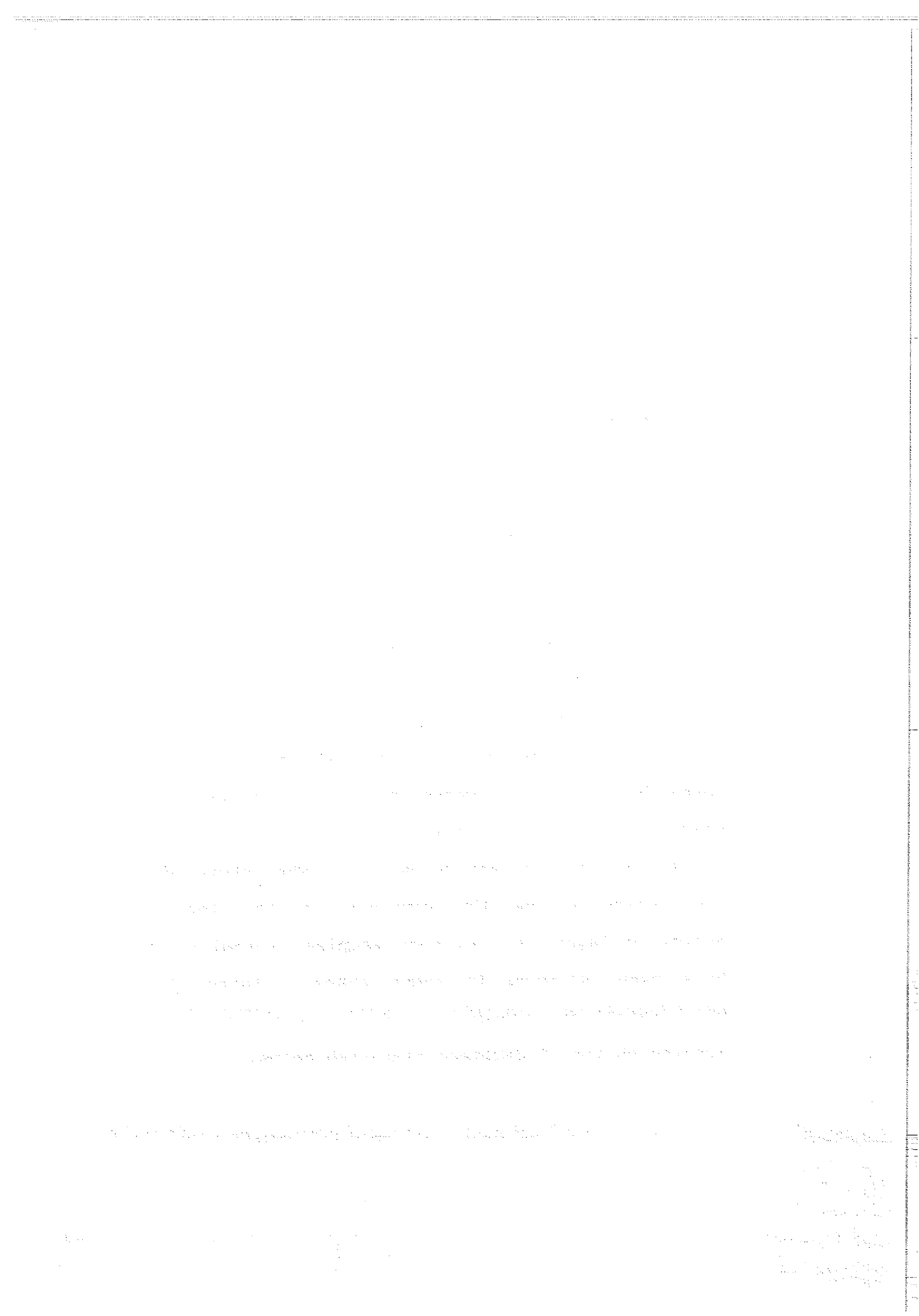

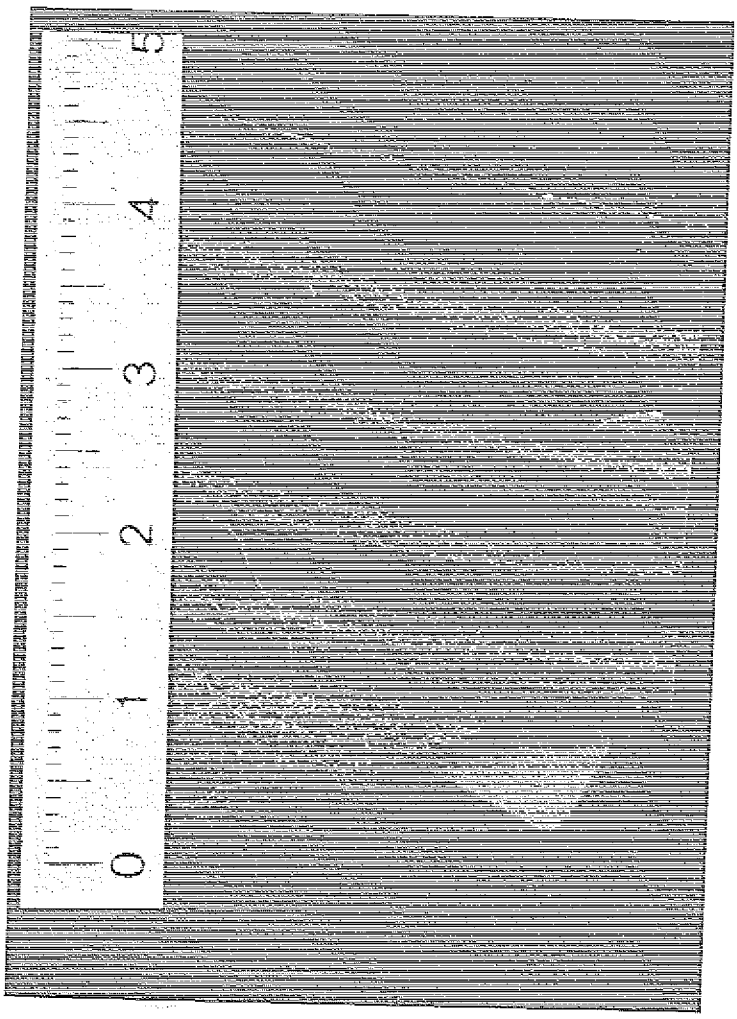

Fig. 16: Photomicrograph of the laminated anhydrite lithofacies. (Scale is in cm).

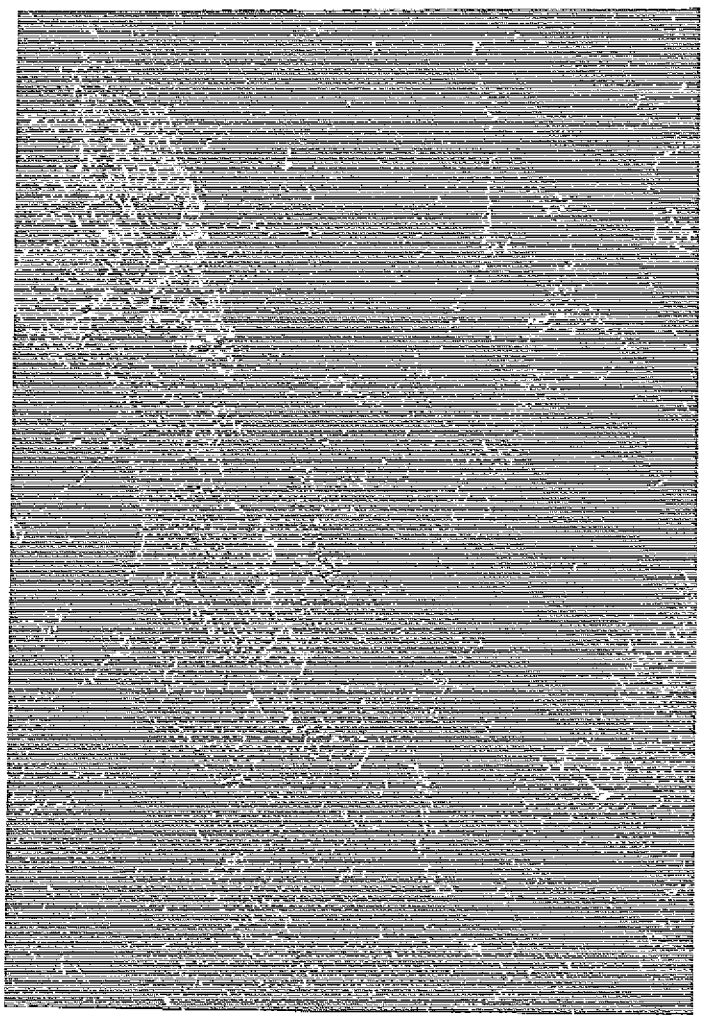

Fig. 17: V-shaped crystal outline of polycrystalline anhydrite, pseudomorphic after gypsum. (Crossed polars. Field of view is 360 μm wide).

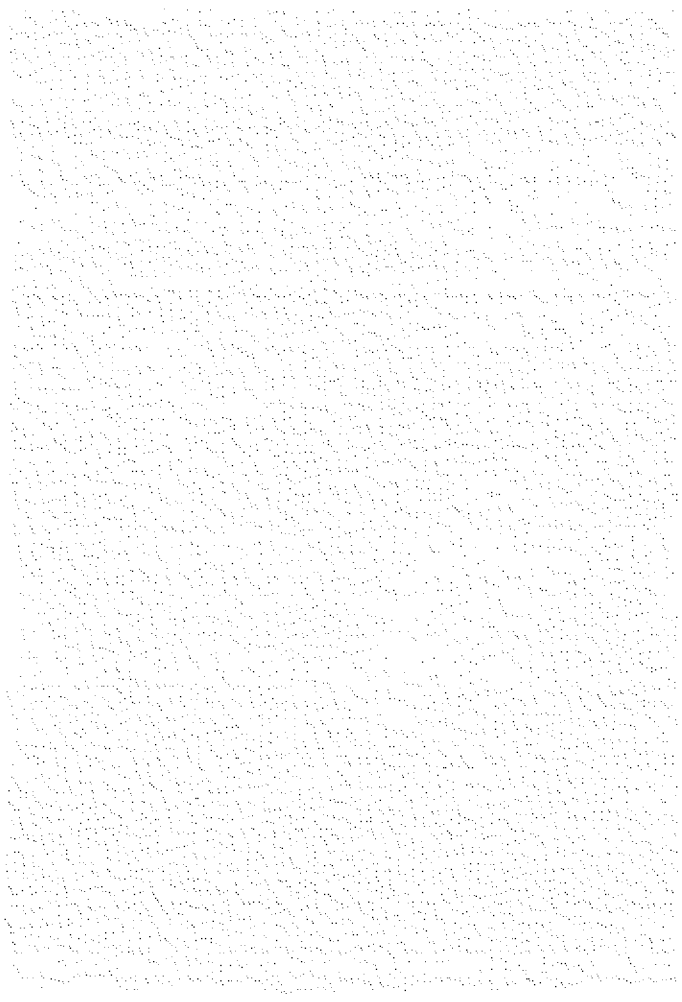

Fig. 18: Photomicrograph of the laminated anhydrite lithofacies. The lamination is defined by alternating anhydrite and marl layers. The clear white areas are halite cement. (Plane-polarized light. Field of view is 5.7 mm wide).

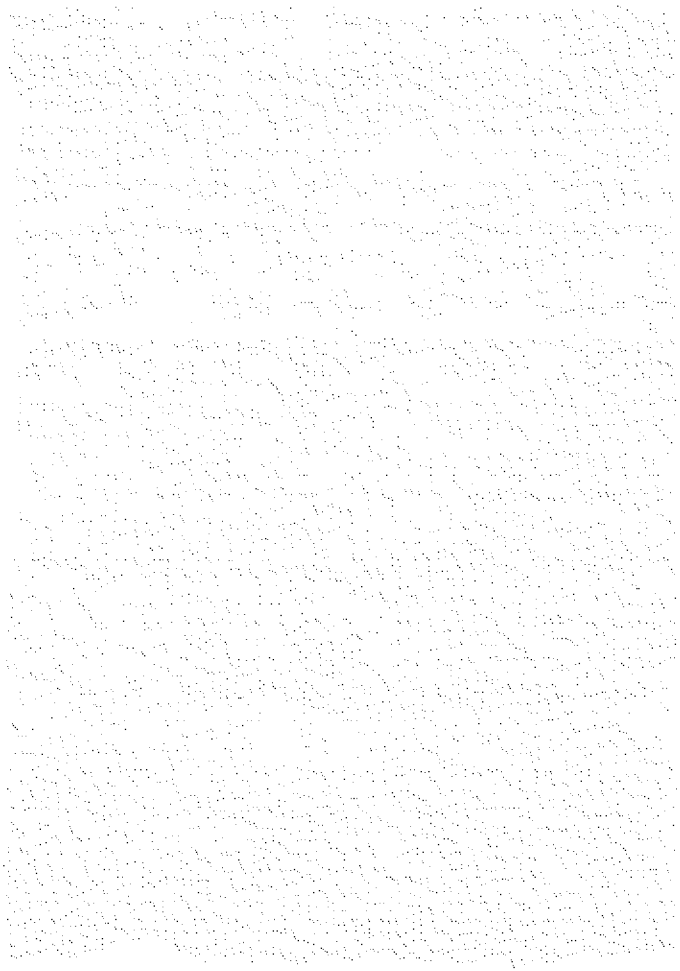

3.4.2.3 Massive Anhydrite

Massive anhydrite occurs in 1-10 cm thick layers (Fig. 19). In cut hand samples it is light gray to dark steel gray. The massive layers are sometimes disrupted by widely spaced, bedding parallel, clay-rich seams, which can be up to 5 mm thick. The anhydrite is composed of a dense network of prismatic, randomly oriented crystals (Fig. 20). Rarely, two prismatic anhydrite crystals have grown together to form V-shaped double crystals. The pore space between the anhydrite network is filled with clear halite cement or with dolomite rhombs. Dolomite can also replace anhydrite.

Minor amounts of dispersed pyrite occurs as subhedral to euhedral cubic crystals.

3.4.3 Halite

In the marl- and anhydrite-dominated S unit at Amelie II, halite forms one 7 cm thick massive layer in the lower part of the unit. However, it also has been observed in other samples, where it occurs either in layers (up to 2 cm thick; Fig. 21) with irregular boundaries or distributed in patches.

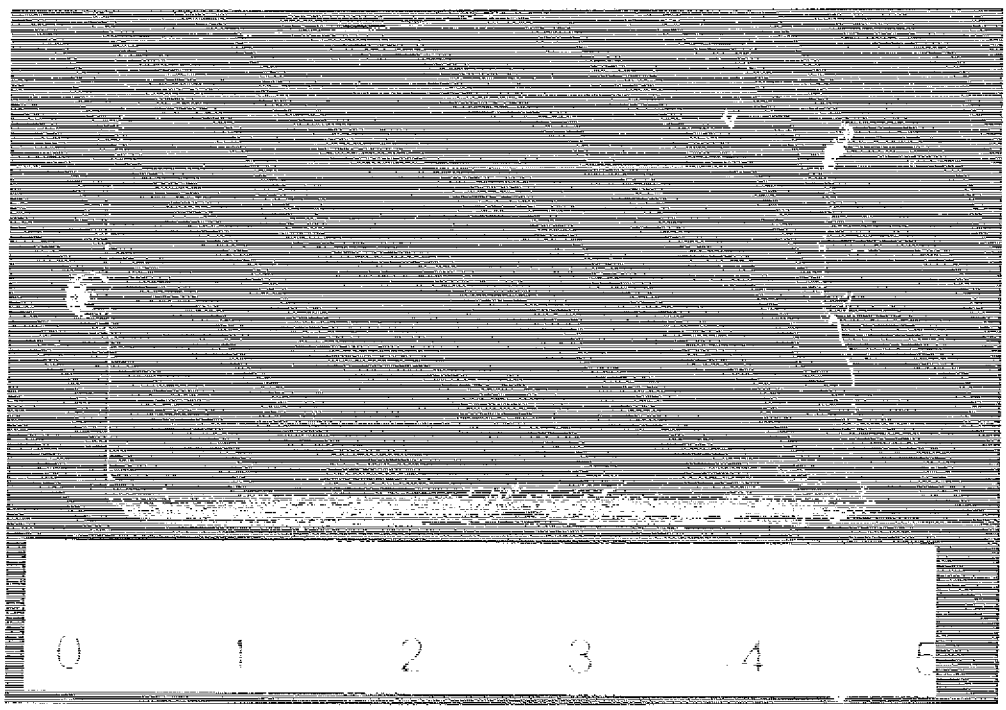

Fig. 19: Photograph of a slab taken from the massive anhydrite lithofacies. (Scale is in cm).

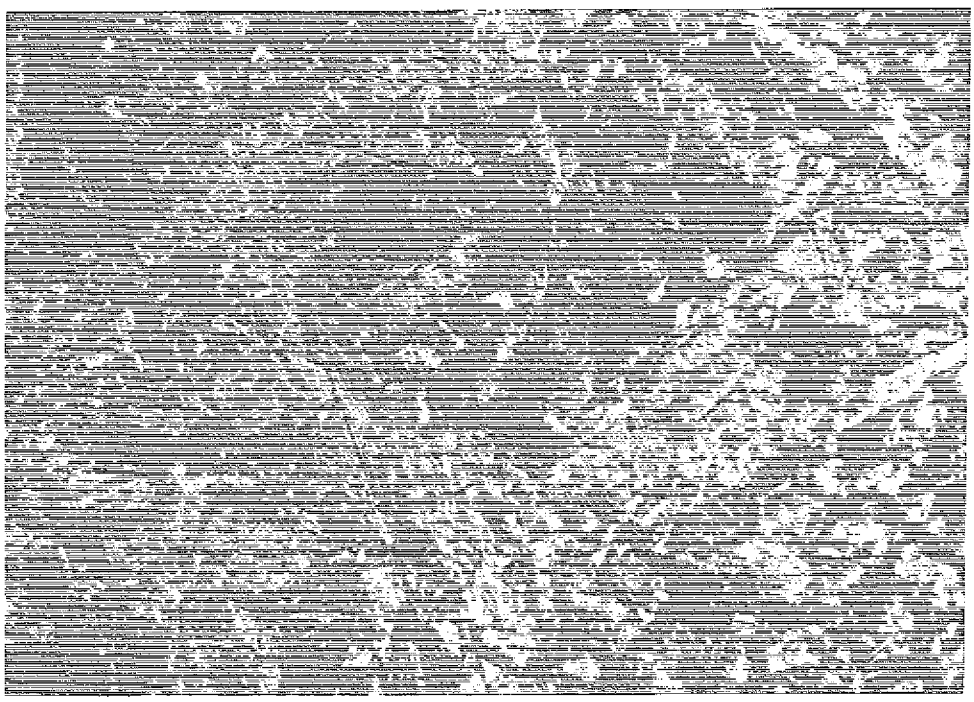

Fig. 20: Photomicrograph of the massive anhydrite lithofacies. Note the dense network of prismatic crystals. (Crossed polars. Field of view is 360 μm wide).

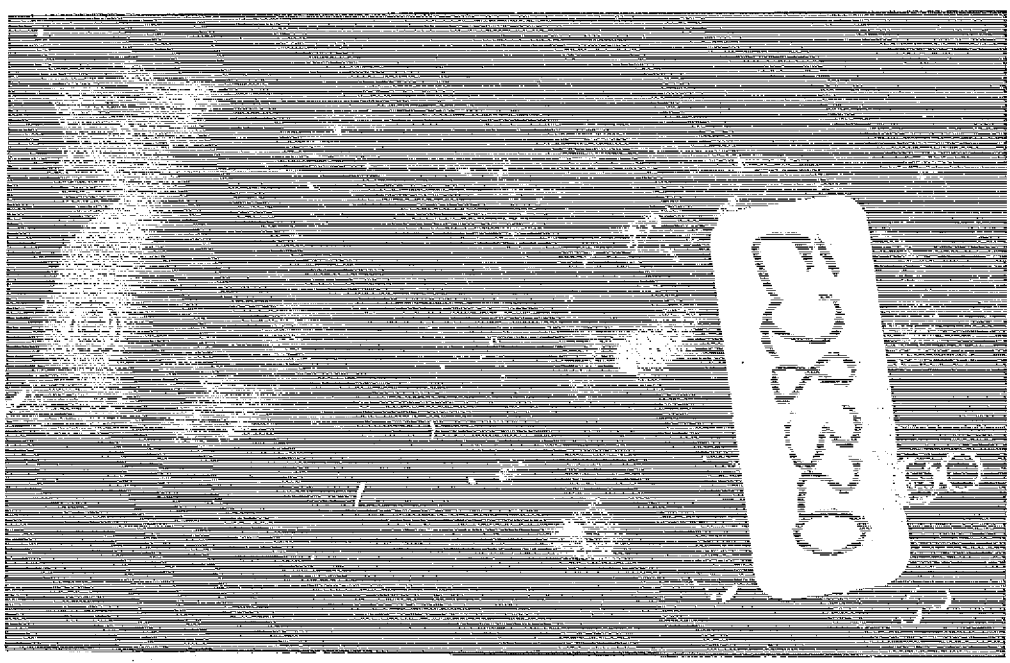

Fig. 21: Photograph of a halite layer. (Sample is 4.5 cm wide).

In general, the halite layers are commonly disrupted by impurity seams that are composed of clay minerals, anhydrite and pyrite. Halite occurs in three morphologies: 1) fluid inclusion-rich halite with preserved relic textures in the form of chevrons, cornets and hoppers (Fig. 22); 2) fluid inclusion-rich and clay-contaminated cement; and 3) clear cement. Anhydrite and carbonate minerals are also present. Anhydrite occurs as needles and rosettes that nucleate on impurity seams and penetrate neighbouring halite grains. Carbonate, probably dolomite or ankerite, forms single rhombohedral crystals dispersed throughout the halite layers.

The halite-dominated units S1 and MI are characterized by massive, thick halite beds (up to 8 m) that alternate with anhydrite and marl beds (up to 30 cm thick). The massive halite is composed of layers of dark, impurity- and clay-rich horizons and by clear, impurity-poor horizons.

Fig. 22: Photomicrograph of a hopper crystal. The morphology is outlined by fluid inclusions. (Plane-polarized light. Field of view is 8 mm wide).

3.5 FACIES MODEL

In order to understand the dynamics of sedimentation and the accumulation of organic matter in a paleodepositional environment, it is essential to develop a model that is internally consistent and can describe the mode of formation of each sedimentary facies. Each sediment type, as well as its organic matter, contains information that allows constraints to be placed on the paleoenvironmental conditions. The sedimentary structures and the chemistry of the evaporite minerals, especially within the evaporitic environments, allow the reconstruction of the physical conditions (e.g. water salinity, basin circulation, sediment accumulation rate, position of wave base, etc.) of a basin.

3.5.1 General Conditions for Evaporitic Sedimentation

In the following chapter possible modes of formation for each of the recognized facies are discussed and a genetic sequence is developed (i.e. facies model). To ensure a better understanding of this discussion a few remarks on the dynamics of evaporitic systems will be made first.

"Evaporite deposits can form in any region of the earth where evaporation exceeds rainfall. This can occur in continental settings, on the margin of a sea in the

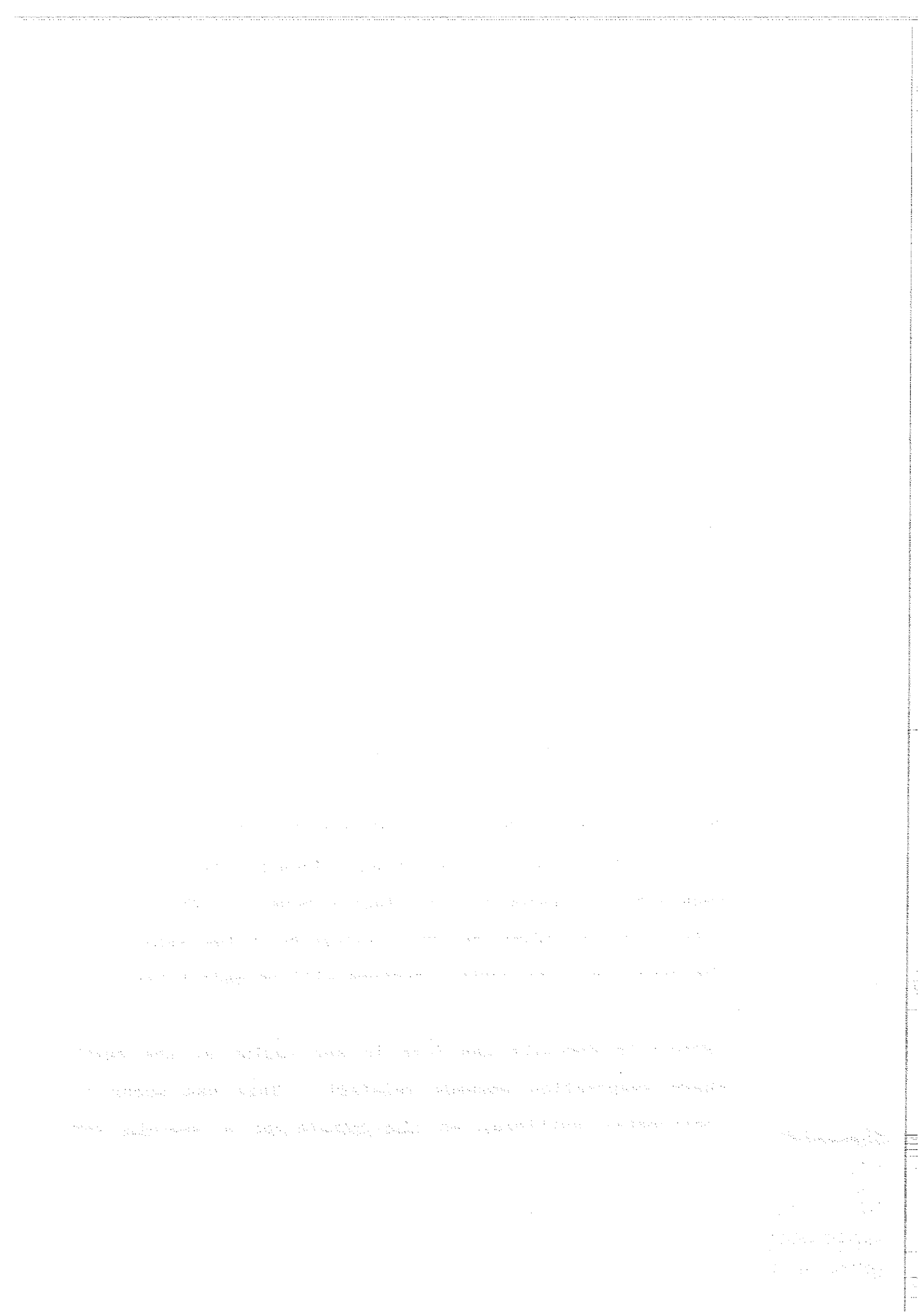

supratidal zone, or within a restricted water body, large or small" (Schreiber, 1986). Even though all of these systems have very different geographical settings, they have a number of characteristics in common. Evaporation causes a water body to lose H_2O and to become enriched with respect to dissolved ions such as Ca^{2+}, Mg^{2+}, Na^{+}, K^{+}, CO_3^{2-}, SO_4^{2-}, and Cl^{-}. As a function of progressive enrichment, the evaporite brine becomes saturated or even supersaturated with respect to various minerals, which as a consequence start to precipitate. The mineral sequence that will be precipitated from a brine depends on the relative abundance of dissolved ions (Eugster and Hardie, 1978).

In an evaporite sequence that resulted from the continuous evaporation of seawater, the first minerals to form are carbonates (aragonite, calcite and dolomite), followed by sulfates (dominantly gypsum and minor anhydrite), chlorites (mainly halite), and potassic salts of various compositions. This complete precipitation cycle occurs only in either closed systems that do not receive a continuous influx of water from outside the system or in open systems when the water loss caused by evaporation exceeds by far the inflow of water into the system. Natural systems, however, rarely show a complete evaporation cycle and may only reach, for example, sulfate saturation before the brine receives renewed influx of

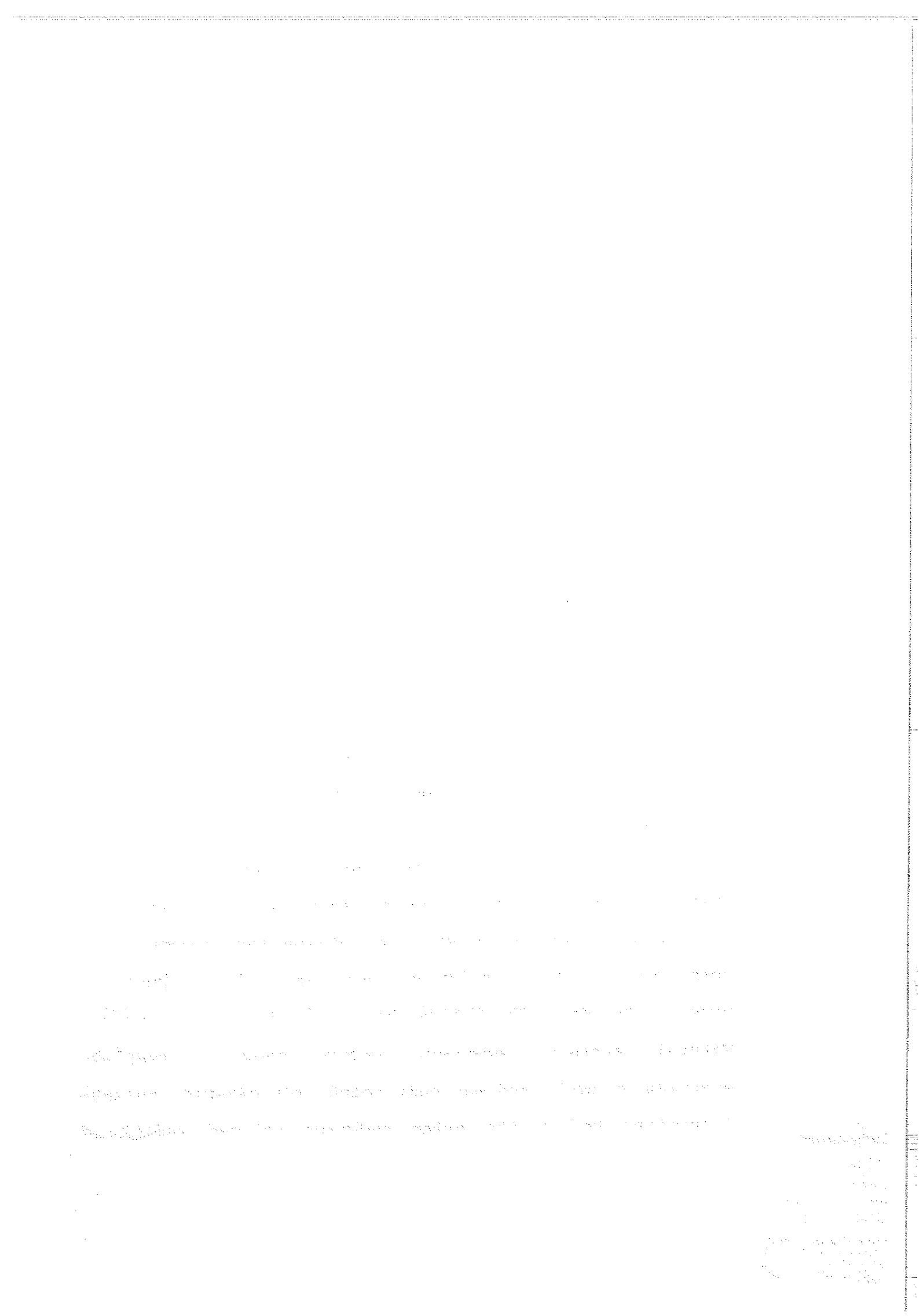

water. However, the idealized mineral precipitation sequence provides a guideline to the interpretation of the sedimentary facies and their mineralogical composition in both modern and ancient evaporite environments. The interpretation of ancient evaporite environments is further complicated by mechanical, mineralogical and chemical changes occurring during the burial of a rock sequence with time.

3.5.2 Setting

The deposition of the Eocene/Oligocene evaporite sequence of the Mulhouse Basin took place in a narrow rift valley (approximately 30 km wide) that apparently had sporadic access to the Tethys Ocean to the south (Ziegler, 1988). The rift system was episodically flooded with oceanic water during its depositional history (Blanc-Valleron, 1991). Further water input may have been received via fluvial systems as indicated by frequent conglomeratic horizons in the sediments deposited near the rift shoulders or from hydrothermal influx along the fault systems (Hardie, 1990; Lowenstein and Spencer, 1990). The Mulhouse Basin was most likely occupied by a standing water body during the deposition of the lower part of the Salt IV series of the lower Oligocene. Evaporation exceeded renewed water influx and resulted in a shrinking water body and a "bulls-eye" depositional pattern of the

resulting evaporite sediments (Fig. 4). The geographic setting provides a framework for the interpretation of the sedimentary facies of the S1 to CI unit.

3.5.3 Facies Interpretation

The idealized facies model presented in Fig. 23 summarizes how the sedimentary facies identified in the S1 to MI unit are related to each other and which transformations they undergo during the ensuing compaction and diagenesis. Post-depositional changes include the compaction-induced dewatering of clay-rich units and loss of crystal-bound water, especially during the gypsum/anhydrite phase transition. Both processes lead to a substantial volume reduction in the original sediment. It should be noted that due to these severe diagenetic overprints, the sedimentary facies that we observe today appear to be only fragmental relics of the original sedimentary structures and their mineralogical compositions.

3.5.3.1 Deposition of Marls

The sedimentary facies are discussed in the sequential order in which they may have formed in the Mulhouse Basin during the evaporation cycle. The first facies to form at the lowest salinities is marl. The most pronounced

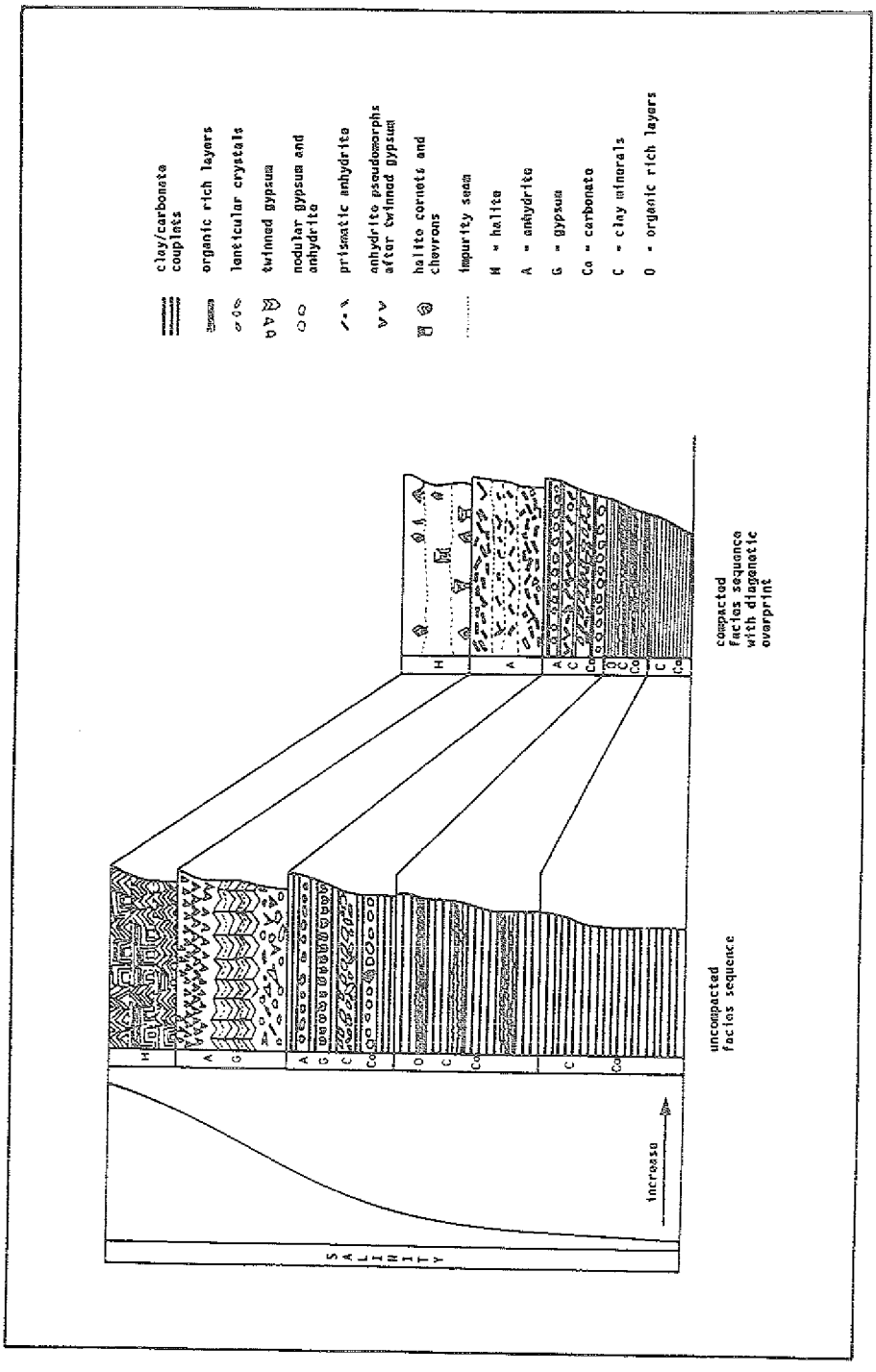

Fig. 23: Idealized facies model for the lithofacies of the S unit of the Mulhouse Basin.

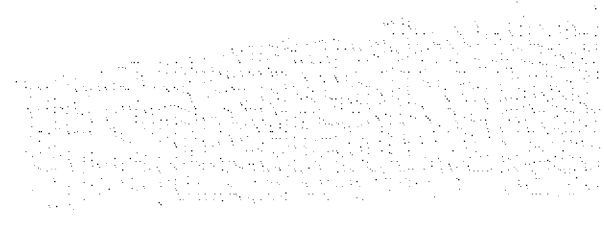

characteristic of these marls is the presence of millimeter-scale lamination and the high total organic carbon (TOC) content. It is generally accepted (Kelts and Hsü, 1978; Eugster, 1980) that the formation and preservation of millimeter-scale laminae, characteristic for so many lacustrine carbonates and oil shales requires special conditions (Eugster, 1985): 1) episodically differentiated particle influx, 2) absence of grazers and burrowers, 3) lack of strong bottom currents, and 4) protection from clastic input. Saline lakes normally are oxygen deficient, with chemical stratification sometimes enhanced by thermal stratification. Consequently, processes of post-depositional destruction of organic matter, such as burrowing and grazing, are not effective, and thus much of the organic matter that has escaped destruction prior to and during sedimentation can be expected to be preserved in the sediment column (Eugster, 1985).

Eugster (1980) presents two models that can cause millimeter scale laminae in lacustrine deposits: the "Lake Zürich" and "Dead Sea" models. In the "Lake Zürich model" (Bradley, 1929; Kelts and Hsü, 1978), annual varves of carbonate/clay couplets form as a result of different climatic conditions during summer and winter. Starting in spring and extending throughout the summer, the warming of the surface water leads to supersaturation with respect to

$CaCO_3$. Supersaturation is enhanced by algal blooms that deplete CO_2. As a consequence, carbonate starts to precipitate. During fall and winter, dead algal material that settles to the bottom and clastic influx caused by winter rains form a dark lamina. The result is an annual carbonate/clay couplet.

Similar couplets have been noted in Dead Sea deposits (Neev and Emery, 1967). Ca^{2+} and HCO_3^- are transported via the Jordan River into the Dead Sea. In response to evaporation, the surface waters become saturated with respect to $CaCO_3$ and a constant rain of carbonate particles develops. The dark, clay-rich laminae are caused by episodic floods bringing in detrital material.

The marls of the Mulhouse Basin are very similar to marls described from Lake Zürich and other lacustrine varved sediments (Anderson and Dean, 1988). Both marls display a distinct lamination caused by light, micrite-rich laminae that alternate with dark, siliciclastic detritus-rich and organic matter-rich laminae (Fig. 24). The presence of this microfacies association, typical for an annual lake cycle in a climate with distinctly different climatic conditions during the spring/summer and autumn/winter seasons, suggests that the couplets of the marls of the Mulhouse Basin can be interpreted as annual

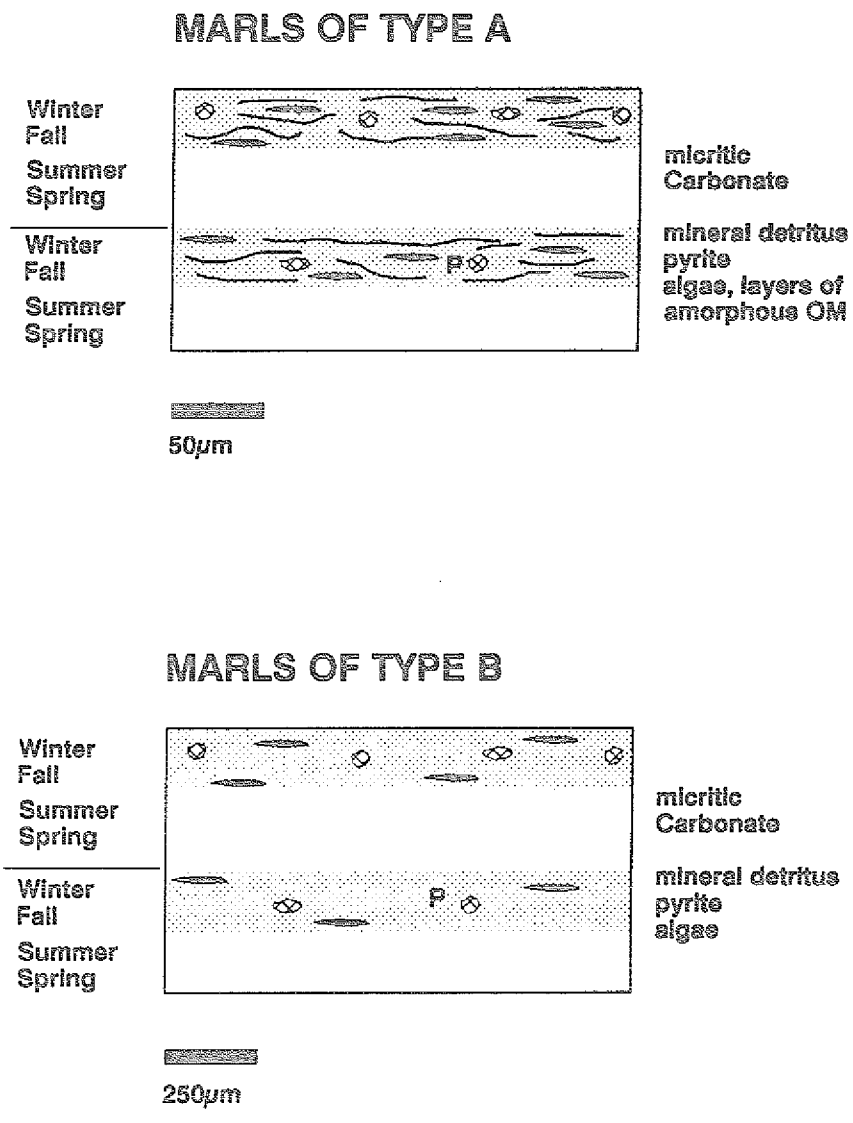

Fig. 24: Interpretation of the laminae of the marls of type A and type B as annual deposits (based on observations given in Figure 12; P = pyrite).

deposits. Following the Lake Zürich model, the carbonate-dominated zones represent spring/summer deposits, which were mainly caused by the removal of CO_2 from the water by enhanced biological activity. The dark laminae, on the other hand, are autumn/winter deposits characterized by the accumulation of dead algal or microbial debris and clastic matter washed into the lake by winter rains (Fig. 24). Further support for this interpretation stems from palynological studies. Schuler (1988) demonstrated that during the deposition of the S1 to CI unit, Mediterranean-type climate conditions prevailed in the lower Rhine Graben area. A Mediterranean climate is characterized by hot summers and rainy winters, and hence provides ideal conditions for the formation of laminated sediments.

Not all marl microfacies in the Mulhouse Basin are the result of an annual deposition cycle. The monotonous deposition of carbonate/clay couplets is sporadically disrupted by formanifera-rich layers. Even though most foraminifera only thrive under normal marine conditions, some species are also adapted to hypersaline* environments (Brasier, 1980). However, it appears unlikely that the occasional layers of foraminiferal tests are caused by the sudden death of a foraminifera assemblage that lived in the hypersaline waters of the Mulhouse Basin. Otherwise a

*Hypersaline: Salinity substantially greater than that of normal seawater.

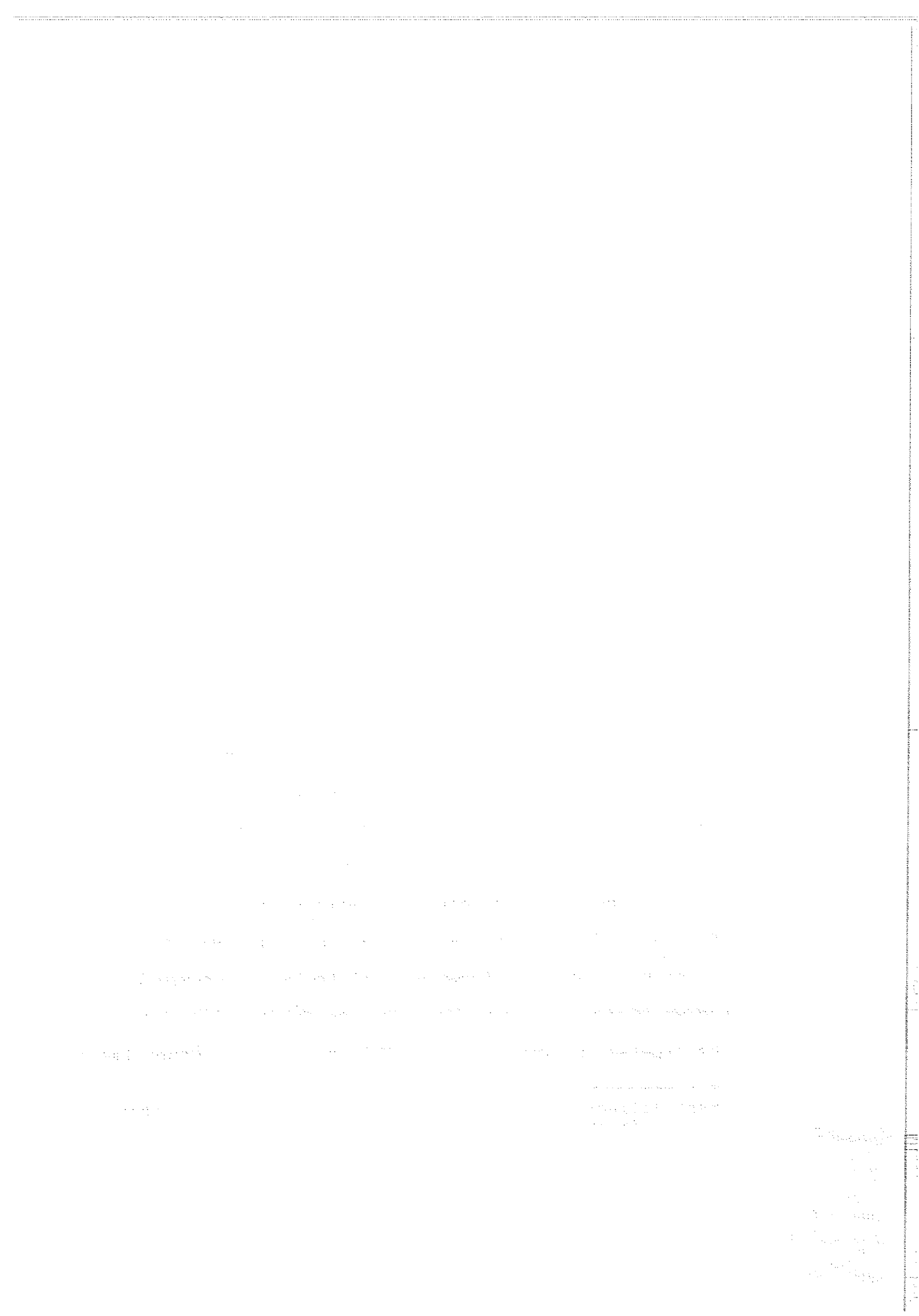

more even distribution of foraminifera tests in the sedimentary section should be expected. It seems more likely that the layers represent sudden flood or storm-like events, when waters from the Tethys ocean swept into the hypersaline Mulhouse Basin.

3.5.3.2 Deposition of Anhydrite

If a brine continues to become concentrated, and hence salinity increases, calcium sulfates start to precipitate. The calcium sulfates can precipitate in three settings: 1) within the sediment in the pore space from saturated interstitial brine, 2) at the sediment/water interface from the surface brine, and 3) in the water column. The facies that form from the interstitial brine are nodular and lenticular gypsum and/or anhydrite. The most common interpretation for nodular anhydrite is that it forms in supratidal sediments of modern sabkhas from mixed water brines of marine and continental origin (Butler et al. 1982; Kendall and Warren, 1988). However the S unit shows no characteristics of supratidal sedimentation such as mud cracks, erosional surfaces, and intra-formational breccias. It is, therefore, believed that the nodular anhydrite facies formed later from interstitial brines in the previously deposited marls during a stage when the surface brine was saturated or even super-saturated with respect to gypsum.

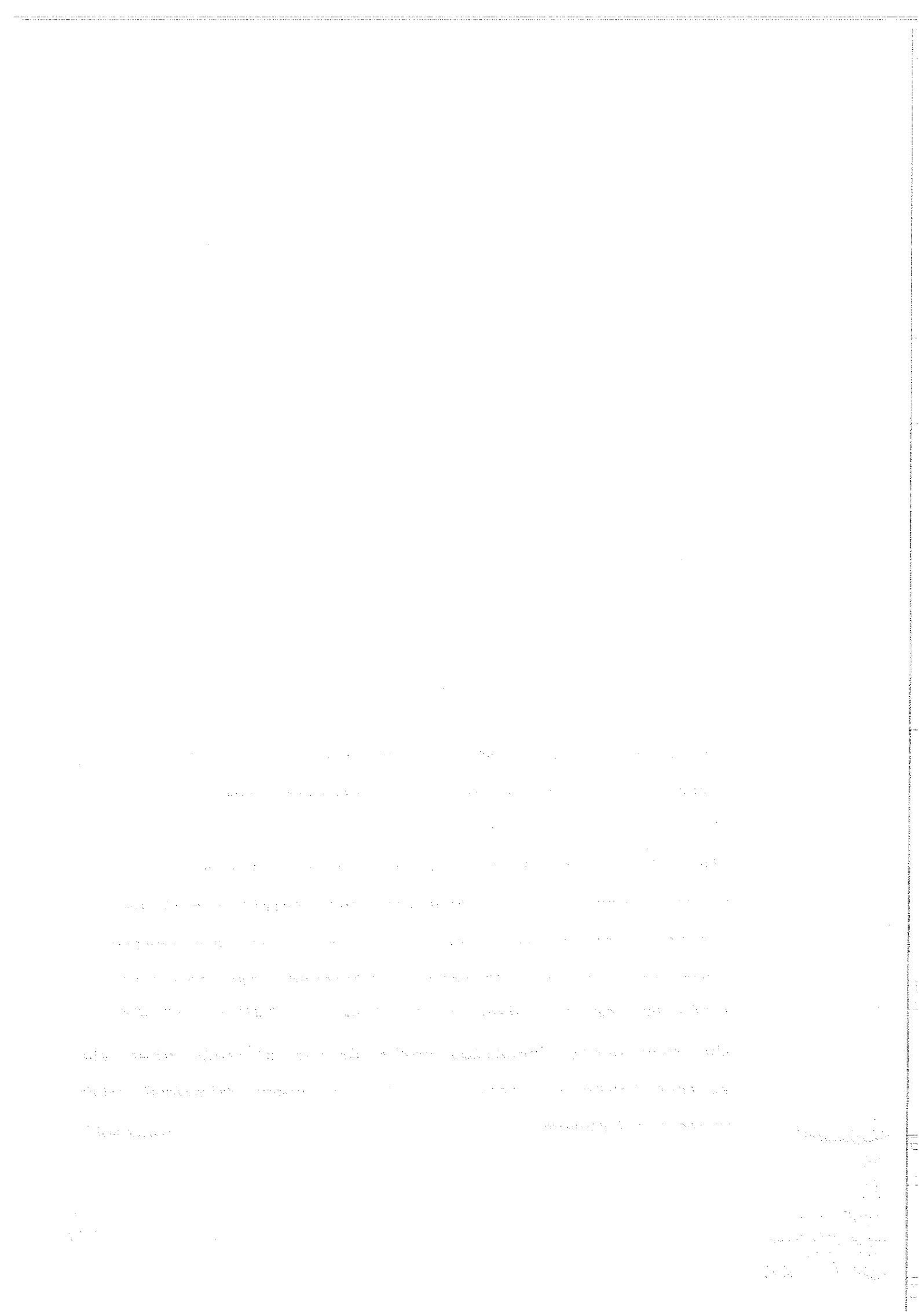

The sulfate nodules grew displacively in the marl matrix and deformed the surrounding sediment. Some of the nodules formed as gypsum; others may have formed as anhydrite. The original gypsum nodules usually can be recognized in thin section because they are composed of what is now polycrystalline lenticular anhydrite. Lenticular crystal morphologies are not known from primary anhydrite but would have mixed lenticular and barrel-shaped forms (see Shearman, 1978, for variants). Purely lenticular morphologies are typical for displacive gypsum that forms in the presence of trace amounts of plant-derived humic acids and have been grown in algal mats of the Trucial Coast under experimental conditions (Cody and Cody, 1988).

Therefore, it appears that organic matter may have played a key role in the formation of the lenticular anhydrite morphologies. The lenticular anhydrite aggregates contain little or no visible organic matter, however, the marl matrix surrounding the lenticular aggregates is usually rich in liptodetrinite layers. Most of the organic matter content of this facies is contained in the marl matrix. The localized concentration of organic acid at sufficiently high levels in these relatively organic-rich layers, with TOC values up to 1.8%, may have induced the growth of lenticular gypsum within this very special

microenvironment. Generally, most of the rock volume in this facies is occupied by anhydrite having a low organic matter content. In marls with low TOC content, organic acid concentrations were apparently not sufficient to result in lenticular gypsum growth.

The lenticular anhydrite facies was also deposited as gypsum and subsequently diagenetically altered to anhydrite. Lenticular gypsum has been noted in algal mats in modern salinas, where it forms nodules, discontinuous horizons and continuous thin layers (Orti Cabo et al., 1984; personal observations). Similar bed forms have also been noted in the S unit.

The facies that are derived from sulfate deposition at or near the sediment/water interface are present as laminated and massive anhydrite. Subaqueous anhydrite is not known to form as a primary phase in modern evaporite environments. Crusts of selenitic gypsum with a massive or laminated character, however, are known from both modern and ancient evaporites (Orti Cabo, 1984; Warren, 1982; Schreiber et al., 1976; Schreiber, 1988). Relic morphologies such as V-shaped twins, simple prismatic crystals, and lenticular crystal outlines have been observed, particularly in the laminated anhydrite facies. They have been described in primary modern and ancient gypsum (Orti Cabo and Shearman, 1977) and here the

anhydrite seems to be pseudomorphous after gypsum. The texture of the massive anhydrite has obliterated most of the primary depositional features. Only in a few cases are V-shaped twinned crystal pseudomorphs present. Most of the massive anhydrite facies is composed of small prismatic crystals, which have been interpreted by Shearman (1985) as syndepositional alterations of primary gypsum.

3.5.3.3 Halite

Halite precipitation is the stage with the highest salinity within the evaporite cycle that can be observed in the S unit. Halite rocks of the S unit also have suffered a strong diagenetic overprint. However, some relics of primary textures such as chevrons, cornets, and halite hopper crystals, as well as thin anhydrite and clay-mineral-lined solution seams, give some indication of the conditions under which the halite was deposited. Bottom-grown halite crusts either grew from bottom-nucleated crystals or on halite rafts or cubes that formed at the air/brine interface and settled through the water column. All of these features have been recognized in modern coastal salinas and salt-pan evaporites (Shearman, 1970; Orti Cabo et al., 1984; Lowenstein and Hardie, 1985). In addition, synsedimentary and diagenetic alterations such as clear halite cement and fluid

inclusion-rich halite cement have been reported from these settings (Shearman, 1970; Casas and Lowenstein, 1989).

3.6 SEDIMENTATION RATES

Sedimentation rates are known to vary considerably in evaporite depositional environments (Schreiber, 1986). Chemical sediments usually accumulate with greater rapidity than associated clastic and biogenic sediments. Sedimentation rates for subaqueously deposited sulfates (usually gypsum) from solar ponds have been reported to range from $1 \times 10^2 - 40 \times 10^2$ cm/ky. Halite deposits from the same depositional environment can even reach sedimentation rates of $10 \times 10^2 - 100 \times 10^2$ cm/ky (Schreiber and Hsü, 1980). All of these rates are optimal for a natural environment and may not be reached in other depositional settings.

Average depositional rates for the sulfate and halite deposits of the Mediterranean Messinian have been determined to be between $3 \times 10^2 - 4 \times 10^2$ cm/ky (Schreiber, 1986). In contrast, sedimentation rates of clastic deposits intercalated with sulfates and halites are often lower by more than one order of magnitude. Kühn and Roth (1979) reported average sedimentation rates for the sediments of reported S1 to MI interval of the Buggingen subbasin of the Mulhouse Basin of 24.4 cm/ky for marls, 156.2 cm/ky for anhydrites and 3030 cm/ky for halite. The magnitude of these sedimentation rates is in good agreement with other evaporite deposits (Schreiber,

1986). Unfortunately, Kühn and Roth (1979) give only a very brief description of how these rates were measured, which is insufficient to reconstruct their methods of sedimentation rate calculation.

A careful study of the sediments in the S1 to MI interval at Amelie II led to the conclusion that only the carbonate/clay and organic matter couplets of the marl beds can be interpreted as annual deposits with a satisfactory degree of confidence. They clearly display characteristics that are also observed in annual deposits of Recent depositional environments (Fig. 24; see previous discussion). Sedimentation rates of marls were estimated by counting carbonate/clay couplets on twenty-three 1-4 cm wide polished slabs and thin sections, and then calculating average sedimentation rates for each sample. The thus-determined sedimentation rates vary from 6-40 cm/ky (Fig. 25). The sedimentation rate of the marls is highest in the halite-dominated stratigraphic intervals (>30 cm/ky) and lowest in the upper part of the marl and anhydrite-rich S unit (<10 cm/ky). Marls that have been classified as type A display generally low (<15 cm/ky) sedimentation rates, while marls of type B are characterized by sedimentation rates greater than 15 cm/ky.

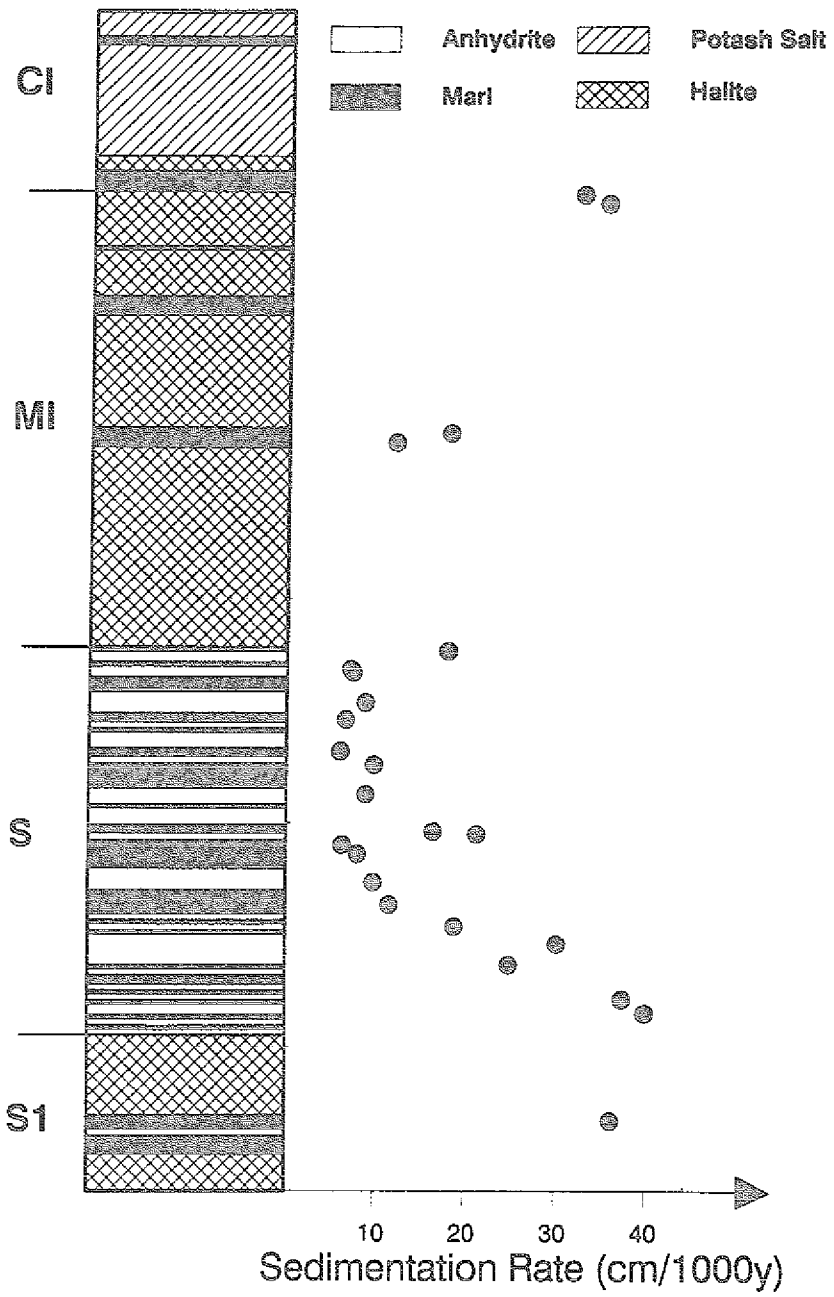

Fig. 25: Sedimentation rates of the marl lithofacies at Amelie II in the stratigraphy interval S1 to CI. The thickness of the depicted interval is 15.5 m.

An improved estimate of the time span represented by the sediments of the S unit can be made based on the measured marl sedimentation rates (Fig. 25). For this purpose, the S unit is divided into a lower section (2.85 m thick) and an upper section (2.78 m thick). Estimated average sedimentation rates are 24 cm/ky for the lower section and 8 cm/ky for the upper section, respectively. The duration of the marl deposition is calculated based on the actual portion of the lithologic column of the S unit represented by marls (163.3 cm in the lower section and 115.8 cm in the upper section) and yields a total deposition time of approximately 21,000 years. The time required for the deposition of the anhydrite and halite beds of the S unit is calculated based on literature data for gypsum and halite sedimentation rates observed in modern evaporite environments (Table 1). The thus determined total time span for the deposition of the sediments of the S unit is 21,065 - 23,598 years.

These results can be used to improve modeling of the evaporite depositional system of the Mulhouse Basin. They also show that the 8248 year time estimate of Blanc-Valleron et al. (1989) for the S unit based on average sedimentation rates published by Kühn and Roth (1979) most likely underestimates the actual duration of deposition.

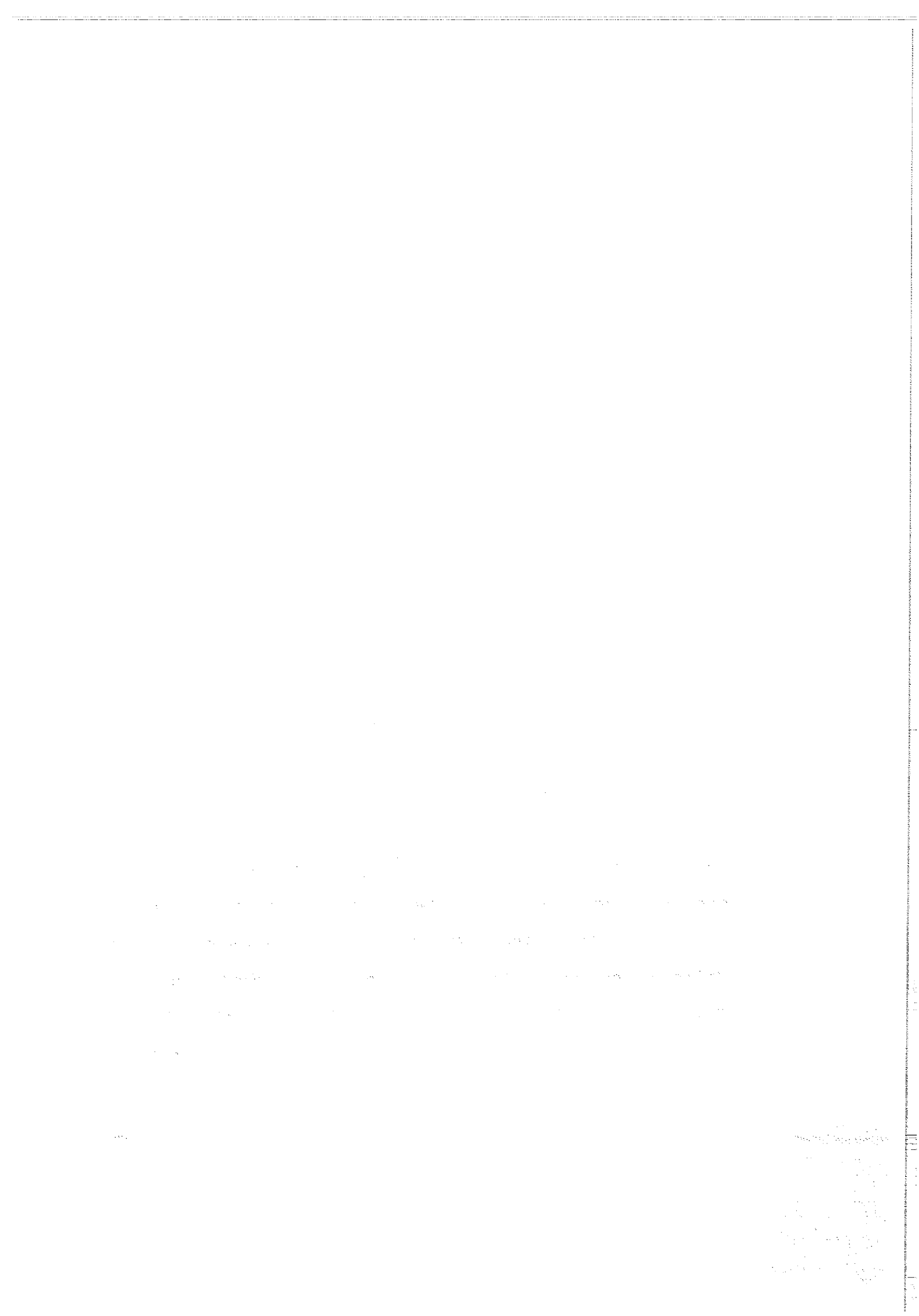

LITHOLOGY	PERCENT OF LITHOLOGY	SEDIMENTATION RATE	TIME FOR DEPOSITION
marl	50%	7-40cm/ky	21,000y
massive anhydrite	23%	100-4,000cm/ky[1)]	33-1,311y
laminated anhydrite	22%	100-4,000cm/ky[1)]	32-1,276y
halite	2%	1,000-10,000cm/ky[1)]	1-11y
lenticular anhydrite	3%	no data	no data
TOTAL	100%		21,065-23,599y

[1)]sedimentation rates for modern evaporite environments (Schreiber&Hsü 1980)

Table 1: Estimate of the time span required for the deposition of the S unit at Amelie. For details see text.

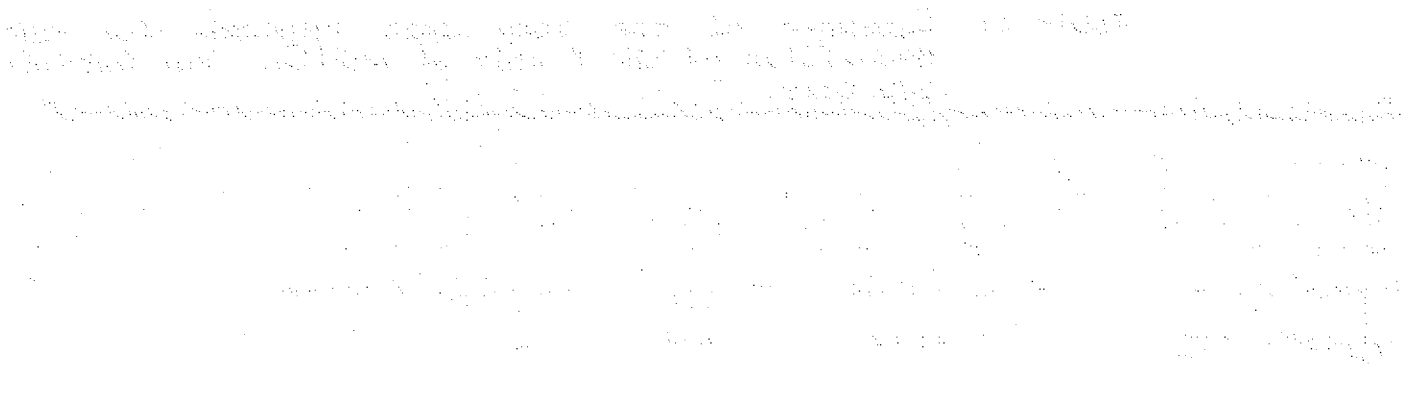

The cause of the variation in sedimentation rates is not known, but may lie in climatic variations, tectonic changes or sea level variations. The results nevertheless show that numerical modeling of rhythmic sedimentation patterns of the Mulhouse Basin evaporite deposits based on average marl sedimentation rates as performed by Blanc-Valleron et al. (1989, 1991) and Carpentier et al. (1991) must be taken with at least a grain of salt, and may render unreliable results.

3.7 ORGANIC MATTER CONTENT OF THE S-INTERVAL

3.7.1 Introduction

The organic content of a lithological unit may be characterized by the abundance and spatial distribution of the organic matter in the source rock, the quality of the kerogens, and the composition of the associated bitumens. The quantity and spatial distribution of the organic matter of a sediment is governed by the physical conditions during its deposition such as nutrient influx (which regulates productivity), sedimentation rate, and preservation conditions. The character of the organic matter is controlled by the type of organisms that contribute to the formation of the kerogen and the degree of oxidation that the organic matter is subjected to prior to and after deposition. The bitumen content (soluble organic matter) of ancient sediments is a mixture of lipids resistant to the formation of larger biomolecules (Tegelaar et al., 1989) and thermal decomposition products of the kerogen. In particular, immature bitumens contain high proportions of compounds inherited from living organisms (with minor chemical alteration), which are considered chemical fossils (synonymous with the term biomarkers; Tissot and Welte, 1984). Experience has shown that a plethora of information regarding the physical, chemical, and biological conditions can be collected by

the study of fossil organic matter. Hence, the information obtained by the careful study of the organic matter of a lithological unit, in conjunction with the understanding of the sedimentological framework of the unit, allows a detailed reconstruction of the paleodepositional environment.

3.7.2 Abundance and Distribution

Previous workers (Blanc-Valleron, 1986; Blanc-Valleron et al., 1990, 1991) noted that the sediments of the lower part of the Salt IV zone of the Mulhouse Basin contain significant amounts of organic matter. Most of the organic material is present in marl and anhydrite dominated units. Halite and potash salt-rich intervals contain relatively small amounts of organic matter. Organic carbon measurements on samples collected in the mines Amelie II, Ungersheim, and Berrwiller showed that the mass of the organic matter is concentrated in marl beds, which contain between 0.47 and 4.59% organic carbon. However, intervals with more than 7% organic carbon content have been reported from marls of the Max core (Blanc-Valleron et al., 1991). The remaining lithofacies generally display lower TOC contents. At the sites Amelie II, Ungersheim, and Berrwiller, the lenticular and nodular anhydrite vary between 0.55 and 1.84% TOC. Laminated anhydrite (0.14 to 0.78% TOC), massive anhydrites (0.08%

to 0.31% TOC), and halites (0.01 to 0.25% TOC) contain even less organic carbon.

3.7.3 Quality of Organic Matter

Organic matter in evaporite sequences stems from two sources: 1) autochthonous material derived from algae and microbes, and 2) allochthonous material carried in by wind and water (residues of higher land plants and recycled organic matter from older sediments).

The term "kerogen" can be defined as the solid organic matter content of a sedimentary rock that is neither soluble in aqueous alkaline solutions nor in common organic solvents (Tissot and Welte, 1984). The potential of kerogen to generate hydrocarbons upon burial depends on its relative proportions of reactive and inert groups. Reactive kerogen can be further subdivided into a labile portion, which is transformed into oil in the temperature realm between 100-150°C, and a refractory portion, which is transformed at somewhat higher temperatures into gas (Mackenzie and Quigley, 1988). The inert part of the kerogen is transformed at very high temperatures and pressures into graphite.

Kerogens derived from algae, bacteria, and some parts of land plants (e.g. spores, cuticles) are comprised chiefly

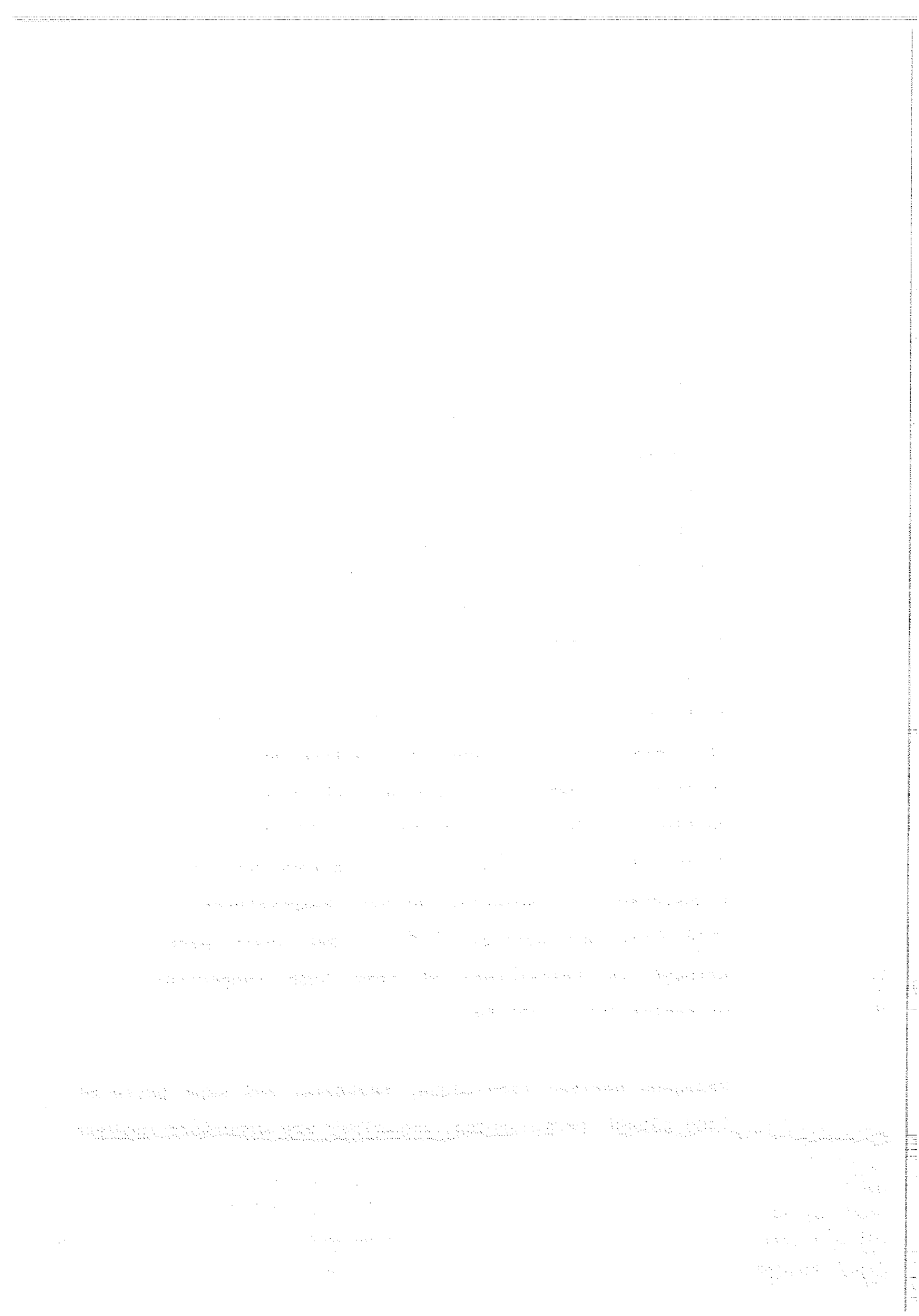

of labile kerogen with small amounts of refractory and inert kerogen. Kerogen derived exclusively from vascular plants is a mixture of refractory and inert kerogen. Environments with a high input of algal- and bacterial-derived organic matter are likely to contain oil-prone source rocks.

One way to assess the quality of kerogen is to determine microscopically the proportions of the visual remains of algae, bacteria, wood fragments and charcoal. Macerals are visually identifiable kerogen particles and are commonly characterized by grouping them according to their biological precursor structures into 1) liptinites (algae, resin, globules, cuticles, spores, etc.), 2) vitrinites (woody fragments with or without plant texture), and 3) inertinites (charcoal-like fragments) (Stach et al., 1982).

Another way to determine the quality of kerogens is by chemical methods. In addition to hydrogen and carbon, organic matter also contains nitrogen, sulfur, and oxygen atoms. The quality of a kerogen, and hence its potential to generate hydrocarbons, can be assessed by elemental composition, i.e., by its atomic hydrogen/carbon and oxygen/carbon ratios (Tissot et al., 1974). Kerogens with high hydrogen/carbon ratios and low oxygen/carbon ratios yield the highest amounts of oil upon maturation. Three

major types of kerogens can be defined based on their hydrogen/carbon and oxygen/carbon ratios (Tissot and Welte, 1984):

Type I refers to a kerogen with high initial hydrogen/carbon (approximately 1.5 or more) and a low initial oxygen/carbon ratio (generally less than 0.1). Kerogens of type I give a high yield of oil. They stem from either a selective accumulation of algal material or a severe biodegradation of organic matter (microbial sources).

Type II kerogen with relatively high hydrogen/carbon and low oxygen/carbon ratios is particularly abundant in many marine petroleum source rocks. Kerogens of type II are usually related to marine sediments with autochthonous organic matter derived from a mixture of phytoplankton, zooplankton and microorganisms (bacteria) deposited in a reducing environment.

Type III refers to a kerogen with relatively low initial hydrogen/carbon and high oxygen/carbon ratios (as high as 0.2 or 0.3). It is essentially derived from continental plants and contains much vegetal debris.

Oil and gas prone kerogens are of type I and II; type III kerogens yield some oil, but predominantly gas. As noted above, the autochthonous production of organic matter in

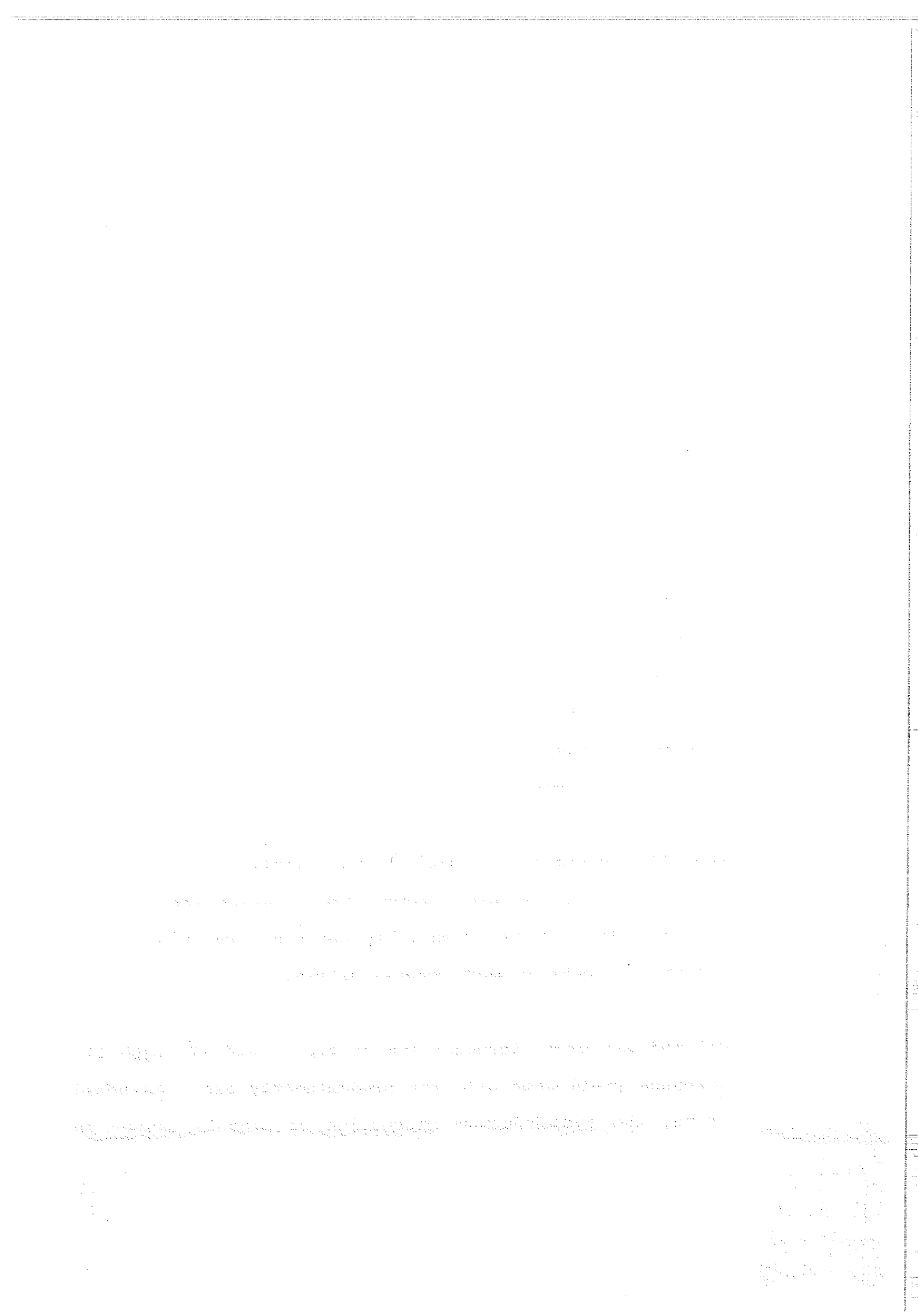

evaporitic systems stems from algal and bacterial sources. These types of kerogens have been reported from a number of evaporite source rocks (e.g. Palmer and Zumberge, 1981, Connan et al., 1986, Mello et al., 1988b). However, kerogens of type III can also be expected in some evaporite depositional environments. In ancient evaporite systems where the paleogeographic reconstruction indicates the presence of a land mass in close vicinity (narrow rift valleys, intracontinental lakes, playas, etc.), type III kerogens are generally to be expected. Type III kerogens can also result from partial oxidation of organic matter in the water column or the top portion of sediments. Such conditions can prevail during periods of continental water influx in any evaporite system.

3.7.4 Organic Petrology

Organic petrology is used to determine the visual remains of organisms that contributed to the formation of kerogen and to determine the quality of the kerogens.

3.7.4.1 Maceral Content

The organic matter content of the S unit is dominated by liptinites (alginite + liptodetrinite) and contains only minor amounts of vitrinites. Inertinite is nearly always absent.

3.7.4.2 Marls

The organic material in the marls of sedimentary facies type A contains on average 41.1% alginite, 54.6% liptodetrinite and 4.3% vitrinite. The algal bodies are flattened parallel to bedding. Individual algae vary between 10 to more than 50 μm in length and only a few microns in width. In addition, layers of amorphous, brightly-fluorescing liptodetrinites (groundmass) are common (Fig. 26). These bedding parallel layers are continuous over several centimeters. The thicknesses vary considerably. In some samples, single layers are only a few microns thick; in others samples, multiple, stacked layers of amorphous fluorescing groundmass can exceed 100 μm in thickness (Fig. 27). Vitrinites are sparse in marls of type A. Individual vitrinite particles vary from less than 10 μm to 50 μm in diameter. Small particles (less than 20 μm) are the most common.

In marls of type B (TOC <2%), layers of amorphous, fluorescent groundmass are completely absent (Fig. 28). Instead, their original organic matter consists of liptinites (alginite (Fig. 29) and liptodetrinite) and generally more than 10% vitrinite. Inertinite occurs

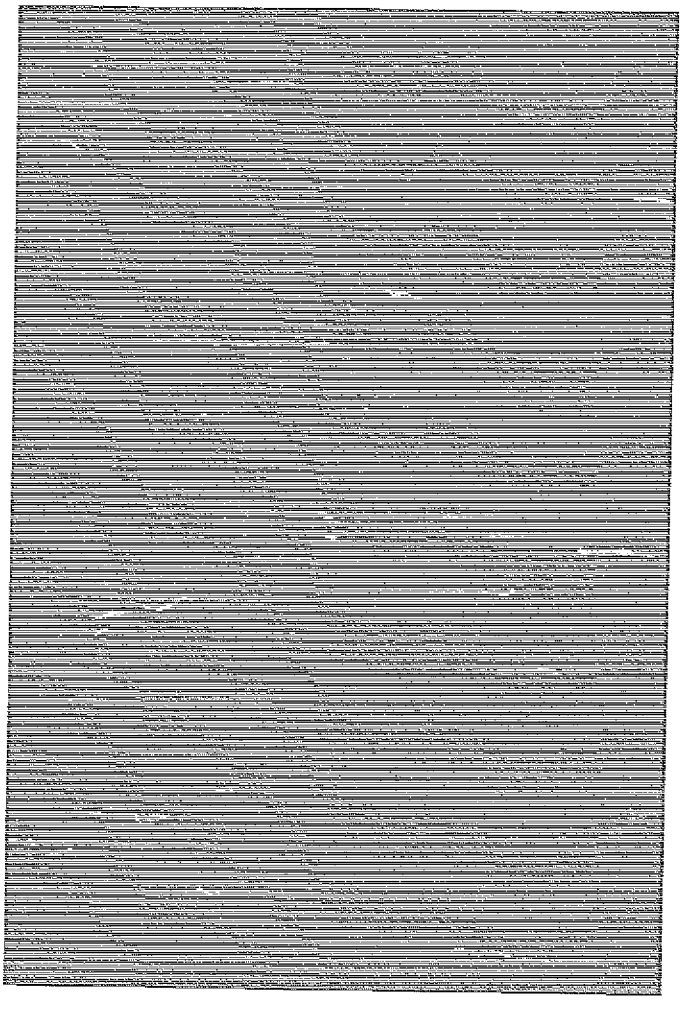

Fig. 26: Photomicrograph of a marl of type A under blue light. Note the brightly fluorescing algal bodies and layers of the amorphous groundmass. (Field of view is 360 μm wide).

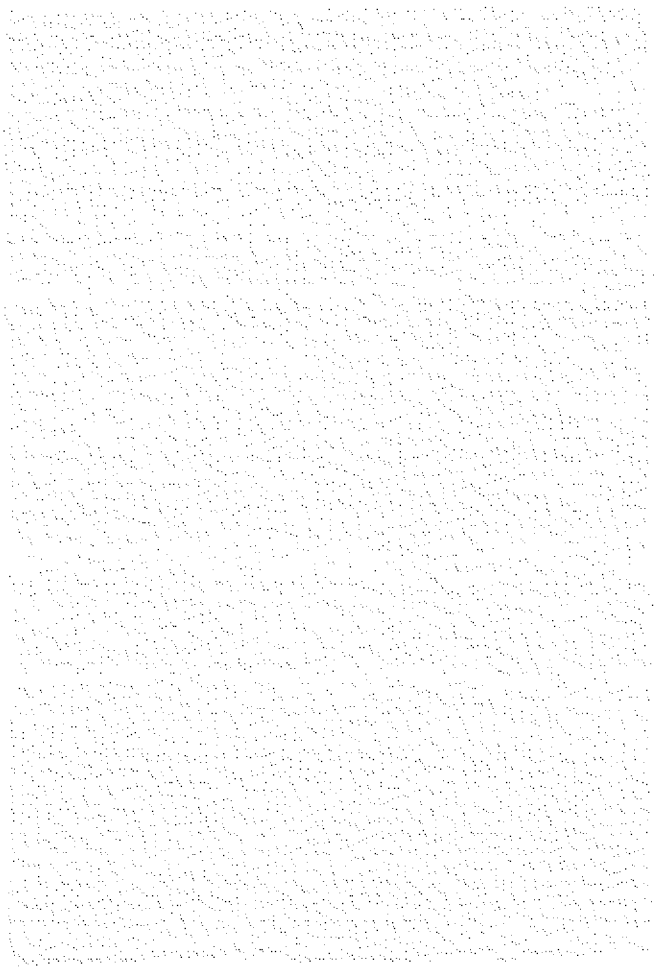

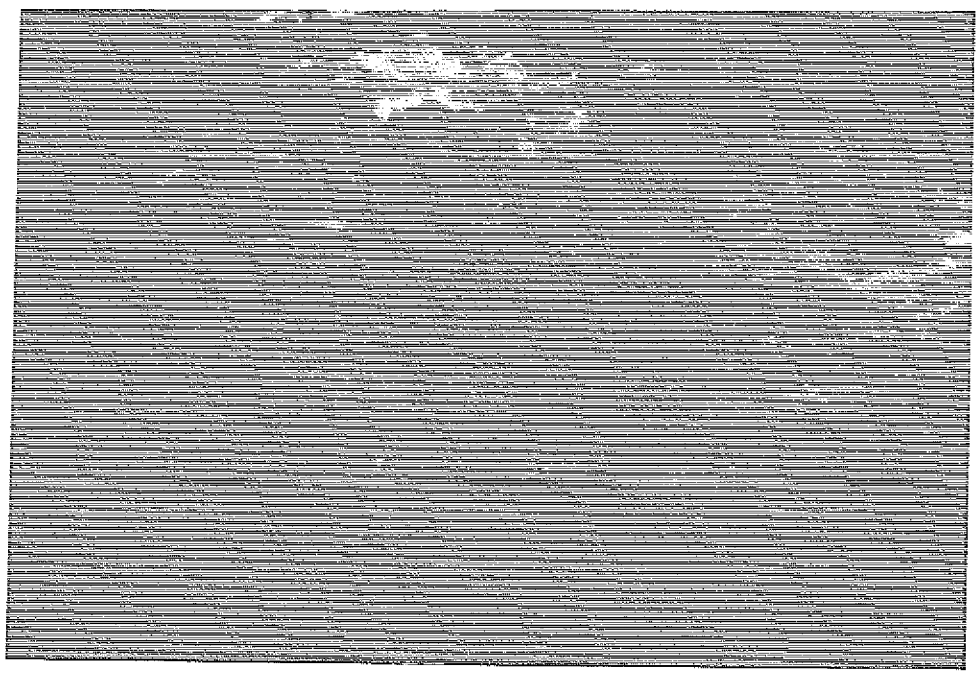

Fig. 27: Photomicrograph of the fluorescing groundmass of organic facies A. (Field of view is 200 μm wide).

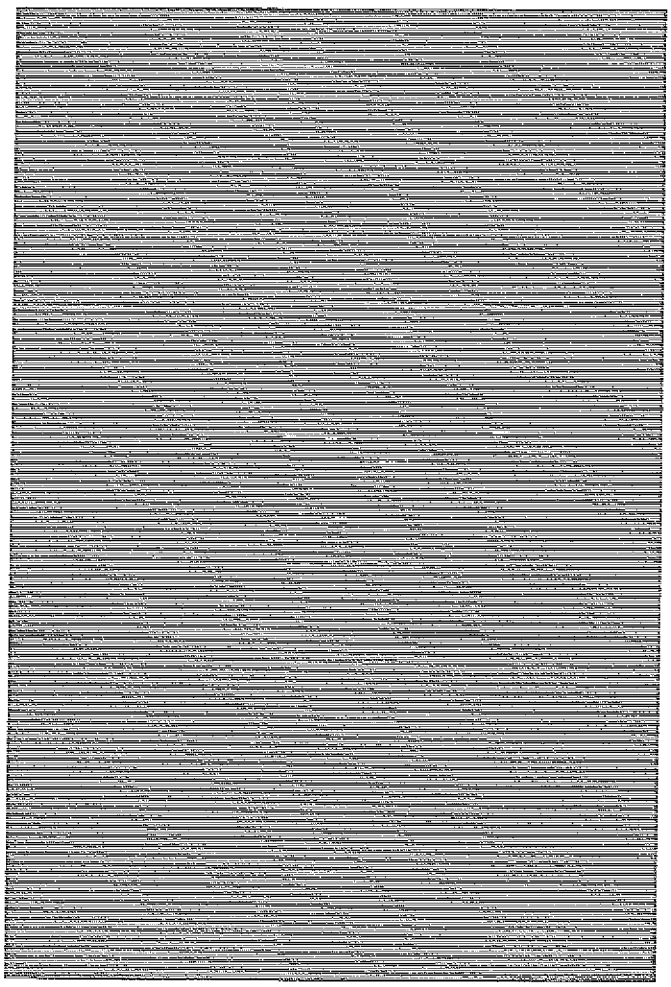

Fig. 28: Photomicrograph of marl of type B under blue light. Fluorescing particles are alginite. (Field of view is 360 μm wide).

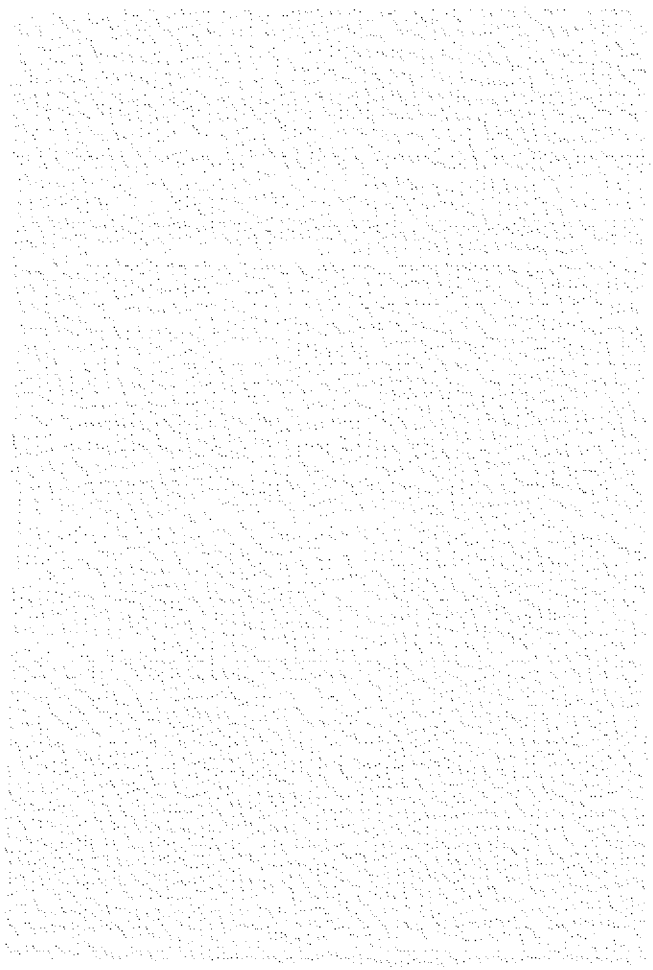

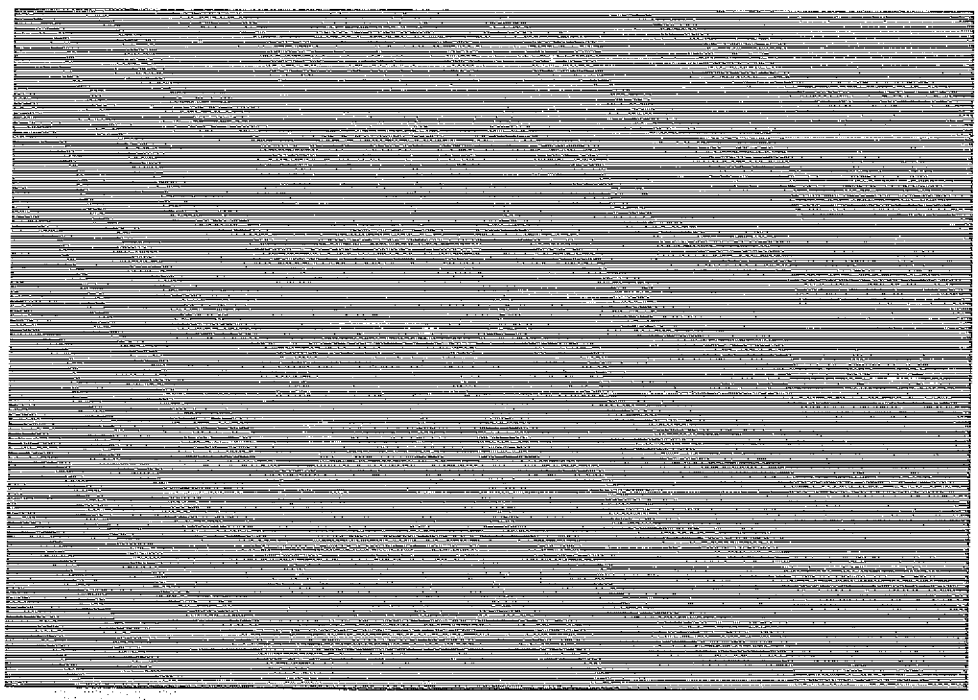

Fig. 29: Photomicrograph of fluorescing compacted algae. (Blue light. Field of view is 200 μm wide).

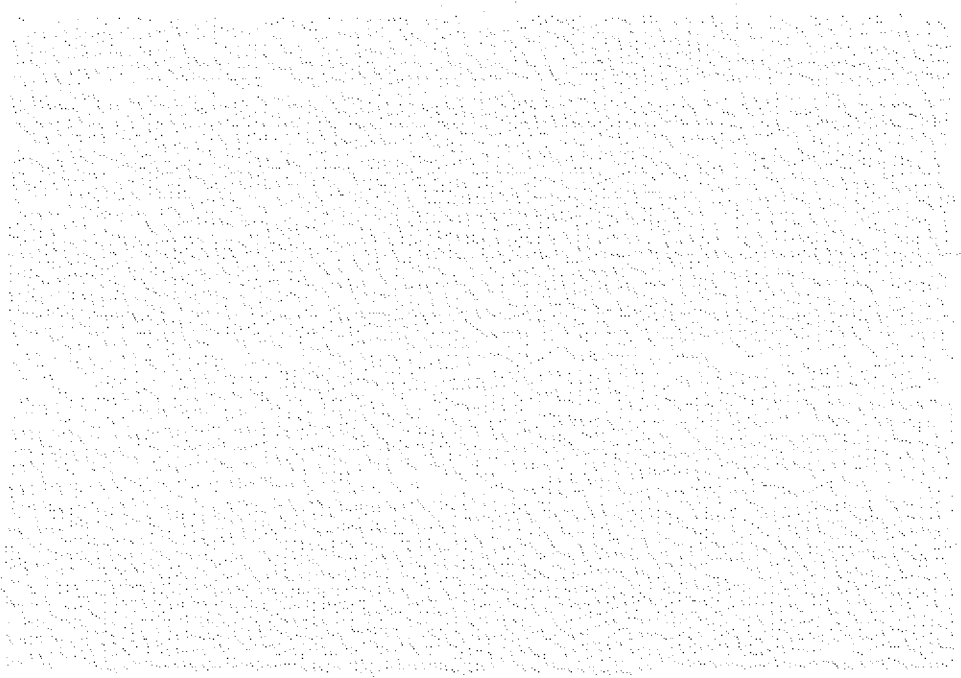

rarely. The alginites and vitrinites of type B display the same characteristics as those of type A. The liptodetrinites, however, are made up of dispersely distributed liptinite fragments (<5 μm).

3.7.4.3 Anhydrites

3.5.4.3.1 Lenticular Anhydrites

Lenticular anhydrite is characterized by disc-shaped anhydrite aggregates that initially formed via displacive growth of gypsum and subsequent anhydritization within a marl matrix (Fig. 30). The anhydrite aggregates contain only a few organic particles. Occasionally algal bodies are preserved within single anhydrite crystals. These algae did not undergo a large degree of compaction, as indicated by their well-preserved spherical shape. Most of the organic content of this sedimentary facies, however, is concentrated in the marl matrix. The organic content of the marls of the lenticular anhydrite facies displays the same characteristics as marls of type A. Ubiquitous features are the layers of amorphous fluorescent groundmass that commonly hug individual lenticular anhydrite aggregates (Fig. 31).

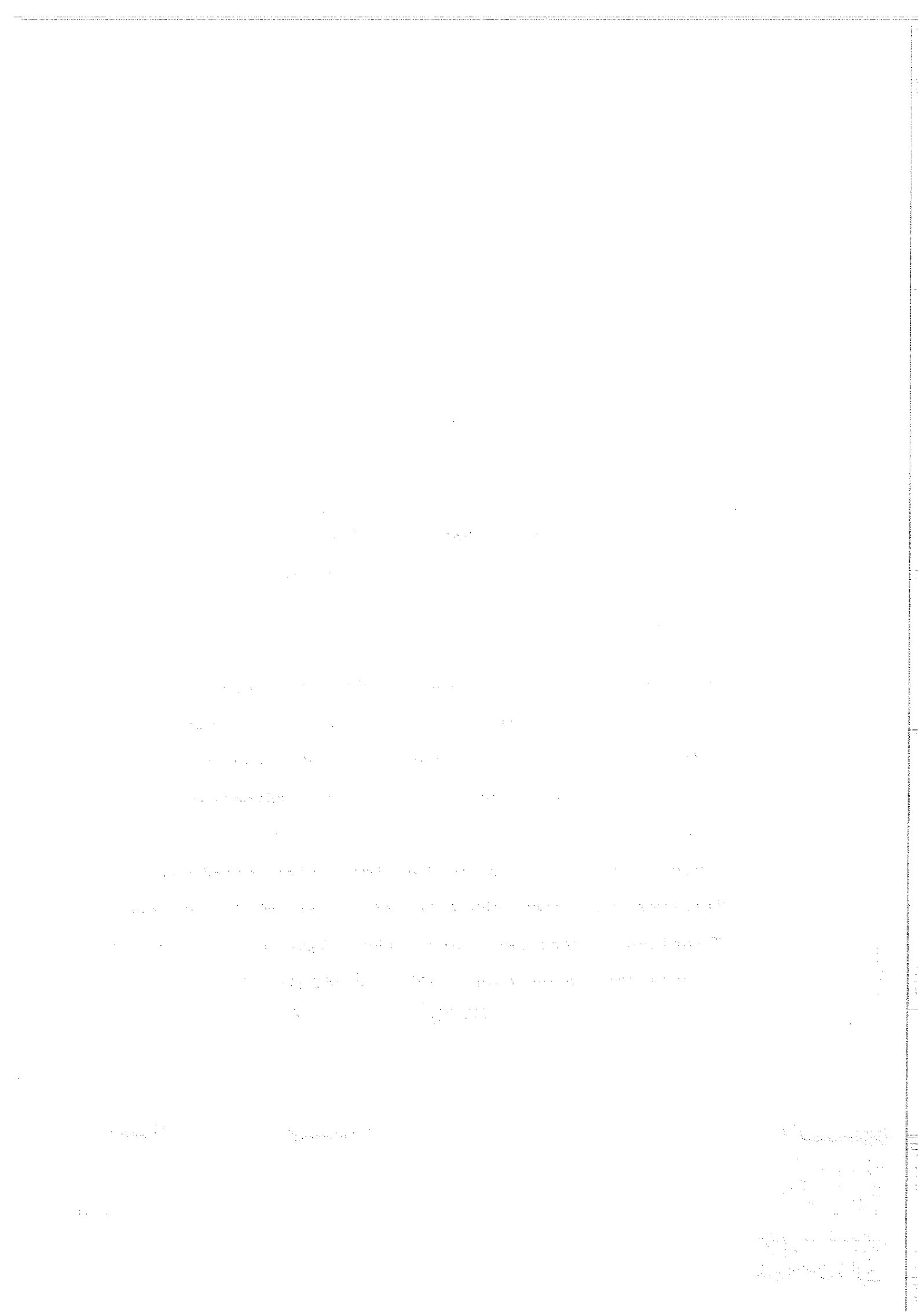

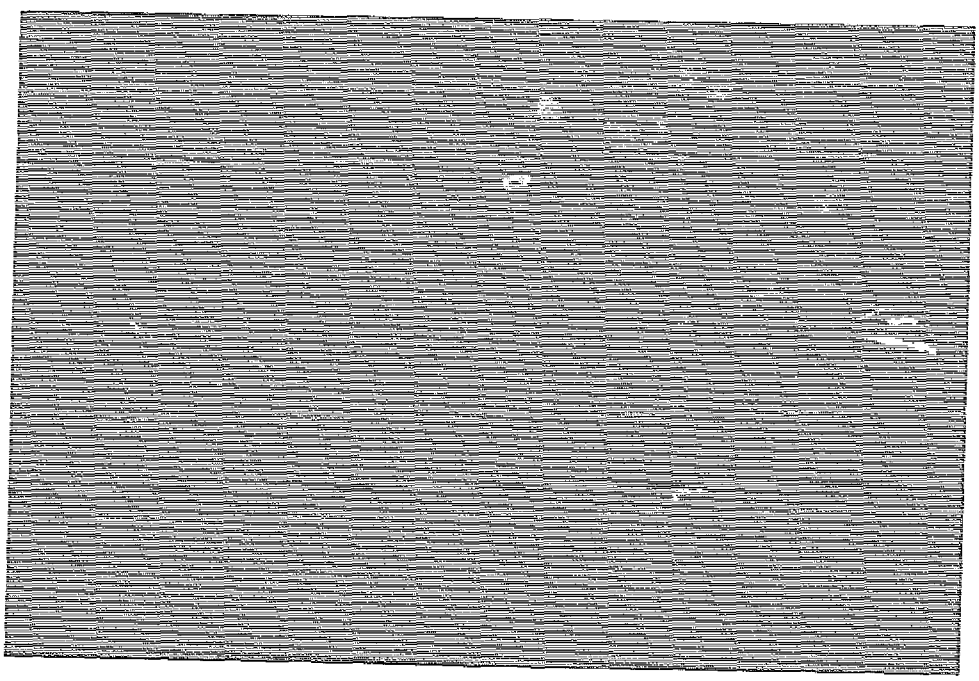

Fig. 30: Alginite in the marl matrix between lenticular anhydrite aggregates. (Blue light. Field of view is 200 μm wide).

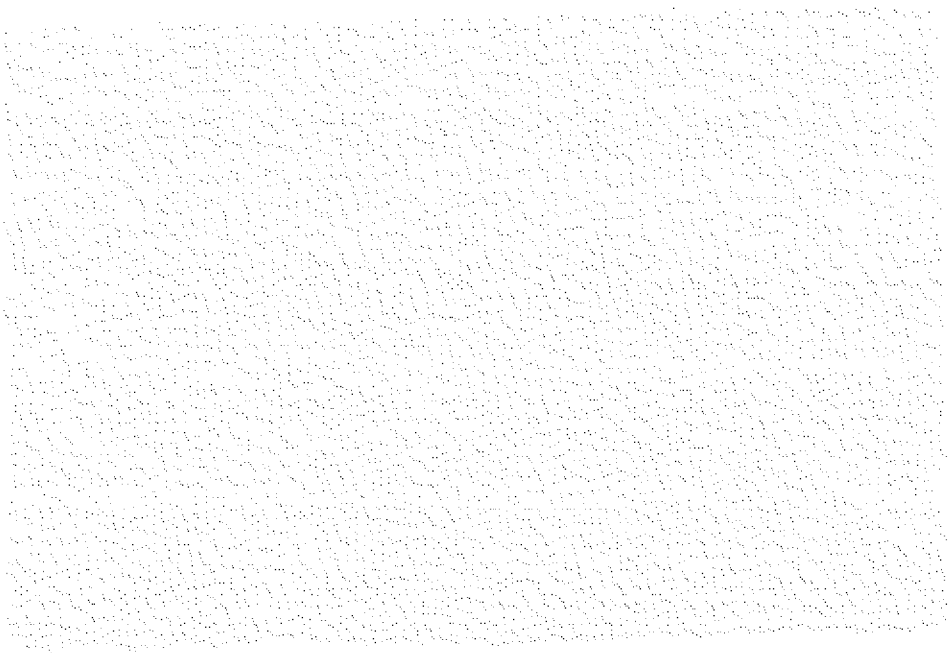

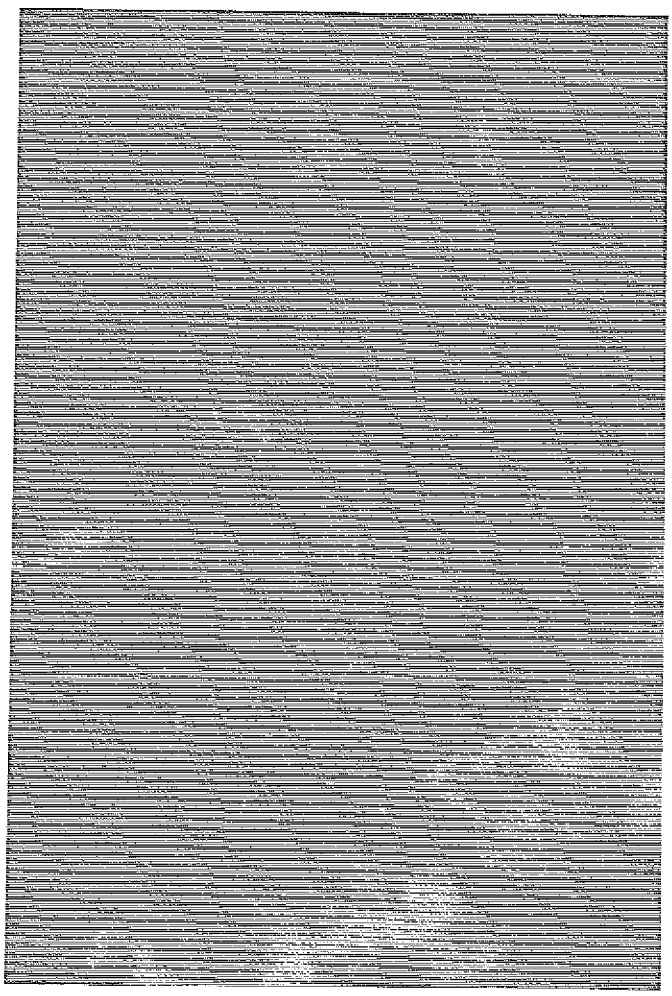

Fig. 31: Fluorescing organic groundmass in a marl matrix of lenticular anhydrite facies. (Blue light. Field of view is 720 μm wide).

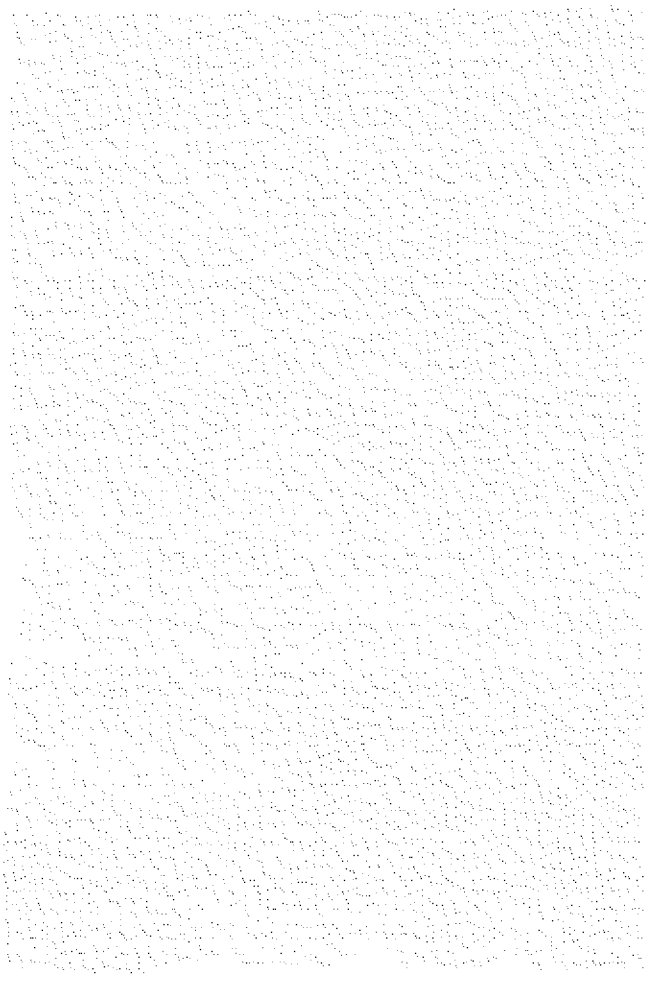

3.7.4.3.2 Laminated Anhydrites

The organic matter in laminated anhydrites is concentrated in clay/carbonate-rich layers that define the lamination in this facies. These layers are interpreted to result from periodic brine refreshment and in conjunction with the renewed influx of nutrients and clastic particles. The organic matter content of the clay/carbonate-rich zones is similar to the organic facies of the marls of type A. Dispersed single algae are common (Fig. 32), and in some zones layers of amorphous liptodetrinite are present. In contrast, the anhydrite-dominated layers only contain a few, individual algae. Vitrinite and inertinite are sparse or absent in this facies.

3.7.4.3.3 Massive Anhydrites

Organic matter is sparse and dispersely distributed in massive anhydrites. In general, uncompacted single algae (Fig. 33) or liptinite fragments (<5 μm) are noted. Vitrinite particles are not abundant.

3.7.5 Halite

Halite contains almost exclusively organic particles smaller than 5 μm. The visually identifiable macerals are

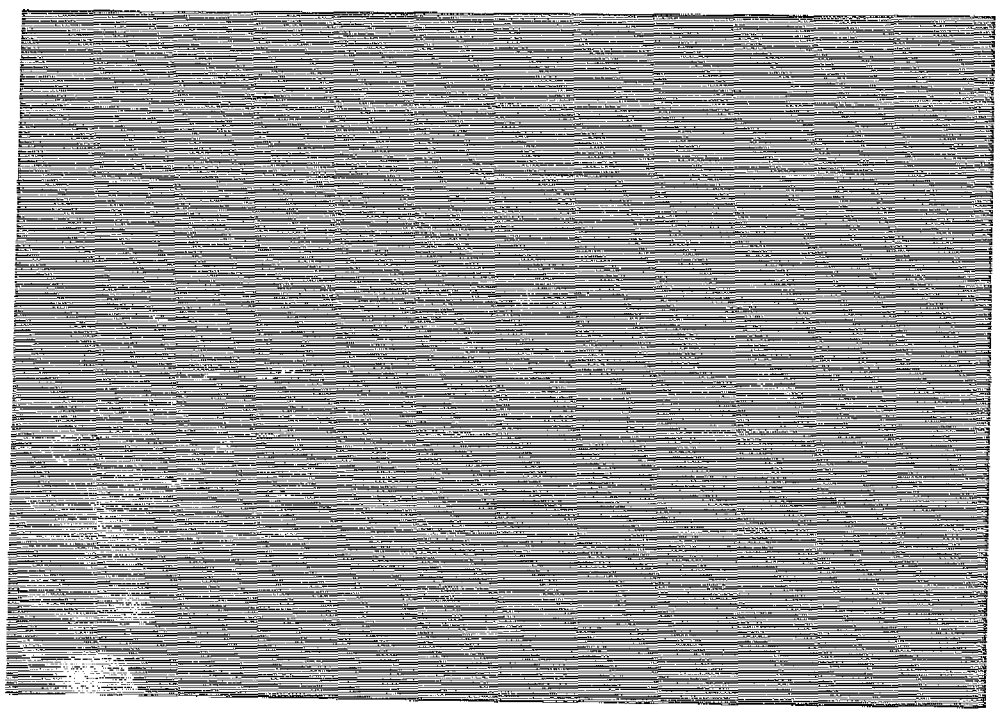

Fig. 32: Disperse algae in marl layer of the laminated anhydrite facies. (Blue light. Field of view is 500 μm wide).

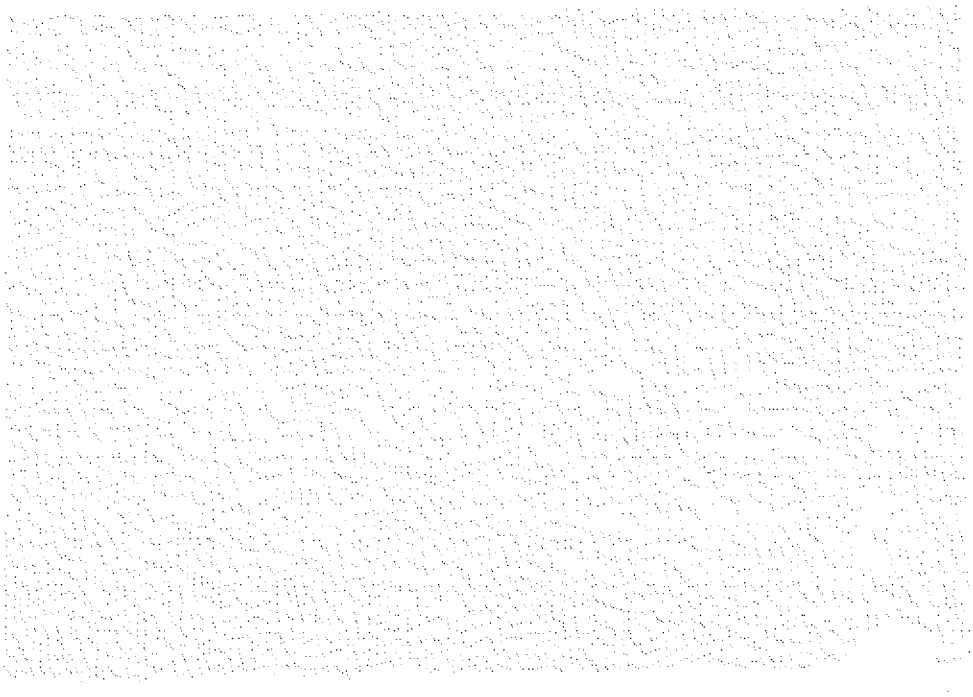

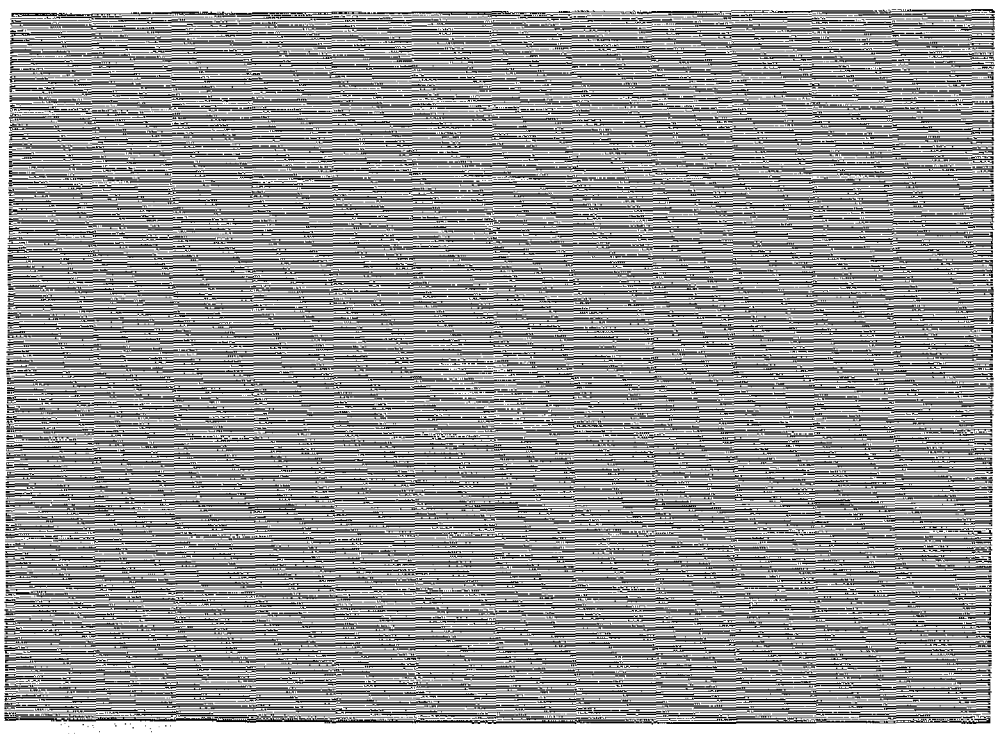

Fig. 33: Single algae in massive anhydrite lithofacies (Blue light. Field of view is 145 μm wide).

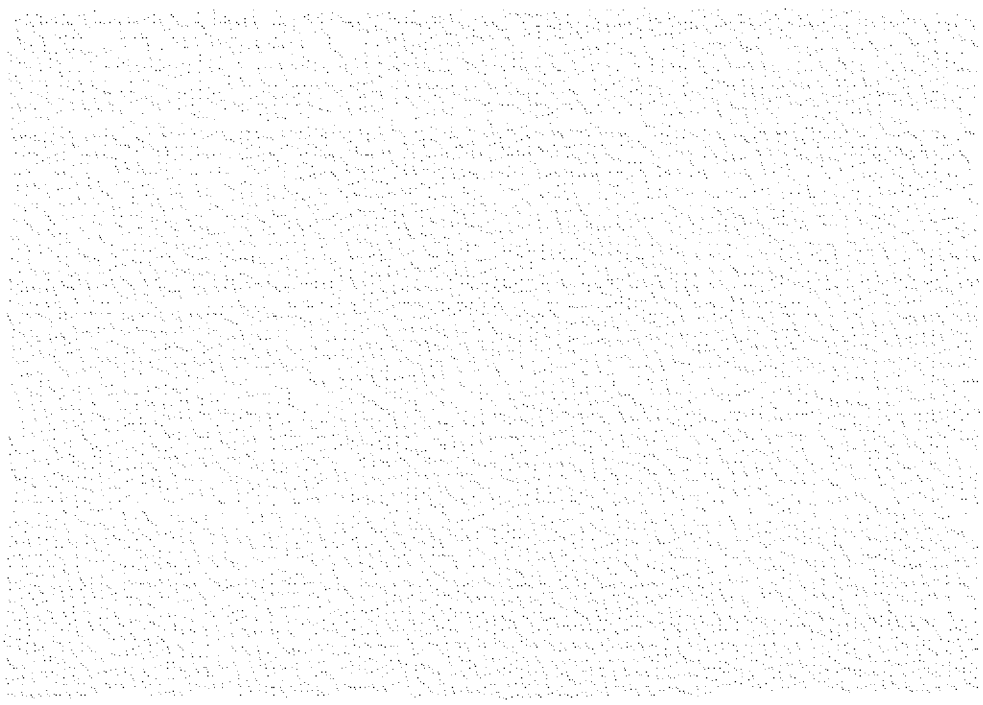

mostly liptodetrinite with only very minor amounts of vitrinite and inertinite. The assessment of the organic matter content of the halite facies and massive anhydrite facies is complicated by the low organic carbon content and the generally small size of the macerals, and, hence, must be interpreted with caution.

3.8 ORGANIC FACIES

The term "organic facies" is used for a mappable rock unit distinguishable by the character of its organic matter without regard to the inorganic aspects of the sediments (Jones, 1984). Microscopic characterization of the kerogens in the S1 to CI unit allows the definition of two organic facies. Organic facies A has an alginite content between 25% and 42% and typically contains more than 50% liptodetrinite. Most of the liptodetrinites are composed of layers of amorphous organic matter, whereas alginite or sporinite debris is sparse. The vitrinite and inertinite content of organic facies A varies between 4% and 21%.

In contrast, organic facies B has a higher alginite content (>50%) than organic facies A. The proportion of liptodetrinite (<35%), however, is distinctly lower than in organic facies A. The liptodetrinites are dominantly composed of alginite debris. Laminated amorphous organic matter, characteristic for organic facies A, is completely absent. Vitrinite is common in organic facies B.

In general, both organic facies A and organic facies B contain varying amounts of algal (alginite) and plant (vitrinite) derived organic matter. The key difference is the proportion of laminated, amorphous organic matter in organic facies A. In both organic facies, aquatic organic

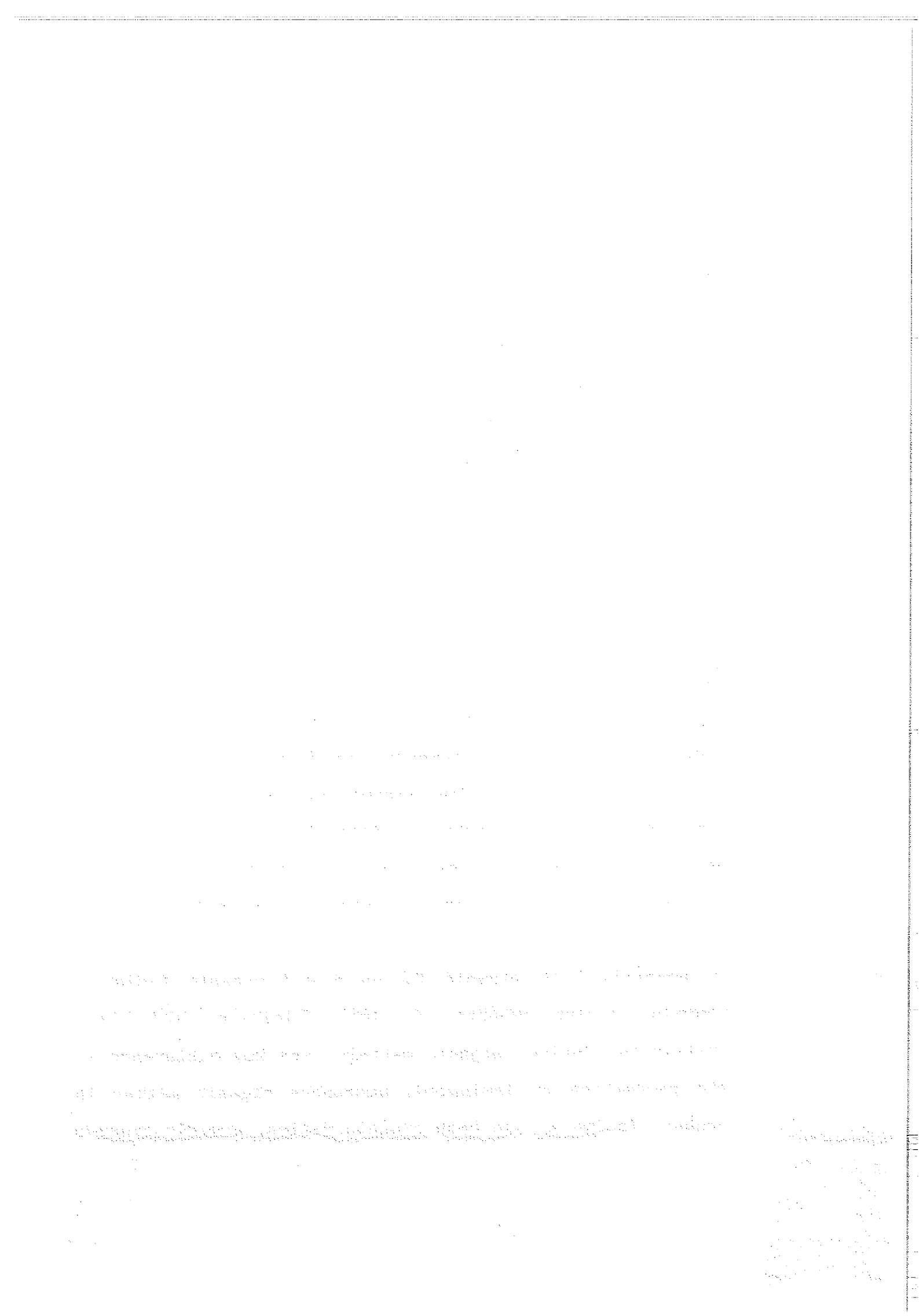

matter (alginite and liptodetrinite) is dominant. Terrestrial-derived organic matter (vitrinite and sporinite) plays a subordinate role. The kerogens of both facies can, therefore, be classified as type II.

A comparison of the maceral content of samples from each described sedimentary facies showed that the organic facies correlates to the sedimentary facies (Fig. 34). Organic facies A is observed in marls of type A, in lenticular anhydrites, and in laminated anhydrites. Organic facies B is present in marls of type B. Massive anhydrites and halites did not contain sufficient amounts of organic matter to perform a meaningful maceral analysis. However, both lithofacies contain minor amounts of alginite, liptodetrinite and vitrinite, and, hence, a maceral content similar to that of the marls of sedimentary facies type B, which contain organic facies B.

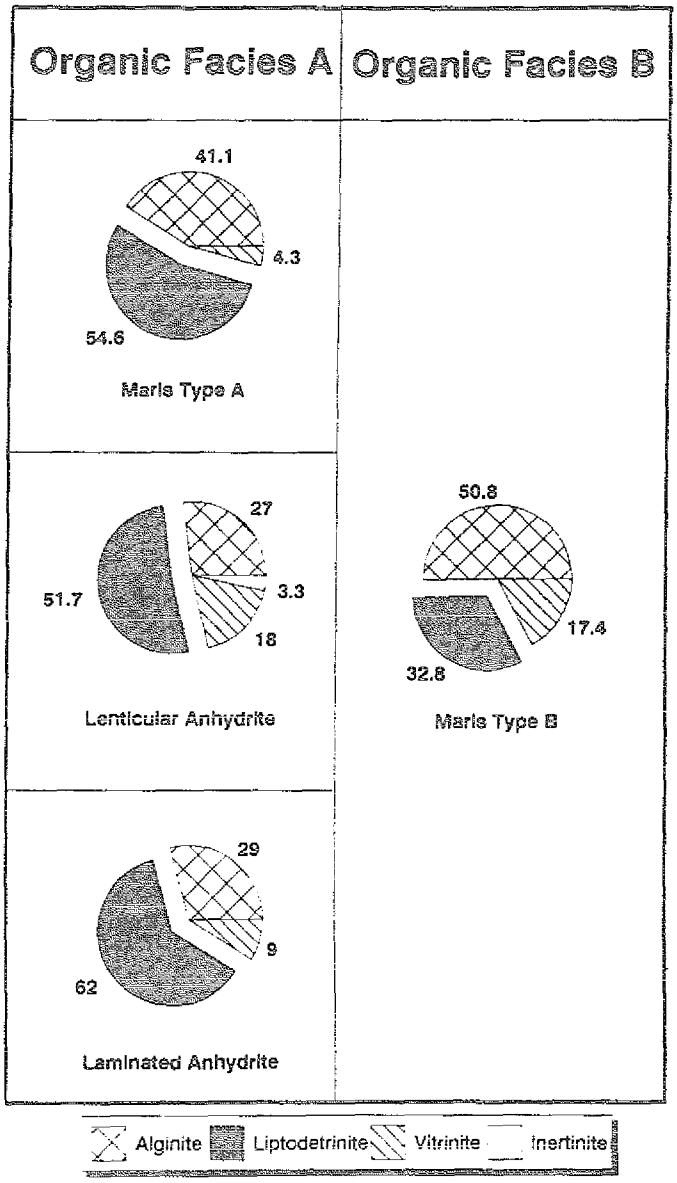

Fig. 34: Average maceral composition of the lithofacies of the S unit.

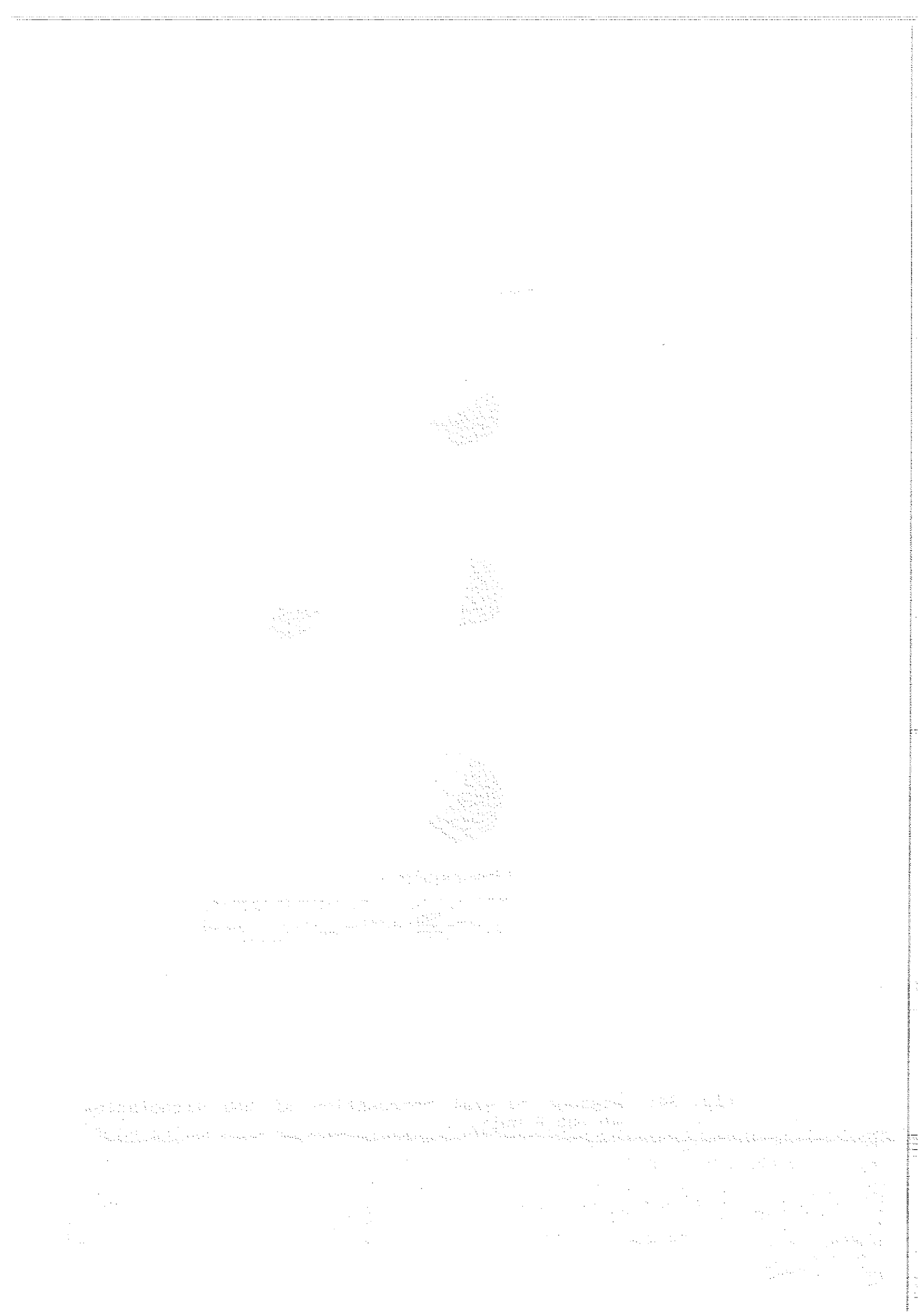

3.9 CHEMICAL CHARACTERIZATION OF THE KEROGENS

Chemical characterization by Rock-Eval pyrolysis of the kerogens of the S unit was conducted for samples from three locations: Amelie II, Ungersheim, and Berrwiller. Results reported here were determined on marl samples and not on anhydrites and halites, since it has previously been demonstrated that low TOC contents and especially the presence of calcium sulfate tends to render results obtained by Rock-Eval pyrolysis useless (e.g. Horsfield and Douglas, 1980; Espitalié et al., 1984; Espitalié, 1986; Peters, 1986).

The kerogen type is characterized by the hydrogen index and the oxygen index. Hydrogen and oxygen indices measured by Rock-Eval pyrolysis correlate with hydrogen/carbon and oxygen/carbon ratios measured by elemental analysis of kerogen (Espitalié et al., 1977). They can, therefore, be used in the same way as hydrogen/carbon and oxygen/carbon ratios for kerogen typing. Chemical kerogen classification can be performed when the hydrogen index and oxygen index data obtained by Rock-Eval pyrolysis are plotted in a van Krevelen-type diagram (Espitalié et al., 1977). The values of hydrogen and oxygen indices of marls from the S unit taken from

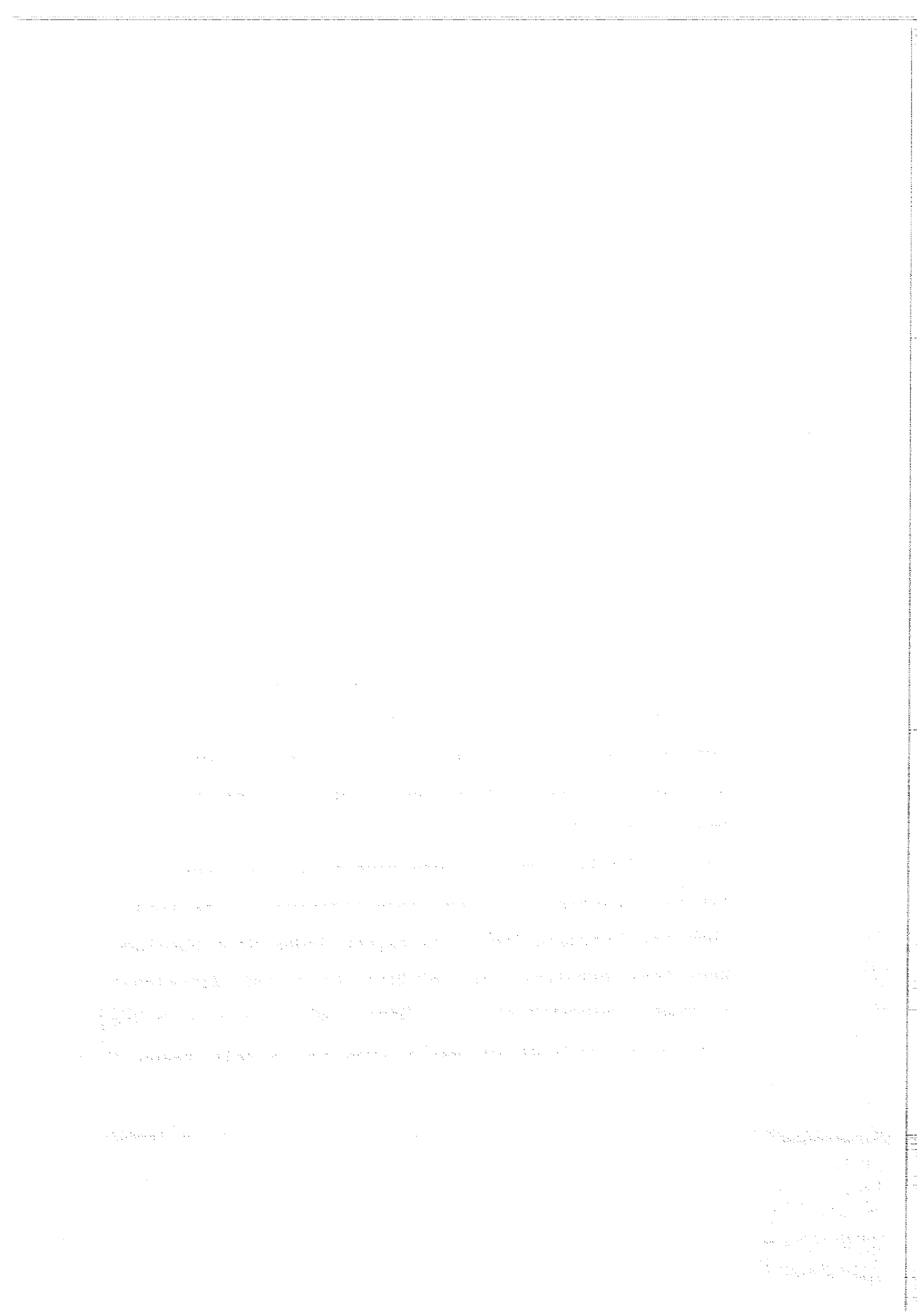

Amelie II, Ungersheim, and Berrwiller are similar (Fig. 35). All data plot between the kerogen type II evolution paths and hence can be classified as type II. This classification is in good agreement with the data from petrology. The kerogens from Amelie II, Ungersheim, and Berrwiller have approximately the same range of hydrogen and oxygen indices and can hence be considered suites of kerogens of comparable quality (Tissot and Welte, 1984). Low T_{max} (temperature of maximum hydrocarbon generation during pyrolysis) values (on average approximately 435°C) indicate that the organic matter at each location is thermally immature.

3.9.1 Organic Facies

A compilation of hydrogen index and oxygen index values for marl samples classified by kerogen microscopy into organic facies A and organic facies B (Fig. 36) shows that both facies can also be differentiated on a chemical basis. Marls containing organic facies A display hydrogen indices between 570 and 380 mg hydrocarbons/g TOC and oxygen indices between 50 and 250 mg CO_2/g TOC. In contrast, marls of facies B display hydrogen indices from 450 to 200 mg hydrocarbons/g TOC and oxygen indices from 100-500 mg CO_2/g TOC. Based on these data, organic facies A has a better petroleum potential than organic facies B.

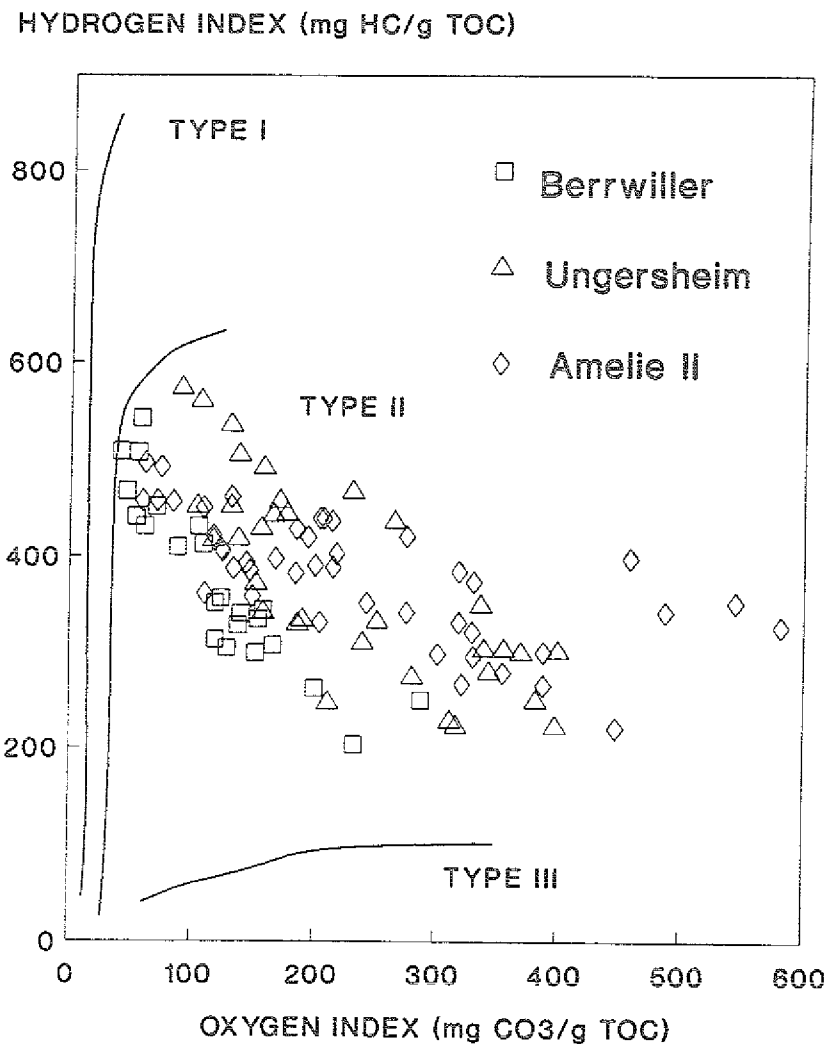

Fig. 35: Hydrogen index versus oxygen index diagram for kerogen typing (Espitalié et al., 1977).

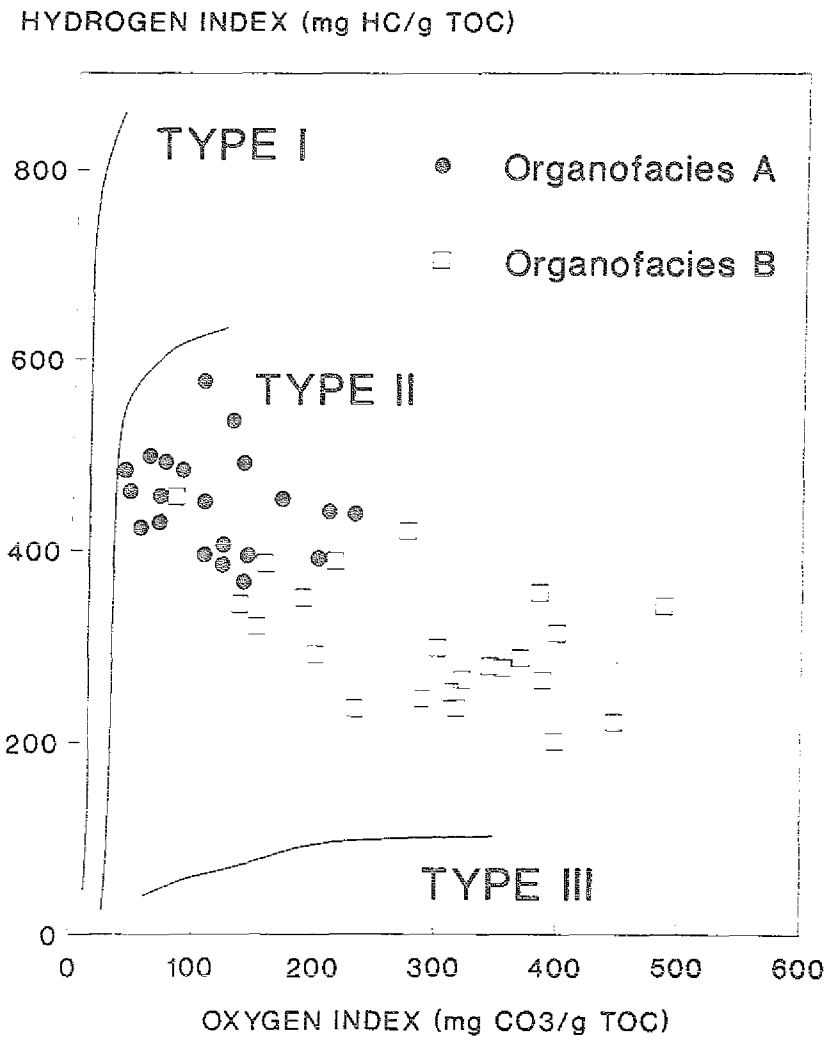

Fig. 36: Discrimination of organic facies A and B of marl samples on the basis of hydrogen and oxygen indices.

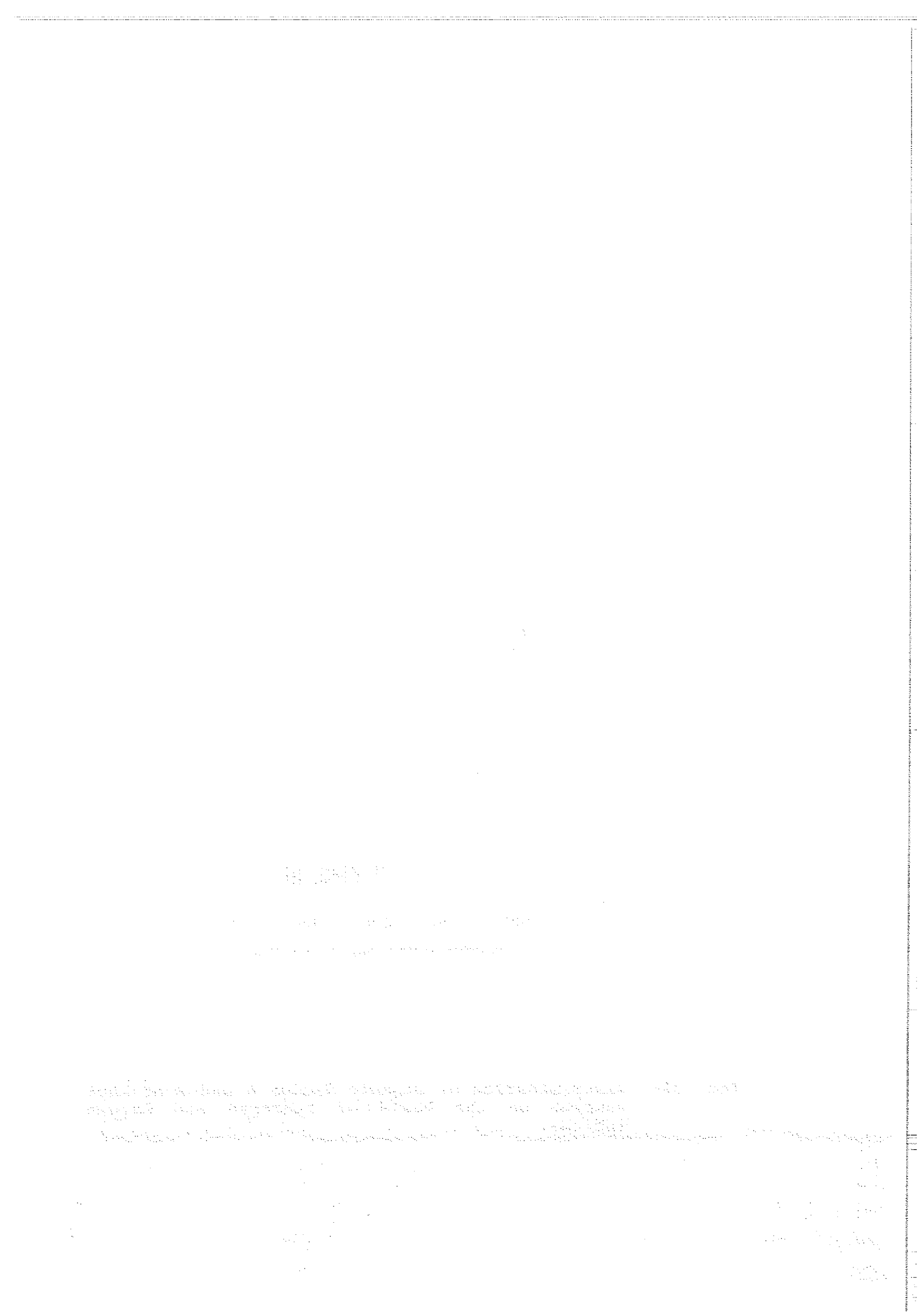

3.9.2 Influences on Kerogen Quality

The quality of the S unit kerogens show marked variation. Even though there is considerable scatter in the hydrogen index data, a general systematic trend with stratigraphic age of the hydrogen index can be observed (Fig. 37). Kerogens from marls at the base of the S unit display hydrogen indices generally lower than 300 mg HC/g C_{org}. The hydrogen indices gradually increase when moving upward through the S unit and peak in the top region at close to 500 mg HC/g C_{org}.

The hydrogen index of kerogens is influenced by the type of initial organic matter, the degree of its preservation during deposition, and the maturity of the kerogens. Maturation processes cause a severe depletion of hydrogen from the kerogen. The transformation of organic matter under thermal stress is an overall disproportionation of the hydrogen of the initial kerogen. On the one hand, hydrogen is enriched in the products generated (hydrocarbons); on the other hand, the residual kerogen becomes increasingly depleted with respect to hydrogen. However, because the kerogens from one sampling site of the S unit have passed through the same thermal history, maturity differences should play no significant role in explaining the observed hydrogen index variation.

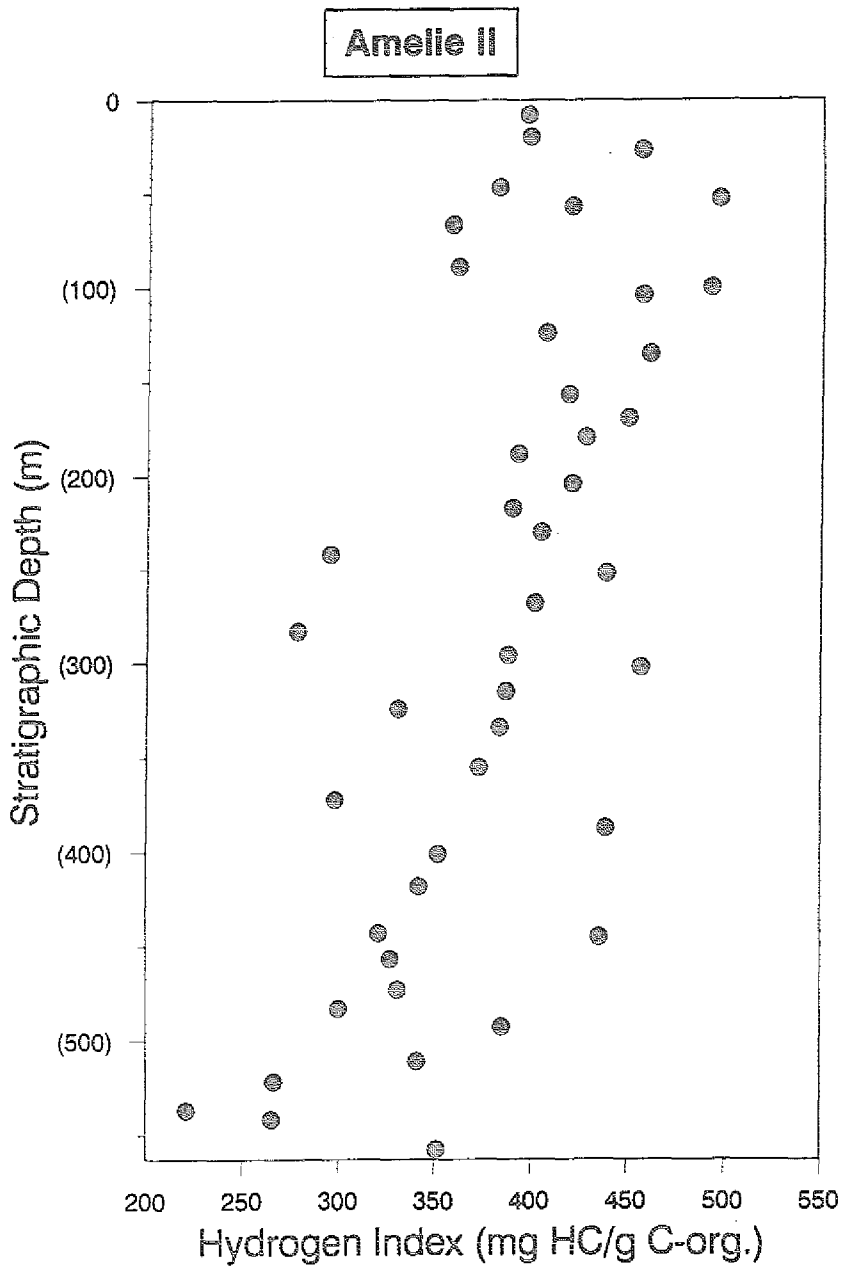

Fig. 37: Variation of the hydrogen index of the marl samples of the S unit with stratigraphic depth at Amelie II. The same variation has been observed at Ungersheim and Berrwiller.

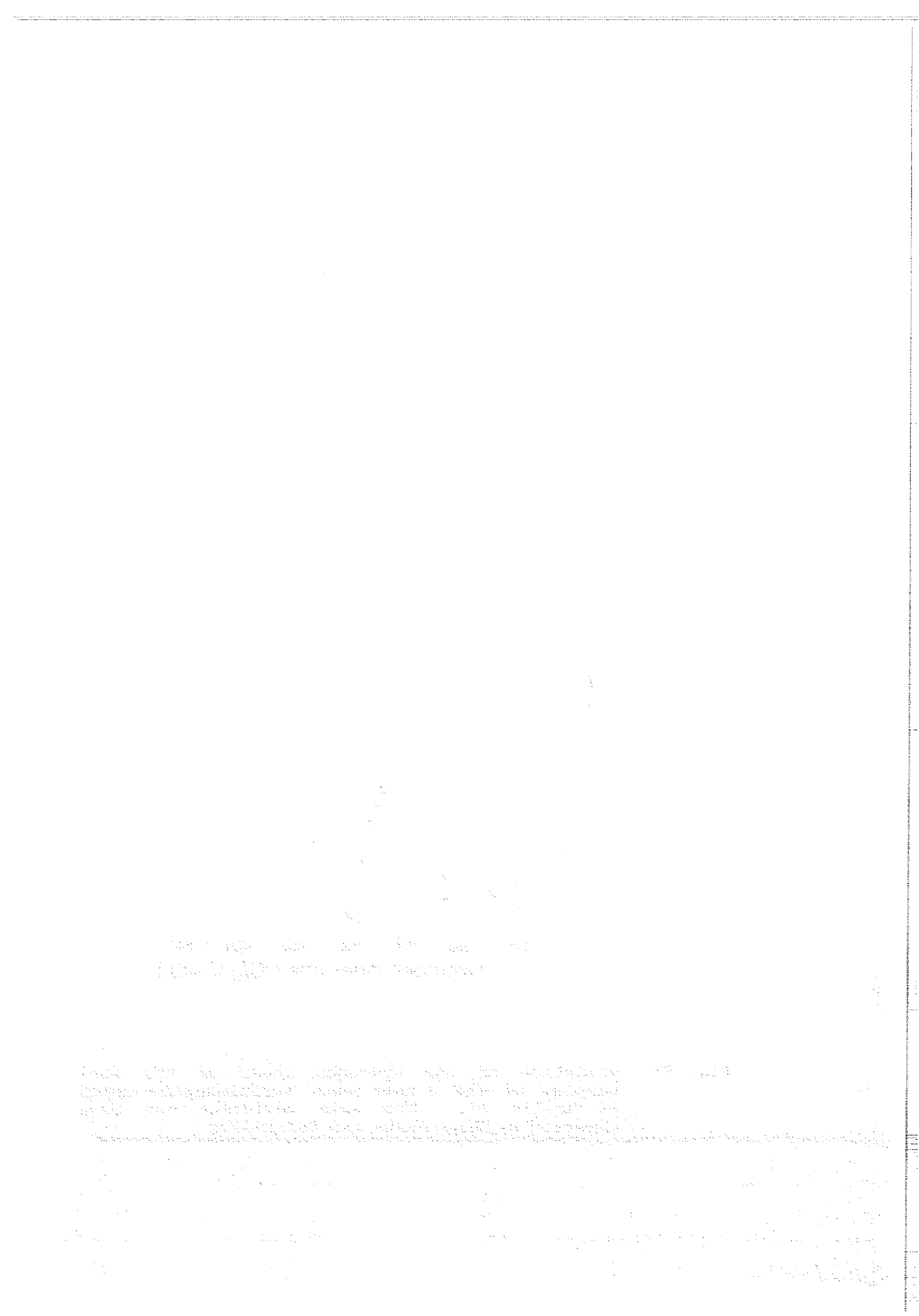

The type of organisms that contribute to the formation of kerogen is another parameter that influences the hydrogen index. The fact that organic matter from different sources has varying chemical composition has been used as the basis for kerogen typing (Tissot and Welte, 1984). Kerogens derived from land plants (mainly composed of huminite/vitrinite) have hydrogen indices of approximately 200 mg HC/g C_{org}, while kerogens of aquatic organic matter have considerably higher hydrogen indices (greater than 500 mg HC/g C_{org}). Various combinations of hydrogen-rich aquatic organic matter and hydrogen-poor terrigenous organic matter can produce kerogen suites with varying hydrogen indices. The influence of the proportion of terrigenous organic matter on the hydrogen indices of marl samples of the S unit becomes evident when hydrogen indices are compared to relative proportions of vitrinite and inertinite (Fig. 38). Both maceral groups are interpreted to represent terrigenous organic matter. Samples with low hydrogen indices contain higher amounts of terrigenous organic matter, whereas samples with higher hydrogen indices are low in terrigenous organic matter.

Preservation conditions can influence hydrogen indices, because oxidized organic matter generally has low hydrogen indices (Tissot and Welte, 1984). However, preservation conditions during the deposition of the S unit are thought

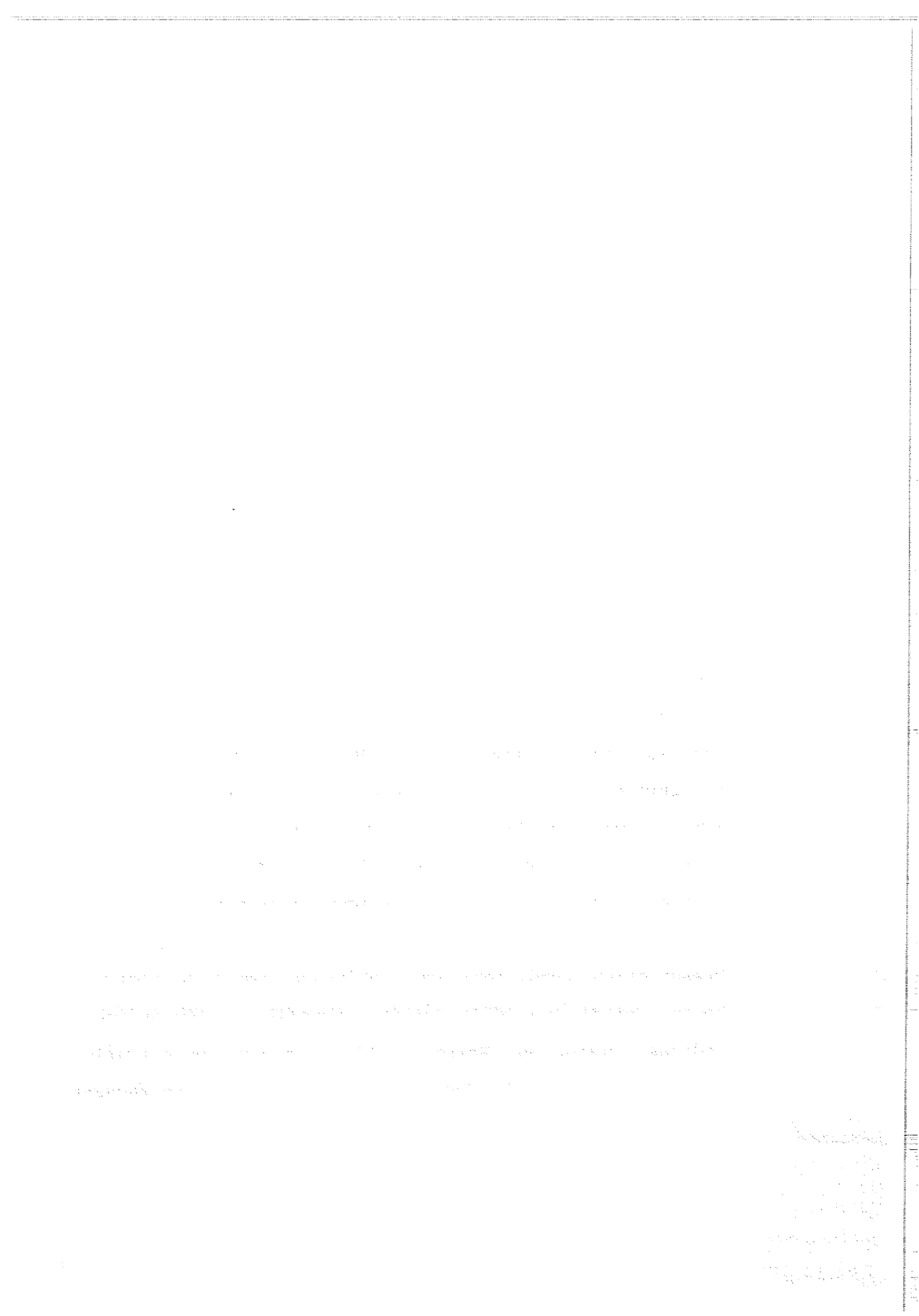

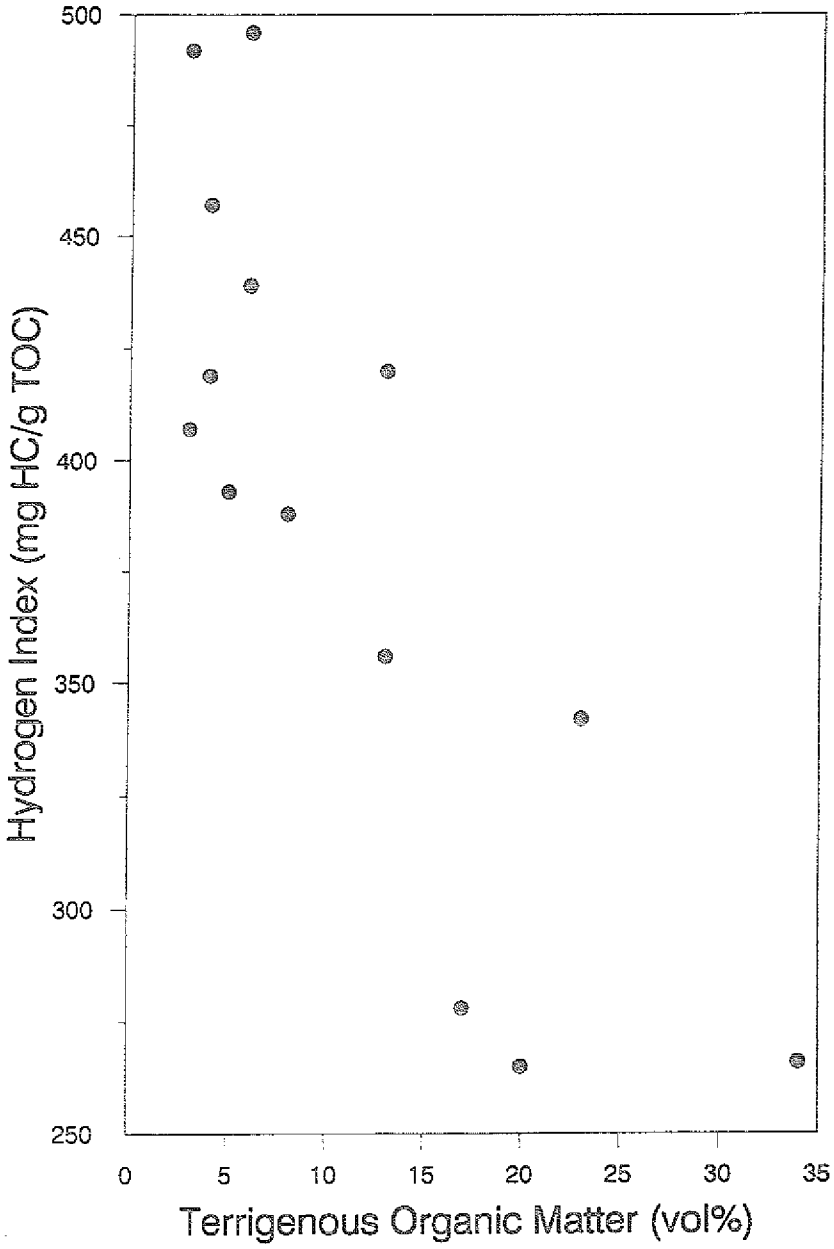

Fig. 38: Variation of the hydrogen index of the marl samples with the terrigenous organic matter content.

to have been good (see discussion under Rhythmic Carbon Sedimentation, Chapter 3.11). Therefore, it is more likely that the presence of terrestrial matter determines the hydrogen indices and hence the kerogen quality of the organic matter, rather than preservation conditions or salinity, as suggested by Hollander and Huc (1991).

3.10 CHARACTERIZATION OF THE SOLUBLE ORGANIC MATTER

The portion of the organic matter that can be extracted from a rock with an organic solvent is called bitumen. Compounds from the bitumen of a petroleum source rock can be divided into four major groups: 1) aliphatic hydrocarbons, 2) aromatic hydrocarbons, 3) nitrogen, sulfur, or oxygen containing compounds (NSO compounds), and 4) asphaltenes (e.g. Tissot and Welte, 1984). All of these subfractions of the bitumen contain a multitude of compounds, however, only a comparatively small number have yet been identified, and even a smaller number are routinely analyzed.

To aid further the reconstruction of the depositional environment, selected aliphatic, aromatic hydrocarbons, and NSO compounds were analyzed. The value of these compounds in paleoenvironmental reconstruction lies in the information that can be obtained regarding the primary contributors to the organic matter, physio-chemical conditions during deposition, and also in supporting the discrimination of organic facies.

3.10.1 Aliphatic Hydrocarbons

3.10.1.1 N-Alkanes

The analysis of n-alkanes from a total of 86 samples, including examples of each sedimentary facies, resulted in the recognition of two distinctly different n-alkane distribution patterns (Patterns A and B of Gely and Huc, 1990). Pattern I is characterized by a bimodal n-alkane distribution (Fig. 39). The modes are at n-C_{16} and n-C_{24}. The minimum of pattern I is recorded at n-C_{21}. In the C_{22}-C_{29} range a slight even/odd predominance is observed. In contrast, pattern II (Fig. 40) is dominated by the C_{15} and C_{17} n-alkanes. N-alkanes in the C_{20}-C_{29} range occur in lower concentrations than n-alkanes in the C_{15}-C_{19} range. In most cases a slight odd/even predominance is developed in the C_{22}-C_{29} range. It should be noted, however, that n-alkane distribution pattern I has been recognized in marls of type A, laminated anhydrites and lenticular anhydrites (Fig. 41). Pattern II is associated with the marls of type B, the massive anhydrites, and the halite lithofacies (Fig. 41).

Both facies show light hydrocarbon preference (sum of n-alkanes $C_{17}+C_{18}+C_{19}$ over sum of n-alkanes $C_{27}+C_{28}+C_{29}$)

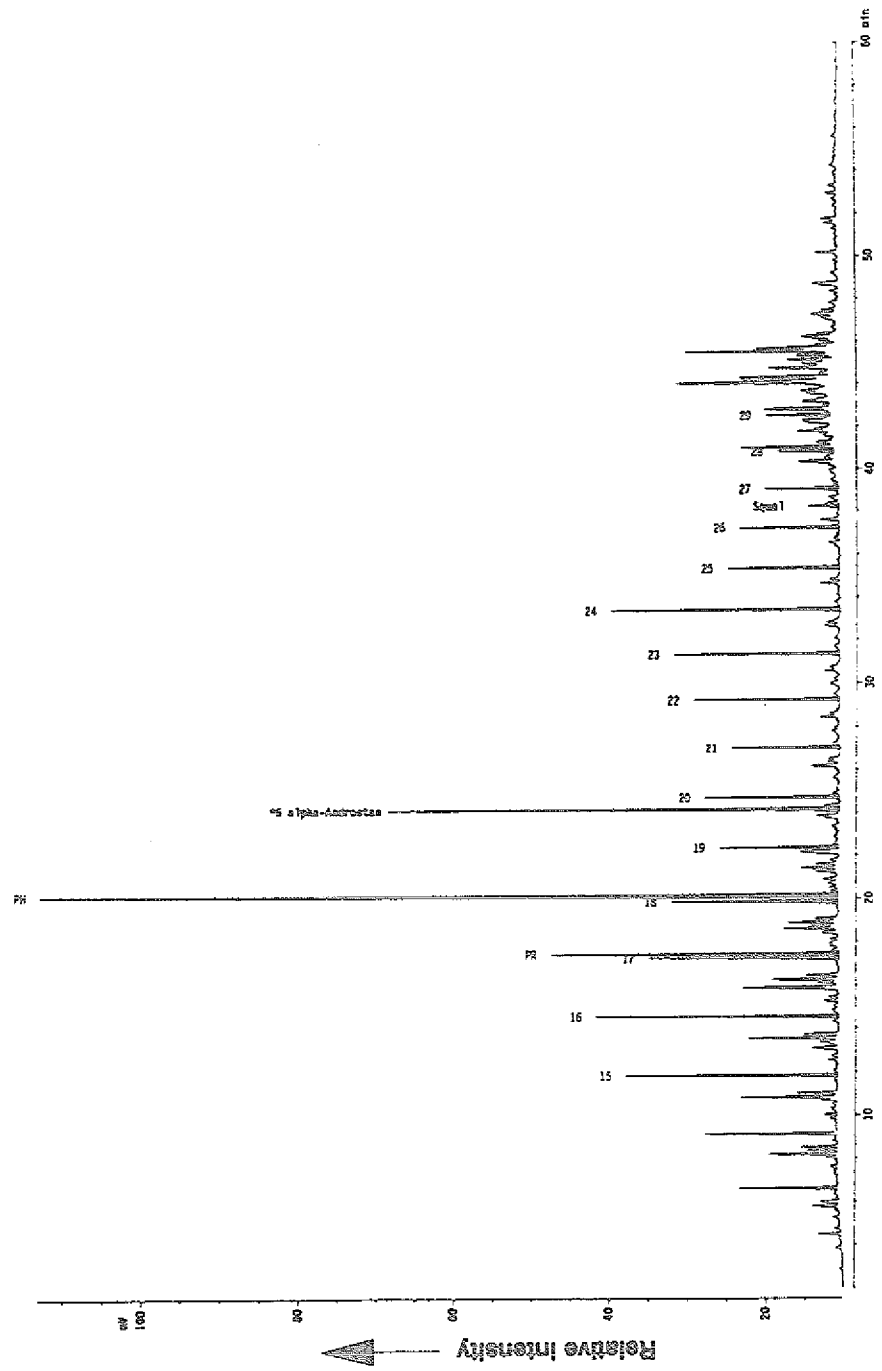

Fig. 39: N-alkane distribution pattern I. Note the bimodal distribution with modes at n-C_{16} and n-C_{24}. (PR = pristane, PH = phytane, squal = squalane).

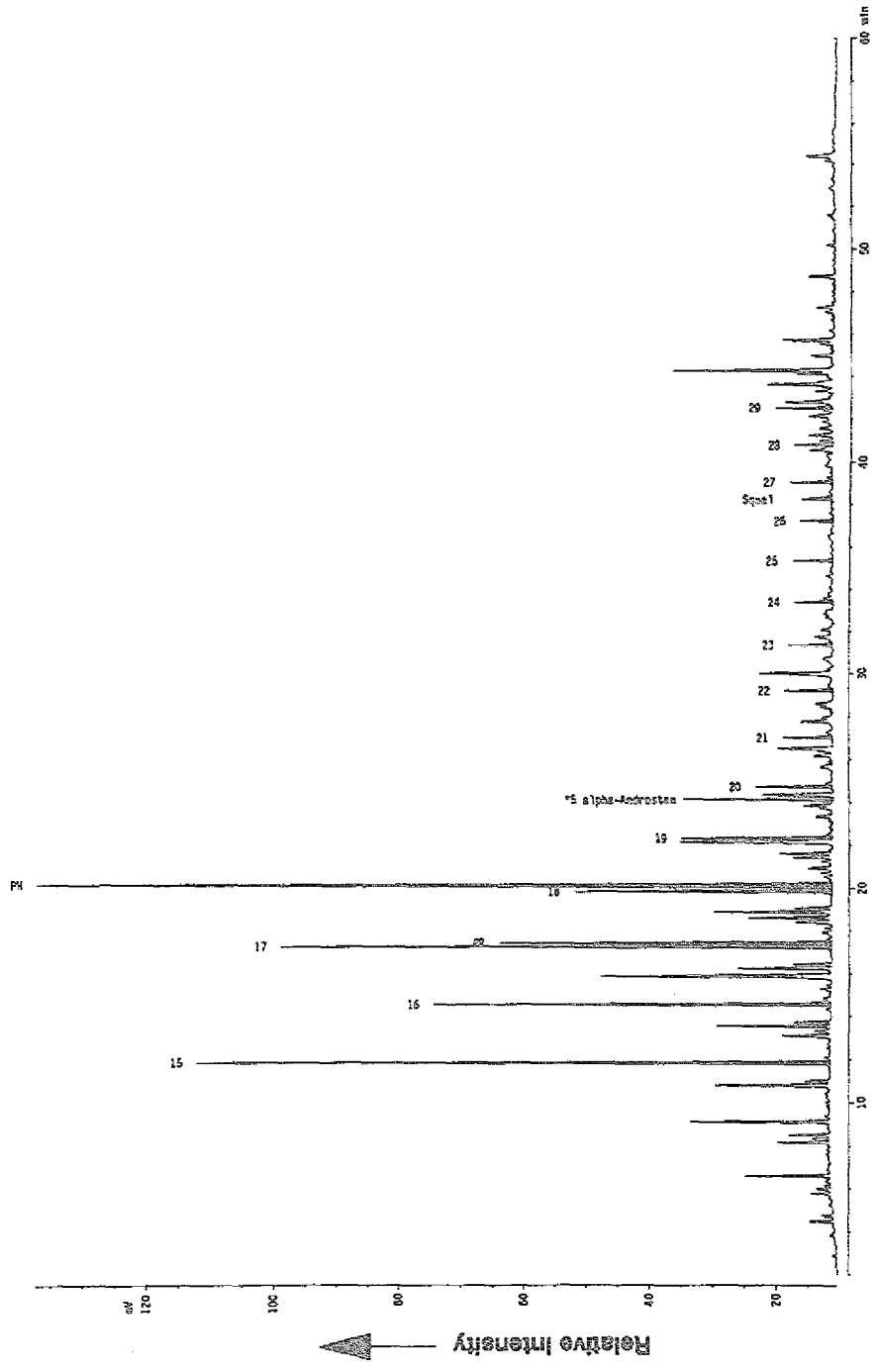

Fig. 40: N-alkane distribution pattern II. (PR = pristane, PH = phytane, squal = squalane).

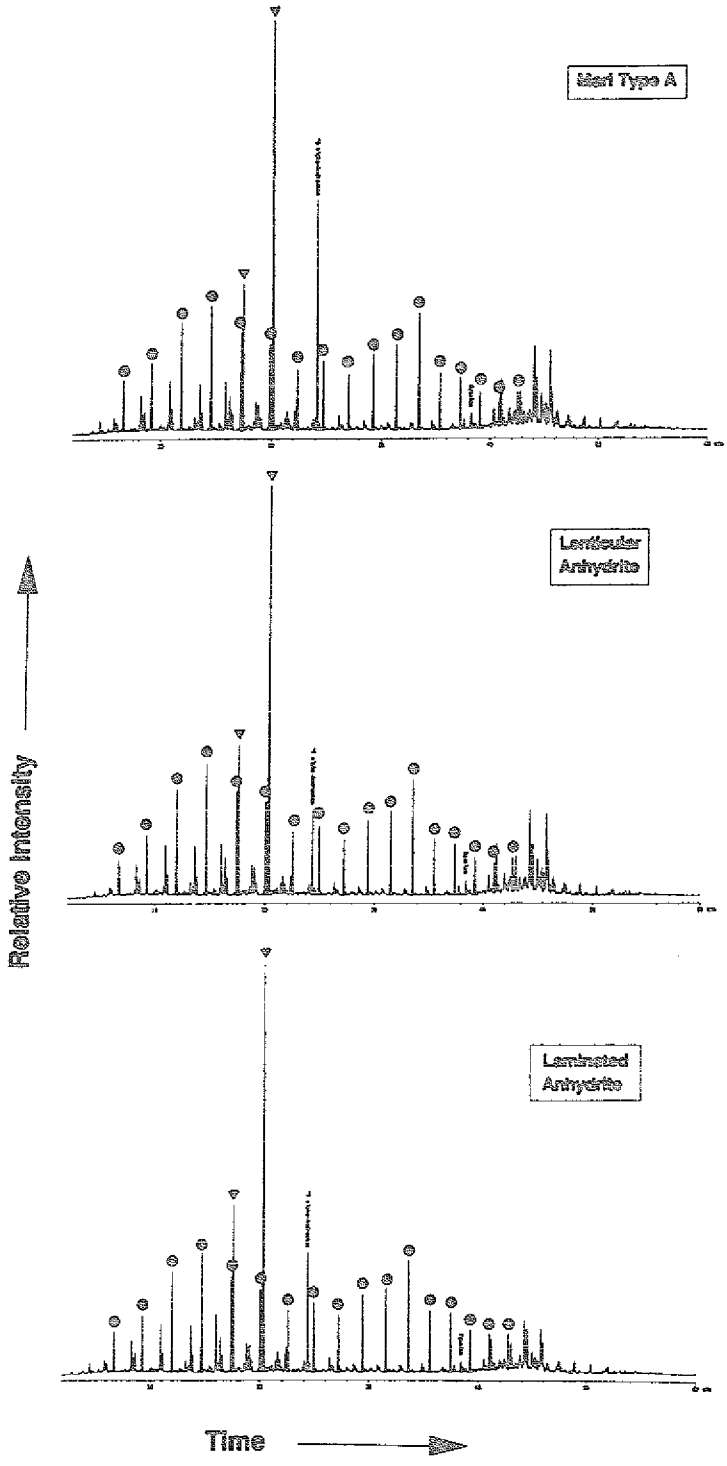

Fig. 41: Examples of the n-alkane distribution patterns of each lithofacies. (Continued on following page.)

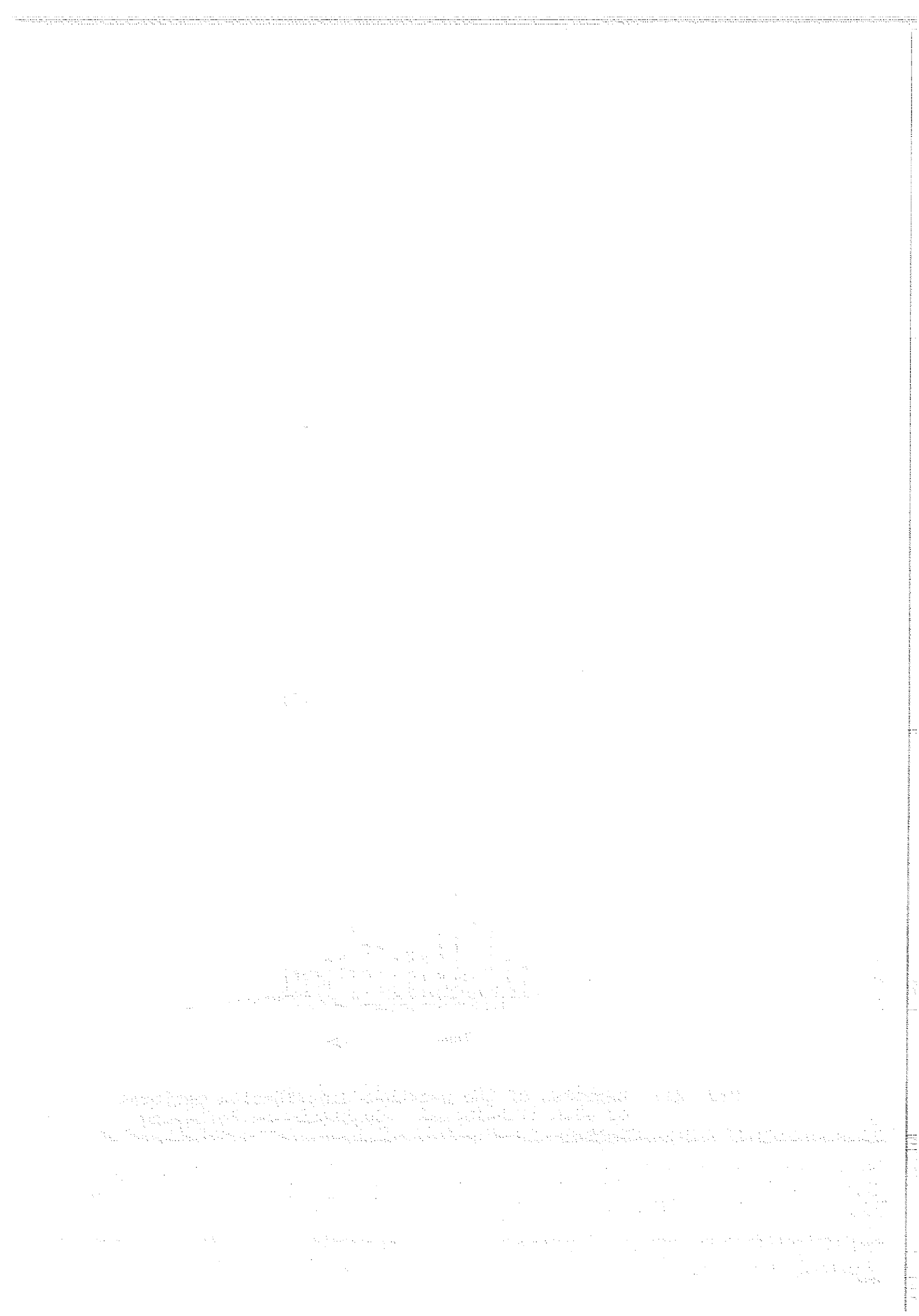

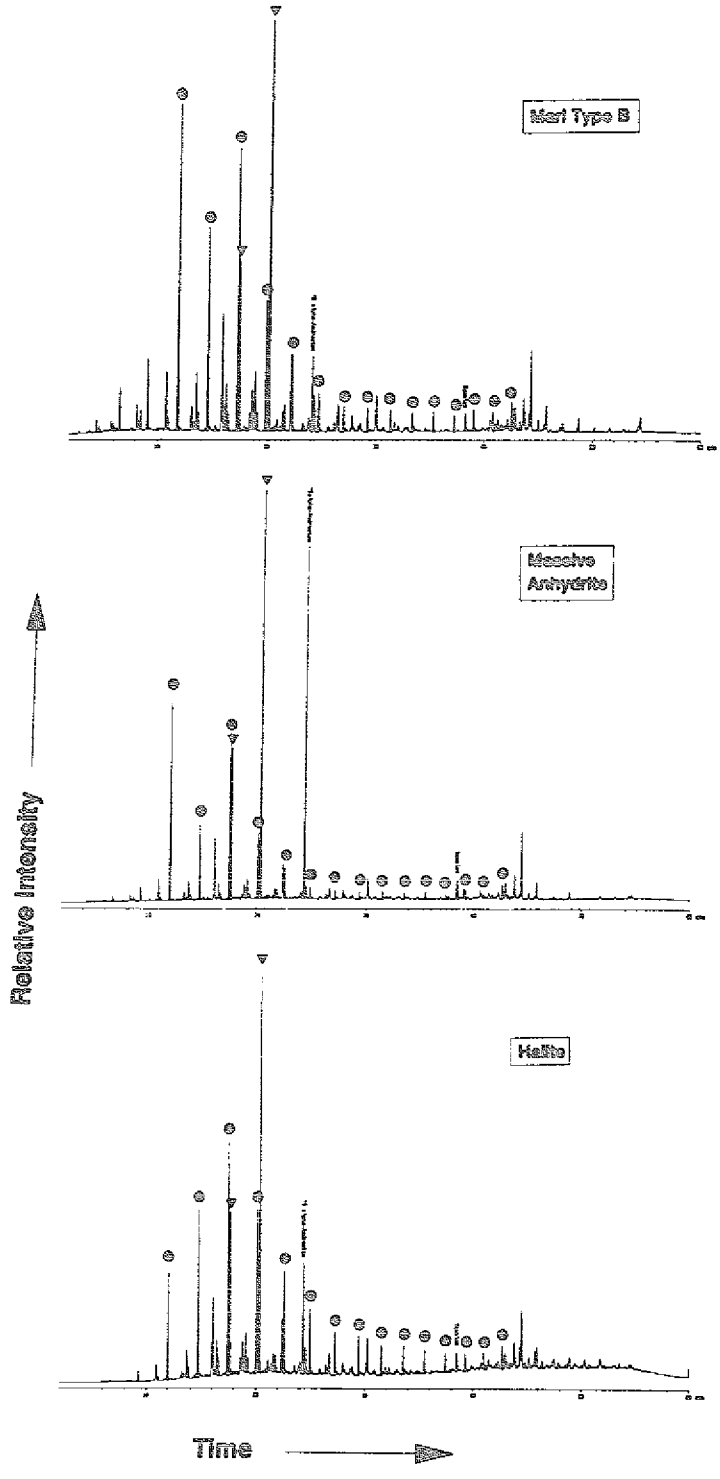

Fig. 41: (Continued from preceding page.) Examples of the n-alkane distribution patterns of each lithofacies.

indices of greater than 1. However, pattern II shows significantly higher light hydrocarbon preference indices (greater than 2.5) than pattern I.

The bimodal n-alkane distribution of pattern I is very similar to n-alkane patterns reported from recent cyanobacteria in New Zealand (Shiea et al., 1991). Extracts of the mats as well as extracts from colonized samples of the mat-building organism *Chlorobium sp.*, a green, sulfur-photosynthetic bacterium, show bimodal n-alkane distributions with n-alkane maxima at C_{17} and C_{25}. N-alkanes in the C_{15} to C_{18} range have also been interpreted to be characteristic for microbial input (Han and Calvin, 1969; Bird and Lynch, 1974). The interpretation of these patterns deriving from microbial mats is further supported by kerogen microscopy, which clearly identifed mat-like structures of amorphous organic matter. Terrestrial contributions to the n-alkane pattern I seem to be of minor importance, because n-alkane components greater than C_{30} are present in relatively low concentrations when compared to the short chain n-alkanes. This interpretation is consistent with the commonly held theory that long chain n-alkanes represent terrestrial (higher plant) input and that short chain n-alkanes represent aquatic input (e.g. Cardoso et al., 1976).

The dominant n-alkanes in pattern II are C_{15} and C_{17}, which are generally attributed to algal sources (Oró et al., 1967; Gelpi et al., 1970; Blumer et al., 1971). This interpretation is also supported by microscopic observations, because alginite (fossil algae) contributes to more than 50% of the visual organic matter of samples that display n-alkane distribution patterns II. The longer chain n-alkanes of pattern II display odd to even carbon preference indices (C_{20}-C_{29} range), which is generally attributed to terrestrial input (e.g. Tissot and Welte, 1984).

3.10.1.2 Isoprenoid Hydrocarbons

The isoprenoid hydrocarbons pristane, phytane and squalane were quantitatively determined. In both patterns I and II (Figs. 39 and 40), phytane is the single most common compound. Pristane is approximately two to six times less abundant than phytane, which gives rise to pristane/phytane ratios ranging from 0.17 to 0.47. Squalane occurs in pattern I in lower quantities than the n-alkanes in the C_{25}-C_{29} range and in pattern II in similar quantities to the n-alkanes in the C_{25}-C_{29} range.

The pristane/phytane ratio in all samples is very low. The common precursor for both of these isoprenoids is the phytol sidechain of chlorophyll (e.g. Didyk et al., 1978).

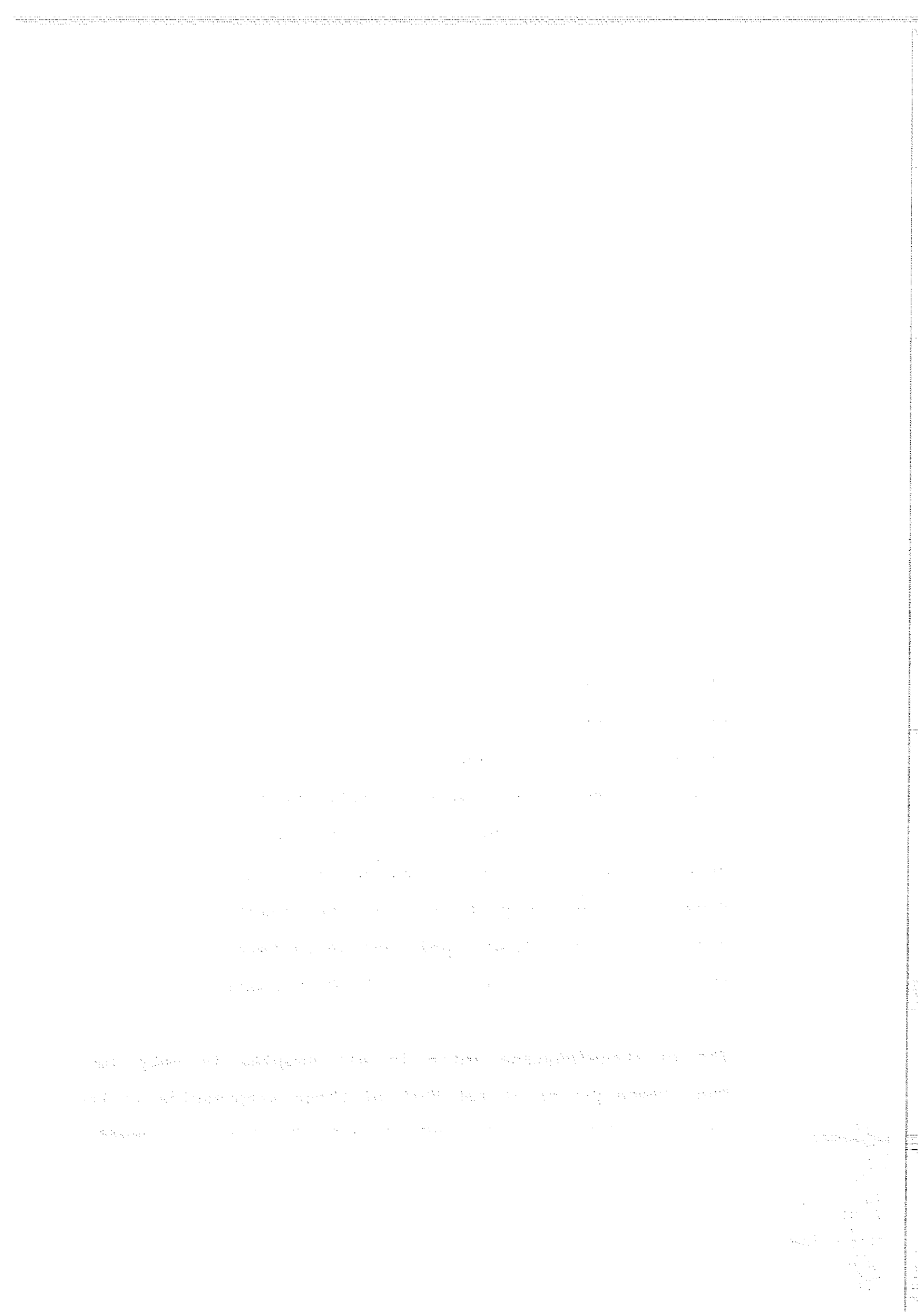

Phytol, a chlorophyll-derived alcohol, has been reported to be the major lipid component in Recent sediment from a Spanish salina in carbonate, gypsum and halite crystallization ponds (Barbe et al., 1990). It is well known that phytol may be a precursor of phytane under reducing conditions. High concentrations of phytane may, therefore, be considered to be an indication of both an input of photosynthetic organisms to the biomass and good preservation conditions. Phytane has also been linked to a phospholipid found in halophilic bacteria (Kaplan and Baedecker, 1970; Nissenbaum et al., 1972) that can be transformed into phytane via the natural breakdown of the isoprenoid glycolether during diagenesis (Welte and Waples, 1973; Waples et al., 1974; Albaiges and Torradas, 1974). These observations led ten Haven et al. (1985) to suggest that low pristane/phytane ratios are not only indicative of a high degree of anoxicity (Didyk et al., 1978), but also can be a salinity indicator.

Squalane, a C_{25} isoprenoid, is present in each sample. Ten Haven et al. (1988) found squalane in bitumen and oils from evaporite rocks from Italy. Fu Jiamo et al. (1986) also reported squalane as a major component from a Paleogene saline lake in China. This compound has also been reported in bitumen from evaporite source rocks and derived oils from Brazil (Mello et al., 1988a, 1988b). Squalane has been interpreted to originate either from

methanogenic or halophilic bacteria (Holzer et al., 1979; Brassell et al., 1981), and hence can be used as an indicator for bacterial input.

3.10.2 Aromatic Hydrocarbons

Selected naphthalenes and phenanthrenes were quantitatively determined from the aromatic hydrocarbon fraction. All analyzed samples showed very similar distribution patterns of these compounds. Neither of these compounds is known to occur in living organisms or in unpolluted Recent sediments (Radke, 1987). Thus, low molecular weight aromatic hydrocarbons, which generally represent major portions of the crude oils, are not likely to be derived from early diagenetic processes (Radke, 1987), and hence do not contain significant paleoenvironmental information. The absolute quantities of these compounds, however, vary from sample to sample and are useful in addressing problems in hydrocarbon generation and migration (see Chapter 4).

Sinninghe Damsté et al. (1990) and Betts et al. (1991) recorded two distinctly different alkyltoluene and alkylbenzene patterns, which correspond respectively to the two organic facies previously defined (see Characterization of Kerogens, Chapter 3.9.1). The environmental significance of these compounds is not yet

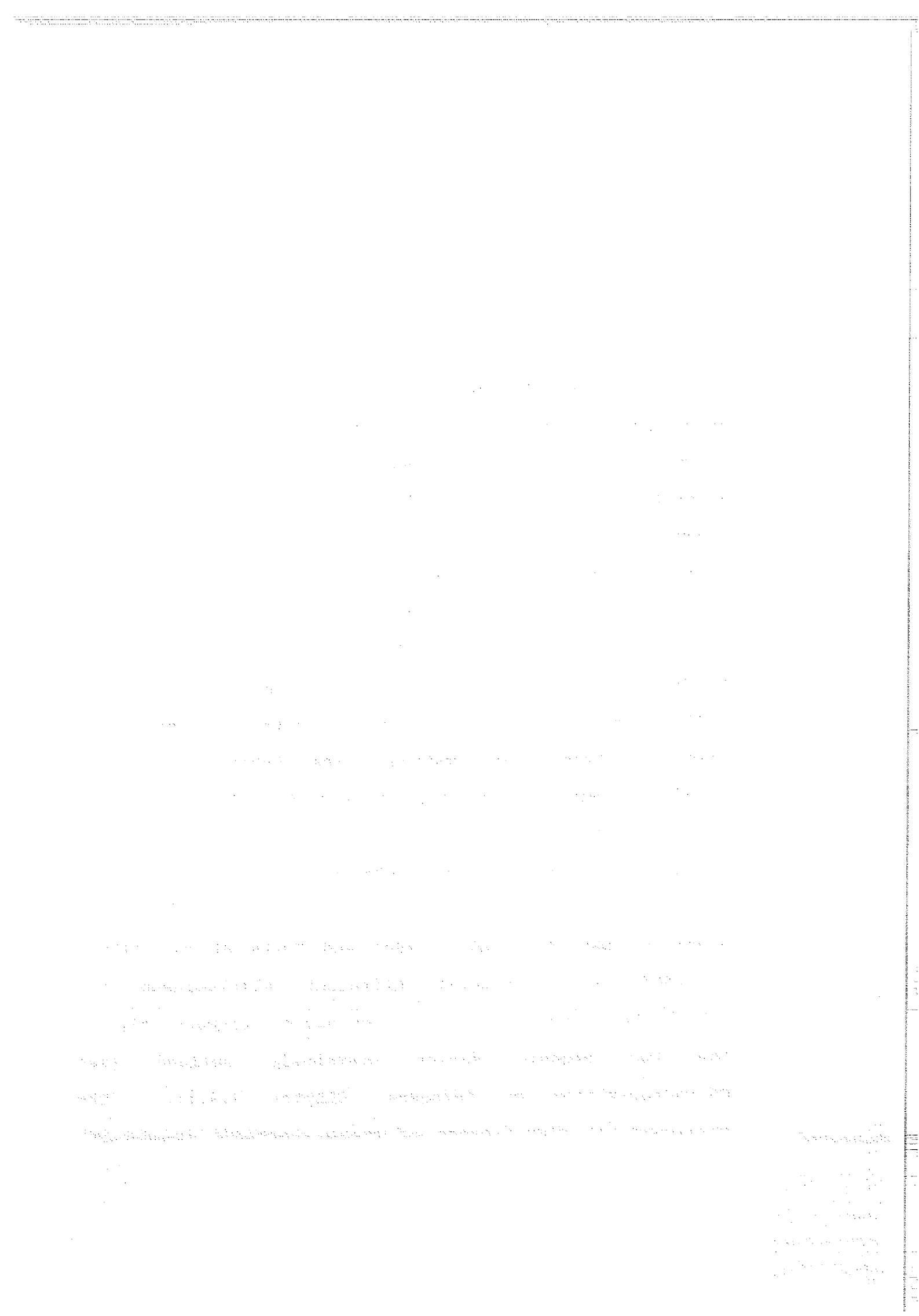

known. However, the predominance of individual long chain alkylbenzenes and alkylnaphthalenes in samples from a sabkha environment led Connan et al. (1986) to suggest a genetic relationship of these compounds to rather common structures in various bacteria. In the extracts from samples that contain kerogens of organic facies A, Sinninghe Damsté et al. (1990) also identified two alkylbenzenes with isoprenoid side-chains, which are derived from archaebacteria and have been suggested to be indicative of hypersaline paleoenvironments (Sinninghe Damsté et al., 1988).

3.10.3 Sulfur Aromatic Hydrocarbons

The distribution of selected alkylbenzothiophenes, dibenzothiophenes and alkyldibenzothiophenes was determined for samples of all observed lithofacies. For several samples from marls of type A and marls of type B the concentration of dibenzothiophene and methyldibenzothiophene was also quantitatively assessed. Two general distribution patterns, which correlated with previously defined organic facies A and B, could be discriminated. The sulfur aromatic distribution pattern associated with organic facies A is characterized by similar relative abundances of the major peaks of the alkylbenzothiophenes on the one hand and the dibenzothiophenes and alkyldi

benzothiophenes on the other hand (Fig. 42). In samples containing organic facies B, dominance of the dimethylbenzothiophenes and trimethylbenzothiophenes over the dibenzothiophene and alkyldibenzothiophenes was observed (Fig. 43). Generally, marls of type A that contain organic facies A are richer in dibenzothiophenes and methyldibenzothiophenes than are marls of type B and organic facies B, respectively.

Even though the geochemistry of sulfur in fossil fuels has received growing interest in the last 15 years (e.g. Orr and White, 1990), little is known about the origin and behaviour of organic sulfur compounds in petroleum and bitumen. It is generally believed that many organic sulfur compounds form during early diagenesis, because organic-bound sulfur in natural organisms is exceedingly rare (Orr and Sinninghe Damsté, 1990). Benzothiophenes and dibenzothiophenes are known to be present in low quantities in immature rocks (for rocks from hypersaline environments, see e.g. Kenig and Huc, 1990; Rullkötter et al., 1990), but become the dominant organic sulfur compounds in mature oils (Thompson, 1981). Cyclicitation and aromatization of selected dialkylthiophenes have been interpreted to be major pathways for the formation of alkylbenzothiophenes (Perakis, 1986; Sinninghe Damsté et al., 1987, 1988). Even though the benzothiophenes and

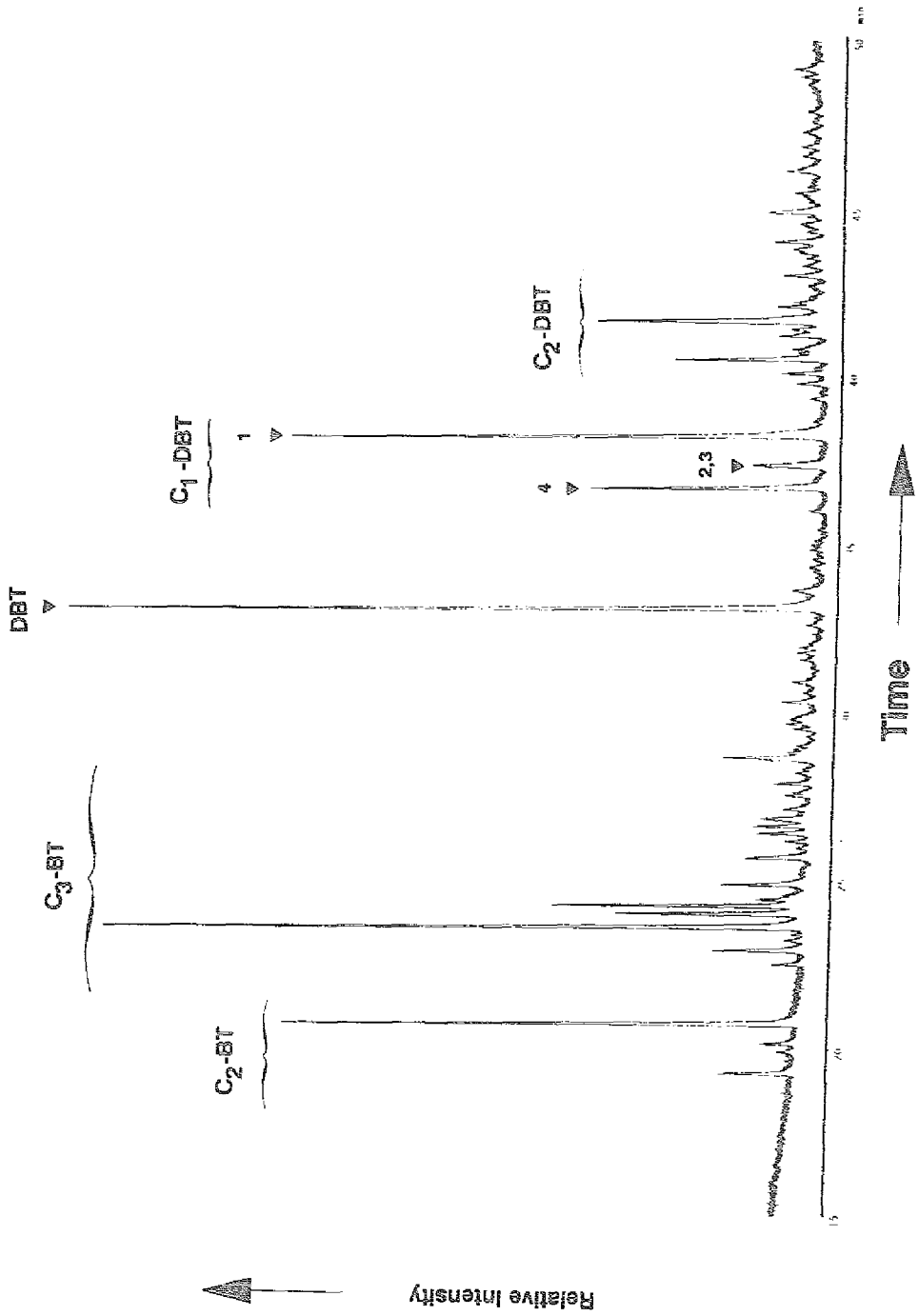

Fig. 42: Distribution patterns of selected sulfur aromatic compounds. The pattern is representative for the marls of type A, laminated anhydrite and lenticular anhydrite lithofacies. (C_2-BT = dimethylbenzothiophenes, C_3-BT = trimethylbenzothiophenes, DBT = dibenzothiophene, C_1-DBT = methyldibenzothiophenes, C_2-DBT = dimethyldibenzothiophenes).

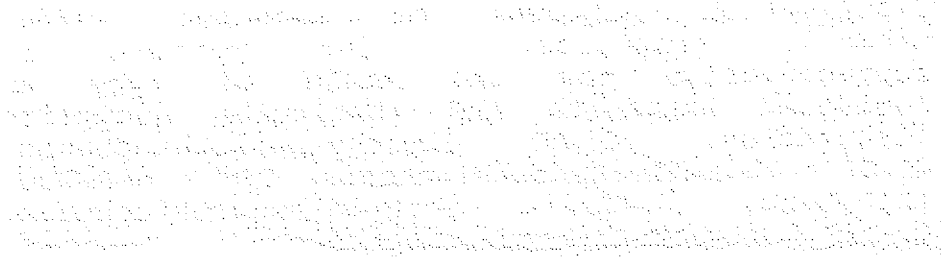

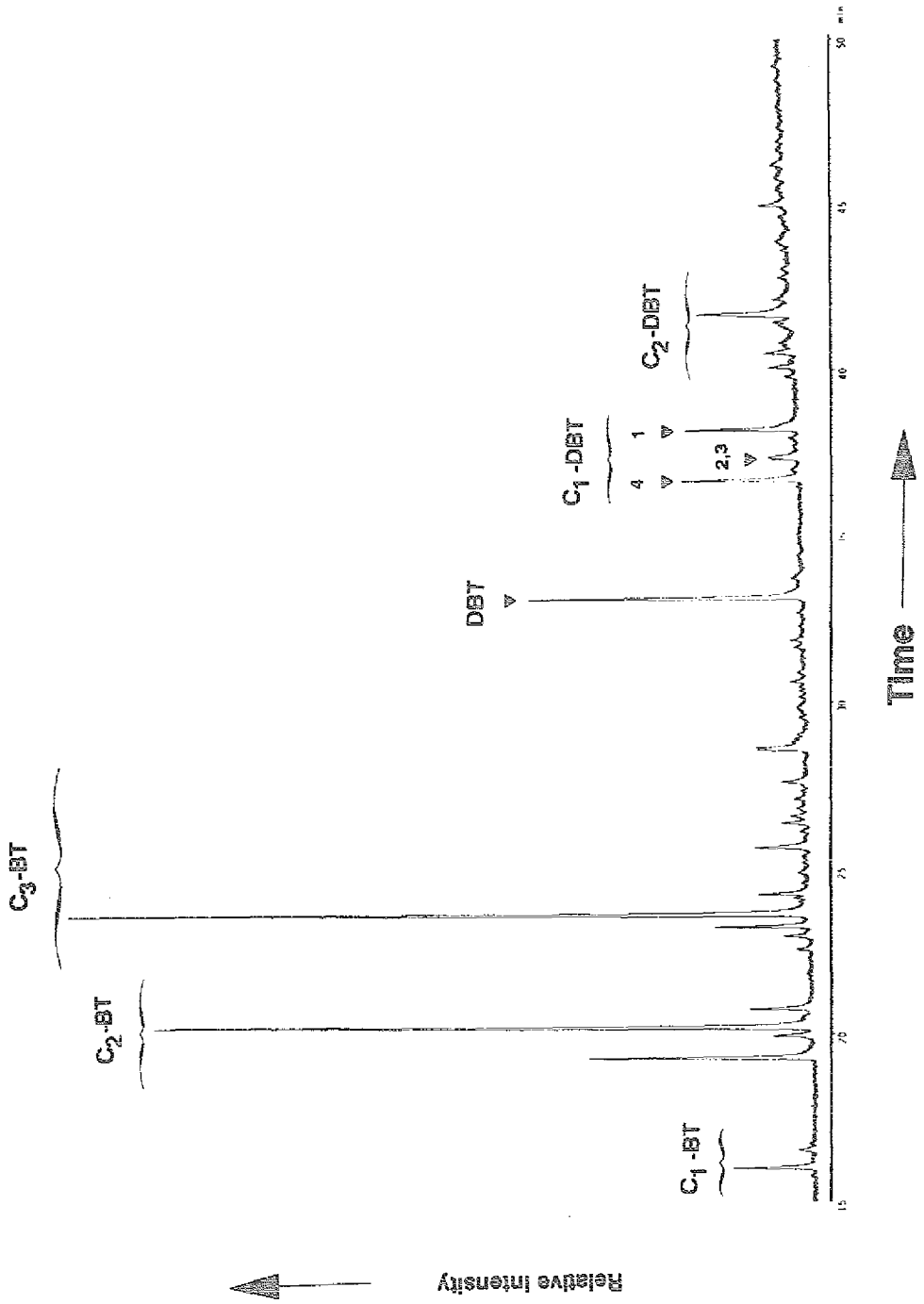

Fig. 43: Distribution patterns of selected sulfur aromatic compounds. The pattern is representative for the marl of type B, massive anhydrite and halite lithofacies. (C_2-BT = dimethylbenzothiophenes, C_3-BT = trimethylbenzothiophenes, DBT = dibenzothiophene, C_1-DBT = methyldibenzothiophenes, C_2-DBT = dimethyldibenzothiophenes).

dibenzothiophenes cannot, therefore, be considered biological markers, they have been noted to be useful in maturity studies and kerogen classification (Radke et al., 1986; Hughes, 1984; Philp and Lewis, 1987). The close correlation between the petrologically defined organic facies and the molecular composition of aromatic sulfur compounds gives rise to hopes that benzothiophenes and dibenzothiophenes will prove to be useful facies indicators in the future.

3.11 RHYTHMIC ORGANIC CARBON SEDIMENTATION

The sedimentation of organic matter associated with marl beds of the Salt IV unit has been interpreted to follow cyclic depositional patterns (Blanc-Valleron, 1991; Blanc-Valleron et al., 1991). Each cycle is characterized by a variation of the organic carbon contents of its marl beds. A cycle starts with a low organic carbon content (usually on the order of 0.5% TOC) and reaches a "TOC maximum," (up to 7% TOC) and then drops back to carbon contents below 1% TOC. One of these "TOC cycles" was noted in the stratigraphic interval ranging from the upper part of the S1 unit to the top part of the CI unit (Fig. 44). At Amelie II, the organic carbon content at the base of the cycle (S1 unit) is approximately 0.8% TOC. Going up through the cycle, the TOC increases gradually up to 4.6% TOC and drops back to approximately 1% TOC (CI unit). A single depositional cycle can contain different quantities of organic carbon at different locations in the basin. At the Max site a maximum TOC of 7% is reached (Blanc-Valleron et al., 1991), whereas at Joseph Else 4%, Ungersheim 3.7%, and Berrwiller 4.3% TOC maxima have been measured.

To elucidate the nature of the observed TOC cycles in the marls of the S unit, site Amelie II was studied in more

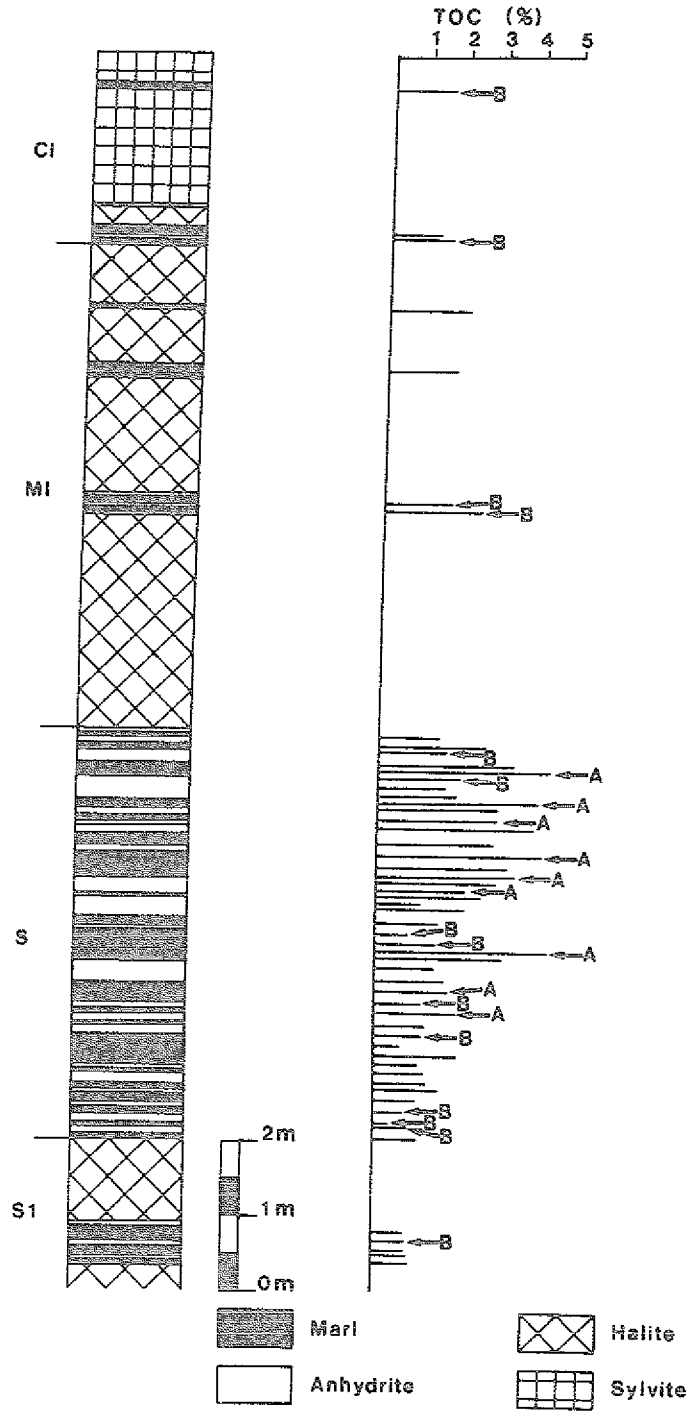

Fig. 44: TOC content of the marl beds at Amelie II. Note the cyclic increase and decrease of the organic carbon content from S1 to the CI unit. The samples marked with A and B refer to samples containing organic facies A and B.

detail. The rate of carbon accumulation of sediments in any environment is dependent on primary productivity, preservation conditions and sedimentation rate (e.g. Demaison and Moore, 1980). Primary productivity and preservation conditions are generally difficult to assess. Sedimentation rates, however, can under certain circumstances be measured within a satisfactory degree of confidence (see Chapter 3.6). A comparison of the amount of organic carbon and the sedimentation rates of marl samples of the entire "TOC cycle" shows that a linear relationship exists between both parameters (Fig. 45). Samples with high amounts of organic carbon correspond to low sedimentation rates, whereas samples with low amounts of organic carbon correspond to samples with high sedimentation rates. This observation suggests that the joint effects of bioproductivity and preservation conditions remained fairly constant throughout this time interval. Varying sedimentation rates led to a dilution or concentration, respectively, of the more or less constant organic matter inputs. This relationships suggests that at least in a first order approximation, sedimentation rate variation can be held responsible for the observed rhythmic TOC sedimentation. Furthermore, this relationship also explains the low TOC content of the anhydrite and halite samples, because sulfates and halite usually have substantially higher sedimentation rates than

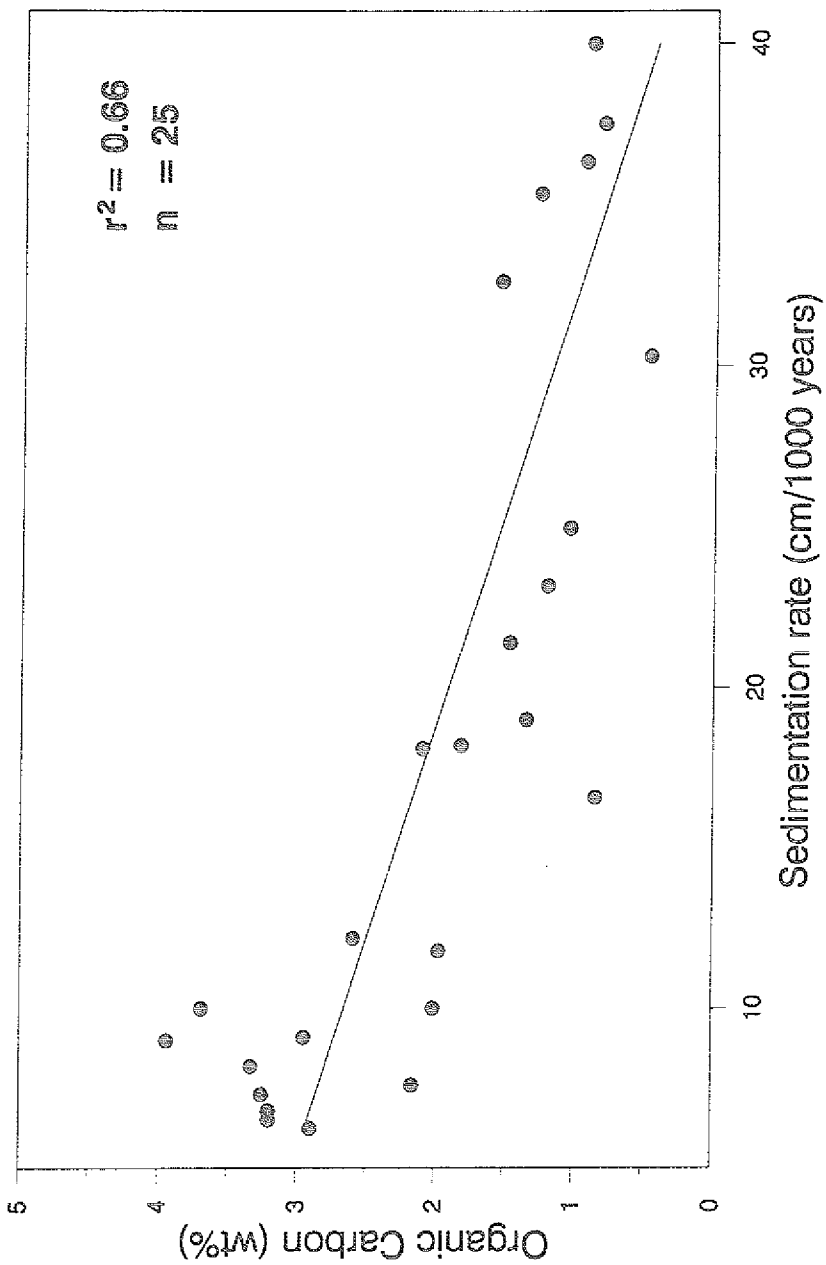

Fig. 45: Relationship between sedimentation rate and organic carbon content of the marls at Amelie II. (n = number of samples. r^2 = correlation coefficient).

marls (sulfates 1-40 m/10^3 years; halite 10-100 m/10^3 y; Schreiber and Hsü, 1980). The scattering of the data indicates that although edimentation rate is probably the key factor in regulating organic carbon accumulation (Fig. 45), other influences cannot be completely ruled out.

3.12 ORGANIC CARBON ACCUMULATION RATE

The relationship between organic carbon content and sedimentation rate can also be expressed as the "organic carbon accumulation rate" (for calculations see Methodology, Chapter 2). The calculated organic carbon accumulation rates for the "TOC cycle" at Amelie II demonstrate that organic matter accumulation is generally high (0.4-1.4 gC/cm^2ky). Stein et al. (1989a and 1989b), Stein and Littke (1990), and ten Haven et al. (1990) report significantly lower carbon accumulation rates for clastic sediments from Baffin Bay and the upwelling area off northwest Africa, the Oman margin, and the Peru margin (ODP sites 645, 658, 679, and 723, respectively) of 0.05 to 0.5 gC/cm^2ky. The highest organic carbon accumulation rates of the lower Salt IV zone are recorded from marl beds that were deposited in halite-dominated intervals (calculated greater than 1 gC/cm^2ky; Fig. 46, S1, MI, CI). Organic carbon accumulation rates for marls from the anhydrite and marl-rich S unit, however, show considerable variation and generally lower values than halite-rich intervals. Three factors can influence the organic carbon accumulation rates: 1) changing preservation conditions, 2) fluctuation in paleoproductivity, and 3) variations in the degree of influx of terrestrial organic matter.

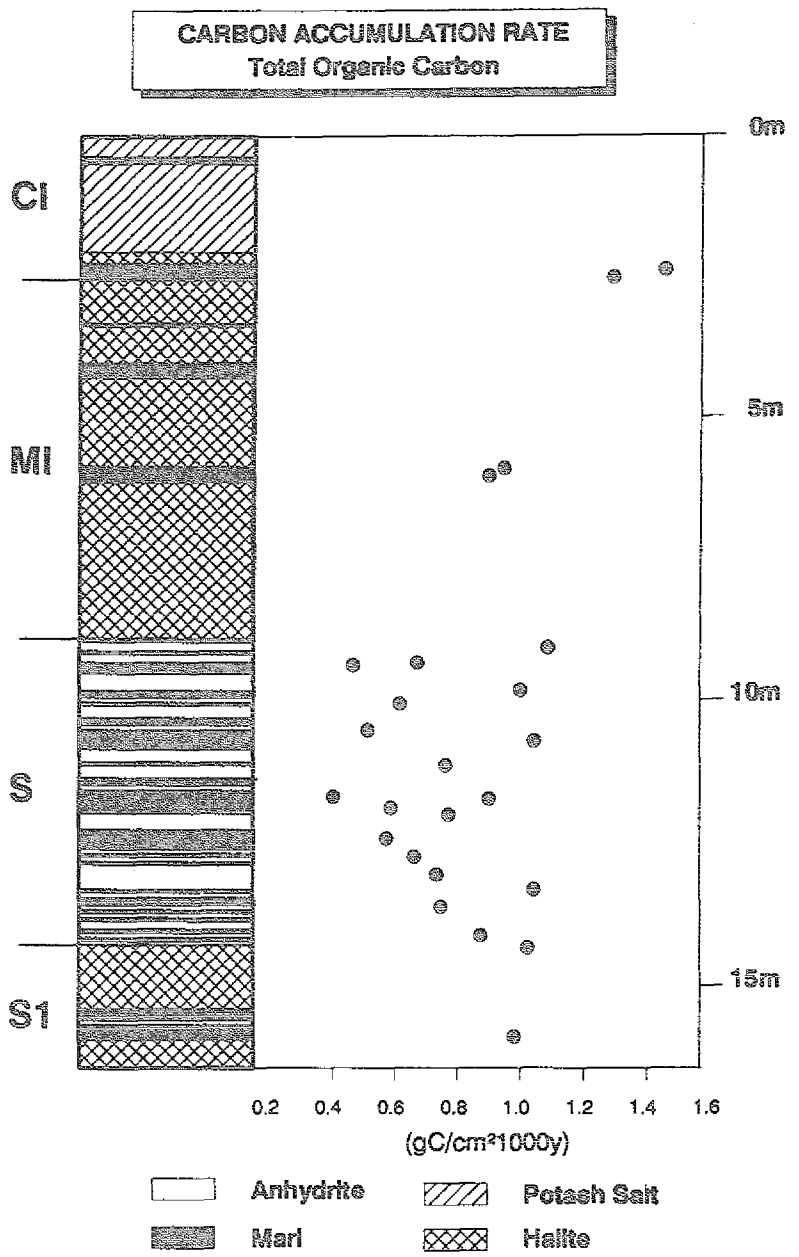

Fig. 46: Organic carbon accumulation rate for the marls at Amelie II. (For details see text and methodology chapter).

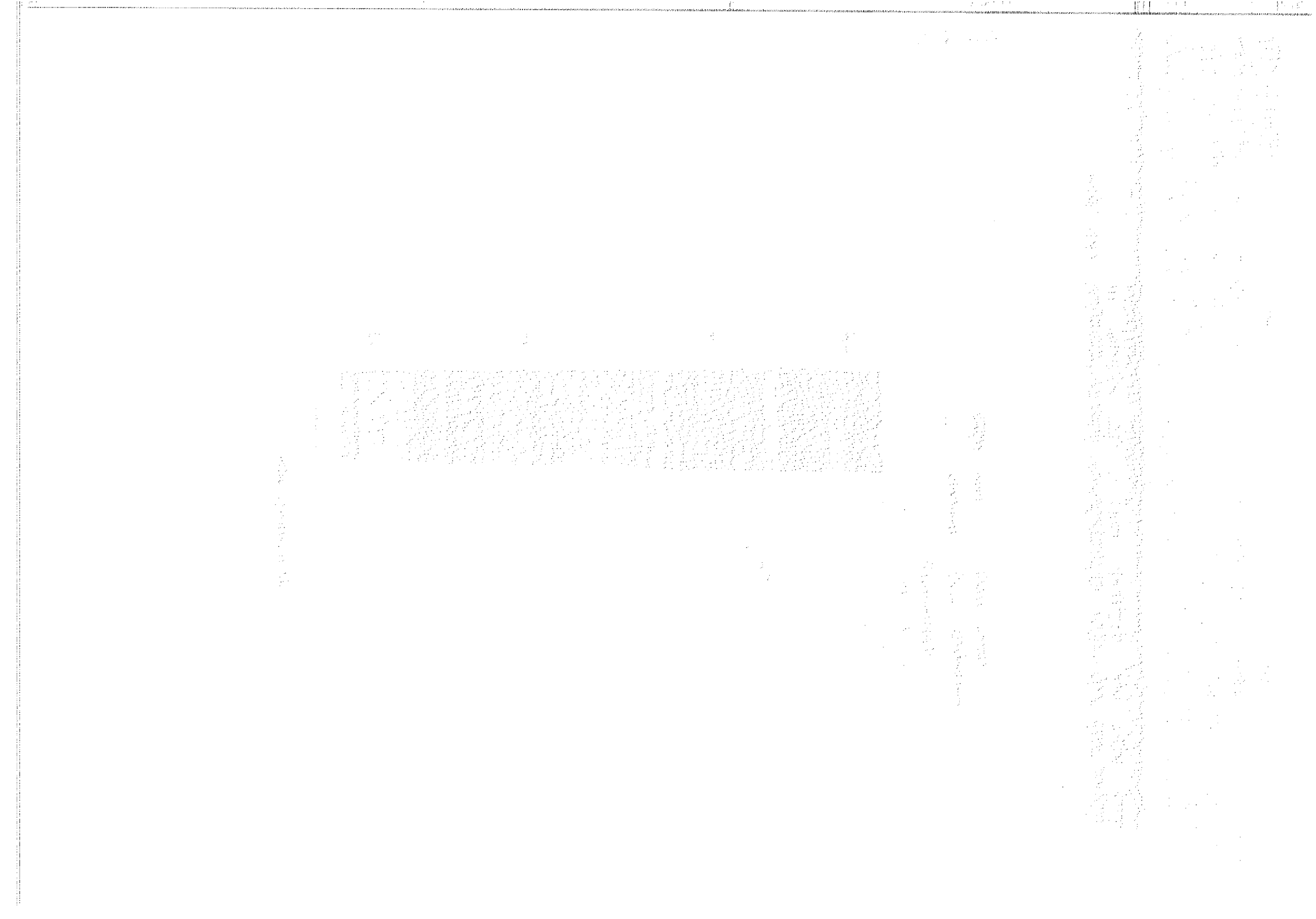

3.13 PRESERVATION CONDITIONS

It is generally agreed that extensive preservation of organic matter requires anoxic conditions (Demaison and Moore, 1980; Deuser, 1971; Hunt, 1979; Tissot and Welte, 1984). Keys to the reconstruction of the level anoxicity in ancient depositional environments are 1) little to no bioturbation of the sediment, 2) in environments with detrital Fe^{2+} influx, the presence of early diagenetic pyrite (Berner, 1981, 1983), and 3) low pristane/phytane ratios of the bitumen (Didyk et al., 1978).

Bioturbation is caused by bottom dwelling organisms that require oxic conditions to sustain life. A general characteristic of bioturbated sediments is a well reworked substrate that lost most of its depositional structures. The marls of the S1 to CI units, however, show a well developed lamination that was not disrupted on any visible scale. It is, therefore, unlikely that bioturbation took place during or after the deposition of the marls from this interval.

Another indicator for reducing depositional environments and hence conditions that favor the preservation of organic matter is the presence of early diagenetic pyrite. Pyrite is a common mineral in all marl samples studied. Most of the pyrite occurs as framboids and is closely

interconnected with organic matter. It is generally accepted that framboidal pyrite represents an early diagenetic mineral phase (Berner, 1983). The formation of early diagenetic pyrite requires the presence of abundant H_2S resulting from bacterial sulfate reduction. Reducing conditions are favorable for the preservation of organic matter. The high abundance of pyrite in the marls of the S1 to CI unit is, therefore, a good indicator for the prevalence of reducing conditions in the pore waters of the sediments during and even after deposition.

The pristane/phytane ratio of bitumens has been suggested as a chemical measure for the degree of anoxicity (Didyk et al., 1978). Low pristane/phytane ratios (< 1) in extracts from immature sediments are interpreted to be indicative of anoxic conditions during the deposition of the sediments. Pristane-phytane ratios greater than 1 are thought to develop when oxic conditions prevail during sedimentation. All sediments of the S1-CI unit display pristane/phytane ratios lower than 0.47. A plot of the organic carbon normalized yields of pristane and phytane (Fig. 47) shows a covariation of both compounds, indicating a constant and uniform source for both isoprenoids and similar preservation conditions for all samples.

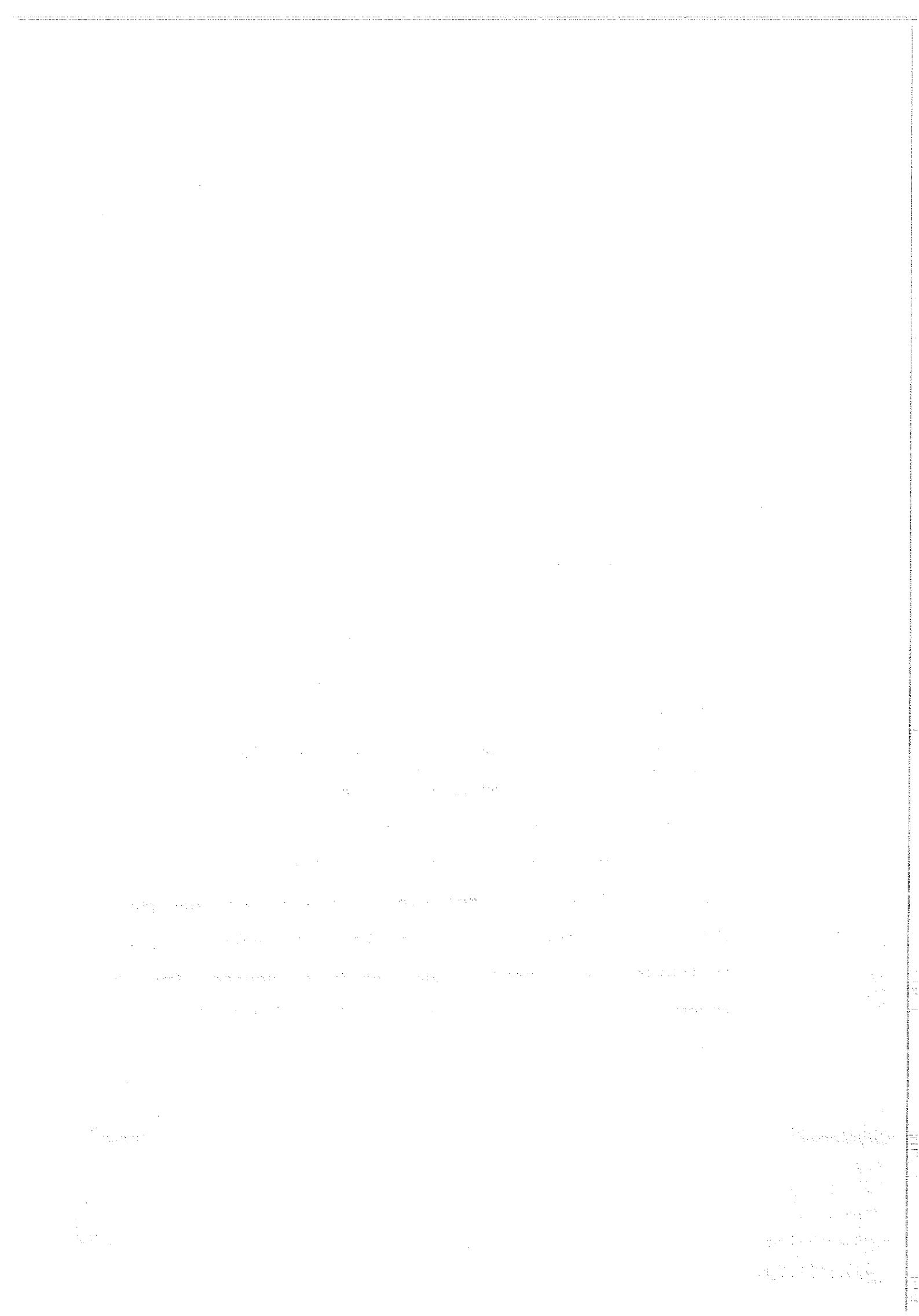

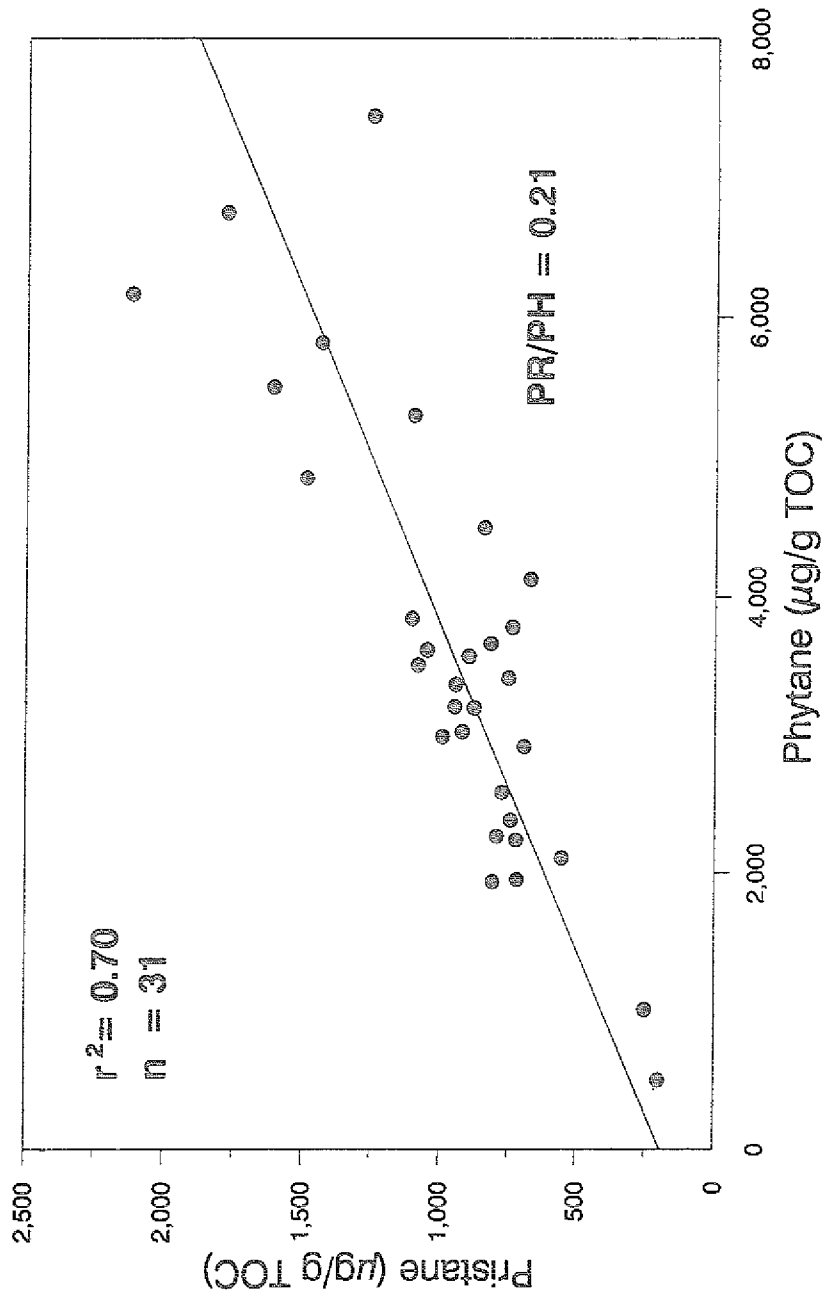

Fig. 47: Co-variation of pristane and phytane content of the sediments of all lithofacies at Amelie II.

3.14 PALEOPRODUCTIVITY AND ACCUMULATION OF TERRESTRIAL ORGANIC MATTER

Because three lines of evidence indicate that the preservation conditions for organic matter at the time of deposition were excellent and fairly uniform for all marl samples of the S unit, there must be additional reasons for the observed variation in the apparent accumulation rate of organic carbon (Fig. 46).

The organic matter of a rock can basically be derived from terrestrial or aquatic sources. Terrestrial organic matter consists mainly of humite/vitrinite (remnants of woody tissues) and inertinite (charcoal-like fragments), but can also contain specific liptinite macerals (e.g. sporinite, cutinite). Aquatic organic matter consists mainly of alginite and liptodetrinite of algal and bacterial origin (Stach et al., 1982; Teichmüller, 1986). Based on this division, accumulation rates of terrestrial and aquatic organic matter for the S unit can be calculated (Fig. 48; see Methodology). The accumulation rates for terrigenous organic matter show a decrease in carbon accumulation from initially 2-3 gC/cm^2ky at the base of the S unit to rates of less than 0.5 gC/cm^2ky in the middle part. The accumulation rates stay fairly constant at 0.5 gC/cm^2ky from the middle part of the

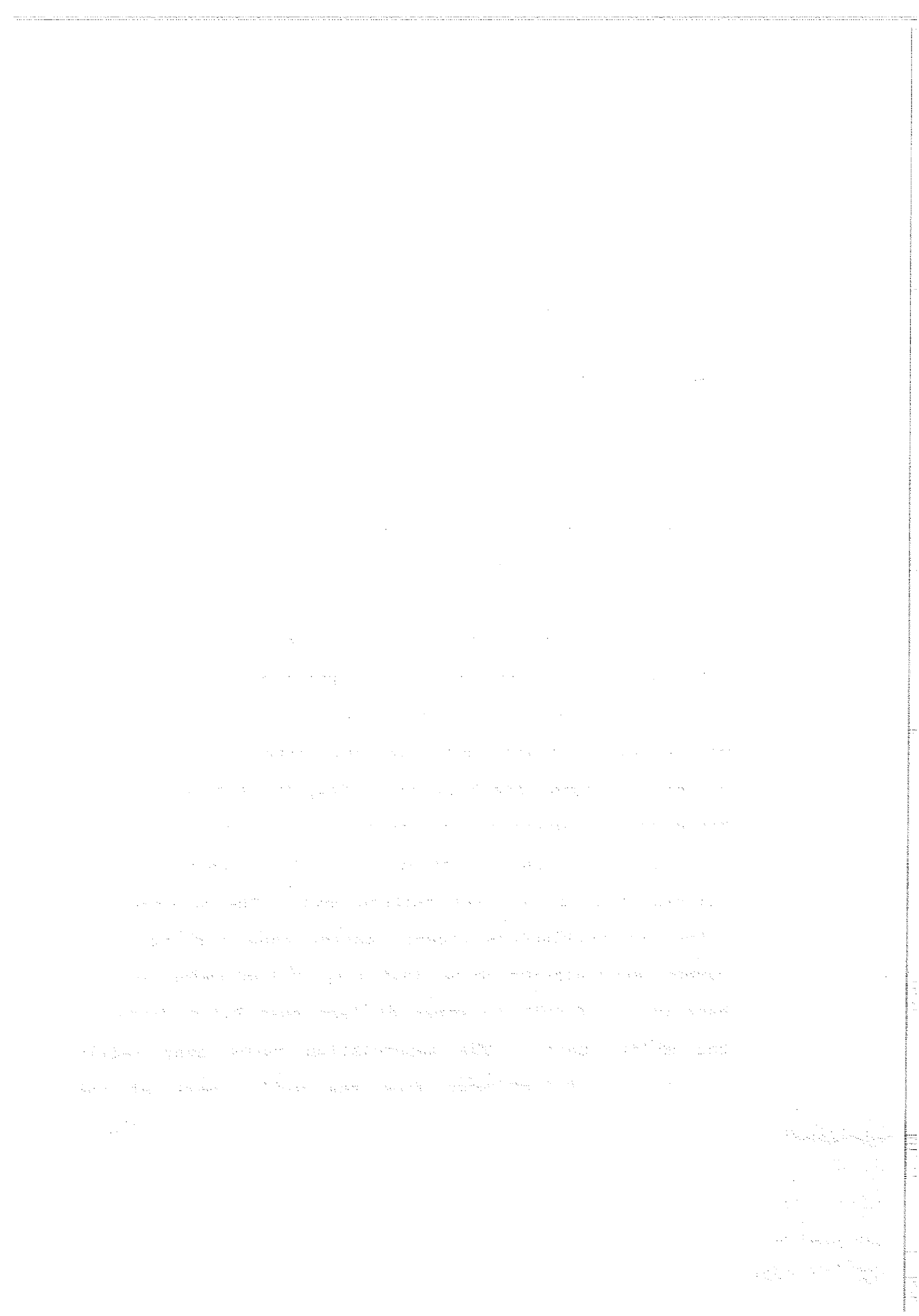

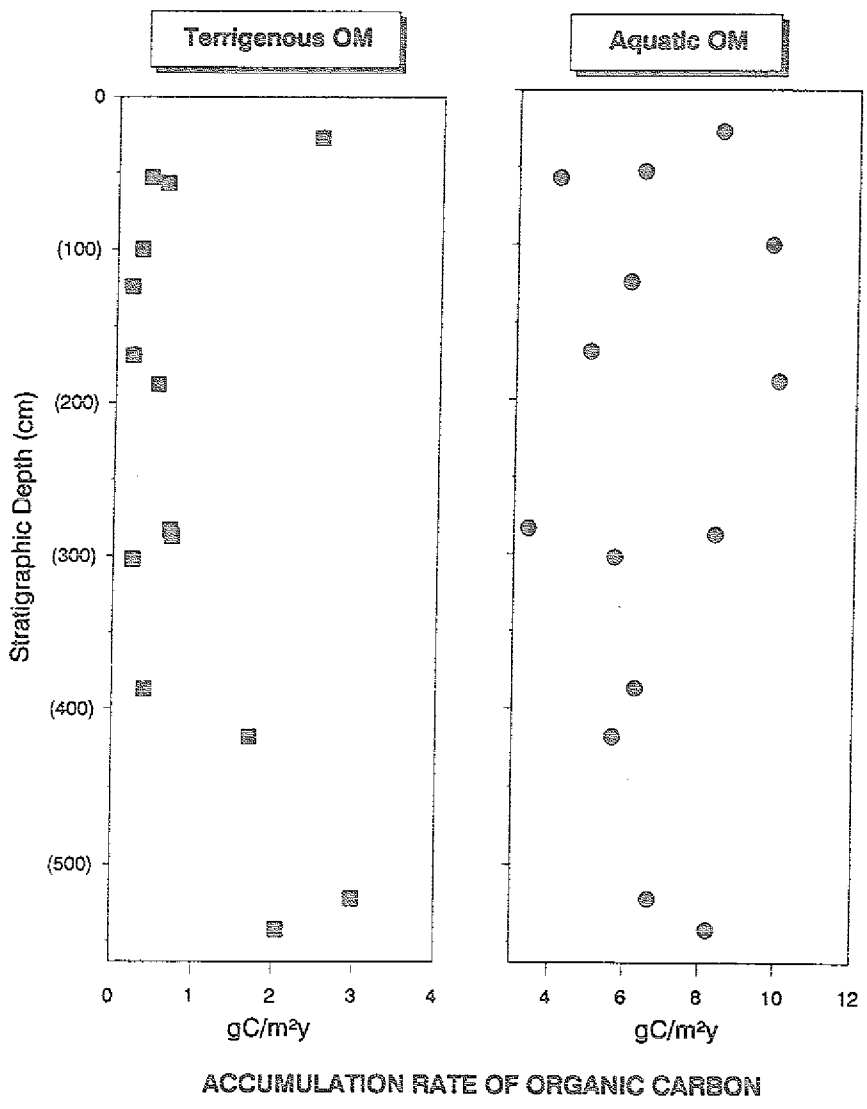

Fig. 48: Accumulation rates for terrigenous and aquatic organic matter of the marls at Amelie II. (For details see text).

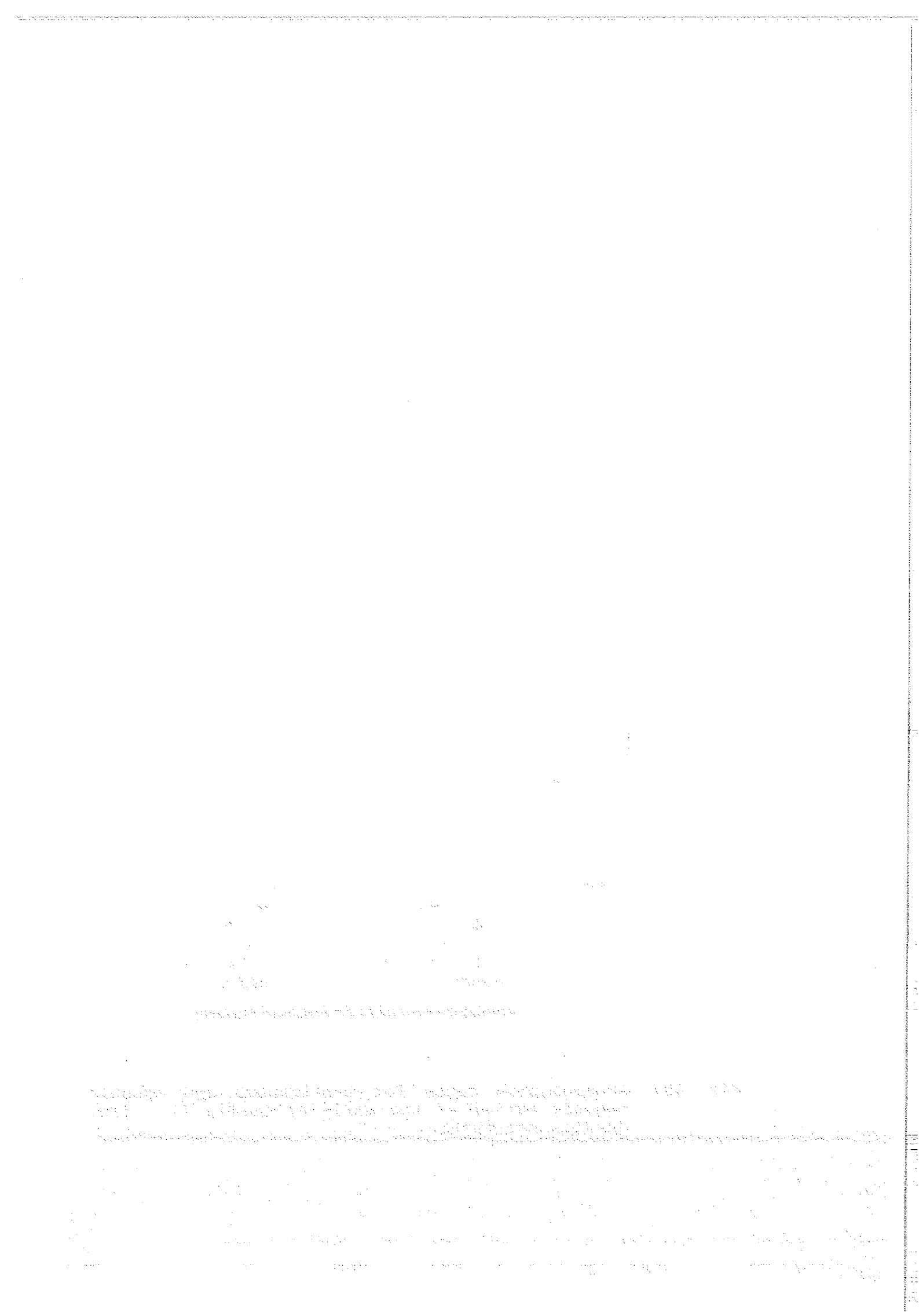

S unit almost to the top, when an abruptly higher influx of terrestrial organic matter occurs (~2.5 gC/cm^2ky). The accumulation rates for aquatic organic matter are considerably higher (3-10 gC/cm^2ky) and show stratigraphy-related fluctuations (Fig. 48).

Terrigenous organic matter is relatively resistant to oxic decomposition (Tissot et al., 1979; Waples, 1983), therefore, changes in the accumulation rate of such terrigenous materials are primarily controlled by changes in rates of supply rather than variations in preservation (Stein and Littke, 1990). Furthermore, the size of the organic particles is mainly a function of transport mode, distance, and transport energy and can, therefore, also be used as a paleoenvironmental indicator (e.g. Stein et al., 1988; Stein and Littke, 1990). The gradual decrease in the accumulation rates of terrigenous organic matter in the lower part of the S unit therefore reflects a change in the rate of supply of organic matter from terrigenous sources. The small size of most of the particles of terrigenous organic matter suggests that the source of the organic matter may lie some distance away from the area of deposition. The cause of the fluctuation of the accumulation rate may then either be changes of the productivity of the source area or changes in the mode (fluvial or wind driven) or rate of transportation.

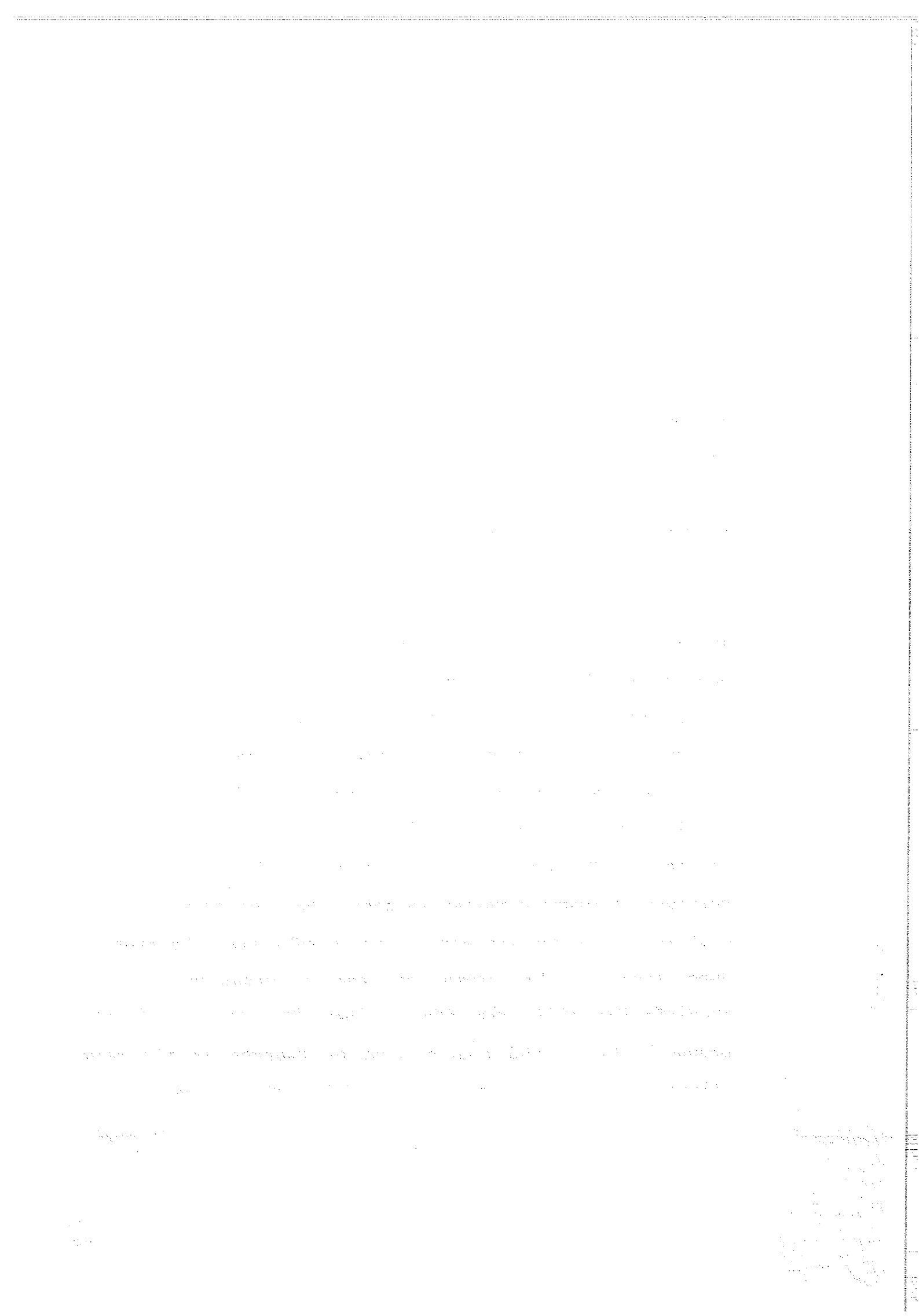

Aquatic organic matter, in contrast to terrigenous organic matter, stems from autochthonous rather than allochthonous sources. The accumulation rates of organic carbon derived from aquatic organisms are mainly controlled by the rate of supply (bioproductivity) and/or preservation conditions (Tissot and Welte, 1984). Because preservation conditions appear to have been fairly uniform during the deposition of the S unit (see previous discussion), the variation in the accumulation rate data for aquatic organic carbon most likely reflects paleoproductivity variations. At this stage of investigation, it is not yet possible to estimate paleoproductivity from aquatic carbon accumulation rates. Unlike those for the open oceans (e.g. Stein and Littke, 1990), carbon fluxes from the productive water column to accretion in the sediment pile have not been determined for evaporite environments.

If changes in the accumulation rate of aquatic organic matter are interpreted as a function of paleoproductivity, then conditions favorable for primary production must have prevailed during the deposition of the upper part of the S unit. Primary organic matter production in hypersaline environments is favored by a high nutrient flux. The nutrients that govern primary productivity in a modern evaporite setting are NH_4^+, NO_3^-, and PO_4^{3-} (Javor, 1989). Phosphate concentrations are usually lower than NH_4^+ and NO_3^- concentrations in many modern hypersaline environments

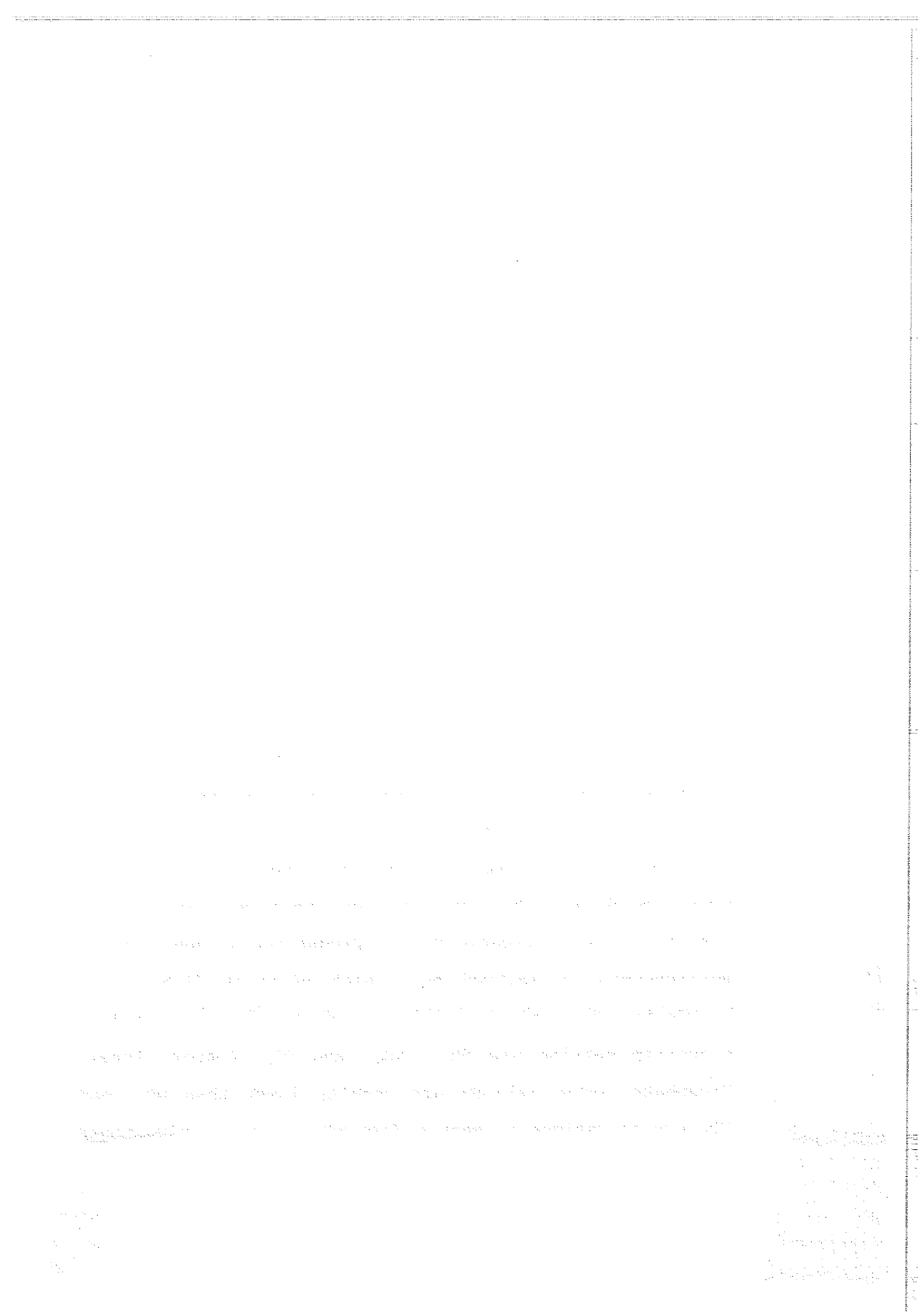

other than soda lakes (Javor, 1989). Ammonia, however, is known to be concentrated by evaporation and may accumulate in evaporite salts (Sonnenfeld, 1984). The importance of nitrogen compounds as nutrients in the organic matter of the S unit is supported by observations of Hollander and Huc (1991). They demonstrated that extremely heavy $\delta^{15}N$ values of the kerogens (+11 to 16 per mil) in all marl facies imply that there was an active nitrogen cycle operating (nitrate and/or ammonia uptake and denitrification). Evaporation causes a concentration of nutrients in the remaining brine concomitant with an increase in salinities. A higher nutrient supply may result in periods of higher productivity. The influence of increasing salinity on the accumulation of organic matter-rich rocks in the upper part of the S unit has also been postulated by Sinninghe Damsté et al. (1991). He and his co-workers measured chroman ratios that indicate that marls of type A were deposited under more saline conditions than marls of type B.

3.15 CONTROLLING FACTORS IN THE FORMATION OF ORGANIC-RICH BEDS IN THE S UNIT

Recently Pedersen and Calvert (1990) reexamined the controls on the formation of organic carbon-rich sediments and sedimentary rocks in oceanic environments. They came to the conclusion that anoxia, *per se*, does not produce organic-rich shales, but that temporal and spatial variation of primary production is a more plausible explanation for the sporadic occurrence of carbon-rich shales (Parrish and Curtis, 1982). In source rocks from the Mulhouse Basin, the paleoproductivity, which was measured indirectly via the accumulation rate of aquatic organic carbon, shows no direct relationship to the amount of aquatic organic carbon. The primary control on the accumulation of organic-rich source rocks in this shallow evaporite basin is the rate of sedimentation. Organic-rich marls (TOC > 2%) accumulate only when the sedimentation rate is low. However, high primary production of organic matter as recorded in many modern environments aids the rapid formation of evaporite source rocks (e.g. Javor, 1989 and many references therein). However, high productivity alone in a depositional regime with high sedimentation rates will not necessarily lead to the deposition of organic matter-rich rocks.

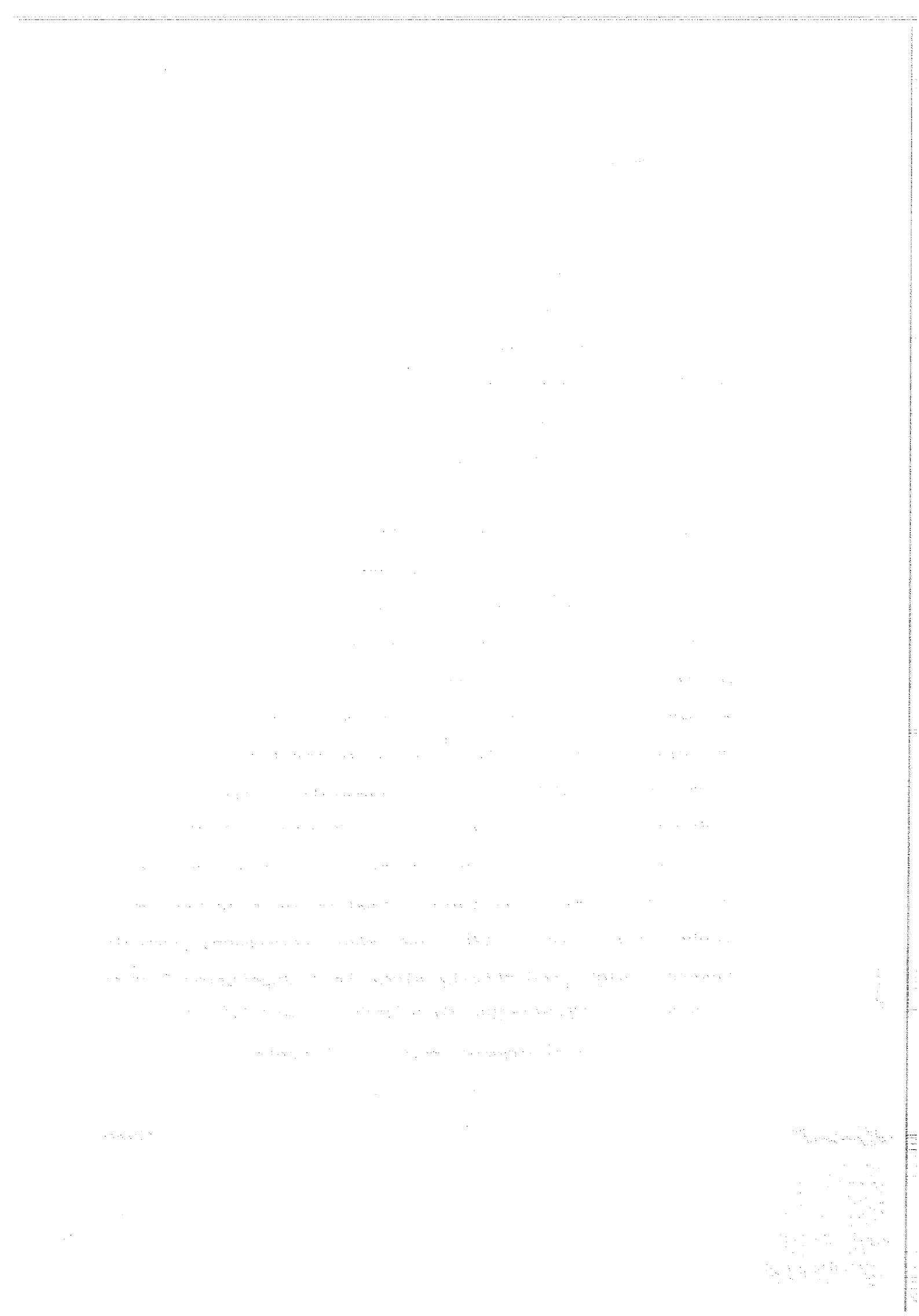

The least understood component in evaporite environments is still the degree of preservation. In the case of ancient evaporite deposits, the preservation conditions can only be assessed by circumstantial evidence (see previous discussion, Chapter 3.13). It has frequently been quoted that evaporite depositional environments are oxygen poor, barren of bottom-dwelling organisms and hence ideally suited for the preservation of organic matter (Kirkland and Evans, 1981; Demaison and Moore, 1980; Sonnenfeld, 1985; Warren, 1986; Evans and Kirkland, 1988). Other organic matter degrading organisms, however, especially sulfide-reducing bacteria and methanogens, both of which are effective biodegraders, are known to thrive under these conditions (Goldhaber and Kaplan, 1974; Froelich et al., 1979; Berner, 1980). A well-studied evaporite environment, Solar Lake on the Arabian Peninsula is known to show substantial rates of at least partially bacterial-induced degradation and transformation of organic matter (Friedman and Krumbein, 1985, and references therein), despite the presence of anaerobic, hypersaline conditions (Cohen et al., 1980; Aizenshtat et al., 1983; Boon, 1984; Edmunds and Eglinton, 1984). However, even though substantial amounts of organic carbon are lost during deposition and burial of organic matter at Solar Lake, preservation conditions are sufficient to permit the existence of organic-rich layers (4.5% TOC) at

shallow depth (60-70 cm) and hence the formation of source-rock prone intervals.

Based on the data set for the SI-CI unit of the Mulhouse Basin, it appears that during periods of moderate to high primary productivity in conjunction with good preservation conditions, the deposition of marls containing rhythmically varying amounts of TOC is governed dominantly by sedimentation rate. Sedimentation rate, on the other hand, is in most cases directly dependent on climatic conditions or sea level.

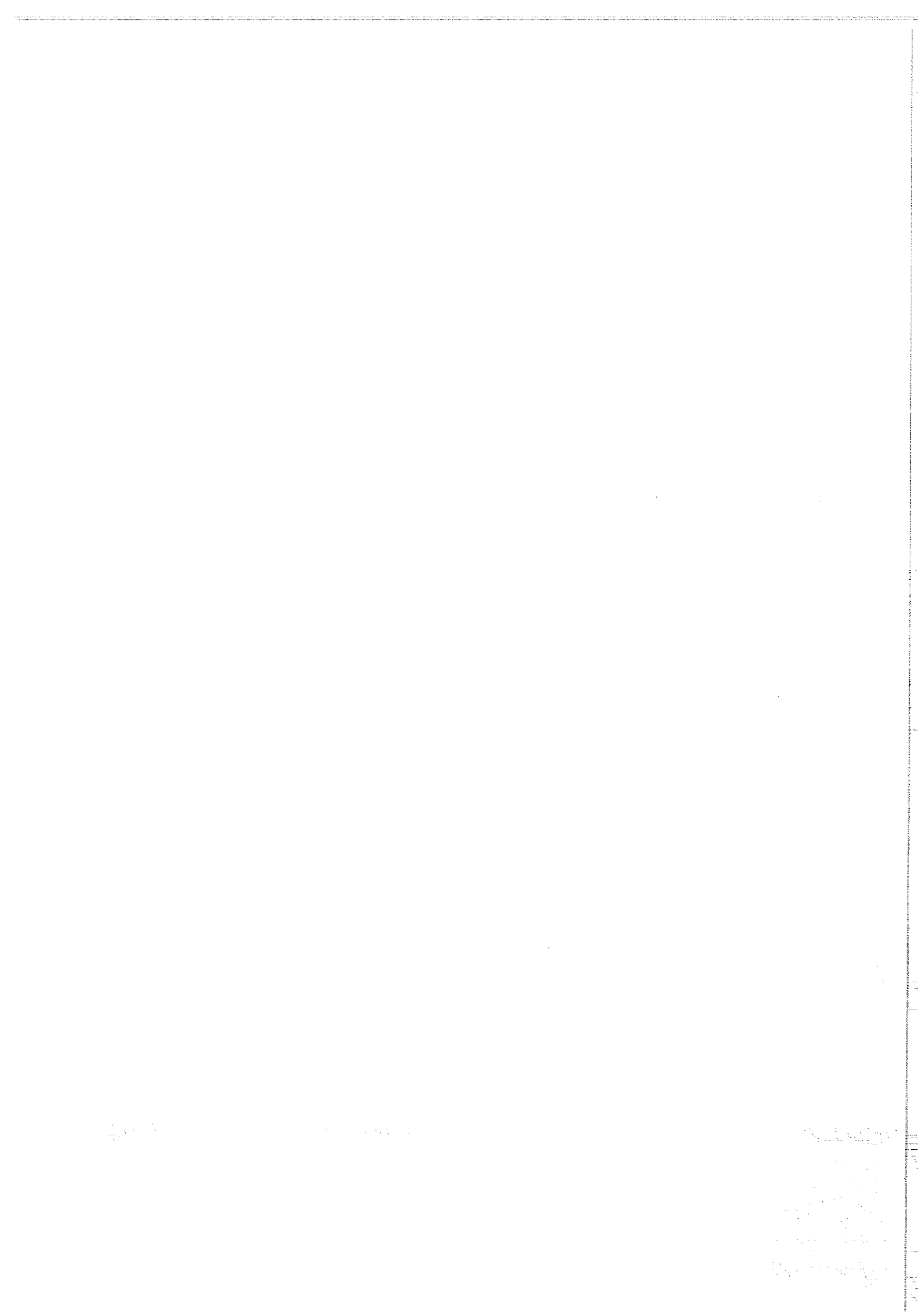

3.16 SYNTHESIS:

RECONSTRUCTION OF THE PALEODEPOSITIONAL ENVIRONMENT

The integration of sedimentological, bulk organic and molecular geochemical data allows the reconstruction of the paleoenvironment. As a result a model is proposed here that describes and explains the observed data.

The overall depositional environment of the evaporites from the Mulhouse Basin was an evaporite lake in a narrow rift valley setting (Illies, 1974). The area was permanently filled with water during the deposition of the S1 to CI unit. All of the sediments deposited in this stratigraphic interval indicate sedimentation took place in a water body with quiescent water conditions. There is no evidence for extensive current movements or periodic desiccation of the basin. The lake level varied considerably as indicated by the concentric-elliptical sedimentation pattern (Blanc-Valleron, 1991). The lake level was highest during the deposition of the marl and gypsum (later converted to anhydrite), and considerably lower during halite and sylvite deposition.

The sediments of "Lake Mulhouse" stem from both terrigenous and marine sources. The terrigenous input consists of wind and water transported siliciclastic matter as well as plant debris. Groundwater and

hydrothermal water contributions may also not be ruled out (Hardie, 1990). Common marine influx is indicated by abundant layers of marine planktonic foraminifera tests in the marl horizons. The sedimentation dynamics of the perennial lake can be described as a succession of meromict lake stages (stratified water bodies) alternating with monomict lake stages (unstratified water bodies) (Fig. 49). Sedimentation of marls of types A and B occurred during the meromict stage. During that period the terrigenous influx dominated. The siliciclastic components of the marls varies between 40% and 80%. Meromict conditions may have been disturbed by marine incursions, which appear to have been sudden, punctuated events (e.g. storms or high floods) and resulted in the deposition of millimetric layers only. The overall sedimentation pattern during marl deposition was governed by the prevailing Mediterranean-type climate. Laminated (varved) deposits composed of carbonate alternating with siliciclastic debris and organic matter-rich layers forming couplets are characteristic of this period. It seems that an annual deposition cycle was operating. During spring and summer (dry season), carbonate was deposited resulting from the consumption of CO_2 by the bloom of phytoplankton. During the wet season (fall and winter), abundant dead organic matter (bacterial and algal in origin) and siliciclastic debris accumulated.

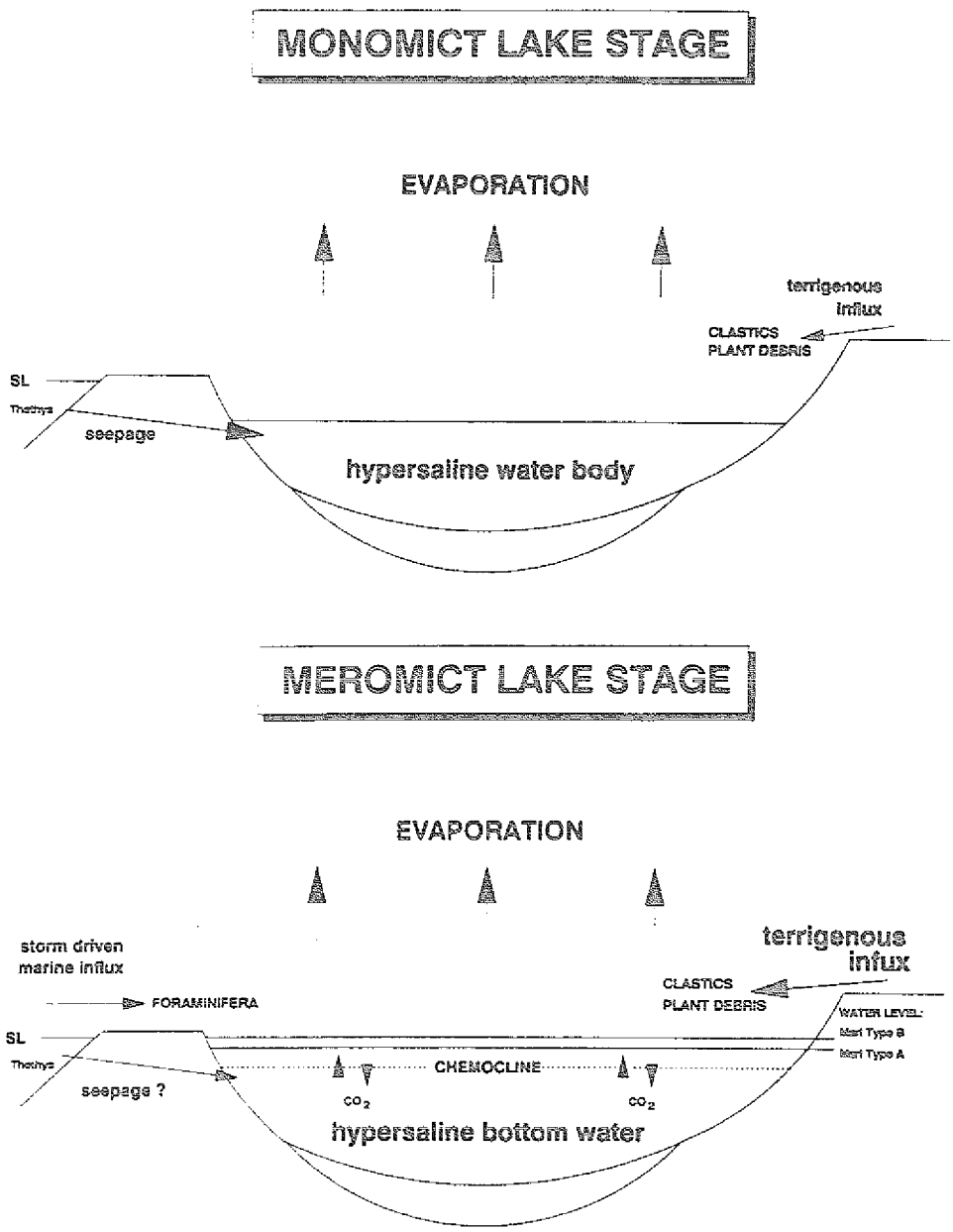

Fig. 49: Schematic model of the monomict and meromict stages of "Lake Mulhouse."

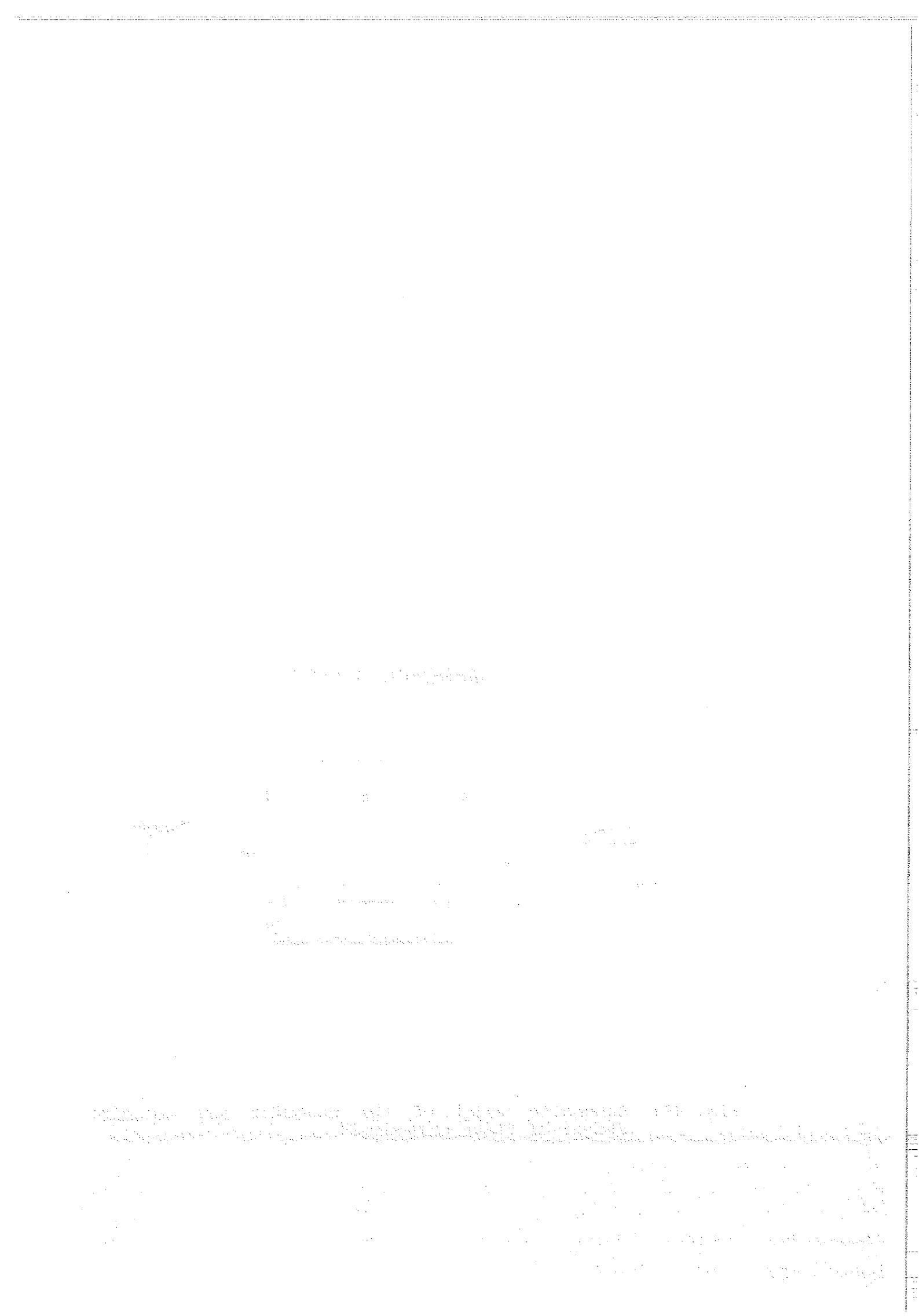

Two substages can be defined during the deposition of marls in the meromict lake stage, which led to the deposition of type A and type B marls. During the deposition of marls of type B (Fig. 50), a density and perhaps thermally stratified water column was established, which was divided into an upper and a lower water body. The bottom waters were most likely oxygen deficient (disaerobic to anaerobic) and hypersaline, as indicated by the lack of bottom-dwelling organisms and bioturbation. Preservation conditions were good (indicated by low pristane/phytane ratios and high phytane content) and this allowed the accumulation of organic-rich marlstones. The upper water body was most likely less saline, but still hypersaline (foraminifera death assemblages). The upper water body was characterized by the occurrence of extensive nutrient recycling (low $\Delta\ \delta^{13}C$-values; Hollander and Huc, 1991). The presence of extended porphyrins (Keely et al., 1990) indicates that the chemocline was in the photic zone, implying a relatively shallow upper water body.

Primary production was moderate (lower aquatic carbon accumulation rates than in the marls of type A) and took place in the upper water body. Algae were the dominant primary producers of organic material in this lake stage (high alginite content, $C_{15} + C_{17}$ rich n-alkane patterns).

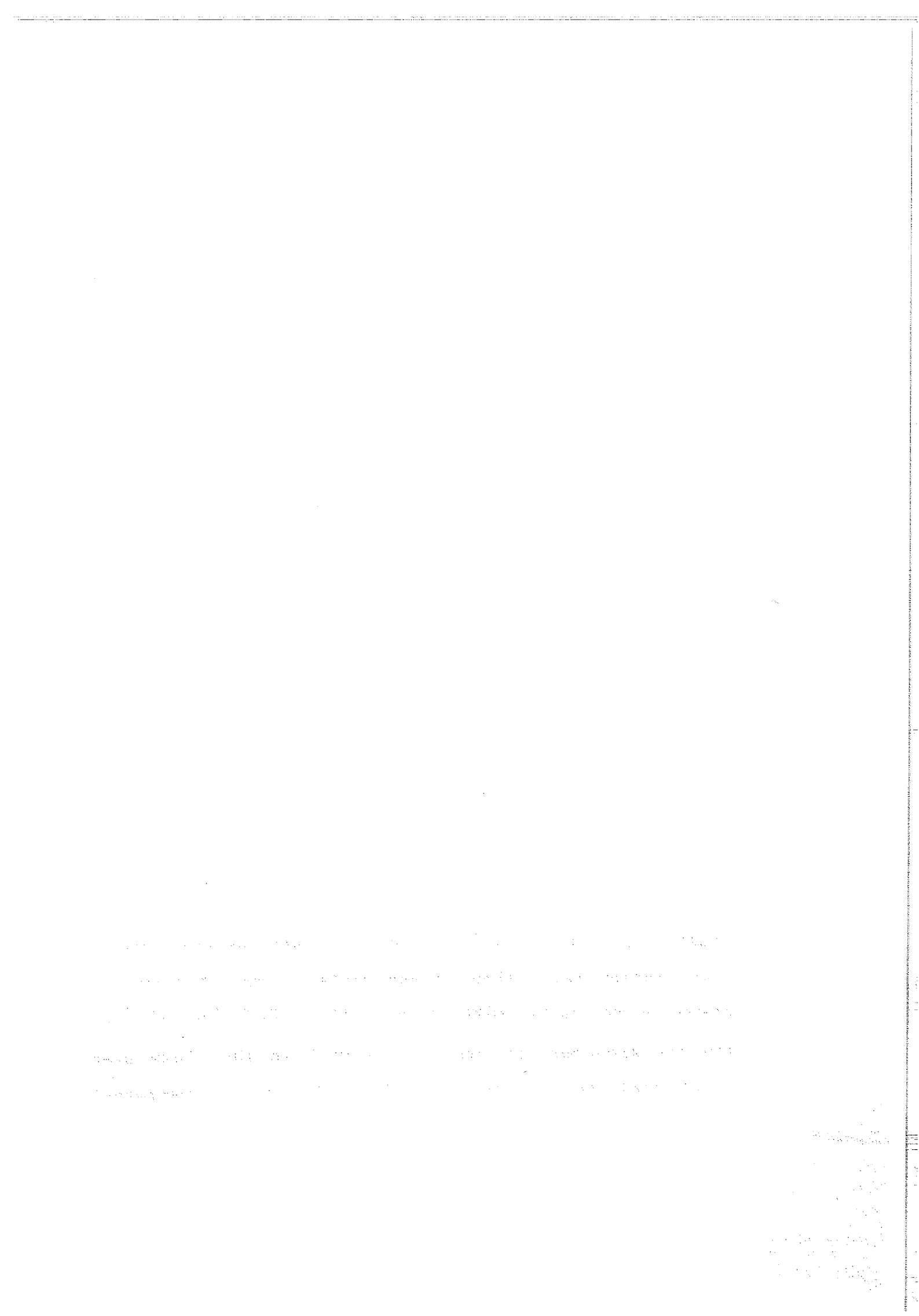

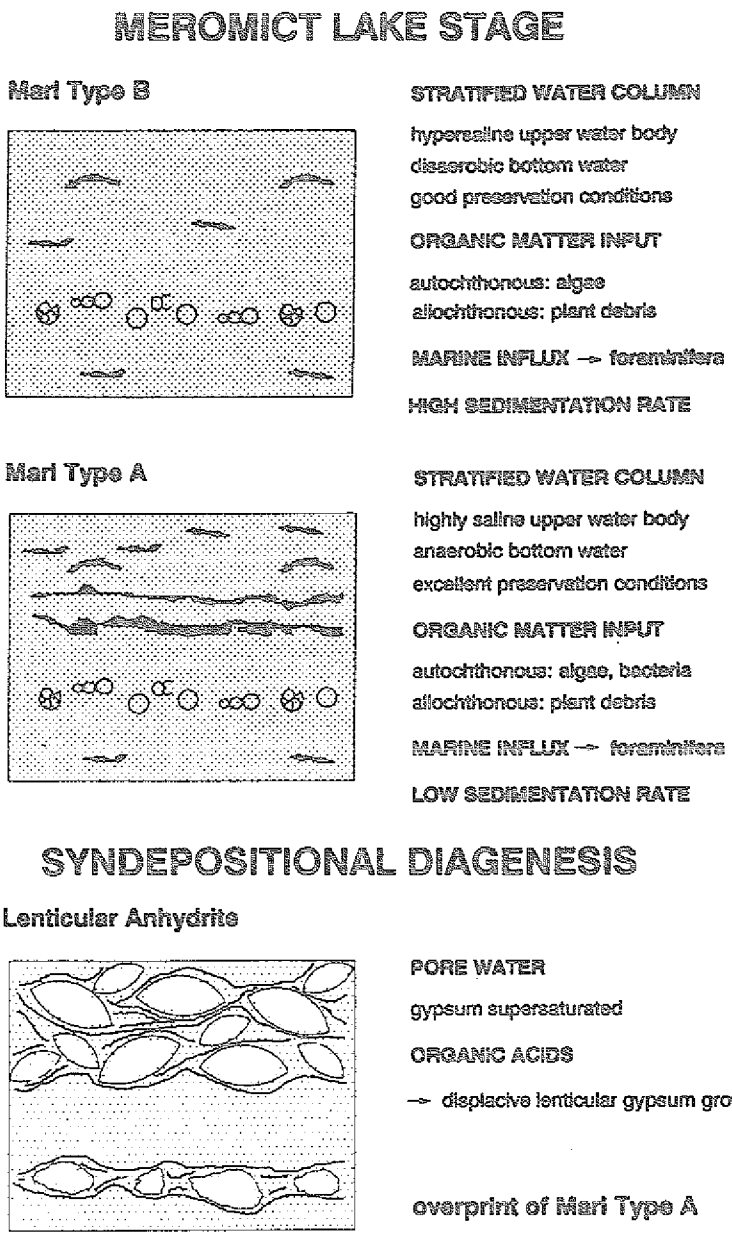

Fig. 50: Relationship between sedimentary facies, organic facies and the physical lake conditions during the deposition of the S unit of the Mulhouse Basin. (Continued on following page.)

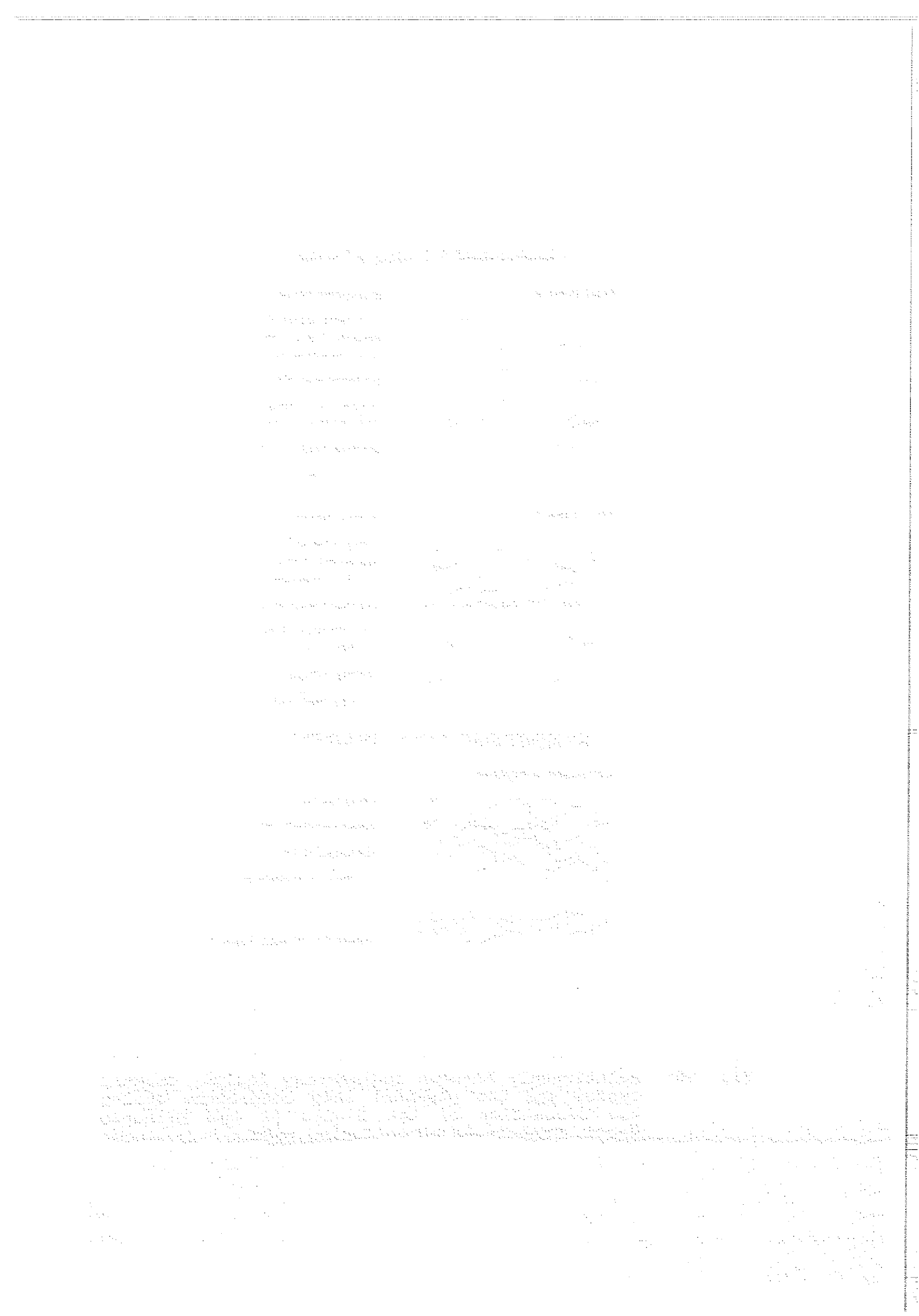

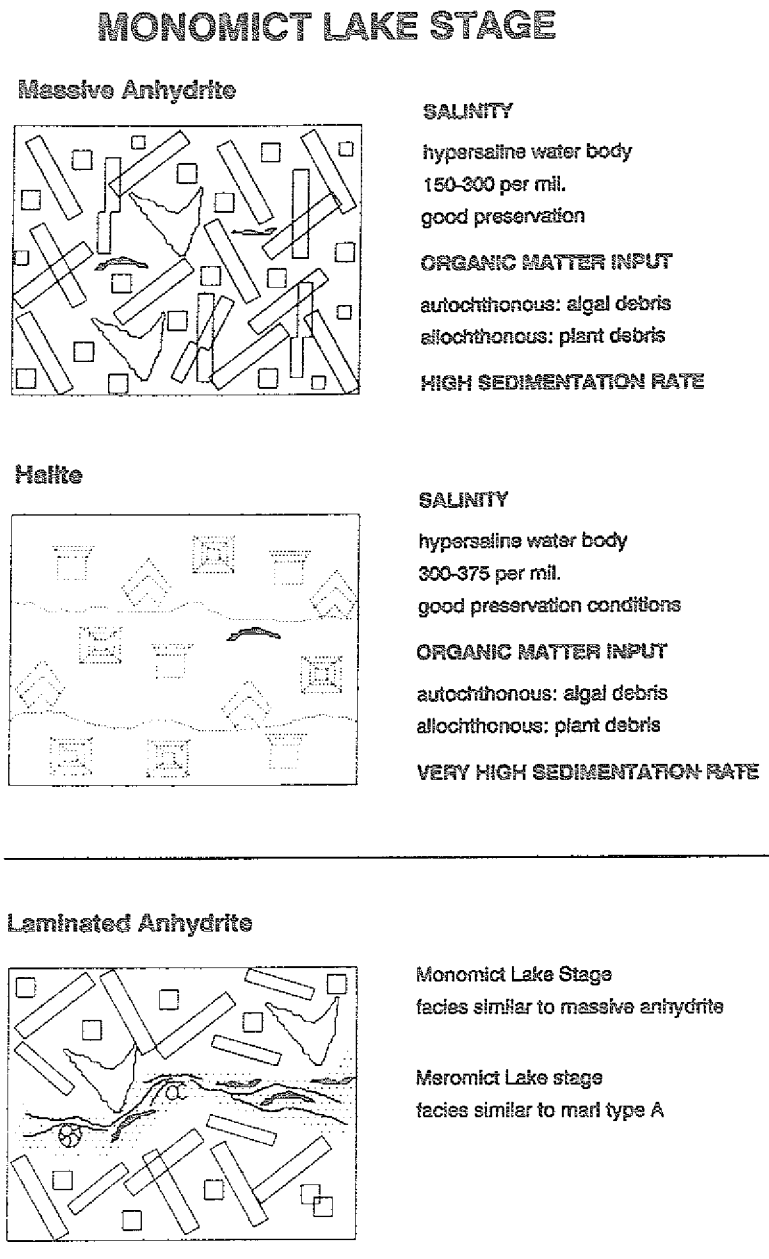

Fig. 50: (Continued from preceding page.) Relationship between sedimentary facies, organic facies and the physical lake conditions during the deposition of the S unit of the Mulhouse Basin. (cont.)

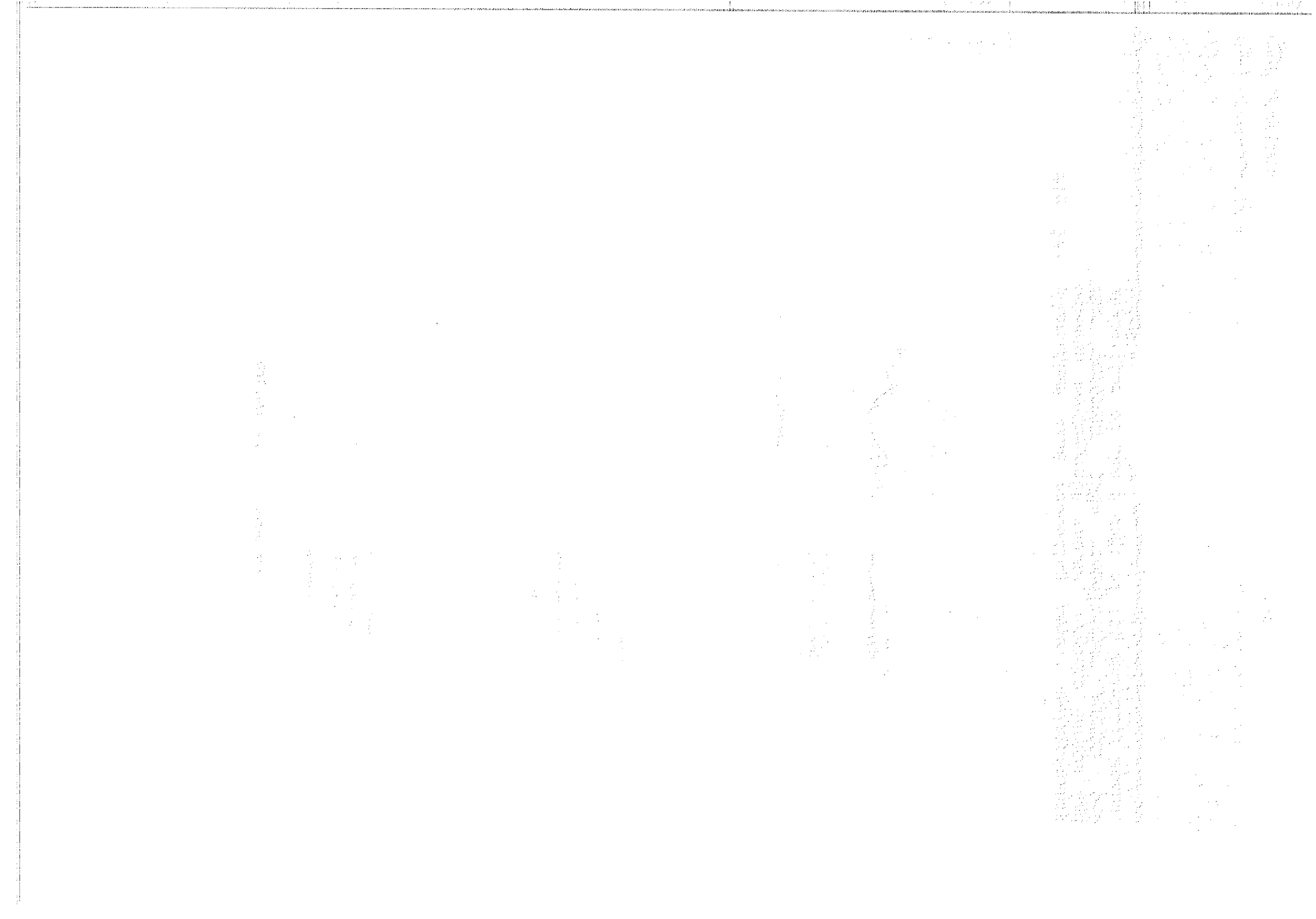

The accumulation of organic matter was also favored by relatively high sedimentation rates and moderate productivity, which led to the formation of marls with organic contents between 0.5 and 2% TOC. The high sedimentation rates also provided a constant influx of plant debris, which is expressed by higher accumulation rates for higher terrigenous organic matter than in marls of type A, which led to a moderate quality of the kerogen (hydrogen index between 200-350 mg HC/g TOC).

The deposition of marls of type A (Fig. 50) also occurred in a stratified water body. The lower part of the water body was again devoid of bottom-dwelling organisms and hence of bioturbation (well-developed lamination). Preservation conditions were excellent. The hypersaline bottom waters were strictly anaerobic and extensive sulfate reduction occurred (high pyrite content of the sediments). The upper part of the water body was also hypersaline (foraminiferal death assemblage). Primary production was extensive (high aquatic organic matter accumulation rates), indicating a high nutrient supply. The primary producers of organic material were algae and bacteria (possibly photosynthetic bacteria; n-alkane spectrum, alginite content). Due to low sedimentation rates and high primary productivity, TOC-rich marls (2-4% TOC) accumulated. The quality of the organic matter is good (oil-prone) because terrigenous organic matter is

sparse (low accumulation rate of terrigenous organic matter, hydrogen index 300-500 mg HC/g TOC).

The generally lower sedimentation rates during the deposition of type A marls when compared to type B marls may have resulted from a highly saline upper water body that allowed bacterial mats to thrive at the chemocline and which protected them from grazing organisms owing to the salinity of the water. A similar phenomenon has been observed from hypersaline ponds in heliothermic lakes (Kirkland et al., 1983). Heliothermic lakes are stratified water bodies with a warm, stagnant, more saline water mass underneath a cooler, less saline, upper water mass that undergoes periodic circulation. Algae and bacteria grow within these hypersaline water bodies, sometimes forming bacterial plates at the interface between the two water masses (Kirkland et al., 1983; Evans and Kirkland, 1988). If these bacterial plates settle into the sediment and can be preserved, they may form laminae of amorphous organic matter very similar to those observed in the marls of type A in the S unit.

The deposition of the massive anhydrites occurred during monomict lake conditions (Fig. 49). The shallow upper water body that covered the basin during the deposition of the marlstones evaporated. Continuing evaporation led to gradual concentration of the brine and finally to

precipitation of gypsum (salinity 150-300 per mil; Fig. 50). The high salinity of the water body led to disaerobic to anaerobic conditions (Warren, 1986) and allowed good preservation of organic matter (low pristane/phytane ratio). The primary producers in this environment were salinity-tolerant algae (alginite content, C_{15} + C_{17} n-alkanes). The formation of organic matter-rich layers was inhibited by dilution due to high sedimentation rates, which led to total organic carbon contents between 0.08% and 0.5%.

Laminated anhydrite is a sedimentary facies composed of a combination of elements of marls of type A and massive anhydrite (Fig. 50). The anhydrite layers are extremely poor in organic matter, whereas the marl-dominated zones are rich in organic matter. The organic facies of the laminated anhydrite is, therefore, dominated by the molecular signal of the organic matter of the marl horizons.

The formation of the halite beds also took place under monomict lake conditions. The salinity of the water body must have exceeded 300 per mil in order to achieve precipitation. Primary producers of organic material were dominantly algae. The highly saline waters provided ideal preservation conditions. Organic accumulation, however,

was extremely low due to the attenuation by high sedimentation rates.

Lenticular anhydrite (Fig. 50) is a result of syndepositional diagenesis of marls of type A. The lenticular aggregates originally formed as gypsum crystals. Usually, displacive gypsum forms as tabular crystals. However, the growth of the gypsum crystals took place at a time when the pore waters of the marls were saturated with respect to gypsum and contained significant amounts of organic acids that "poisoned" the crystal faces (Cody and Cody, 1988). The level of organic acid required for this type of crystal growth was apparently only present in the organic matter-rich marls of type A.

4. FORMATION OF HYDROCARBONS AT LOW MATURITY RANGES

4.1 Introduction

Among the reasons evaporite-carbonate source rocks have attracted increasing attention are 1) they usually contain higher amounts of lipid-like extractable organic matter per unit organic carbon than shale source rocks in a thermally immature state (0.3-0.5% vitrinite reflectance, e.g. Palacas, 1988; Baskin and Peters, 1992), and 2) they appear to generate oils at extremely low maturity levels (T_{max} 429-435°C, Connan et al., 1986). Two principle hypotheses have been put forward to explain the phenomenon of significant yields of lipid-like soluble organic matter at low levels of thermal maturity. Orr (1986) suggests that during early diagenesis, in highly reducing, iron-poor environments where H_2S is abundant, sulfur becomes incorporated into the kerogen structure. Cleavage of thermally weak sulfur-carbon bonds results in the generation of resin- and asphaltene-rich petroleum at low maturity levels. An alternate explanation is that the extremely reducing conditions of the depositional environment cause retardation of the condensation reactions of precursor molecules and their incorporation into the kerogen structure (Powell, 1984).

Based on theoretical considerations, Sonnenfeld (1985) and Warren (1986) have argued that petroleum migration can occur in evaporite source rocks at early stages of diagenesis. Leythaeuser (1988a, 1988b) and Leythaeuser and Schaefer (1984) demonstrated that primary migration of hydrocarbons alters the chemical composition of the residual oil remaining in the source rock after expulsion and carries a signal that can be used to detect such processes and mechanisms of primary migration of hydrocarbons.

Both low temperature generation and expulsion of bitumen and hydrocarbons from evaporite source rocks are important concepts for oil and gas exploration. A consequence of these concepts is that oil and bitumen accumulations in commercial quantities may exist at shallow depths, which is usually not taken into consideration. The understanding of the processes that take place during petroleum generation and migration can improve the capability of the exploration geochemist to predict and locate oil fields.

Based on theoretical considerations, Sonnenfeld (1985) and Warren (1986) have argued that petroleum migration can occur in evaporite source rocks at early stages of diagenesis. Leythaeuser (1988a, 1988b) and Leythaeuser and Schaefer (1984) demonstrated that primary migration of hydrocarbons alters the chemical composition of the residual oil remaining in the source rock after expulsion and carries a signal that can be used to detect such processes and mechanisms of primary migration of hydrocarbons.

Both low temperature generation and expulsion of bitumen and hydrocarbons from evaporite source rocks are important concepts for oil and gas exploration. A consequence of these concepts is that oil and bitumen accumulations in commercial quantities may exist at shallow depths, which is usually not taken into consideration. The understanding of the processes that take place during petroleum generation and migration can improve the capability of the exploration geochemist to predict and locate oil fields.

4.2 Approach

Three general approaches have been applied to the study of hydrocarbon generation in source rocks: 1) recognition of the geochemical effects of petroleum generation by analysis of source rock sequences from the same depositional environment at increasing maturity levels (e.g. Tissot et al., 1971), 2) experimental simulation of hydrocarbons by pyrolysis methods (for a summary see Horsfield, 1984), and 3) numerical models for conversion of kerogen to oil and gas based on mathematically and experimentally derived kinetic rate parameters (Lewan, 1985; Sweeney et al., 1987; Tissot et al., 1987; Mackenzie and Quigley, 1988; Burnham and Braun, 1990). Experimental studies have the advantage that all products formed during the hydrocarbon generation stage can be monitored. However, due to the experimental necessity of applying much higher temperatures than actually prevailed in nature because of limited pyrolysis times compared with geological time, the experimental results often do not match the natural products. Numerical models have to rely on bulk kinetic parameters determined under experimental conditions and also can only approximate that naturally occurring processes. Therefore, the first approach is chosen here to ensure that representative results are obtained.

The basic approach to this study consists of the establishment of a mass balance of all organic components involved (quantity of initial and residual kerogen involved as well as of generated products) for a maturity sequence. The organic content of sediments from a well-defined stratigraphic unit with a known depositional history but which were buried to two different depths during the development of the basin are compared with each other. The key prerequisite allowing such a study is to ensure that two rock sequences with identical sedimentary facies and organic contents are accurately correlated. It is essential that the organic facies be the same at each site, because only then can the products of petroleum formation be supposed to have the same original composition and thus comparable with each other. Identical sedimentary facies ensure that the conditions during deposition of the organic matter were similar. This implies that the type of organic matter and the degree of preservation of organic matter during deposition were the same at each site. An additional advantage of the comparison of samples from identical sedimentary facies is that the catalytic effects of the mineral matrix on petroleum formation should be identified. If the sedimentary facies and organic facies are identical at both sites, then the bitumen and kerogen content at each site can be quantitatively assessed and an inventory of the amounts of individual petroleum product can be

compiled. A mass-balance of the concentrations of individual petroleum products from certain maturity intervals can then grant insight into the processes of hydrocarbon generation and migration.

4.3 Comparison of the Sampling Sites

Sampling of the S unit of the Mulhouse Basin was made possible by Mines de Potassé d'Alsace at the locations Amelie II, Ungersheim, and Berrwiller. The sampling sites lie within a 5 km radius of each other. Locations were chosen based on their present-day burial depth. An attempt was made to cover the maximum range of depths available. Amelie II corresponds to a present-day burial depth of 580 m, Ungersheim to 700 m and Berrwiller to 1040 m. The complete S unit could be sampled at Amelie II and Ungersheim, while only the upper two-thirds, approximately, of the unit are exposed in a mine exposure at Berrwiller.

4.3.1 Paleobasin Morphology

An isopach map for the period of deposition of the S unit to the TS unit shows that at least two depocenters existed (Fig. 6). A northern depocenter was located in the vicinity of Ensisheim and a southern depocenter was located north-west of Mulhouse. The sampling sites Amelie II and Berrwiller lie within the southern subbasin, whereas Ungersheim is located in the northern subbasin.

4.3.2 Sedimentology

The existence of two subbasins apparently had little influence on the development of the sedimentary facies and organic facies of the sediments of the S unit of the Mulhouse Basin. A sedimentary survey showed that identical sedimentary facies are present at each sampling site. Each site contains marls of type A, marls of type B, lenticular anhydrites, laminated anhydrites and massive anhydrites. Halite was encountered at Amelie II and Ungersheim. Halite beds could not be sampled at Berrwiller because halite usually occurs in the lower part of the S unit, which was not completely exposed at Berrwiller. The carbonate content of the marls of the S unit is also similar at each site. Marls at Amelie II contain 15-65 wt% carbonate, marls at Ungersheim 15-55 wt% and at Berrwiller 21-60 wt%. At each site marls with low carbonate content (15-20 wt%) are encountered in the lower part of the S unit and marls with high carbonate content (40-65 wt%) are present in the middle part of the unit (Figs. 51, 52, 53). The sedimentological similarities encountered at the three sample sites appear to indicate uniform depositional conditions for the entire basin.

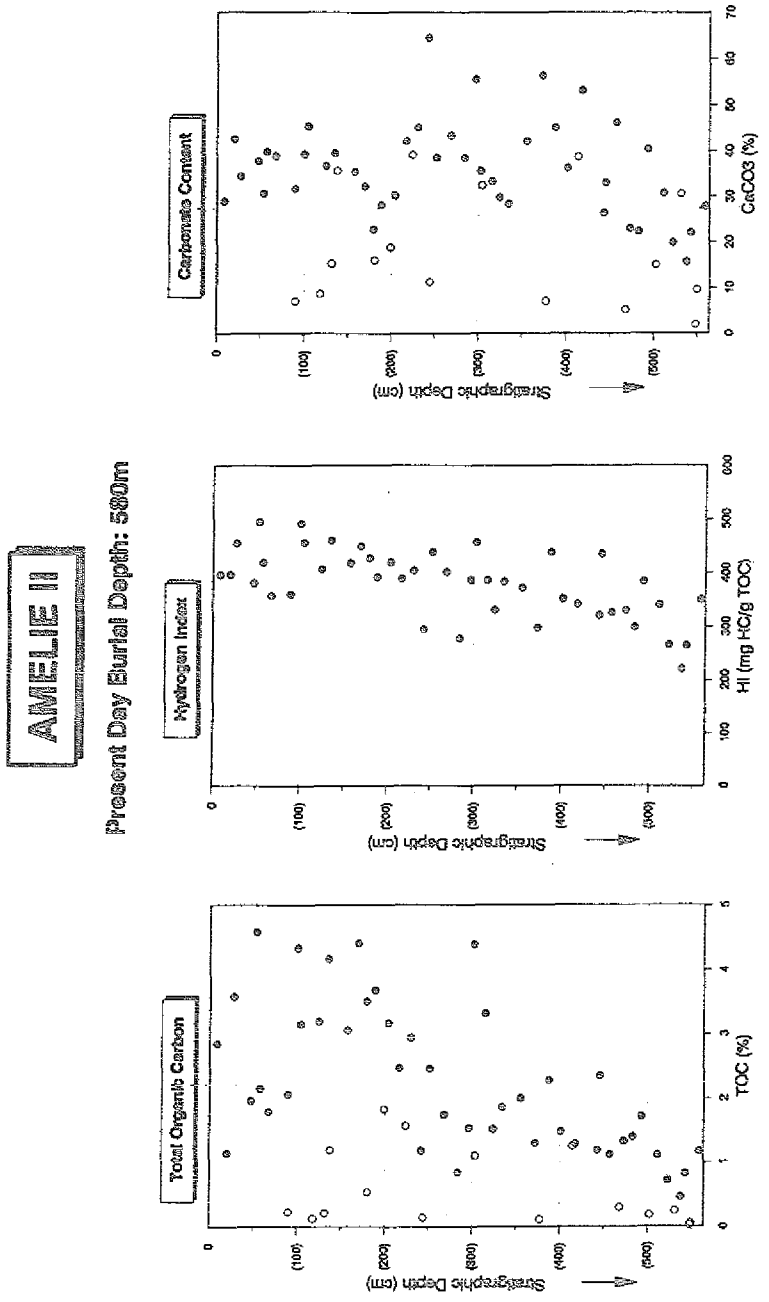

Fig. 51: Variation of the total organic carbon content, hydrogen index and carbonate content within the S unit at Amelie II.

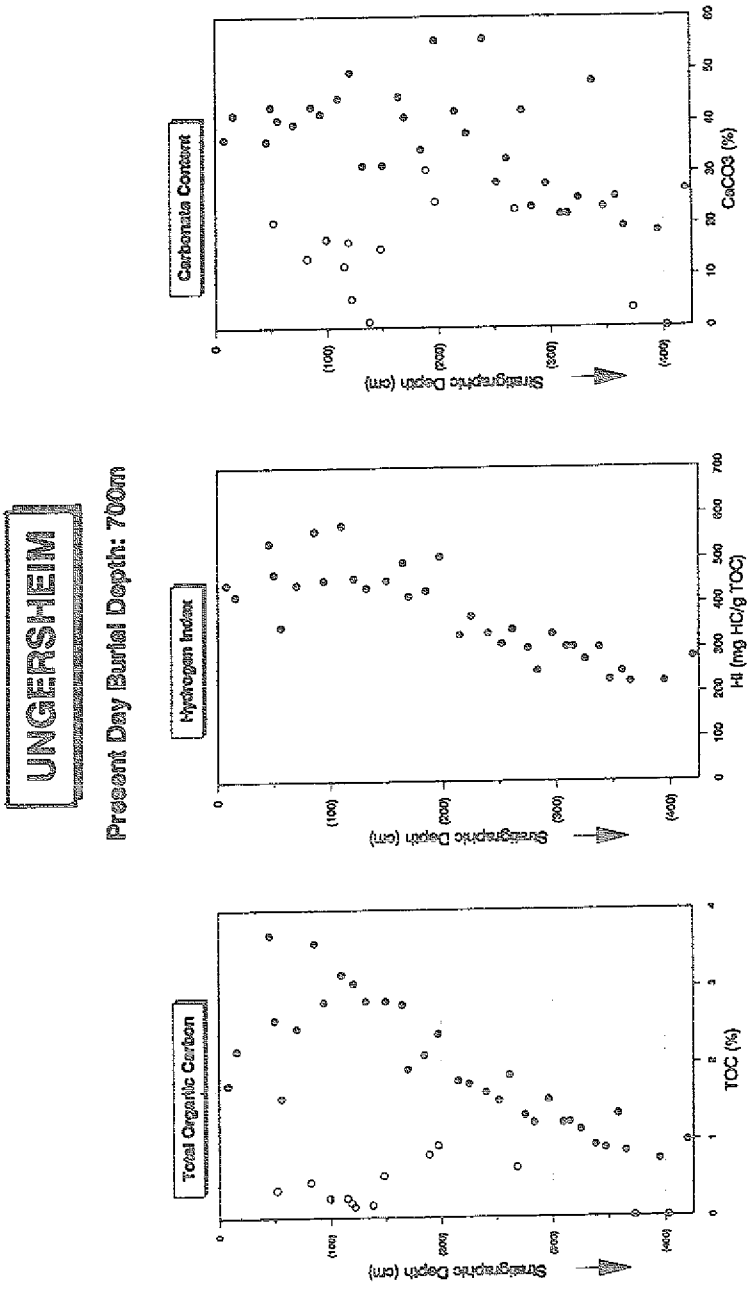

Fig. 52: Variation of the total organic carbon content, hydrogen index and carbonate content at Ungersheim.

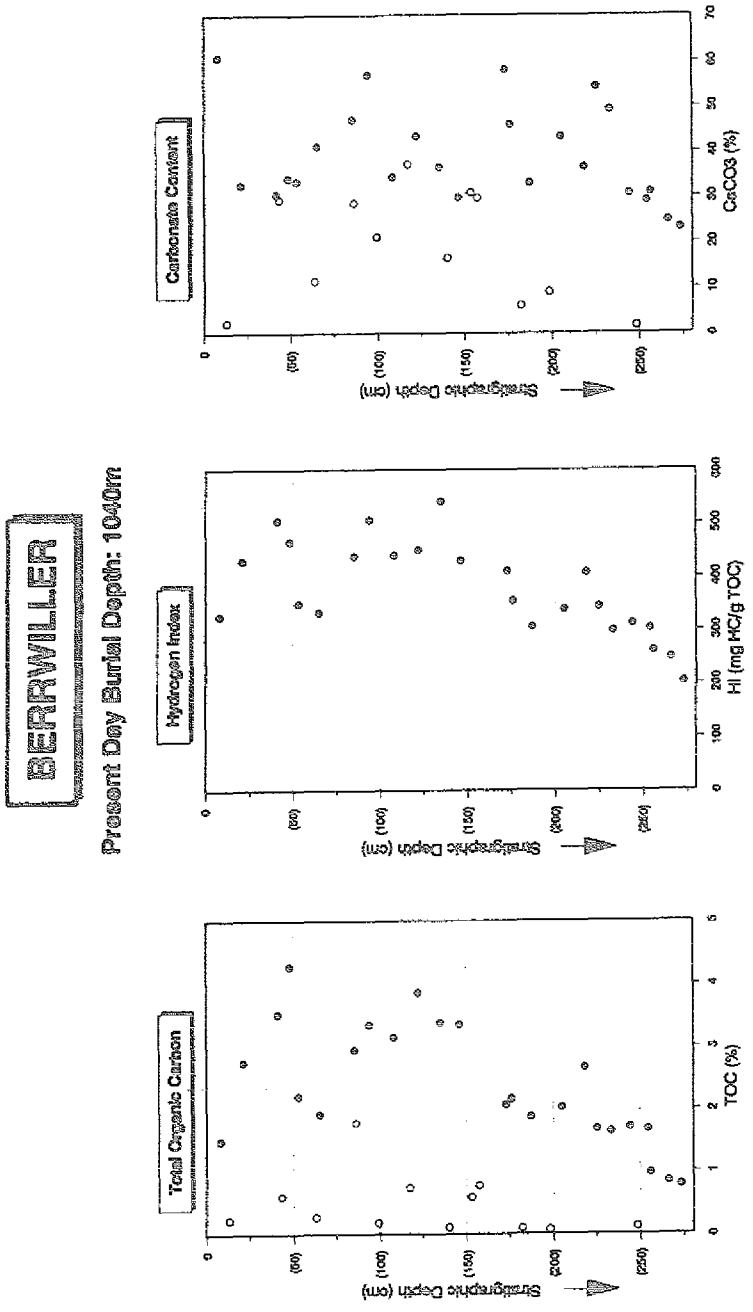

Fig. 53: Variation of the total organic carbon content, hydrogen index and carbonate content at Berrwiller.

4.3.3 Organic Petrography

The S unit displays a systematic vertical variation in the amount of organic matter (TOC content) and kerogen quality (hydrogen index) of the marl beds. The total organic carbon content of marls located at the base of the S unit is generally less than 1 wt% and increases gradually towards the top of the unit, where TOC values greater than 3 wt% are common. A parallel trend can be observed for the hydrogen indices. Hydrogen indices between 200-300 mg hydrocarbon/g TOC are common at the base of the unit. The hydrogen index increases gradually to approximately 500 mg hydrocarbon/g TOC in the upper part of the S unit. Similar trends for organic carbon content as well as for the kerogen quality (hydrogen index) are present at Amelie II, Ungersheim, and Berrwiller (Figs. 51, 52, 53).

4.3.4 Organic Geochemistry

The extracted bitumens of the marls, anhydrites and halite beds at each of the three locations can be grouped into organic facies A and B based on their n-alkane distribution patterns (see also Part I). Organic facies A shows a bimodal n-alkane distribution with maxima at n-C_{17} and n-C_{24} (Fig. 54). In contrast, organic facies B is characterized by a high n-C_{15} and n-C_{17} content and a low concentration of n-alkanes in the C_{20}-C_{29} range (Fig. 55).

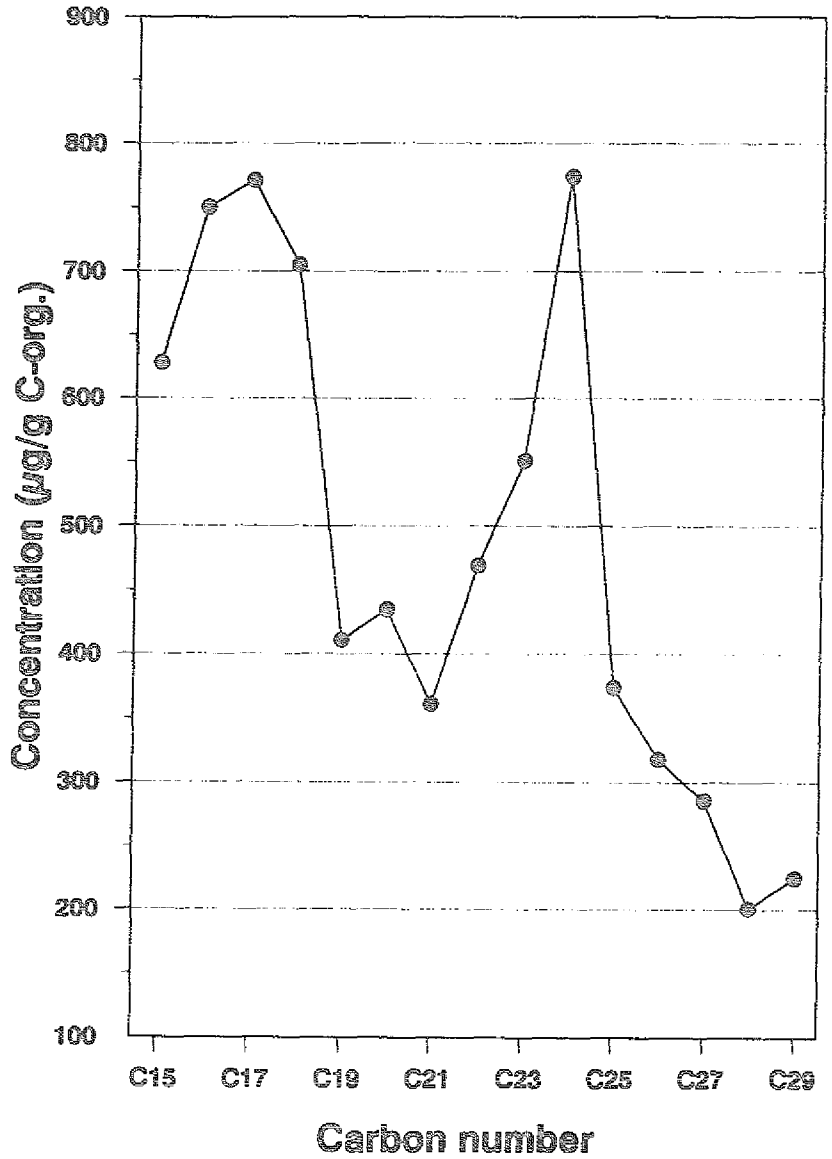

Fig. 54: Example of an n-alkane distribution pattern representative for organic facies A.

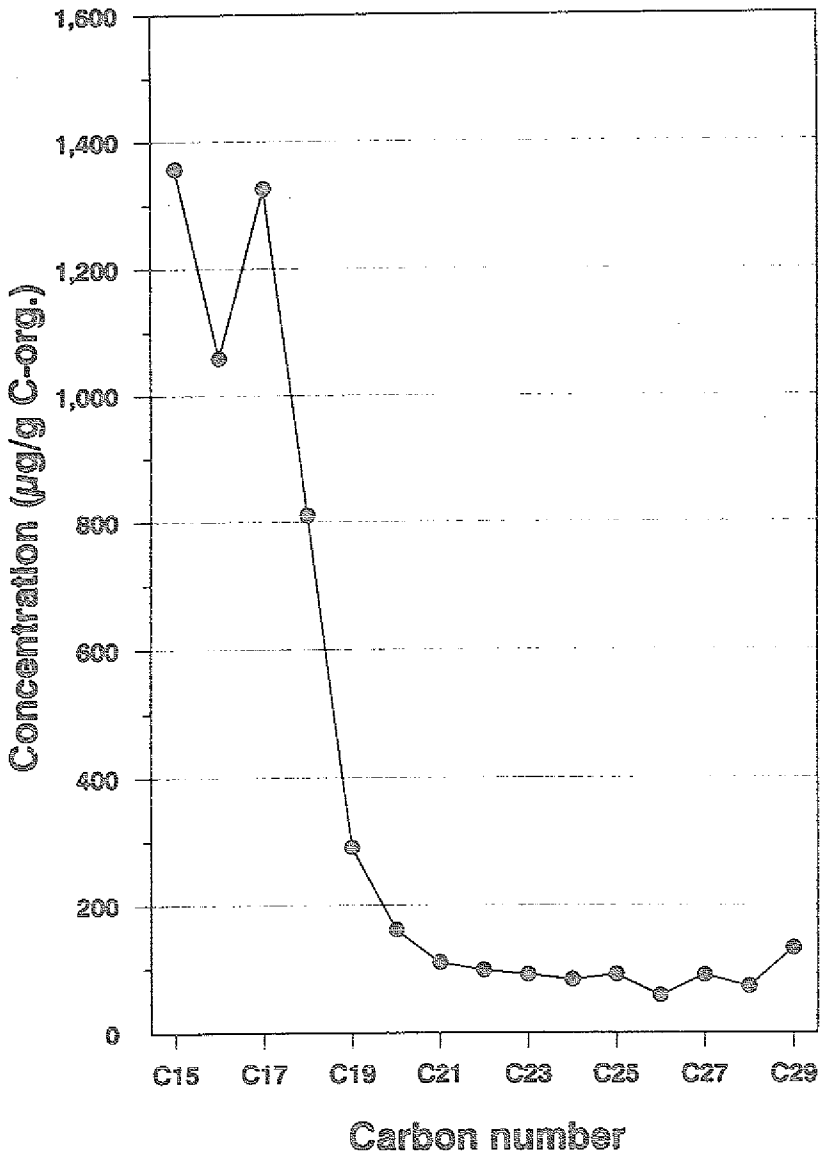

Fig. 55: Example of an n-alkane distribution pattern representative for organic facies B.

The observed similarities within the S unit at Amelie II, Ungersheim, and Berrwiller with respect to sedimentology, amount of organic matter, quality of the kerogens and composition of selected bitumen fractions ensures that a meaningful mass balance can be performed.

4.3.5 Maturity Assessment

The maturity of the organic matter content of the sediments of the Mulhouse Basin was determined by measurements of random vitrinite reflectance, the T_{max} parameter of Rock-Eval pyrolysis and by selected maturity parameters based on sulfur aromatics measured on marl sample extracts. Although vitrinite generally occurs sparsely in the sediments of the Mulhouse Basin, vitrinite reflectance measurements could be performed. A sufficiently large number of vitrinites (n>50) was present only in the marl samples.

Vitrinite reflectance measurements on marl samples indicate a comparatively low maturity for each of the three sampling sites. The maturity of the sediments at Amelie II, Ungersheim, and Berrwiller corresponds to 0.35% (±0.05) R_o, 0.42% (±0.05) R_o, and 0.45% (±0.05) R_o, respectively. The increase in vitrinite reflectance corresponds to the present-day burial depth of the samples

(Fig. 56). The determined maturities are comparable to the range of maturities reported by Robert (1985) for sediments from the southern Rhine Graben in a similar depth range.

The maturity assessment of the organic matter content of the marls based on T_{max} shows on average similar maturities for the sites Amelie II and Ungersheim with 432±3°C. According to this parameter, the organic content of the marls at Berrwiller is slightly more mature (435±3°C).

The methyldibenzothiophene ratio was introduced as a maturity indicator by Radke et al. (1986). This parameter uses the lower thermal stability of the 1-methyldibenzothiophene isomer relative to the 4-methyldibenzothiophene isomer to assess maturity. The methyldibenzothiophene ratio relies on a shift in predominance from thermally relatively unstable towards more stable isomers with progressive maturation (Radke, 1988). It has been proposed that the methyldibenzothiophene ratio be used preferentially for the maturity assessment of soluble organic matter derived from kerogens that break down to yield petroleum at relatively low temperatures, such as Type II kerogens (Radke et al., 1986).

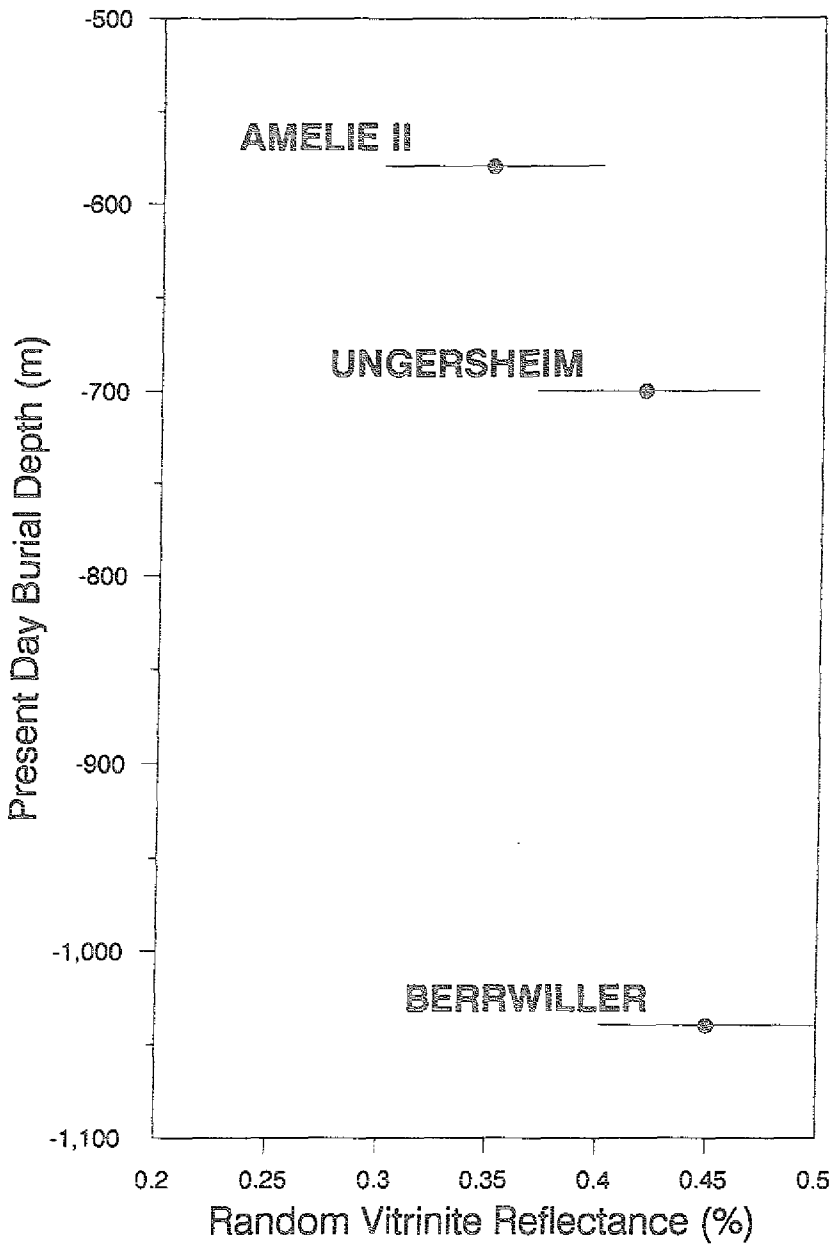

Fig. 56: Maturity level expressed as vitrinite reflectance and present day burial depth of the S unit at Amelie II, Ungersheim and Berrwiller (bars indicate range of standard deviation).

Measurements performed on extracts of marls from the sites Amelie II, Ungersheim, and Berrwiller display a wide range of methyldibenzothiophene ratios (0.4-1.6; Fig. 57). At very low maturities there appears to be a relationship between the hydrogen index, and, hence, organic facies, and the methyldibenzothiophene ratio. Samples with maturities of 0.35-0.42% R_o show progressively higher methyldibenzothiophene ratios with decreasing hydrogen index. The samples from the Berrwiller site (R_o = 0.45%) display methyldibenzothiophene ratios of approximately 0.65 regardless of the hydrogen index (Fig. 57).

These observations confirm the findings of Radke et al. (1986), who pointed out the influence of organic matter type on maturity parameters based on sulfur aromatics. It appears that 0.5% R_o is the lower limit for the application of the methyldibenzothiophene ratio as a maturity parameter in carbonate/evaporite source rocks. Below this level of maturity, organic facies-induced variations clearly render this ratio useless.

Each of the applied maturity parameters documents that the most pronounced maturity differences exist between the organic matter content of the samples from the sites Amelie II and Berrwiller. The organic matter at the site

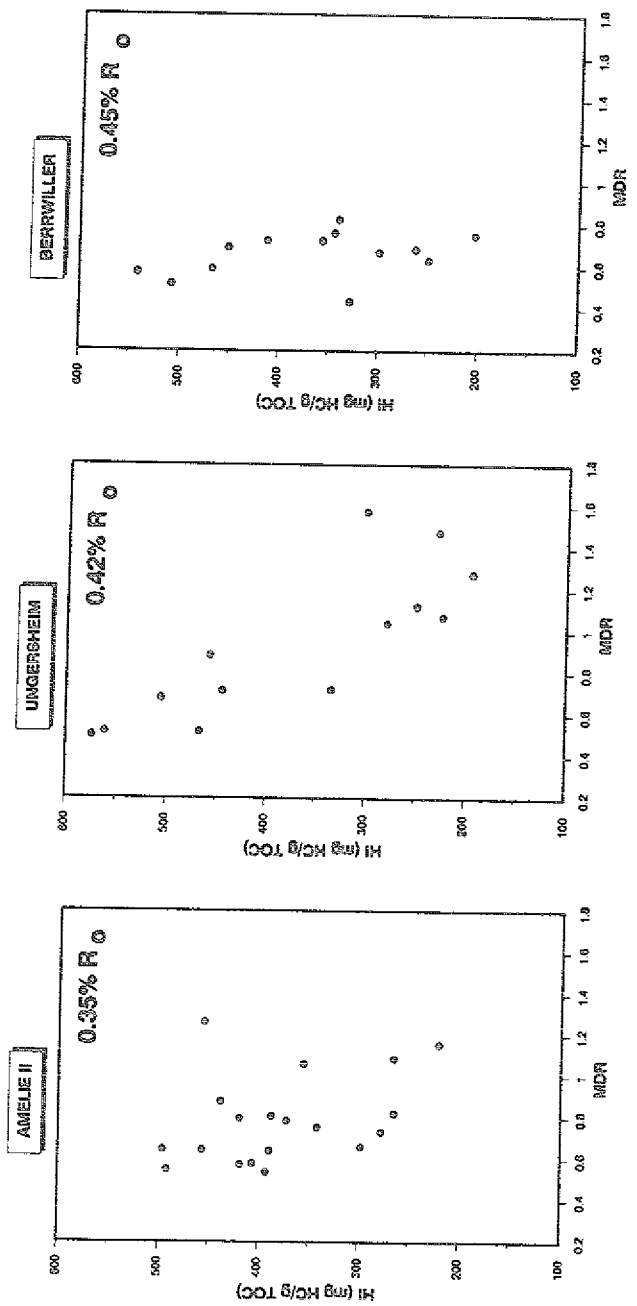

Fig. 57: Variation of the methyldibenzothiophene ratio (MDR) with kerogen quality, expressed as hydrogen index (HI).

Ungersheim reached a maturity level intermediate between the less mature site Amelie II and the relatively more mature site Berrwiller.

4.4 Sample Selection

The above discussion and the results discussed in Chapter 3 show that sedimentary facies and organic facies are virtually identical at each of the sampling sites. Organic matter maturity differences are most pronounced when the sites Amelie II and Berrwiller are compared. The maturity of the organic content of the sediments from Ungersheim is intermediate between Amelie II and Berrwiller. Therefore, in order to cover a reasonable maturity interval, samples from Amelie II and Berrwiller, which correspond to maturities of R_o = 0.35% and R_o = 0.45%, respectively, are compared with each other.

Sample selection was performed under the following premises: The presence of two distinct organic facies at each of the sampling sites (Amelie II, Ungersheim, and Berrwiller) is indicated by the results of the organic petrological study, the chemical characterization of the kerogens (Rock-Eval) and the analysis of the bitumen fractions, in particular the n-alkane distribution patterns and the sulfur aromatic distribution patterns (reported in Chapter 3). Each of the two organic facies occurs in three sedimentary facies:

1) Organic Facies A
   - marls of type A

- lenticular anhydrite
- laminated anhydrite

2) Organic Facies B
   - marls of type B
   - massive anhydrites
   - halites

To monitor the progress in bitumen and hydrocarbon formation, three to four samples from each lithofacies were selected from the less mature site Amelie II and the more mature site Berrwiller. The stratigraphic position of the samples in the S unit at the sites Amelie II and Berrwiller are indicated in Figure 58. Samples of the same sedimentary facies selected from both Amelie II and Berrwiller share the same organic facies, similar total organic carbon contents and carbonate contents (Table 2). In the case of the sedimentary facies of marls of type A and marls of type B, samples with similar hydrogen indices, and hence similar petroleum potential and kerogen type were chosen (Table 2).

The emphasis of the sample selection was to ensure that the organic matter content and the quality of the organic matter were virtually identical in samples of one sedimentary facies, even though the samples were selected from two different geographic locations.

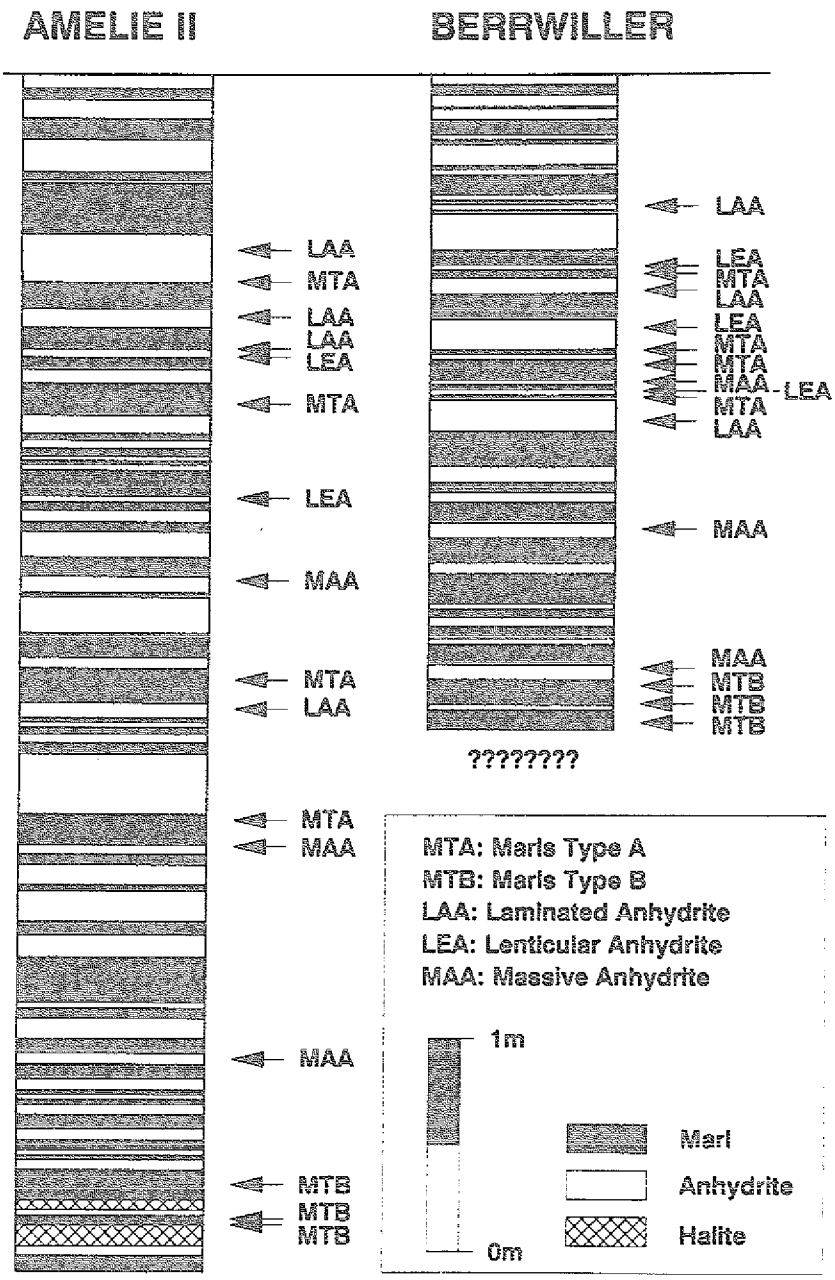

Fig. 58: Stratigraphic position of the samples of the lithofacies compared in the mass-balance of Chapter 4 at Amelie II and Berrwiller.

Sample #	Carbonate Content	TOC	Hydrogen Index	Organic Facies
	(%)	(%)	(mg HC/g TOC)	
Marls Type A				
AMELIE II				
28259-1	39.48	4.34	492	A
28280	28.32	3.69	393	A
28291	42.40	2.01	373	A
28299	35.74	4.40	457	A
BERRWILLER				
29651	57.06	3.35	484	A
29654	43.48	3.86	427	A
29655	36.57	3.38	422	A
29659	58.14	2.07	394	A
Marls Type B				
AMELIE II				
28318	22.16	0.83	265	B
28319	15.74	0.47	221	B
28321	19.99	0.73	266	B
BERRWILLER				
29675	30.99	0.98	292	B
29676	24.74	0.85	246	B
29677	23.07	0.79	235	B
Lenticular Anhydrite				
AMELIE II				
28266	35.74	1.20	n.d.	A
28278	18.99	1.84	n.d.	A
28298	32.57	1.12	n.d.	A
BERRWILLER				
29650	28.66	1.78	n.d.	A
29654	37.15	0.74	n.d.	A
29657	30.82	0.59	n.d.	A
Laminated Anhydrite				
AMELIE II				
28255	7.16	0.24	n.d.	A
28258	8.83	0.14	n.d.	A
28264	15.41	0.22	n.d.	A
BERRWILLER				
29648	11.58	0.28	n.d.	A
29652	21.24	0.19	n.d.	A
29658	29.66	0.78	n.d.	A
Massive Anhydrite				
AMELIE II				
28272	11.33	0.15	n.d.	B
28288	7.16	0.12	n.d.	B
28306	5.25	0.31	n.d.	B
BERRWILLER				
29656	16.66	0.12	n.d.	B
29660	6.16	0.10	n.d.	B
29664	9.08	0.08	n.d.	B
29672	1.75	0.13	n.d.	B

n.d.: not determined
HC: Hydrocarbons

Table 2: Summary of the organic geochemistry parameters of the samples used for the mass-balance calculations in Chapter 4.

4.5 Methods

To quantify the maturation progress of the organic matter of the S unit in the depth interval between 580 and 1040 m, corresponding to R_o = 0.35% and R_o = 0.45%, respectively, kerogen concentration, extract yields, and selected n-alkanes, naphthalenes, phenanthrenes and sulfur aromatics were identified and quantified for a number of samples from each lithofacies.

The analyzed compounds were chosen because they represent major organic matter constituents of an organic-rich sediment. Kerogen is the solid component of the organic matter. Bitumen is a complex mixture of organic compounds that can be extracted with an organic solvent from a rock. Owing to the analytical procedure applied, only higher molecular weight compounds (C_{15+}) are recovered. Lower molecular weight compounds of the gas and gasoline range can only be analyzed in a quantitative fashion if sealed canned samples are collected from a freshly drilled core immediately after recovery (Schaefer et al., 1978). Because freshly drilled material was not available for both maturity levels, a quantitative assessment of the gas phase would not be relevant.

The bitumen extract of the samples was separated by medium pressure liquid chromatography into aliphatic

hydrocarbons, aromatic hydrocarbons, and NSO-compounds (Radke et al., 1980). The concentration of the asphaltene fraction (n-hexane insoluble fraction) was determined by differences between the total bitumen extract yields and the sum of the aliphatic hydrocarbon, aromatic hydrocarbon and NSO-compound yields. Selected molecular species of the aliphatic and aromatic hydrocarbons were identified by gas chromatography and quantified. N-alkanes, naphthalenes, phenanthrenes, and dibenzothiophenes were chosen because these compound classes are major fractions of crude oils and bitumens and have been successfully used to solve questions of hydrocarbon generation and migration (e.g. Leythaeuser et al., 1988a, 1988b).

Mass Balance Approach

In order to monitor the generation progress over the studied maturity interval, organic carbon normalized concentrations of selected compounds were assembled to a mass-balance. The soluble organic matter yields of a number of samples from each of the sedimentary facies from both maturity levels were averaged and compared to each other. If a yield increase was observed, it is interpreted to reflect progressive petroleum formation. A mass balance is then established:

$$\text{Compound Yield}_{\text{generated}} =$$
$$\text{Compound Yield}_{\text{more mature sample}} - \text{Compound Yield}_{\text{less mature sample}}.$$

A number of samples (three or four) from each facies from both locations was averaged to get a reliable trend. The selection of samples for this mass balance calculation was based on bulk organic geochemical characteristics. The samples of each facies group chosen from Amelie II and Berrwiller contain similar contents of organic carbon (TOC), similar hydrogen index values (in the case of the marl samples), very similar carbonate contents ($CaCO_3$), and, at the same maturity stage, similar yields of extract (see Appendix).

4.6 Inventory of Chemical Changes of the Lithofacies of the S unit of the Mulhouse Basin over the Maturity Interval 0.35-0.45% R_o

The first step in establishing a mass balance is to inventory the abundance of the studied compounds at each maturity level. In the this chapter a data base for each compound class is established. For the lithofacies of each maturity interval, first the solid organic matter (kerogen concentration) is presented, followed by the extractable organic matter concentration . The compound classes of the organic matter are then presented with their hydrocarbon subfractions (Tables 3 and 4).

4.6.1 Kerogen

Most petroleum geologists accept that the bulk of petroleum hydrocarbons are generated by thermal decomposition of kerogen in source rocks during long periods of burial (Hunt, 1979; Tissot and Welte, 1984). The process of petroleum formation is thought to occur as a decomposition of the labile portion of the kerogen into liquid bitumen and finally a partial decomposition of this bitumen into oil and gas (Lewan, 1992). A consequence of this process is a continuous decrease in the kerogen content of a source rock and at the same time, an increase

Table 3: Concentration of the kerogen and extract yields of the lithofacies of the S unit in gram carbon per gram total organic carbon.

Lithofacies	Ro	Aliphatic HCs	Aromatic HCs	NSO–compounds	Asphaltenes	Kerogen
	(%)	(mg C/g TOC)	(mg C/g TOC)	(mg C/g TOC)	(mg C/g TOC)	(mg C/g TOC)
Marl Type A	0.35	16.28	2.87	24.4	86.45	870.00
	0.45	21.65	7.85	19.51	139.08	811.91
Marl Type B	0.35	25.77	3.45	40.89	11.74	918.15
	0.45	38.24	6.78	53.57	101.74	799.67
Lenticular Anhydrite	0.35	17.25	4.64	8.76	79.43	889.92
	0.45	34.44	19.24	5.38	57.04	883.90
Laminated Anhydrite	0.35	14.69	4.55	5.13	59.57	916.06
	0.45	31.76	18.8	5.59	45.99	897.86
Massive Anhydrite	0.35	12.04	3.76	6.31	63.18	914.71
	0.45	9.52	10.24	2.74	20.96	956.54

Table 4: Concentration of the extract yields of the lithofacies of the S unit.

Lithofacies	Ro	Aliphatic HCs	Aromatic HCs	NSO-compounds	Asphaltenes	Total Extract
	(%)	(mg/g TOC)	(mg/g TOC)	(mg/g TOC)	(mg/g TOC)	(mg/g TOC)
Marl Type A	0.35	18.50	3.12	32.98	112.35	166.95
	0.45	24.61	7.22	26.36	187.97	246.16
Marl Type B	0.35	29.29	3.76	55.26	15.85	104.16
	0.45	43.46	7.38	72.40	137.78	261.02
Lenticular Anhydrite	0.35	19.61	5.05	11.85	107.37	143.88
	0.45	39.14	20.92	7.28	77.11	144.45
Laminated Anhydrite	0.35	16.70	4.95	6.94	80.51	109.10
	0.45	36.10	20.44	7.56	62.16	126.26
Massive Anhydrite	0.35	13.69	4.09	8.54	85.39	111.71
	0.45	10.82	11.14	3.71	28.54	54.21

in the liquid organic matter portion, as long as no petroleum is expelled.

In order to document kerogen conversion as a consequence of the maturation progress, the average carbon content of the kerogens normalized to the total organic carbon content of the sediments was calculated for samples of each sedimentary facies at 0.35% R_o and 0.45% R_o, respectively. As a first step, the total organic carbon content of the sediment was measured. In a second step, the actual carbon content of the bitumen fraction was calculated. The aliphatic hydrocarbon and the aromatic hydrocarbon fractions, the NSO-compounds and the asphaltenes of the bitumen were converted into the actual carbon content of each fraction by multiplying the organic carbon-normalized yields of each fraction by a correction factor. The correction factors proposed by Tissot and Welte (1984) as appropriate for average bitumens of source rocks are 0.88 for the aliphatic hydrocarbons, 0.92 for the aromatic hydrocarbons and 0.74 for the NSO-compounds and asphaltenes and approximate the actual carbon content of each chemical compound class. By this method, the carbon concentration of the bitumen is determined and can be expressed as a partial concentration of the total organic carbon content (mgC/g TOC). The measurable total organic carbon of a sediment consists of the sum of the carbon of the kerogen, the extractable organic matter, and

liquid and gaseous organic matter that cannot be extracted with organic solvents. Therefore, if the carbon content of the extractable organic matter is removed from the total organic carbon, the remaining carbon content is that of the kerogen and the non-extractable organic matter of the sediment. The carbon content of the kerogen and the non-extractable organic matter cannot be separated by this method. However, it is to be expected that the concentration of organic carbon bound in the kerogen at low maturities exceeds by far the organic carbon bound in the non-extractable organic matter. Therefore, they are both treated as "kerogen" in the concentrations presented in Table 3. The concentrations reported in Table 3 are the carbon concentrations of each organic matter species in one gram of organic carbon.

The results of the calculations (Table 3) show that the "kerogen" portion of the total organic carbon varies between 799 and 956 mgC/g C_{org} or 79.9% to 95.6% of the total organic carbon. The normalized kerogen content generally decreases with increasing maturity (Fig. 59). An exception is that the kerogen content of the massive anhydrite facies increases with degree of maturity.

The decrease in the normalized kerogen content with increasing maturity can be interpreted as indicative of

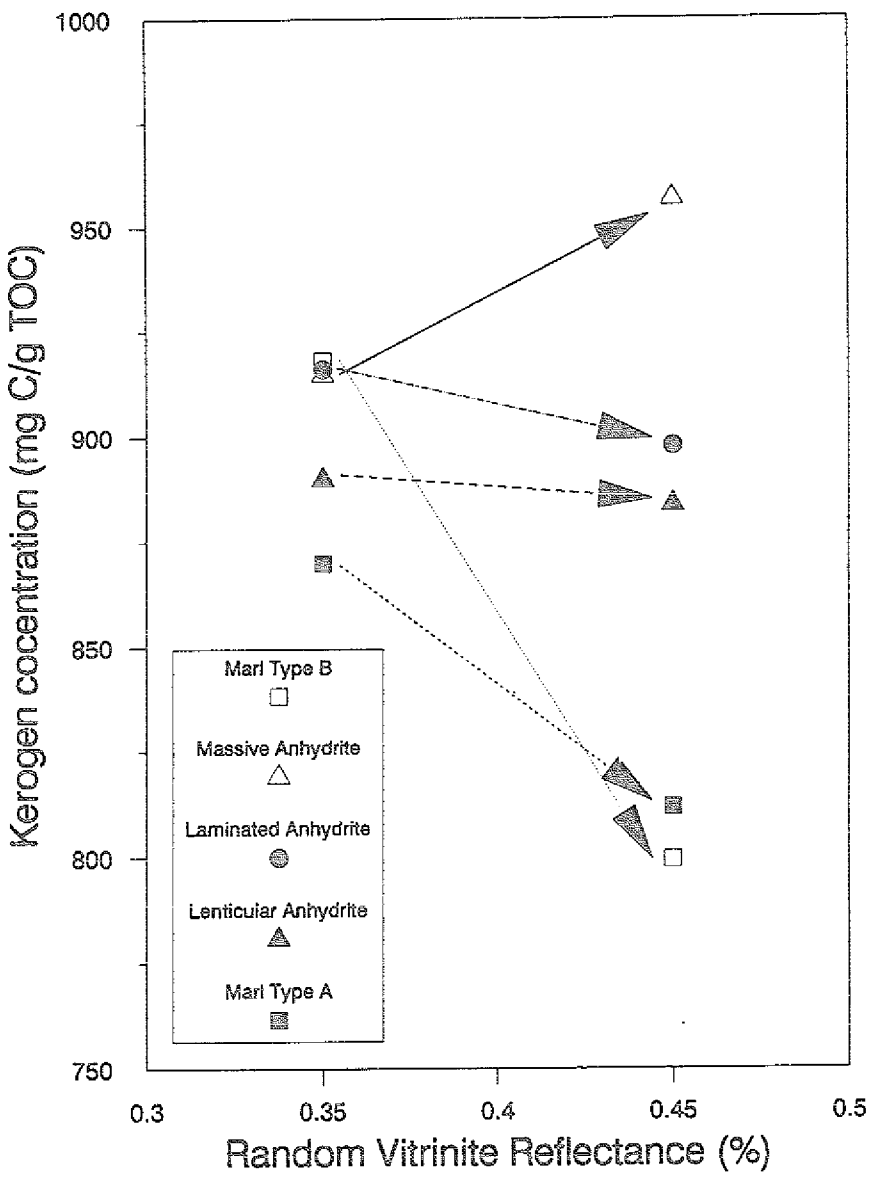

Fig. 59: Variation of the kerogen concentration of the lithofacies of the S unit with maturity.

kerogen conversion into liquid bitumen. The increase of the kerogen portion of the massive anhydrite facies indicates that in this facies, the ratio of kerogen to bitumen has increased.

4.6.2 Total Extracts

The TOC-normalized extract yields depicted in Fig. 60 were obtained by flow blending extraction with dichloromethane (Radke et al., 1978). Extract yields vary between 45 mg/g TOC (massive anhydrite, Berrwiller) and 371 mg/g TOC (marl type B, Berrwiller) (Table 4). Generally, the extract yield of the sediments of the S unit are unexpectedly high, considering their low maturity. Based on the TOC-normalized extract yields, it can be determined that between 10% and 20% of the total organic matter is present in the form of extractable bitumen. There is a trend of increasing extract yields with increasing TOC content.

When the yields within each individual sedimentary facies are compared (Fig. 60), it can be seen that at the less mature site Amelie II, marls of type A have on average the highest extract yields (166 mg/g TOC), followed by lenticular anhydrites (143 mg/g TOC), laminated anhydrites (109 mg/g TOC), massive anhydrites (111 mg/g TOC) and marls of type B (104 mg/g TOC). At the more mature site

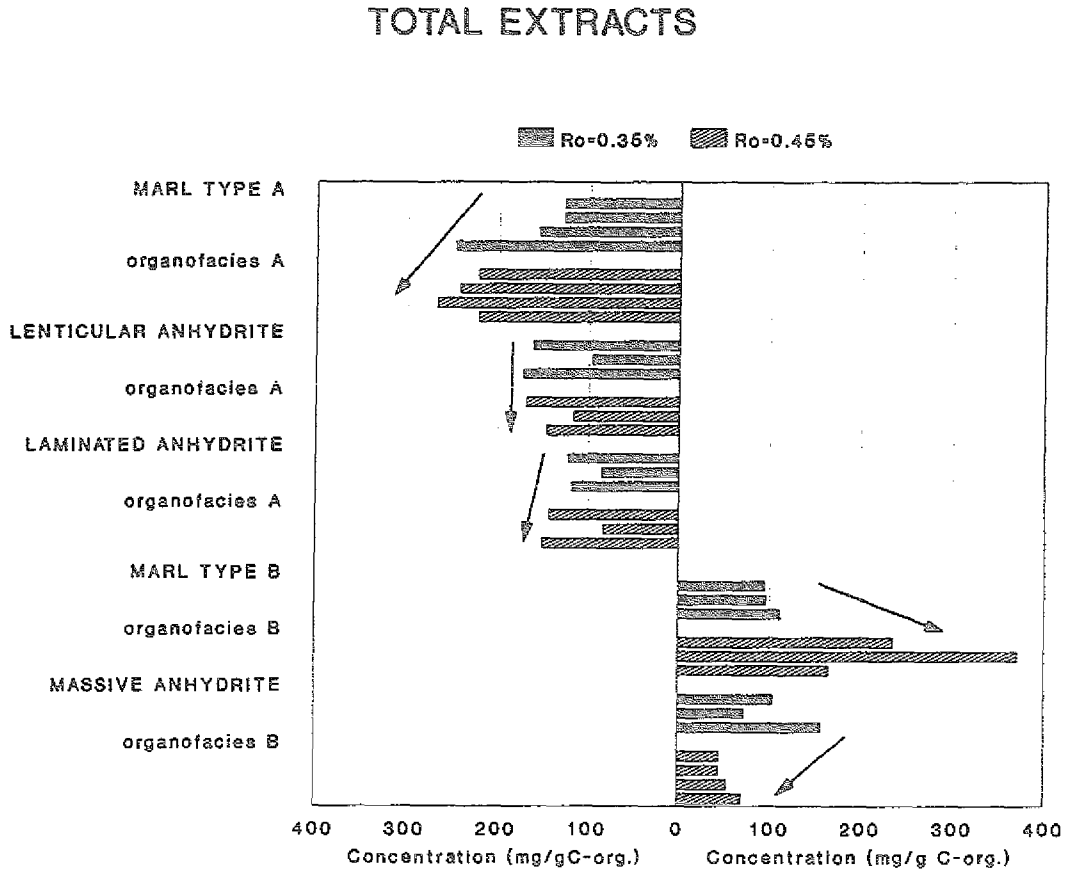

Fig. 60: Extract yields of the lithofacies of the S unit at 0.35 % R_o and 0.45 % R_o.

at Berrwiller, however, the highest yields are associated with type B marls (261 mg/g TOC), followed by type A marls (246 mg/g TOC), lenticular anhydrite (144 mg/g TOC), laminated anhydrites (126 mg/g TOC) and massive anhydrites (54 mg/g TOC).

Surprisingly, even though maturation progresses from site Amelie II (0.35% R_o) to site Berrwiller (0.45% R_o), only marls of type A and of type B show a marked increase in total extract yield (by a factor of 1.48 and 2.50, respectively). The extract yields for laminated anhydrites increase only slightly and for lenticular anhydrites they remain almost constant within this maturity interval. The extract yields of massive anhydrites even decrease by 47% (Fig. 61).

Extract Composition

The bitumens of sediments can be separated into hydrocarbons and non-hydrocarbons. The hydrocarbons of the bitumen are contained in the aliphatic and aromatic hydrocarbon fraction. The NSO-compounds and asphaltenes are heterocompounds that in addition to carbon and hydrogen atoms also contain other atoms, especially nitrogen, sulfur, and oxygen. Immature bitumens are

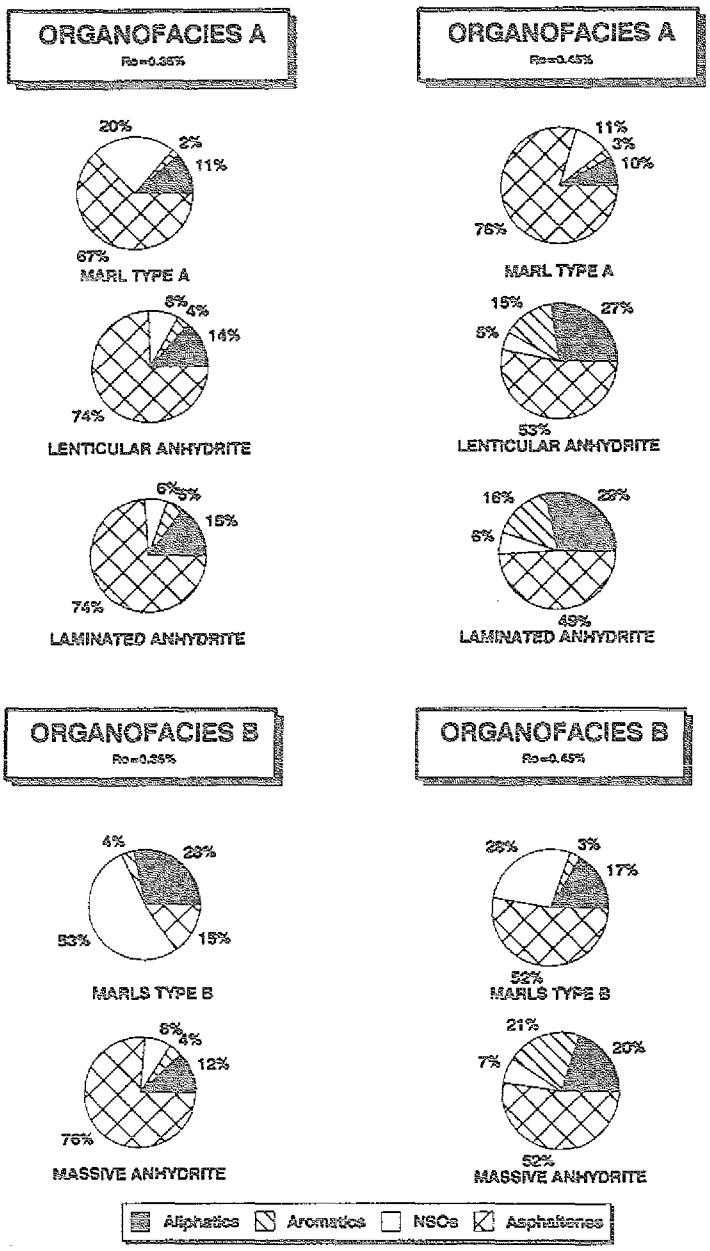

Fig. 61: Composition of the extracts of the lithofacies of the S unit at 0.35 R_o and 0.45 R_o.

characterized by high proportions of asphaltenes and NSO-compounds, whereas mature bitumens are dominated by the hydrocarbon fractions.

The bitumens of the Mulhouse Basin sediments are rich in heterocompounds. Asphaltenes and NSO-compounds constitute between 55% and 87% of the total extract yields (Fig. 61). The non-hydrocarbon fraction of the less mature extracts (R_o of the kerogen = 0.35%) from the sediments at Amelie II is generally dominated by the asphaltenes. An exception is the extracts of the marls of type B. In this sedimentary facies, NSO-compounds dominate the non-hydrocarbon fraction. The hydrocarbon fractions amount to between 13% and 32% of the total extract yields of the sediment at Amelie II (Fig. 61). The sediment extracts from the more mature site at Berrwiller (R_o = 0.45%) are markedly different from the ones from Amelie II. The relative proportion of hydrocarbons is higher in extracts from Berrwiller (13-45% of the total extracts). Anhydrite-rich sediments (laminated, lenticular and massive anhydrite) show sharp increases in the relative amounts of aromatic and aliphatic hydrocarbons when compared to the Amelie II extracts and at the same time a drop in the relative concentrations of the polar fractions. The behavior of the marl extracts, however, is contrary to this trend. The relative concentrations of the polar fractions stays almost the same at Amelie II and

Berrwiller, even though the NSO-compound fraction is reduced in favor of the asphaltene fraction.

The general increase in extract yields in all sedimentary facies from the less mature site at Amelie II to the more mature site at Berrwiller indicates that bitumen formation is associated with an increase in maturity. The formation of bitumen is accompanied by a shift in the composition of the bitumen. In general, hydrocarbon formation appears to take place, while at least in the anhydrite-rich sedimentary facies heterocompounds are either converted into hydrocarbons or formed at a lower rate than hydrocarbons. The differences in bitumen composition in the marls compared to the anhydrite-dominated sediments may point to distinctly different formation mechanisms for each of these lithofacies.

4.6.3 Aliphatic Hydrocarbons

The average aliphatic hydrocarbon yields of the sediments from the less mature site Amelie II range between 13-29 mg/g TOC. The yields of the more mature site Berrwiller are generally higher (11-44 mg/g TOC; Fig. 62) than at site Amelie II. The aliphatic hydrocarbon yields increase for each defined lithofacies with the exception

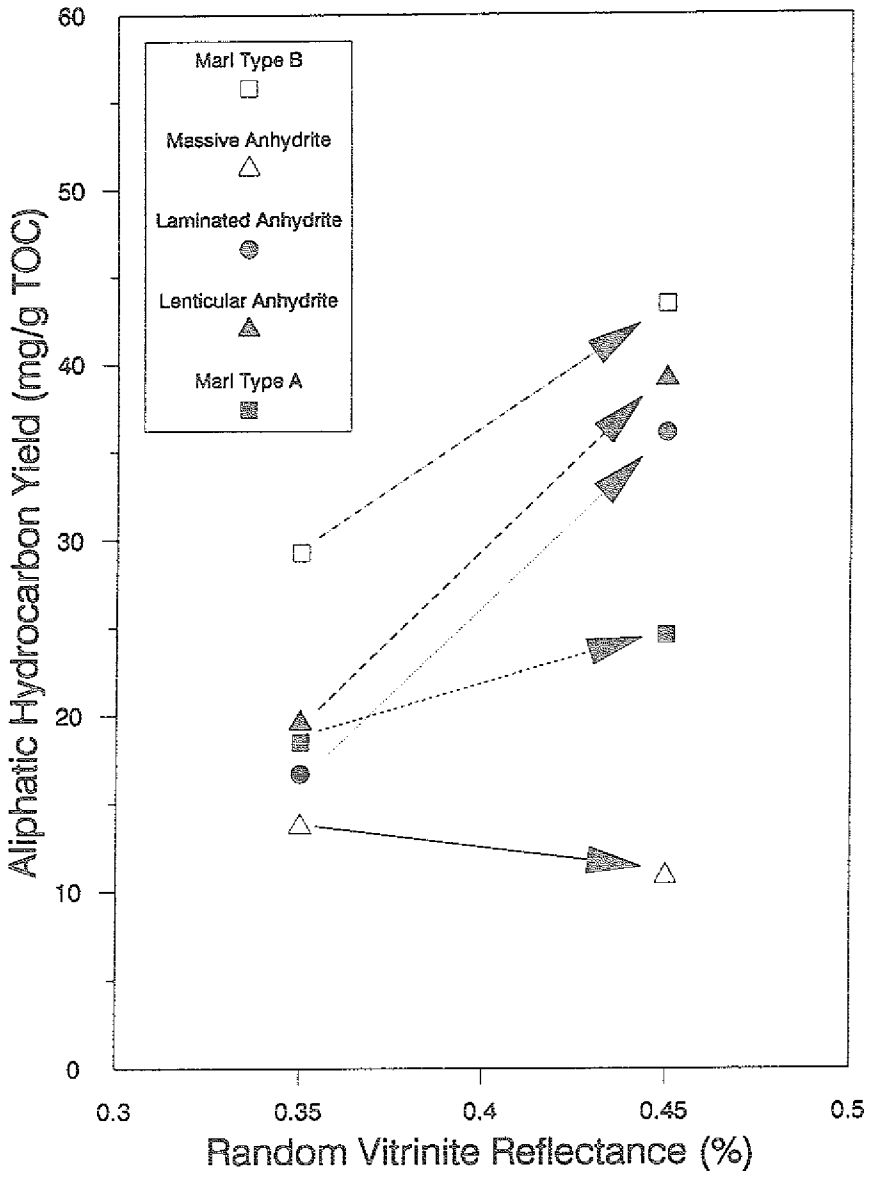

Fig. 62: Aliphatic hydrocarbon yields of the lithofacies of the S unit.

of the massive anhydrites. The aliphatic hydrocarbon yields of this facies are approximately 20% lower at Berrwiller than at the less mature site Amelie II.

4.6.3.1 Bulk Yields of n-alkanes

The n-alkane yield increase over the maturity interval from 0.35% R_o to 0.45% R_o can also be documented on a molecular level. For this purpose the n-C_{15} to n-C_{29} alkanes were identified and quantified by gas chromatography. The n-alkane concentrations range from 1.43 to 8.07 mg/g TOC at Amelie II and from 1.34 to 19.60 mg/g TOC at Berrwiller. The total n-alkane yields, depicted in Fig. 63, show the same trend as the aliphatic hydrocarbon yields. The n-alkane concentrations increase for each lithofacies from the less mature location to the more mature location. The massive anhydrite lithofacies at the maturity level 0.45% R_o, however, contains the lowest n-alkane yields of all lithofacies.

4.6.3.2 Mass Balance on the Molecular Level

For the purpose of a mass balance on the molecular level, the concentrations of individual n-alkanes of a selected number of samples from each lithofacies were compared. Two generally different n-alkane patterns had been

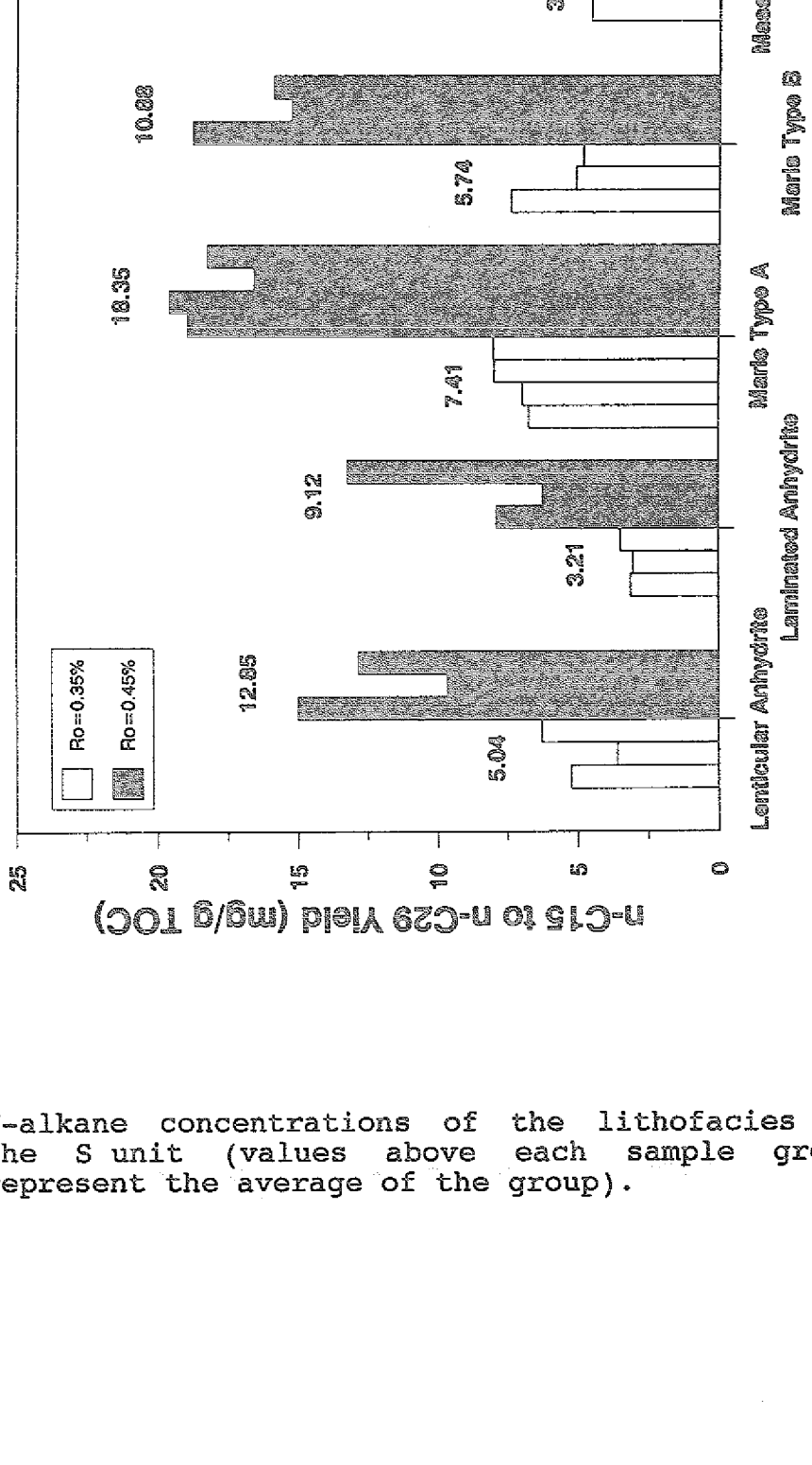

Fig. 63: N-alkane concentrations of the lithofacies of the S unit (values above each sample group represent the average of the group).

previously identified (see Chapter 4.3.4) and assigned to organic facies A and organic facies B. The yield increase on the molecular level is documented in the marls of type A for organic facies A and marls of type B for organic facies B (Figs. 64, 65). Within each organic facies group, the n-alkane yields for samples from the same lithofacies with identical maturity are very similar. The overall distribution patterns stay almost identical over the studied maturity interval. However, the absolute yield increase per n-alkane varies considerably. In order to demonstrate the absolute yield increase per n-alkane, the TOC-normalized n-alkane yields of each sedimentary facies were averaged for each maturity level. The resulting concentrations were subtracted from one another to calculate the absolute yield increase for each individual hydrocarbon over the studied maturity interval.

The results are presented below according to the organic facies present in each lithofacies. First the lithofacies that contain organic facies A are discussed (marls of type A, lenticular anhydrite, laminated anhydrite) and then lithofacies that contain organic facies B (marls of type B, massive anhydrites).

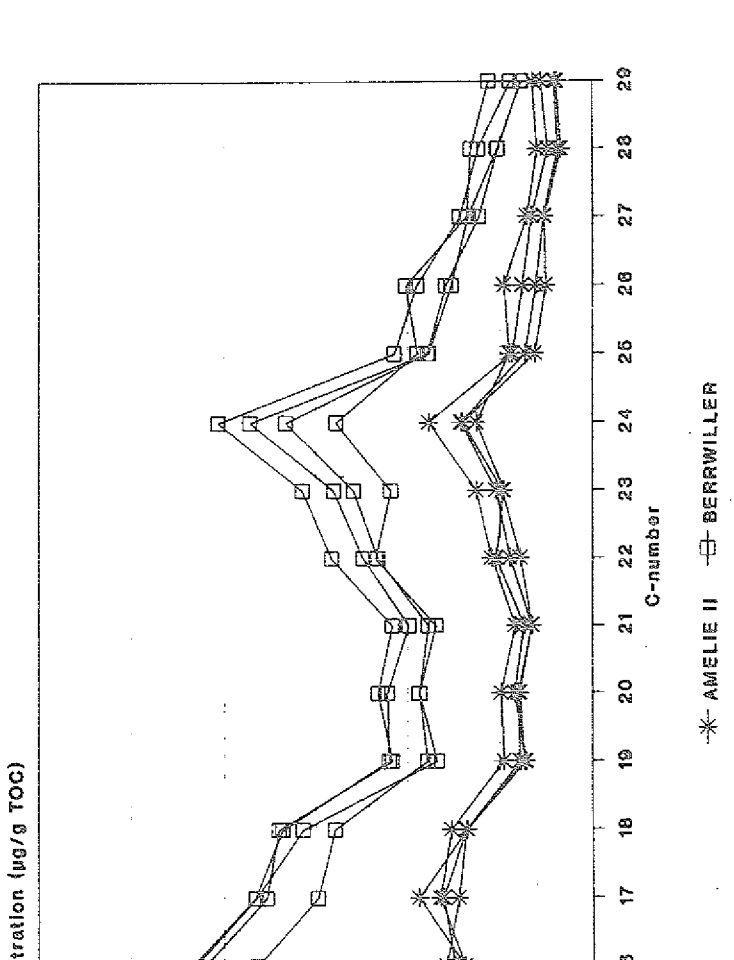

Fig. 64: N-alkane concentration patterns of marl of type A samples from Amelie II and Berrwiller. Note the similar concentrations of samples from each site.

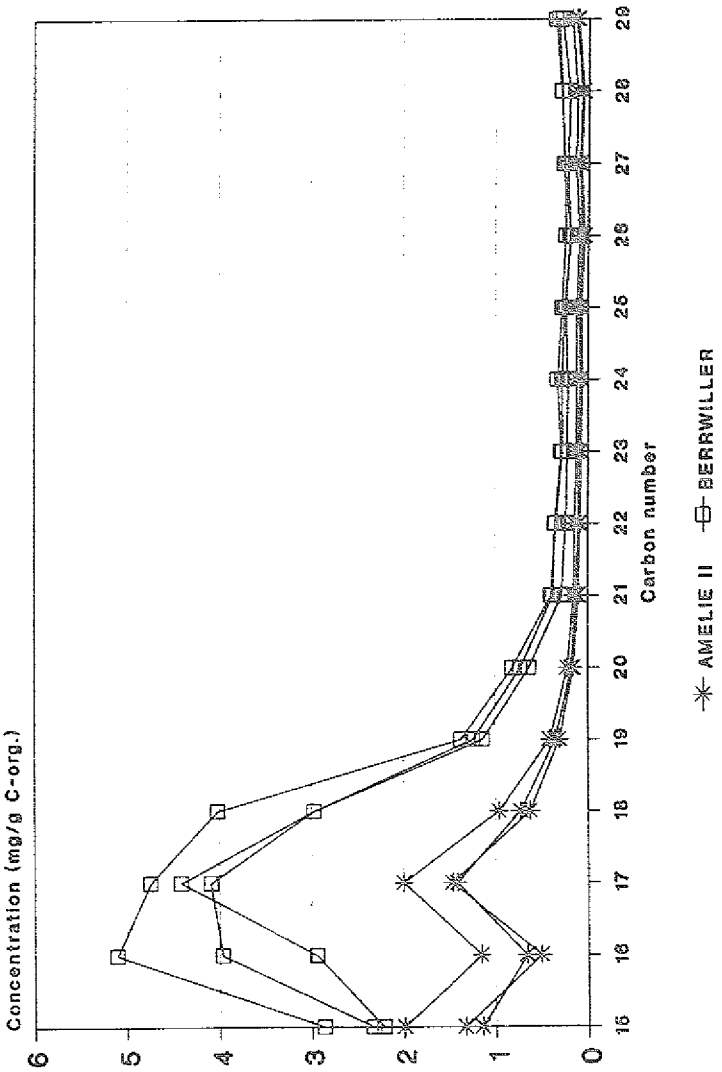

Fig. 65: N-alkane concentration patterns of marl of type B samples from Amelie II and Berrwiller.

Organic Facies A

Marls of Type A

The averaged n-alkane contents of marls of type A from site Amelie II and Berrwiller are depicted in Fig. 66. The absolute yield increase per n-alkane is also shown (curve BE-AM in Fig. 66). This type of presentation of the mass balance results will be followed for all lithofacies.

The results indicate that for each individual n-alkane there is a distinct increase in yield in the maturity interval between 0.35 and 0.45% R_o. This yield increase exceeds the content of n-alkanes that are present in the less mature samples. No preferential generation of any specific n-alkane species is apparent, with the exception of a somewhat higher yield increase in the C_{15}-C_{16} range. However, this type of yield increase is an artifact due to evaporative loss during sample preparation.

Lenticular Anhydrites

Lenticular anhydrites contain lower contents of n-alkanes (normalized to TOC) than marls of type A in both the less and more mature sample suites. The absolute yield

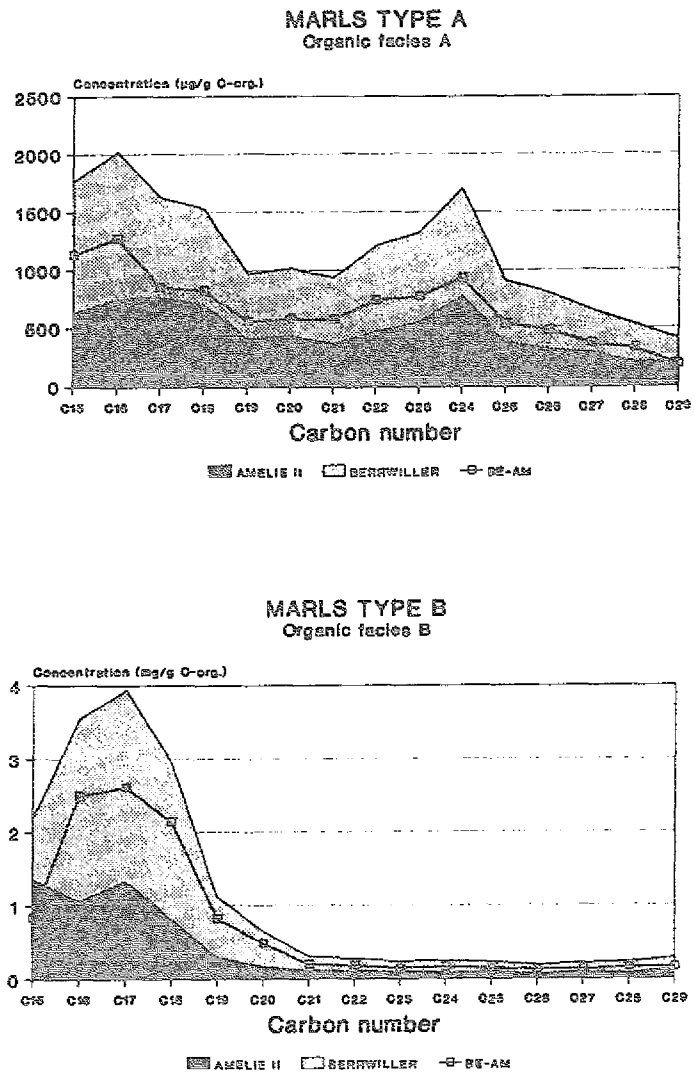

Fig. 66: Average n-alkane concentration patterns and absolute yield increases (BE - AM) of the lithofacies of the S unit. (Continued on following page.)

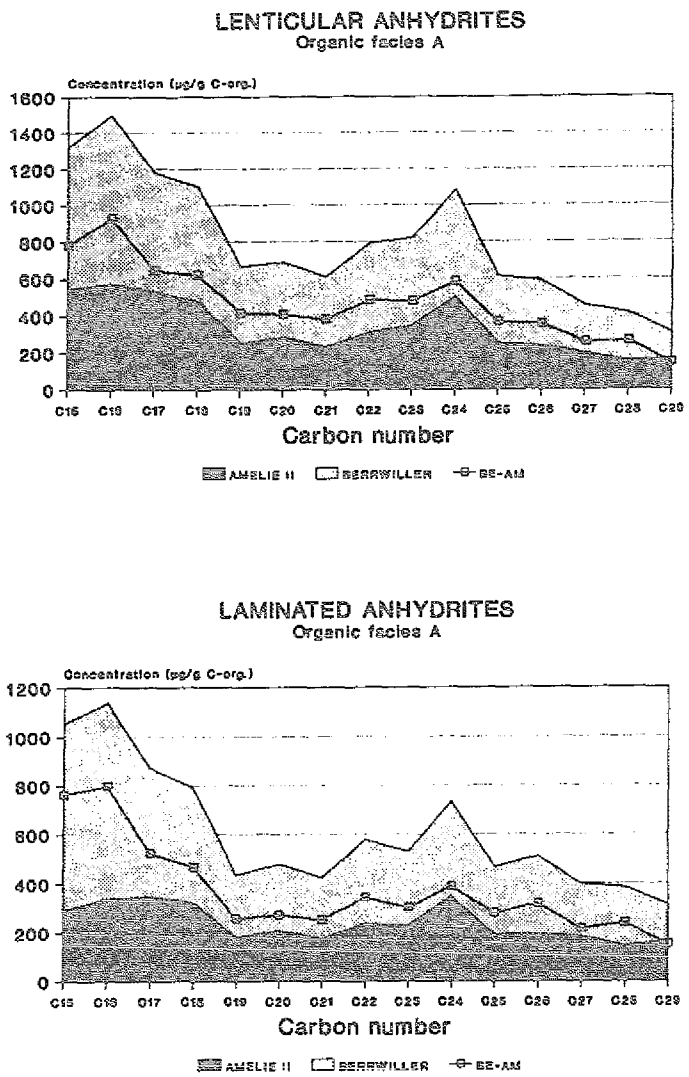

Fig. 66: (Continued from preceding page.) Average n-alkane concentration patterns and absolute yield increases (BE - AM) of the lithofacies of the S unit.

increase over the maturity interval is lower in lenticular anhydrites than in marls of type A (Fig. 66). However, as in marls of type A, the distribution pattern of the newly generated hydrocarbons over the studied maturity interval remains the same as the one from the less mature samples. Also, the absolute yield increase exceeds the n-alkane concentrations of the less mature sample suite from site Amelie II.

Laminated Anhydrites

The distribution patterns of the averaged n-alkane yields of the laminated anhydrites follow the general trend of those of the marls of type A and the lenticular anhydrites (Fig. 66). However, a pronounced even/odd predominance is encountered in the C_{20}-C_{28} range. The even/odd predominance is even more pronounced in the more mature sample suite. Within the organic facies A group, the absolute yield gains for each n-alkane becomes smaller from marls of type A through lenticular anhydrites to laminated anhydrites (Fig. 66).

Organic Facies B

Marls of Type B

The differences in n-alkane distribution patterns between organic facies A and organic facies B were discussed in the first chapters of this thesis. If the same mass balances-type calculations described previously are performed for samples of marls of type B from Amelie II (R_o = 0.35%) and Berrwiller (R_o = 0.45%), a marked increase in the yields of all n-alkanes in the C_{15}-C_{20} range with increasing maturation is observed. With the exception of n-C_{16}, the yield increase exceeds the original content of n-alkanes of the less mature sample set (Amelie II; Fig. 66).

Massive Anhydrites

The mass balance-type calculations for massive anhydrites show a completely unexpected trend which is very dissimilar to the ones discussed above: massive anhydrites from the less mature site Amelie II (R_o = 0.35%) contain higher yields of n-alkanes than massive anhydrites from the more mature site Berrwiller (R_o = 0.45%) (Fig. 67). The absolute yield decrease over this maturity interval is most pronounced for n-alkanes in the

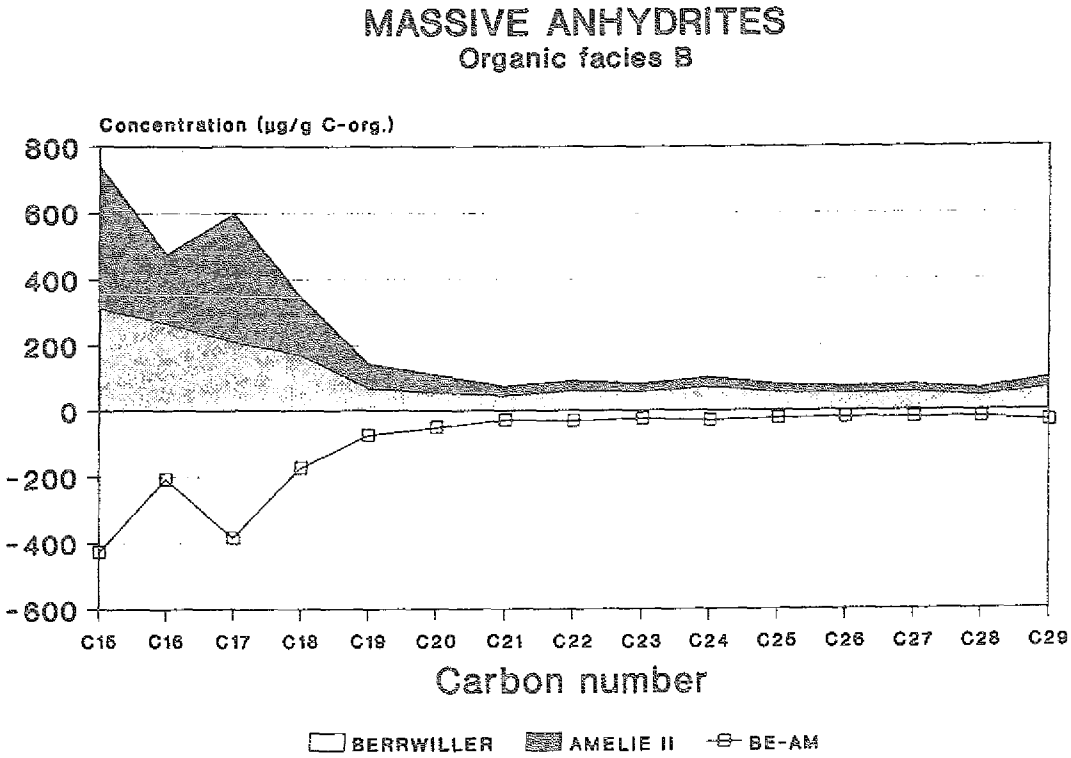

Fig. 67: Average n-alkane concentration patterns of samples of the massive anhydrite lithofacies at Amelie II and Berrwiller. Note the net loss of n-alkanes (BE - AM).

C_{15}-C_{20} range, but in general every n-alkane occurs in lower concentrations (normalized to TOC) at Berrwiller than at Amelie II.

4.6.4 Aromatic Hydrocarbons

The aromatic hydrocarbon yields increase for each lithofacies in the maturity interval from 0.35% R_o to 0.45% R_o (Fig. 68). The most pronounced increase is recorded for the laminated and lenticular anhydrite lithofacies. Their aromatic hydrocarbon concentrations increase by a factor 4, while the concentrations of marls of type A and of type B approximately double. It should be noted that the aromatic hydrocarbon concentration of the massive anhydrite facies also shows a marked gain in the aromatic hydrocarbon yield. This behavior is opposite to yield decreases for this lithofacies with respect to the total extracts, aliphatic hydrocarbons, and n-alkanes.

4.6.4.1 Bulk Yields of Naphthalenes

The naphthalene fraction of the aromatic hydrocarbons is characterized by higher yields in the more mature samples from all lithofacies (Fig. 69). The absolute concentrations vary between 135 and 1951 mg/g TOC. There is generally little variation among the samples of one

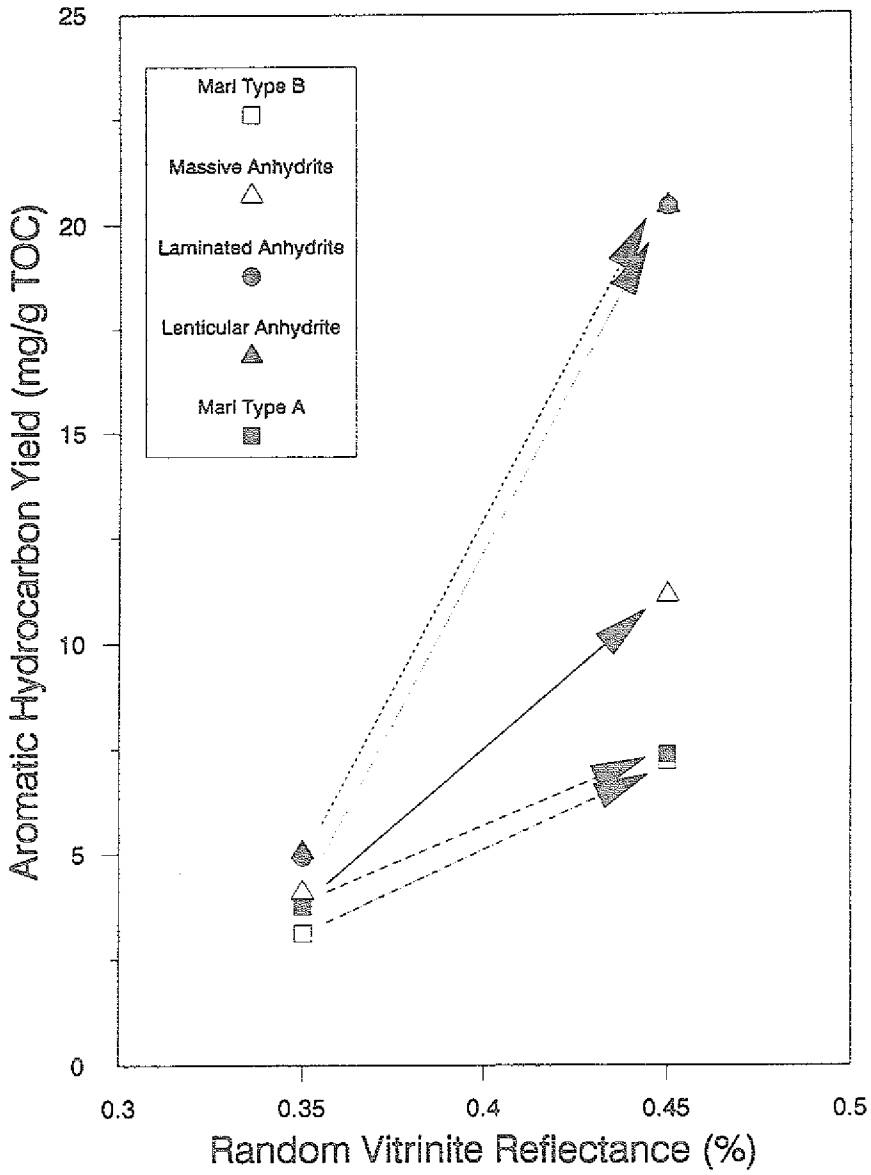

Fig. 68: Aromatic hydrocarbon yields of the lithofacies of the S unit.

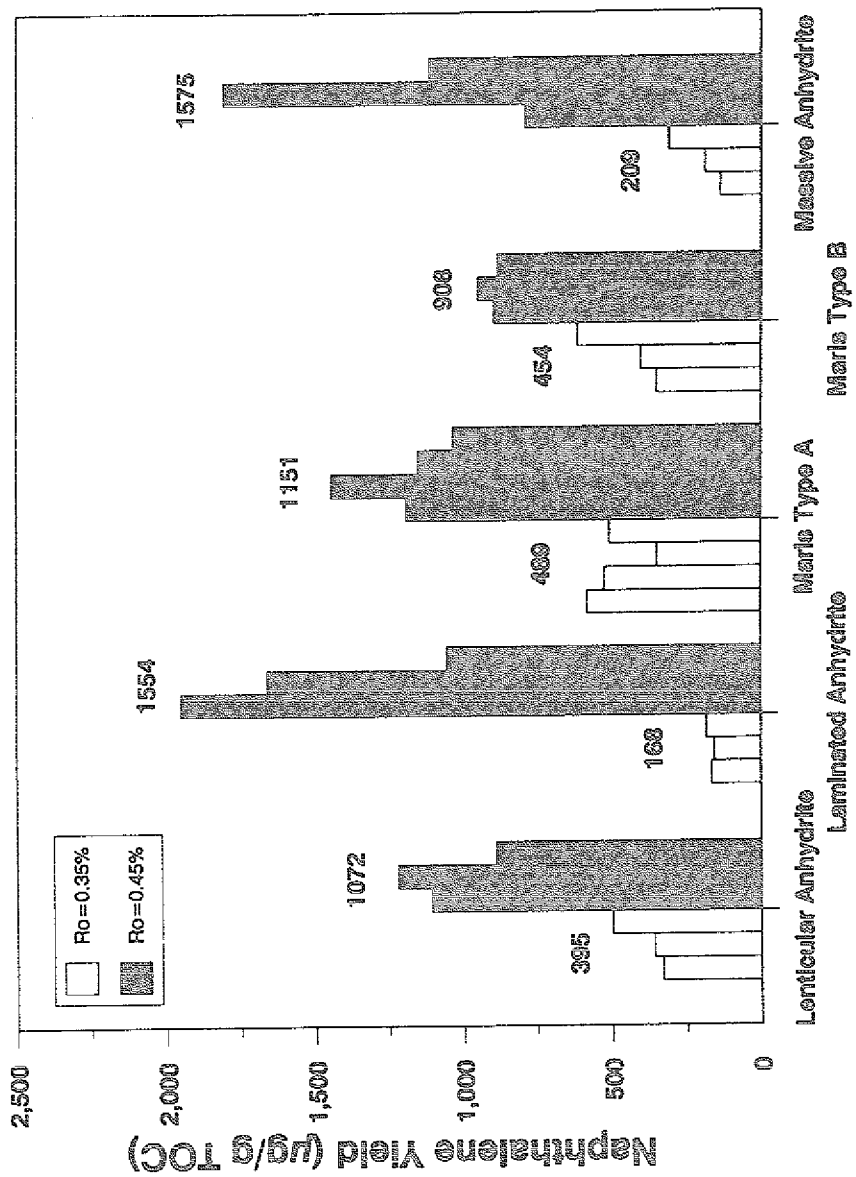

Fig. 69: Naphthalene concentrations of the lithofacies of the S unit (values above each sample group represent the average of the group).

lithofacies from the less mature site, however, considerable differences in naphthalene concentration can occur within each lithofacies among the more mature samples.

4.6.4.2 Mass Balance on the Molecular Level

The concentrations of selected naphthalenes, phenanthrenes and dibenzothiophenes were determined by gas chromatography. An inventory of the individual compounds that have been identified and quantified is given in Table 5.

Naphthalenes

The carbon-normalized naphthalene yields of selected methylnaphthalenes, ethylnaphthalenes, dimethylnaphthalenes and trimethylnaphthalenes show very similar distribution patterns for all lithofacies. The highest concentrations are recorded for the methylnaphthalenes and the dimethylnaphthalenes (Figs 70, 71). The unresolved 1,3 + 1,5 dimethylnaphthalene peak corresponds inallfacies to the most abundant naphthalene. Ethylnaphthalenes and trimethylnaphthalenes usually occur in lower concentrations than the methylnaphthalenes and dimethylnaphthalenes.

Naphthalenes:	1 - Methylnaphthalene (1 MN)[1)] 2 - Methylnaphthalene (2 MN) 1 - Ethylnaphthalene (1 EN) 2 - Ethylnaphthalene (2 EN) 2,6 + 2,7 - Dimethylnaphthalene (1 DMN) 1,3 + 1,7 - Dimethylnaphthalene (2 DMN) 1,4 + 2,3 - Dimethylnaphthalene (3 DMN) 1,5 - Dimethylnaphthalene (4 DMN) 1,2 - Dimethylnaphthalene (5 DMN) 1,3,7 - Trimethylnaphthalene (1 TMN) 1,3,6 - Trimethylnaphthalene (2 TMN) 1,3,5 + 1,4,6 Trimethylnaphthalene (3 TMN) 2,3,6 - Trimethylnaphthalene (4 TMN) 1,2,5 - Trimethylnaphthalene (5 TMN)
Phenanthrenes:	Phenanthrene (PH) 1 - Methylphenanthrene (1 MP) 2 - Methylphenanthrene (2 MP) 3 - Methylphenanthrene (3 MP) 9 - Methylphenanthrene (9 MP) 2,3 + 3,5 - Dimethylphenanthrene (1 DMP) 2,7 - Dimethylphenanthrene (2 DMP) 1,3 + ? - Dimethylphenanthrene (3 DMP)[2)] 1,6 + ? - Dimethylphenanthrene (4 DMP) 1,7 - Dimethylphenanthrene (5 DMP) 2,3 - Dimethylphenanthrene (6 DMP) 1,9 + ? - Dimethylphenanthrene (7 DMP)
Dibenzothiophenes:	Dibenzothiophene (DBT) 1 - Methyldibenzothiophene (1 - MDBT) 2 + 3 - Methyldibenzothiophene (2,3 - MDBT) 4 - Methyldibenzothiophene (4 - MDBT)

1) Abbreviations in brackets correspond to the ones used in the following tables and figures.
2) ? indicates unresolved compounds.

Table 5: List of analyzed aromatic and sulfur aromatic compounds. (Note the abbreviations are used in many of the following figures.)

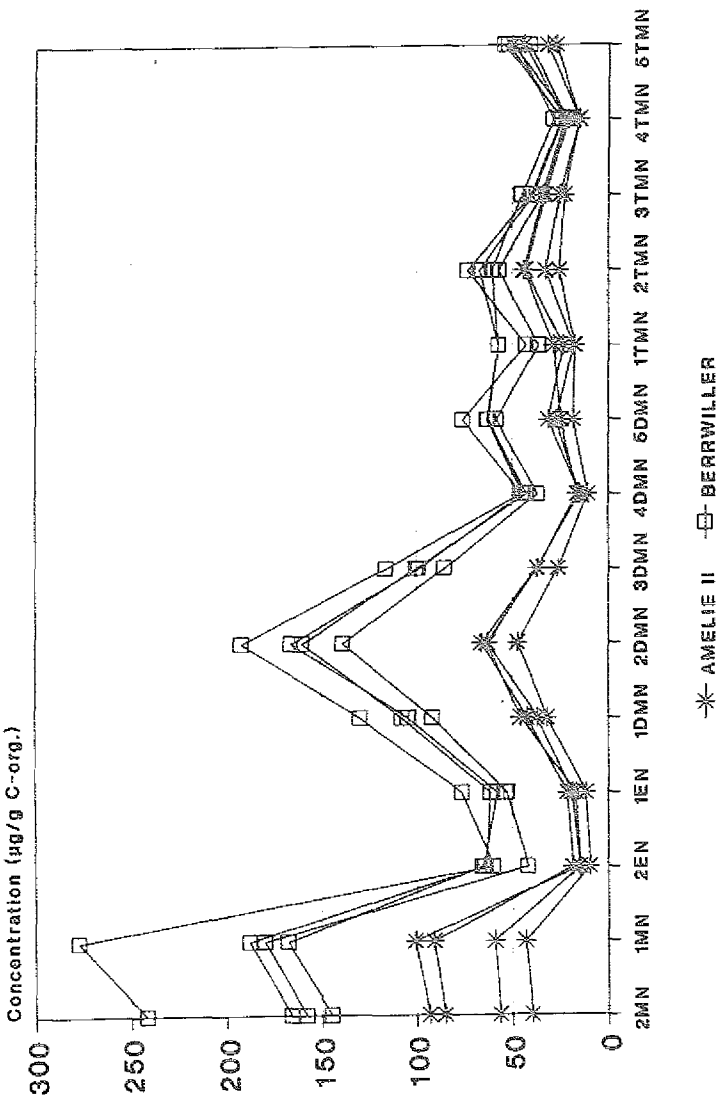

Fig. 70: Naphthalene concentration patterns of marl of type A samples from Amelie II and Berrwiller (abbreviations for individual naphthalene compounds are listed in Table 5).

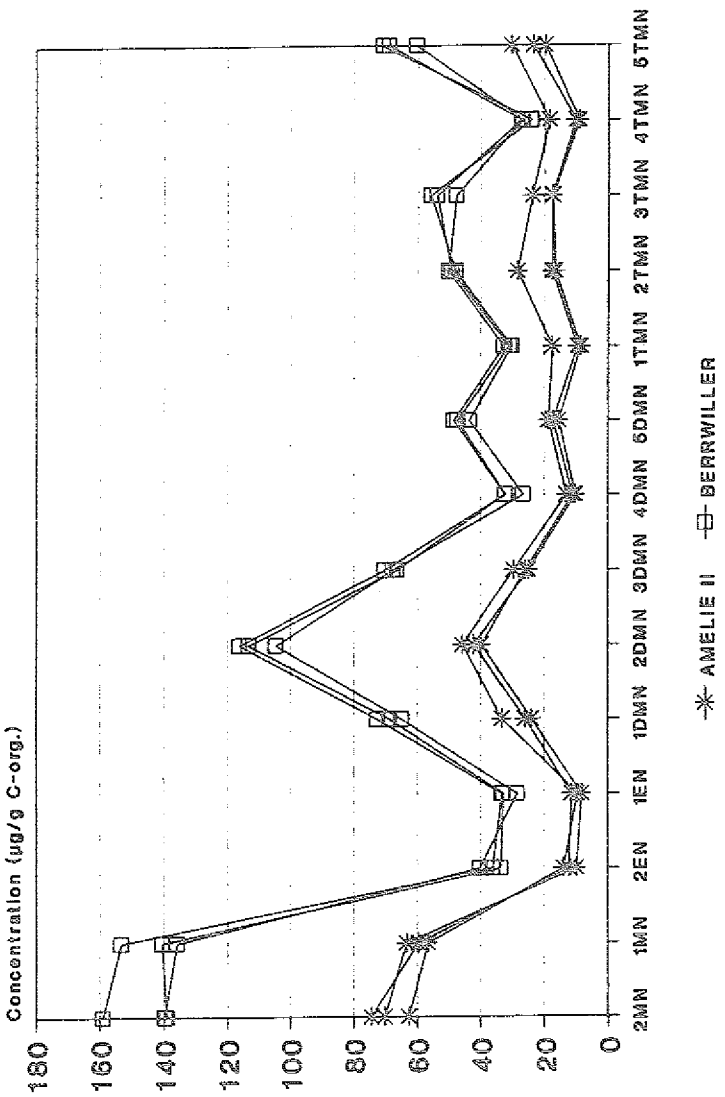

Fig. 71: Naphthalene concentration patterns of marl of type B samples from Amelie II and Berrwiller (abbreviations are listed in Table 5).

The individual naphthalenes of samples of one lithofacies with the same maturity level show only minor variations in concentration. The naphthalene distribution patterns remain the same at both maturity levels studied. However, the absolute concentration increases considerable at the higher maturity level (e.g. marls of type A and B; Figs. 70, 71). The average yield increase of the naphthalenes of each lithofacies is documented in Fig. 72.

Organic Facies A

Marls of Type A

The averaged naphthalene distribution patterns are presented in Fig. 72. The trends of naphthalene yield increases are in general similar to those of the n-alkanes. However, the yield increases in the trimethylated naphthalenes, especially for 1,3,6-TMN (2 TMN), 1,3,4 + 1,4,6-TMN (3 TMN), 2,3,6-TMN (4 TMN) and 1,2,5-TMN (5 TMN) are less pronounced than those for the methylated, ethylated and dimethylated naphthalenes.

Lenticular Anhydrites

The naphthalene yield increase follows the same pattern as in marls of type A (Fig. 72). The absolute yield increase

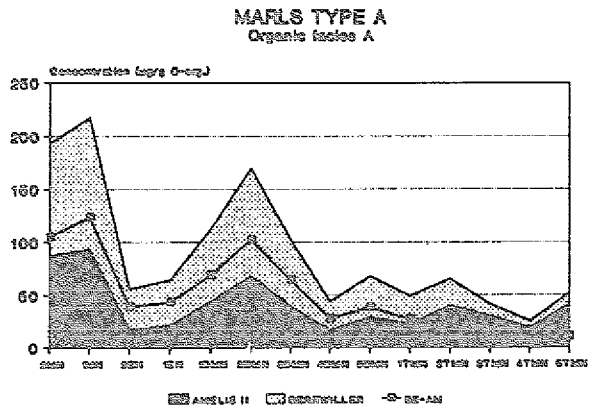

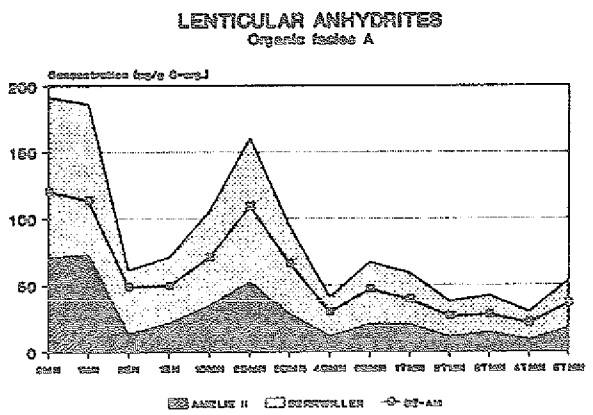

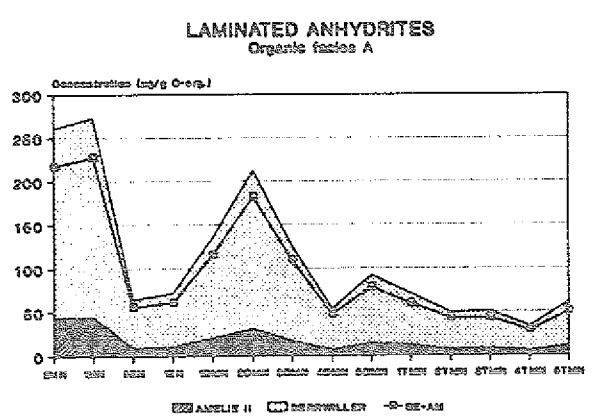

Fig. 72: Average naphthalene concentration pattern and absolute yield increase (BE - AM) of the lithofacies of the S unit. (Continued on following page.)

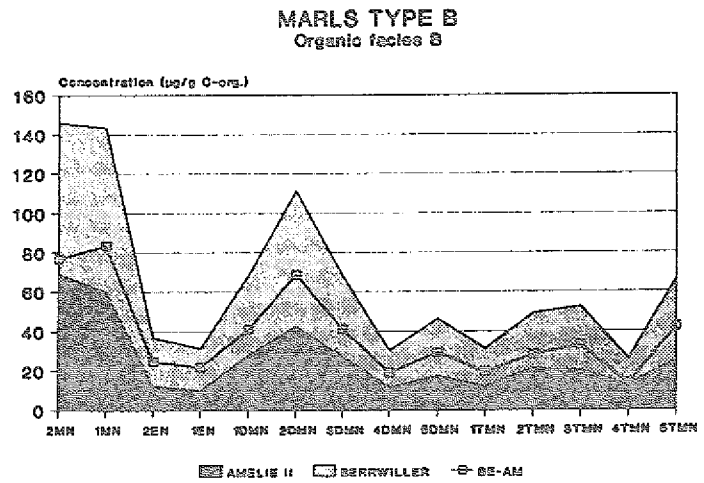

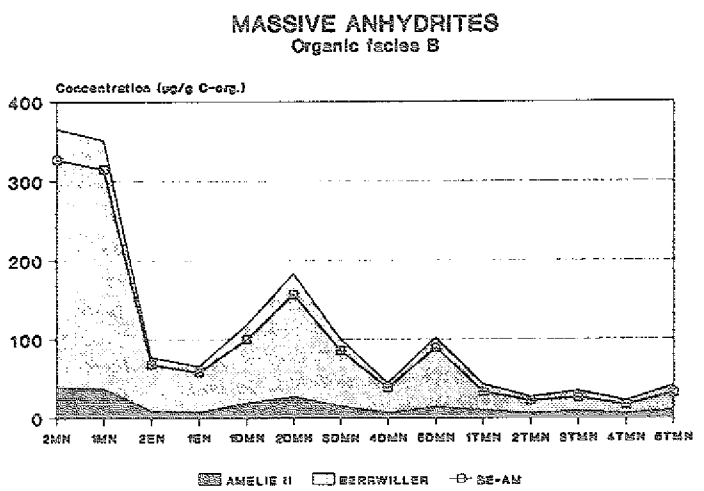

Fig. 72: (Continued from preceding page.) Average naphthalene concentration pattern and absolute yield increase (BE - AM) of the lithofacies of the S unit.

for each naphthalene molecule is almost identical to those observed in marls of type A (Fig. 72). However, in the lenticular anhydrite facies, the absolute increase of the trimethylated naphthalene concentrations exceeds those encountered in the samples from the less mature site Amelie II.

Laminated Anhydrites

Laminated anhydrites from the more mature site Berrwiller display the highest yields per naphthalene compared to samples of lenticular anhydrites and marls of type A (Fig. 72). They also show the highest absolute yield increases within both organic facies for each individual naphthalene molecule (Fig. 72).

Organic Facies B

Marls of Type B

The naphthalene distribution patterns of organic facies A are very similar to those of organic facies B. The average yield increase of each naphthalene molecule (Fig. 72, BE-AM) from Berrwiller to Amelie II exceeds the concentration observed at site Amelie II. The absolute yield increase in the studied maturity interval is lower

for marls of type B than those of the three sedimentary facies that contain organic facies A.

Massive Anhydrites

The mass balance calculation for naphthalene yields, however, show a reverse trend from that of the n-alkanes (Fig. 72). Here, naphthalene yields increase markedly over the studied maturity interval. The absolute yield increase per naphthalene is the highest recorded among all lithofacies (Fig. 72).

Phenanthrenes and Dibenzothiophenes

The phenanthrene and dibenzothiophene concentrations were determined for a selected number of samples from marls of type A and marls of type B. The samples were chosen to represent organic facies A (marls of type A) and organic facies B (marls of type B).

The phenanthrene distribution patterns of the samples from marls of type A and B are very similar (Figs. 73, 74). The most abundant compound is phenanthrene. The methylphenanthrenes generally occur in higher concentrations than the dimethylphenanthrenes. In both the marls of type A and type B considerable variation of the

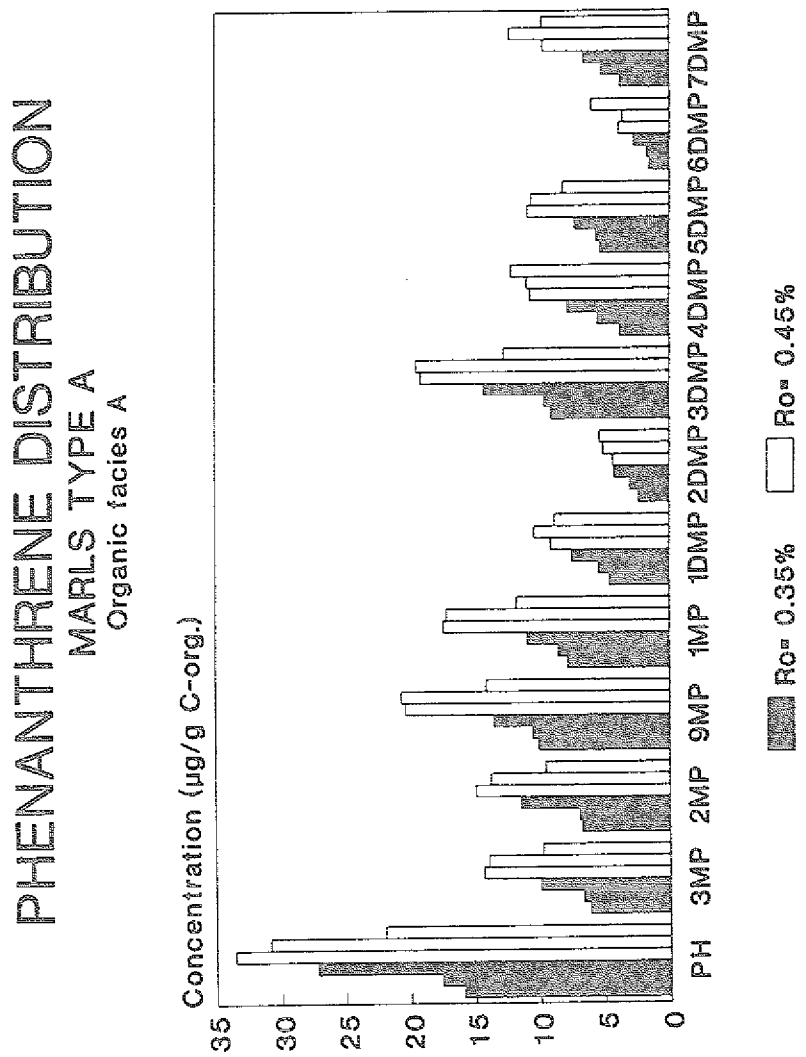

Fig. 73: Phenanthrene concentration patterns of marl of type A samples (abbreviations are listed in Table 5).

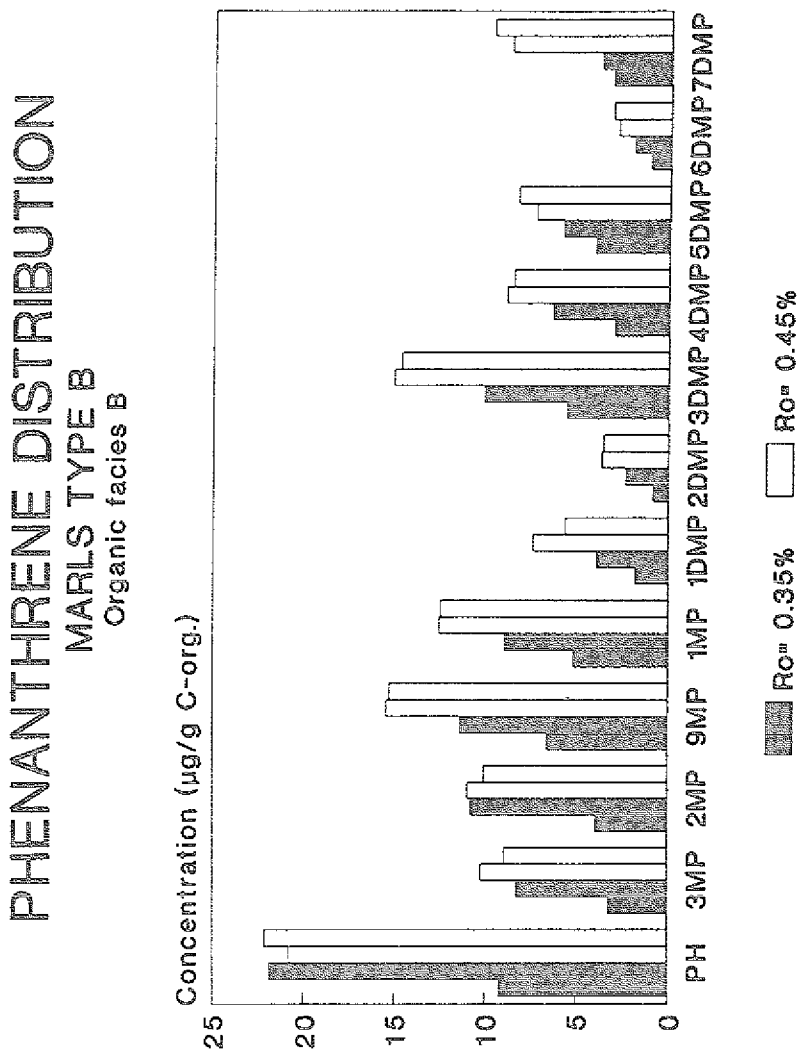

Fig. 74: Phenanthrene concentration patterns of marl of type B samples (abbreviations are listed in Table 5).

concentration of individual phenanthrenes exists among samples of identical maturity from one lithofacies. Even though on average higher concentrations of the individual phenanthrene molecular species generally exist in the more mature samples, there is some overlap in the concentration range of single compounds between the less and more mature samples.

The dibenzothiophene distribution shows the same patterns for marls of type A and of type B (Fig. 75). The dibenzothiopene and 1-methyldibenzothiophene are more abundant than the 4-methyldibenzothiophene and the 2- and 3-methyldibenzothiopene. The concentration of each compound rises with an increase in maturity.

4.6.5 NSO-Compounds and Asphaltenes

The asphaltene and NSO-compounds make up between 59% and 86% of the total extract. Asphaltene concentrations were determined by subtracting the measured yields of the aliphatic and aromatic hydrocarbon fractions and the NSO-compound fractions from the total bitumen extract. The asphaltene fraction is usually the largest compound class.

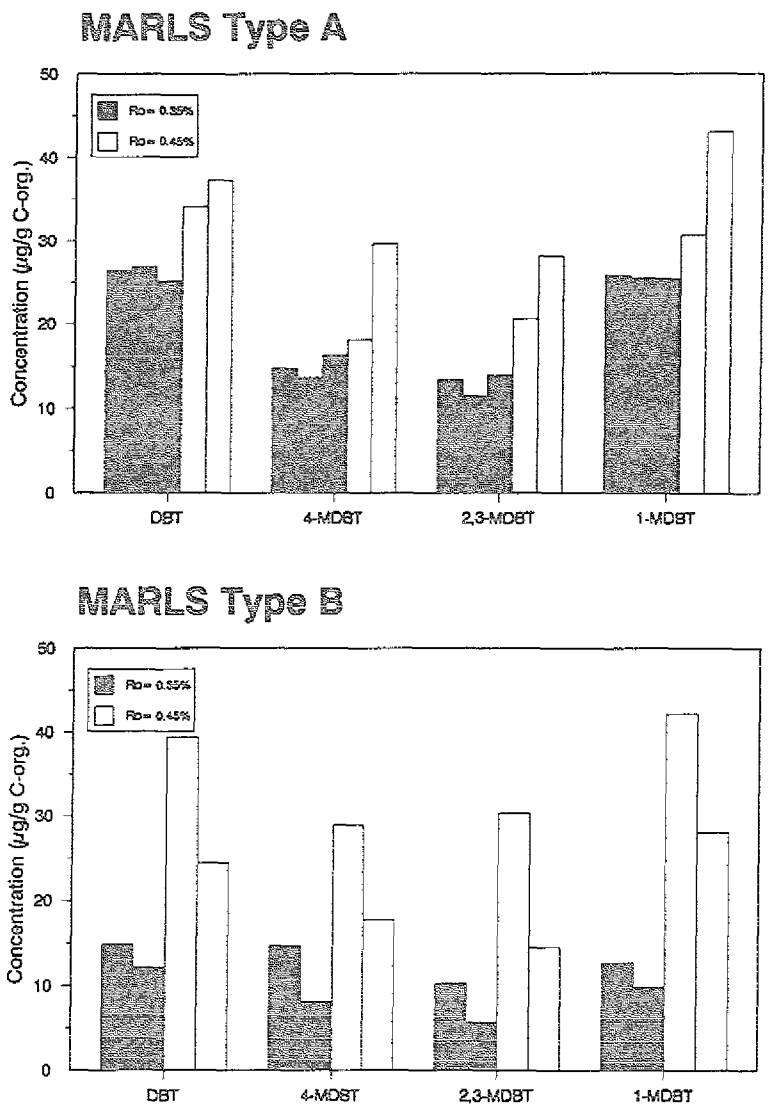

Fig. 75: Dibenzothiophene concentrations of samples from marls of type A and B (abbreviations are listed in Table 5).

The aromatic and aliphatic hydrocarbon fractions display marked yield increases for each lithofacies over the studied maturity interval (exception: aliphatic hydrocarbon yield of the massive anhydrite lithofacies). The NSO-compound and asphaltene yields show a different picture (Figs. 76, 77). The average yields of the marls of type A and marls of type B of both compound classes increase sharply. In contrast, the average yields of the NSO-compounds and asphaltenes of the laminated anhydrite, lenticular anhydrite and massive anhydrite lithofacies decline over the studied maturity interval.

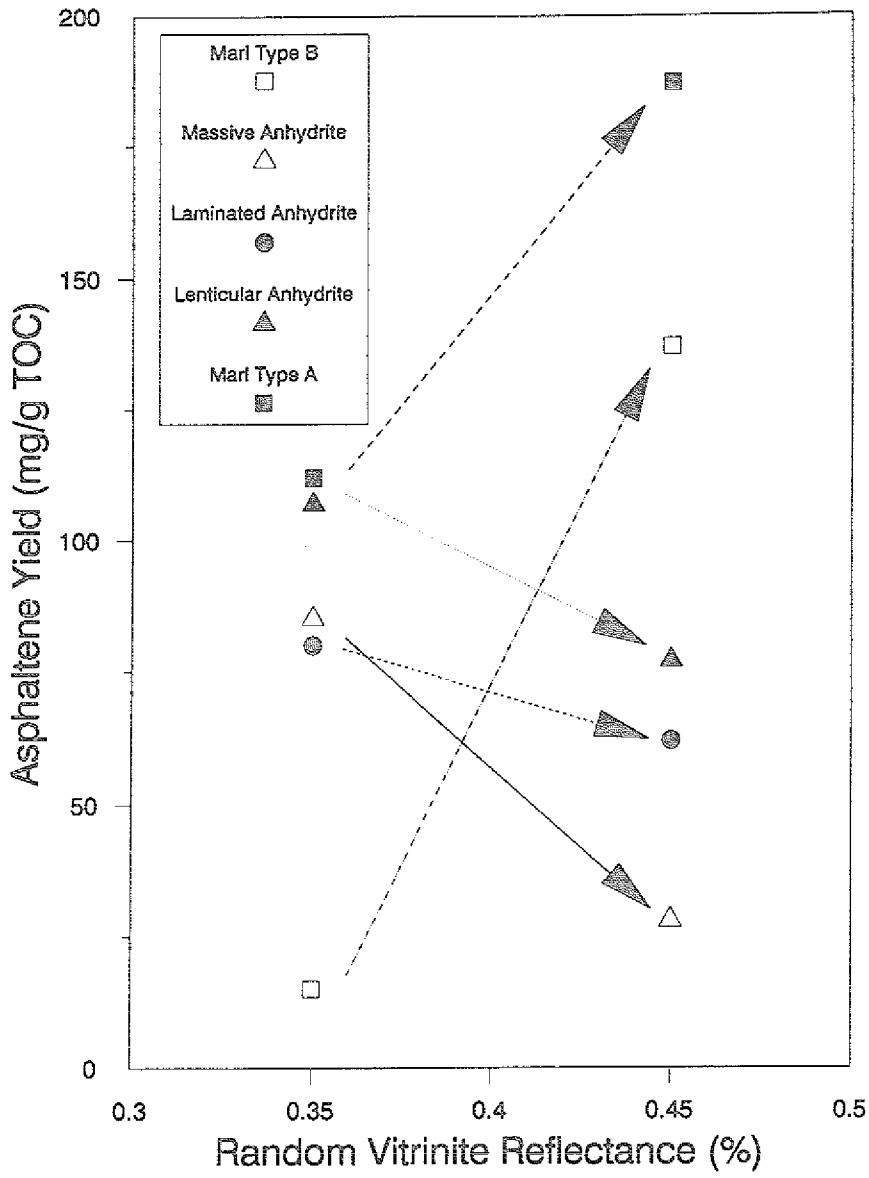

Fig. 76: Asphaltene yields of the lithofacies of the S unit.

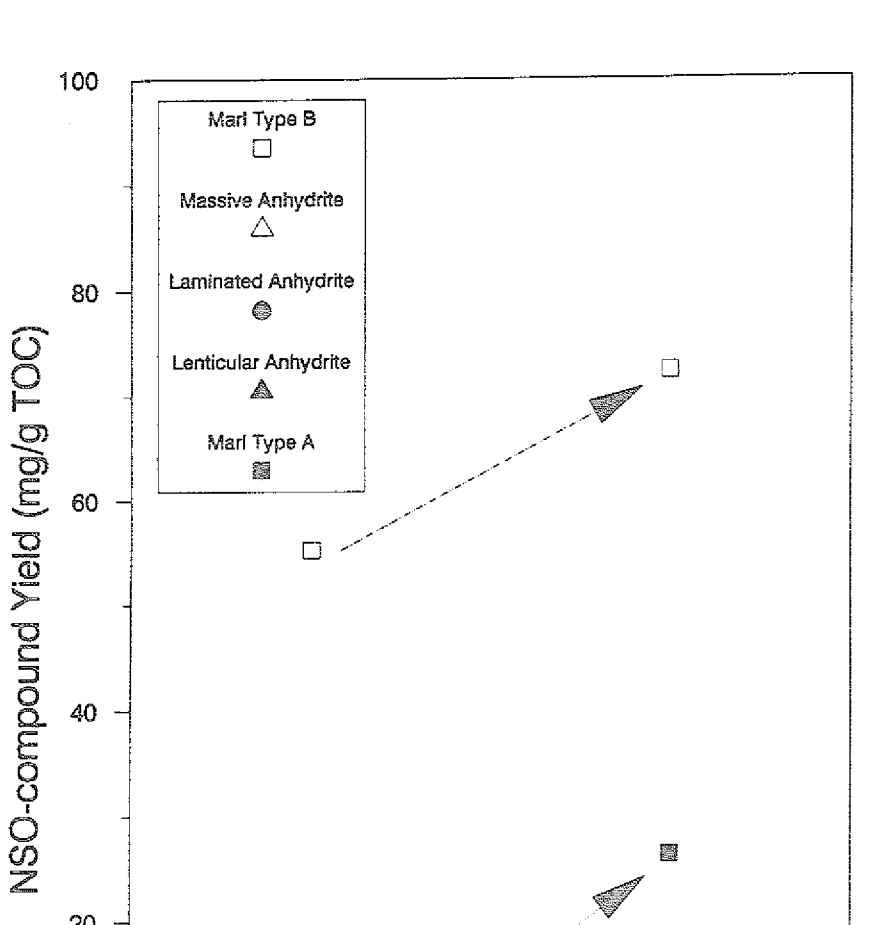

Fig. 77: NSO-compound yields of the lithofacies of the S unit.

4.7 Discussion

4.7.1 Petroleum Generation

Most petroleum geologists accept that the bulk of petroleum hydrocarbons were generated by thermal decomposition of kerogen in source rocks during long periods of burial (Hunt, 1979, Tissot and Welte, 1984). Tissot and Welte (1984) summarize the views of many workers on petroleum formation in the following generalized scheme.

In shallow buried organic-rich sediments, only small amounts of extractable organic matter is present (inherited from living organisms). The only hydrocarbon species generated at this stage is methane (biogenic gas). As burial increases and temperature rises, heteroatomic bonds are broken in the kerogen and CO_2 and H_2O are formed. The first petroleum products liberated by this transformation are bitumens consisting mostly of heteroatomic (NSO) compounds and asphaltenes. As temperature continues to increase during catagenesis, C-C bonds are cracked at incremental rates and aliphatic side-chains are removed from the kerogen and previously formed NSO-compounds. Most of the hydrocarbons formed during this main stage of oil generation are of low to medium molecular weight. The transformation of organic

matter during catagenesis is an overall process of disproportionation of the hydrogen of the initial kerogen. As hydrogen is enriched in the generated products, the residual kerogen becomes increasingly depleted with respect to hydrogen. After most of the labile material has been eliminated through catagenesis, a structural reorganization occurs in kerogen, with the development of a higher degree of ordering. In this stage (metagenesis), no significant amounts of hydrocarbons are generated from kerogen except some methane. Large amounts of methane may, however, result from cracking of pre-existing, unexpelled petroleum.

4.7.2 Bitumen Formation

During early stages of kerogen degradation, NSO-rich products are generated (bitumen). In the bitumens of the Mulhouse Basin, the dominant species at both maturity levels are asphaltenes and NSO-compounds. Clearly, hydrocarbons amount to less than 50% of the total extracts from the sediments of each lithofacies (Fig. 61).

The effectiveness of bitumen formation can be documented when the carbon-normalized extract yields of the sediments of the Mulhouse Basin are compared to other potential source rocks, which originate from different environments

(Fig. 78). Littke et al. (1988) reported extract yields for three lithologically comparable immature potential source rocks, which on average contain less extractable organic matter than the evaporites of the S unit (R_o = 0.35-0.45%; Fig. 78): 1) sulfur-rich lacustrine sediments of Miocene age from the Nördlinger Ries (R_o < 0.35%; Rullkötter et al., 1990), 2) the Messel oil shale (R_o < 0.3%; Rullkötter et al., 1988), and 3) the Posidonia shale (drillhole Wenzen, R_o = 0.48%; Littke et al., 1988). At least in the case of the Posidonia shale (e.g. Rullkötter et al., 1988), and facies equivalents of the Messel oil shale (e.g. Hillebrand and Leythaeuser, 1991), it has been demonstrated that these potential source rocks have generated and expelled hydrocarbons upon maturation. The unusually high extract yields of the evaporite source rocks of the S unit are also in good agreement with observations by Palacas (1983, 1988), Ferguson (1988), and Powell (1984), who also reported high extract yields from immature carbonate-evaporite source rocks from a variety of different locations.

An estimate of the degree of bitumen formation and hydrocarbon generation can be drawn from a comparison of the extract yields versus the hydrocarbon yields of the Mulhouse Basin and those of a classical type II source rock of shale lithology, the Lower Toarcian of the Paris

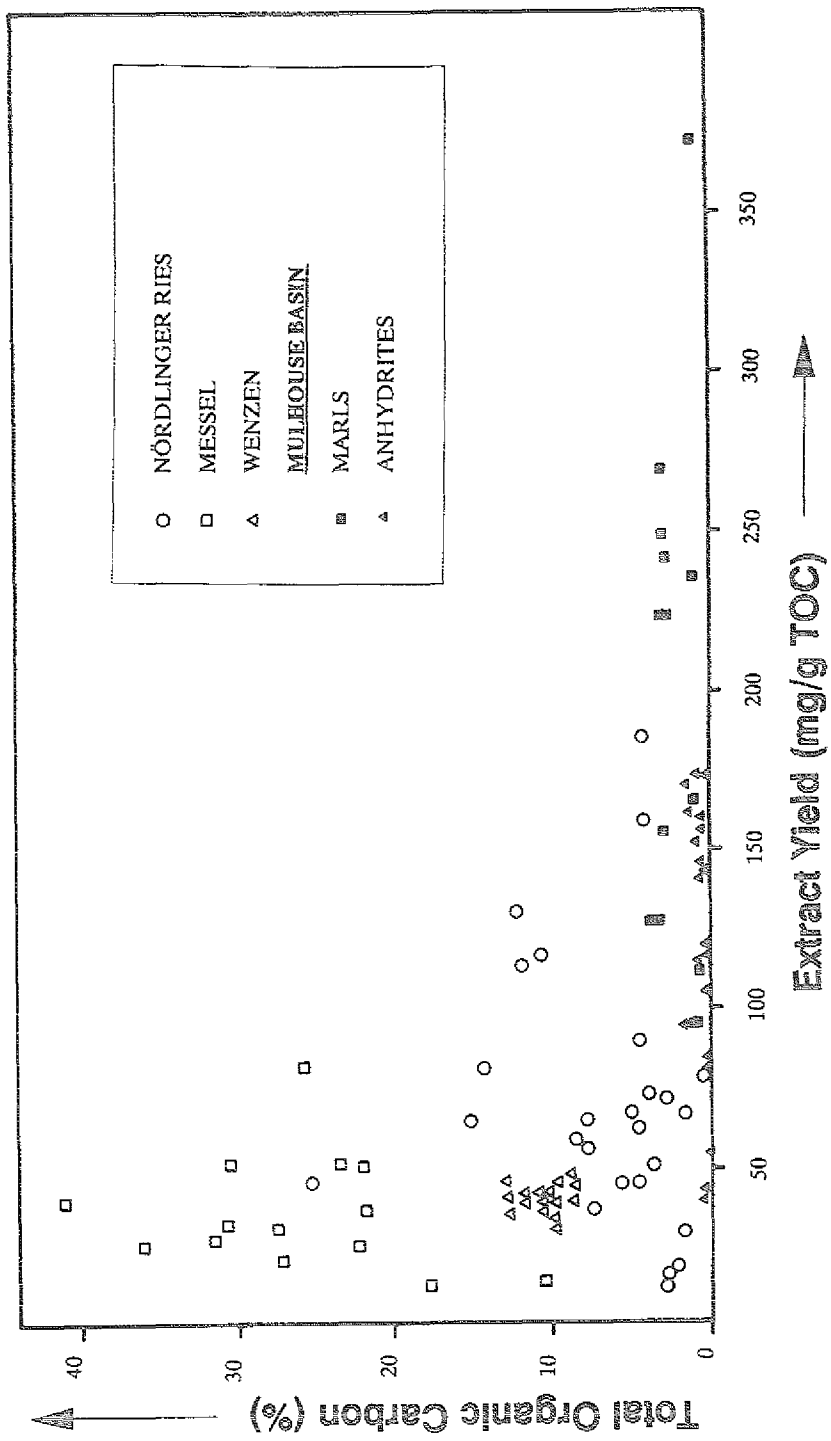

Fig. 78: Comparison of the extract yields of the lithofacies of the S unit with other immature source rocks.

Basin. According to Tissot and Welte (1984), the principal zone of oil formation for the lower Toarcian of the Paris Basin is characterized by extract yields from 70-180 mg of extract per gram organic carbon and hydrocarbon yields of 20-100 mg/g TOC. If the rocks of the Mulhouse Basin are compared to these yield ranges (Fig. 79), it becomes apparent that the extract yields of the sediments of the Mulhouse Basin by far exceed those of the Toarcian from the Paris Basin. On the other hand, the hydrocarbon yields of only a limited number of samples have reached values comparable to those of the lower Toarcian of the Paris Basin. The comparison also confirms the observation that potential evaporite source rocks on average contain much higher extract yields than shale source rocks with similar kerogen quality.

4.7.2.1 Bitumens at Maturity Level R_o = 0.35

As demonstrated in Chapters 3.8 and 3.10, two distinctly different organic facies can be recognized in the sediments of the S unit of the Mulhouse Basin. Organic facies A is present in samples of the lenticular and laminated anhydrite facies as well as in the marls of type A, whereas organic facies B occurs in marls of type B and in the massive anhydrite facies. The bitumen data of the massive anhydrite lithofacies is discussed in detail in

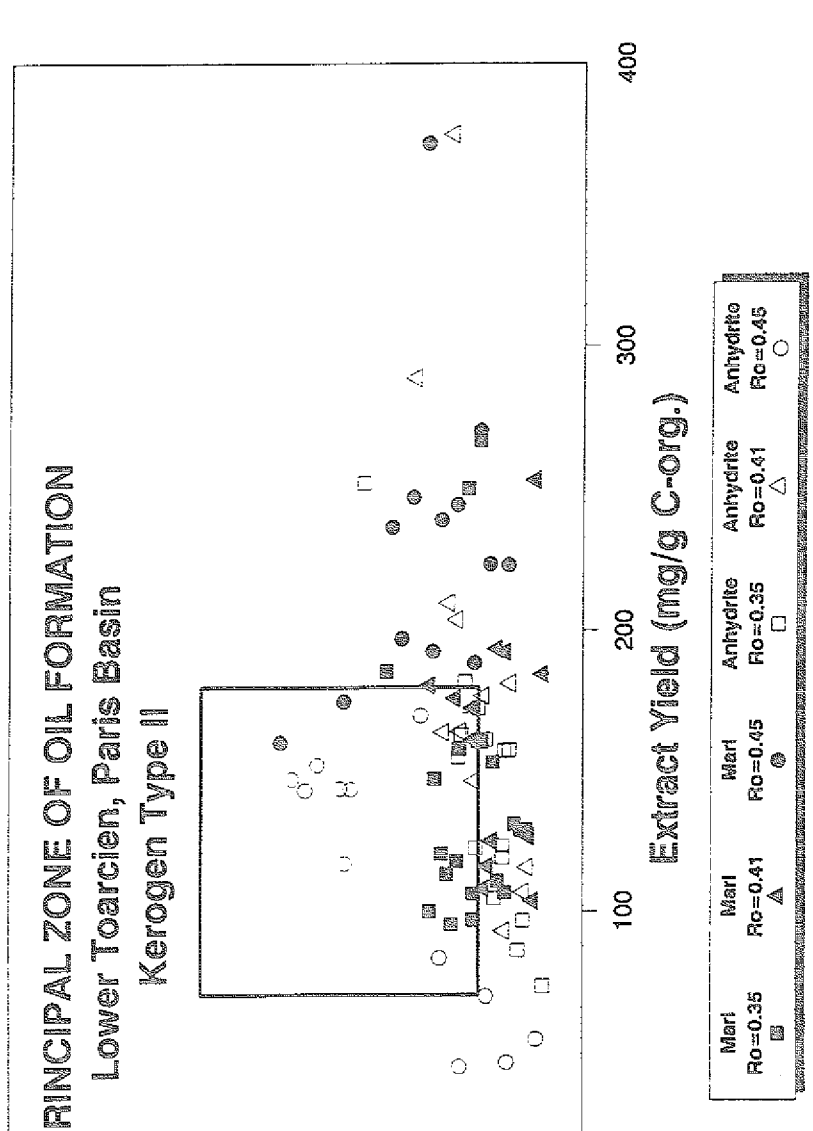

Fig. 79: Comparison of the extract and hydrocarbon yields of the bitumen of the S unit with values for the principal zone of oil formation in the Paris Basin.

the section on hydrocarbon expulsion. As will be documented later, the massive anhydrites have expelled bitumen and, therefore, represent a special case.

The average extract yields of the lithofacies of organic facies A range from 109-166 mg/g TOC and are higher than those of organic facies B (104 mg/g TOC). The aliphatic hydrocarbon yields of the lithofacies of organic facies A vary between 16.70 and 19.61 mg/g TOC. Marls of type B contain 20.20 mg/g TOC. The aromatic hydrocarbon fraction is similar in samples of both organic facies and varies from 3.12 to 5.05 mg/g TOC. The most pronounced differences between organic facies A and organic facies B are encountered in the asphaltene content. Organic facies A contains 80.51 to 112.35 mg/g TOC, whereas the marls of organic facies B contain only 15.85 mg/g TOC. It should be noted that the asphaltene content was determined by calculation (see Chapter 4.6.5) and was not measured directly, and hence may be less accurate than, for example, the concentrations of the aliphatic or aromatic hydrocarbons. However, the differences between organic facies A and organic facies B with respect to the asphaltene content are too large to be attributed to the determination process of the asphaltene concentration. The NSO-compound content is the highest in organic facies B.

It is evident that even though within each organic facies, representative lithofacies display very similar compositions with respect to the extract fractions, marked differences exist between organic facies A and B. The reason for these differences is probably to be found in the composition of the kerogens of each organic facies. The kerogens of organic facies A are dominantly comprised of amorphous organic matter with some alginite and vitrinite. Organic facies B is rich in alginite (>50 vol.%) and contains more vitrinite than organic facies A.

The thermal degradation products of alginites are predominantly n-alkanes and some aromatics (e.g. Largeau et al., 1984, 1986; Derenne et al., 1988). This observation may explain the markedly higher aliphatic hydrocarbon yields of organic facies A over organic facies B, even though n-alkanes are also to be expected from the thermal degradation of other macerals, e.g. cutinite, sporinite, and suberinite (Nip et al., 1986, 1989; Prahl et al., 1985; Tegelaar et al., 1989). The differences in the extract yields from organic facies A to organic facies B may also be the result of different activation energies required for bitumen formation from kerogen. It is well documented that the kinetic energies required for petroleum generation vary considerably with kerogen

quality and type (Quigley et al., 1987; Ungerer and Pelet, 1987).

4.7.2.2 Bitumens at Maturity Level 0.45% R_o

The extract yields of the bitumens of the lenticular and laminated anhydrite facies and the marls of types A and B are higher at maturity level 0.45% R_o than at 0.35% R_o. The lithofacies containing organic facies A shows a moderate increase by a factor of 1.01-1.47. In contrast, the extract yields of marls of type B (organic facies B) displays a 2.5-fold total yield increase (Table 4). The small increase in extractable organic matter from the lithofacies with organic facies A is, in the case of the lenticular anhydrites and laminated anhydrites, characterized by an increase in the aromatic and aliphatic hydrocarbon fractions (approximately 4-fold; Table 4). This shift is significant and raises the hydrocarbon content of both lithofacies to more than 40% of the total extract yield. This value is considerably higher than the hydrocarbon to non-hydrocarbon ratio of shale source rocks at comparable maturity levels. Tissot and Welte (1984) report average hydrocarbon contents of approximately 25% of the total extract for type II kerogens of the lower Toarcian of the Paris Basin at the onset of the principal zone of oil formation. The increase in extract yields of the lithofacies of marls of types A and B are primarily

caused by higher asphaltene contents and/or only a minor rise in the hydrocarbon fractions. The hydrocarbon portions of both lithofacies amount to up to 20% of the total extractable bitumen and, hence, are similar to those reported from the onset of the oil window of the lower Toarcian of the Paris Basin (Tissot and Welte, 1984).

The mass balance for the maturity interval 0.35-.045 R_o expresses the net gains and losses for the extract sub-fraction of each lithofacies (Fig. 80). The net balance over the maturity interval 0.35-0.45% R_o can be considered to be an expression of active hydrocarbon generation. Hydrocarbons are indeed newly formed in each lithofacies regardless of organic facies type.

To interpret the results of the net changes documented in Fig. 80 in a quantitative fashion and delineate the processes of hydrocarbon formation, the following questions need to be addressed: 1) is the observed net gain solely a product of petroleum formation, or 2) is it the combined effect of, for example, simultaneous petroleum formation and migration; or 3) a result of impregnation by migrated petroleum?

A satisfactory answer to the question raised above is exceedingly difficult because little is known about the

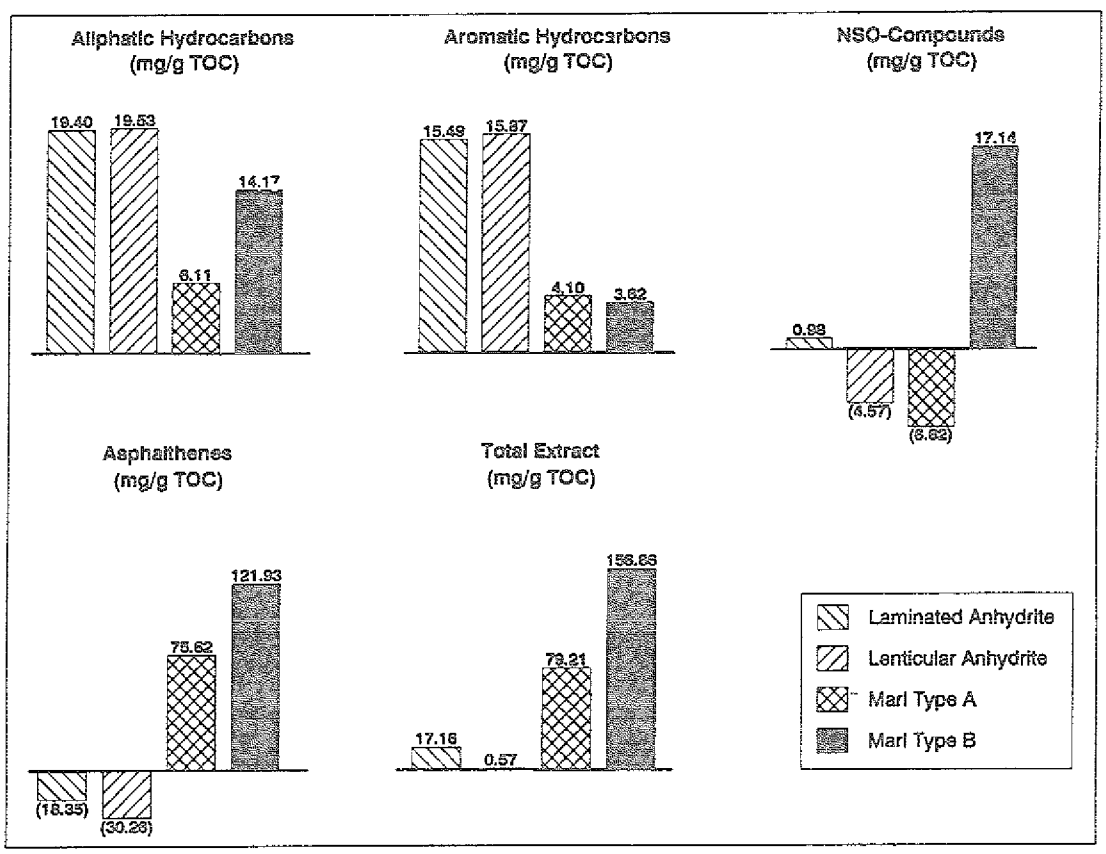

Fig. 80: Net loss and net gains over the maturity interval of 0.35 % R_o - 0.45 % R_o.

details of hydrocarbon formation, especially within a stage of early maturation at comparatively low temperatures. The general consensus of most workers, as summarized by Hunt (1979) and Tissot and Welte (1984), appears to be that petroleum generation at low temperatures is caused by the thermally-induced cleavage of carbon-sulfur, carbon-nitrogen, and carbon-oxygen bonds in the kerogen, which requires considerably lower activation energies than the cleavage of carbon-carbon bonds (e.g. Loudon, 1988). The products liberated from the kerogen matrix by this process should ideally represent a random cross-section of the kerogen constituents. However, reactions of the released products in the bitumen phase itself, which is a complex mixture of compounds of various compositions and chain lengths, will alter the bitumen composition. Therefore, a direct relationship between bitumen composition and kerogen structure cannot be determined (Rullkötter and Michaelis, 1990). In light of this consideration, it is extremely difficult to predict the mode of formation of bitumen from kerogen in a qualitative fashion, much less the quantity of bitumen that will form in a specified temperature interval from any type of kerogen.

Because a direct prediction of the quantity of bitumen expected to form in a specific temperature interval from kerogen is not possible based on the current state of

knowledge in organic geochemistry, indirect reasoning has to be applied to verify whether the bitumen yield increase in a particular maturity interval is a function of the petroleum generation process or a combined effect of several processes. Processes that are known to result in a reduction of the bitumen content in a particular maturity interval are the expulsion of petroleum products and the conversion of bitumen into gas.

At low maturity levels, the most effective method of gas formation is the biochemical generation of methane via fermentation processes. These fermentation processes are apt to produce isotopically light hydrocarbons (e.g. $\delta^{13}C_1$ = -55 to -90 $\%_o$ PDB). Gas analysis of samples from the Mulhouse Basin (Whiticar, 1990) indeed detected a high gas content (up to 19,509 ppb ΣC_1-C_5). The isotopic signature of these gases, however, is isotopically heavier than the gases produced by bacterial fermentation. The carbon ($\delta^{13}C$ = -42.3 to -33.8 per mil PDB) and hydrogen (δD_1 = -220 per mil to -234 per mil SMOW) stable isotope signatures in combination with the molecular composition of the natural gases indicate the hydrocarbons may be of thermogenic origin. Whiticar (1990) concluded that these hydrocarbons could be allochthonous in nature and have migrated in from source rocks at higher maturity levels (0.6-0.8% R_o). However, organic matter from evaporite deposits at Solar Lake have been shown to be significantly

enriched with respect to ^{13}C ($\delta^{13}C$ = -4.4 per mil; Schidlowski et al., 1984) when compared to the isotopic composition of average biogenic matter ($\delta^{13}C$ = -20 to -30 per mil; e.g. Schidlowski, 1982; Hayes, 1983). If the organic matter of the evaporites of the Mulhouse Basin was also enriched in ^{13}C, the anomalously low $\delta^{13}C$ isotopic values may be the result of isotopic fractionation in the depositional environment rather than an indicator for the thermogenic origin of the entrapped gases. It is, therefore, not yet possible to interpret the origin of the gas content of the sediments of the Mulhouse Basin with a satisfactory degree of confidence.

Primary migration could also have altered the amount and composition of the bitumens at both sites and, hence, affected the net balance of the newly-formed products within this interval. Especially in the light of the results for the massive anhydrite facies, which, as will be documented in a later section, has expelled bitumen. The absolute amount of hydrocarbons of this facies, however, is low due to the low carbon content of this lithofacies (0.1-0.3% TOC) most likely only comparatively small quantities and hence only minor amounts of hydrocarbons have actually been expelled.

One way to document hydrocarbon migration is the presence of remnants of the expelled phase such as bitumen-stained

fractures, hydrocarbon-bearing fluid inclusions or sealed microfractures in diagenetic minerals, oil impregnations or seeps. However, none of these migration indicators has been observed at the sampling sites Amelie II and Berrwiller, or in thin sections and/or polished slabs of the studied sample set. These observations make the impregnation of the sediments of the Mulhouse Basin by migrated hydrocarbons rather unlikely. Additionally, if significant hydrocarbon expulsion had taken place, a higher degree of variation with respect to the concentrations of each molecular species would be expected in any one lithofacies at the same maturity level, particularly in the alkane and naphthalene patterns of the samples. However, the n-alkanes and naphthalenes of the samples of each lithofacies at identical maturity level in the Mulhouse Basin display very similar concentrations on a molecular scale (Figs. 64, 65, 70, 71). It appears unlikely that all of these samples have expelled hydrocarbons to the same degree.

The arguments presented above indicate that petroleum generation is probably the most important process to explain the observed trends of bitumen yield increase from the samples from the lenticular anhydrite, laminated anhydrite and marls of types A and B.

Based on this assumption, the net balance presented in Figure 80 can be further interpreted in the following way: The four lithofacies can be divided into two groups based on the net increase of the extract fractions. The first group contains the laminated and lenticular anhydrite lithofacies and the second group contains the lithofacies of marls of type A and type B. The lithofacies of the first group are characterized by high absolute net gains in the aliphatic and aromatic hydrocarbon fractions relative to the lithofacies of the second group, and by a net loss in asphaltenes and only minor gains in total extract yields compared with the second group.

It is especially surprising that the gains in aromatic and aliphatic hydrocarbons of the laminated and lenticular anhydrite facies exceed by far the gain in total extracts. Because the asphaltenes and, in the case of the lenticular anhydrite lithofacies, also the NSO-compounds, decrease at the same time, it appears that the hydrocarbons are formed at the expense of the NSO-compound and asphaltene fractions.

Asphaltenes and NSO-compounds can be considered to be small fragments of kerogen (Louis and Tissot, 1967) and under pyrolysis conditions yield comparable hydrocarbon distribution patterns (Muscio, 1991). Hydrocarbon formation from NSO-compounds and asphaltenes also requires

considerably lower activation energies than the formation from kerogen, as documented by pyrolysis experiments by Muscio (1991). It has been suggested by Pelet et al. (1986) that asphaltenes and NSO-compounds play an intermediate role in hydrocarbon formation. Hydrocarbon formation may either occur directly from kerogen degradation or via intermediate asphaltene and/or NSO-compound formation and subsequent degradation to hydrocarbons.

Further support for the hypothesis that asphaltenes may have contributed to hydrocarbon generation in the samples of the Mulhouse Basin can be drawn from the flash-pyrolysis experiments of Sinninghe Damsté et al. (1990). He and his co-workers demonstrated that upon pyrolysis, asphaltenes and kerogens of the S unit of the Mulhouse Basin formed products very similar to each other. The pyrograms were notably rich in n-alkanes (C_6-C_{26}), n-alk-1-enes (C_6-C_{26}), isoprenoid alkanes and alkenes. In view of these results, the conversion of asphaltenes and possibly NSO-compounds to hydrocarbons in the lenticular and laminated anhydrite facies appears to be at least a viable hypothesis.

If, however, for the anhydrite lenticular and laminated lithofacies, one considers the formation of hydrocarbons in the maturity interval 0.35%-0.45% R_o primarily as a

result of asphaltene/NSO conversion then the lithofacies of marls of type A and type B must follow a different conversion scheme, because the end products are significantly different. Lithofacies of marls of type A and type B display a net gain in total extracts, aliphatic and aromatic hydrocarbons, and asphaltenes. The NSO-compounds of marls of type A display a small loss when compared to the gains in the asphaltene fraction. The mechanism that leads to the formation of hydrocarbons in both of these lithofacies does not only result in hydrocarbon formation, but also favors formation of asphaltenes and, to some extent, NSO-compounds. Therefore, it appears that the marls of type A and type B follow the classical kerogen conversion model that results in formation of minor amounts of hydrocarbons and large amounts of heteroatomic-rich compounds at low maturity levels (Tissot and Welte, 1984; Hunt, 1979). It may be possible that hydrocarbon formation may also occur via asphaltene conversion within these lithofacies. The kerogen conversion process, however, appears to be the more effective process dominating the resulting chemical signal.

4.7.3 Molecular Considerations for Hydrocarbon Generation

In order to study hydrocarbon generation, a mass balance approach previously established by Leythaeuser et al.

(1980) and Radke et al (1986) was applied. The carbon-normalized yields of total extracts, selected n-alkanes and aromatics were compared with increasing maturity. Previous workers in evaporite depositional environments have questioned whether anhydrite and halite rocks are able to preserve organic matter and to release significant amounts of hydrocarbons upon maturation (e.g. Sonnenfeld, 1985; Warren, 1986). To further investigate this question, the same mass balance type approach was performed for all lithofacies of the S unit. The results depicted in Figures 66 and 72 suggest that all lithofacies of the S unit of the Mulhouse Basin reveal increasing yields of n-alkanes and naphthalenes which are interpreted to result from thermal evolution of this rock suite. The only exception was observed for massive anhydrites, whose n-alkane yields decrease with increasing maturity of their organic matter content. This observation will be discussed in the next sub-chapter.

Certain n-alkanes are known to stem directly from the organisms incorporated in the organic matter fraction of source rocks and have been classified as biological marker substances (e.g. Comet and Eglinton, 1987). Naphthalenes, on the other hand, do not occur in living organisms (Radke, 1987 and references therein). However, naphthalenes have been reported to occur widely in ancient sediments and coals, where they are believed to be

derived, at least in part, from degradation of natural terpenoids (Alexander et al., 1985 and references therein). An increase in the yield of naphthalenes with increasing thermal maturity can, therefore, be interpreted as an indication of hydrocarbon generation (Radke et al., 1986). Following these arguments, the increase of the naphthalene and, by analogy, n-alkane yields are interpreted as a result of active hydrocarbon generation.

Having established that at least an initial stage of hydrocarbon generation occurs over the investigated maturity interval, the question of how effective hydrocarbons are formed arises. The relative effectiveness of hydrocarbon formation can be assessed when the carbon-normalized concentration of each compound class in a given sample is divided by the respective concentrations of the less mature sample.

4.7.3.1 Relative Increases in Selected n-alkanes and Naphthalenes

To determine whether any hydrocarbons were formed preferentially over the studied maturity interval, plots of relative yield increases were constructed for selected n-alkanes and naphthalenes of all lithofacies (Figs. 81, 82, 83). The trends shown in these figures represent "generation factors" (= generation rate factors of Leythaeuser et al., 1980) for each hydrocarbon calculated according to:

$$\text{generation factor} = \frac{\text{average hydrocarbon yield}_{\text{more mature site}}}{\text{average hydrocarbon yield}_{\text{less mature site}}}$$

Hence a generation factor of 1 implies no yield increase. Note that no generation factors could be calculated for n-alkanes from massive anhydrites, because the yield per n-alkane decreases over the studied maturity interval.

The generation factors for n-alkanes of samples from organic facies A (marls of type A, lenticular anhydrites and laminated anhydrites) are uniform for the carbon number range from C_{15} to C_{29}, showing a narrow range of variation around a value of 2.5. This implies that the concentrations of most n-alkanes from all sedimentary facies containing organic facies A increased by a factor

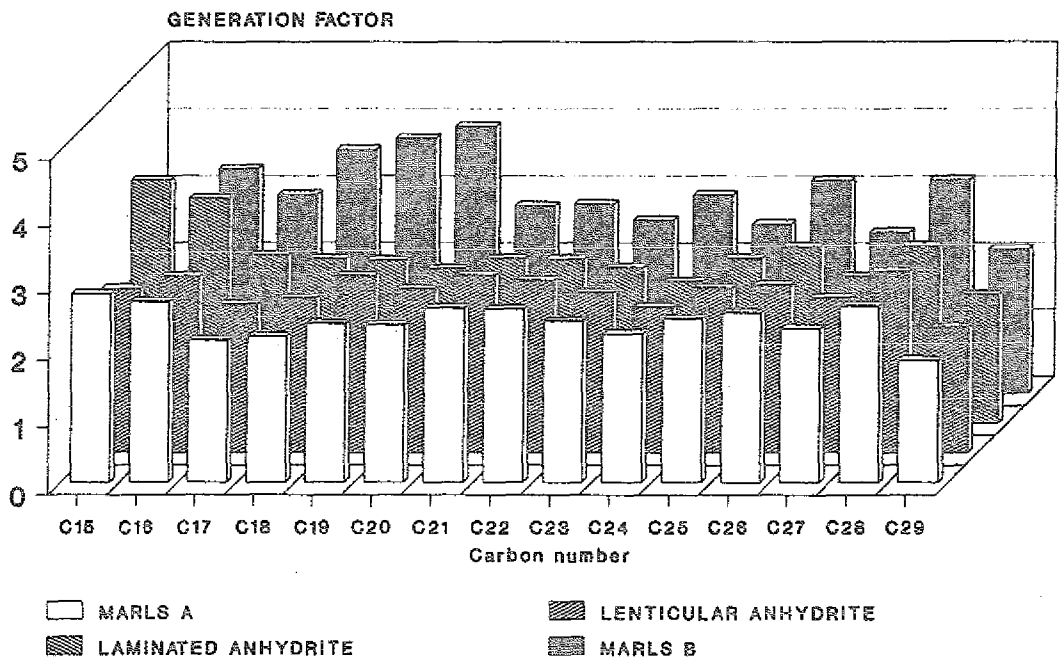

Fig. 81: Generation factors for n-alkanes of the lithofacies of the S unit.

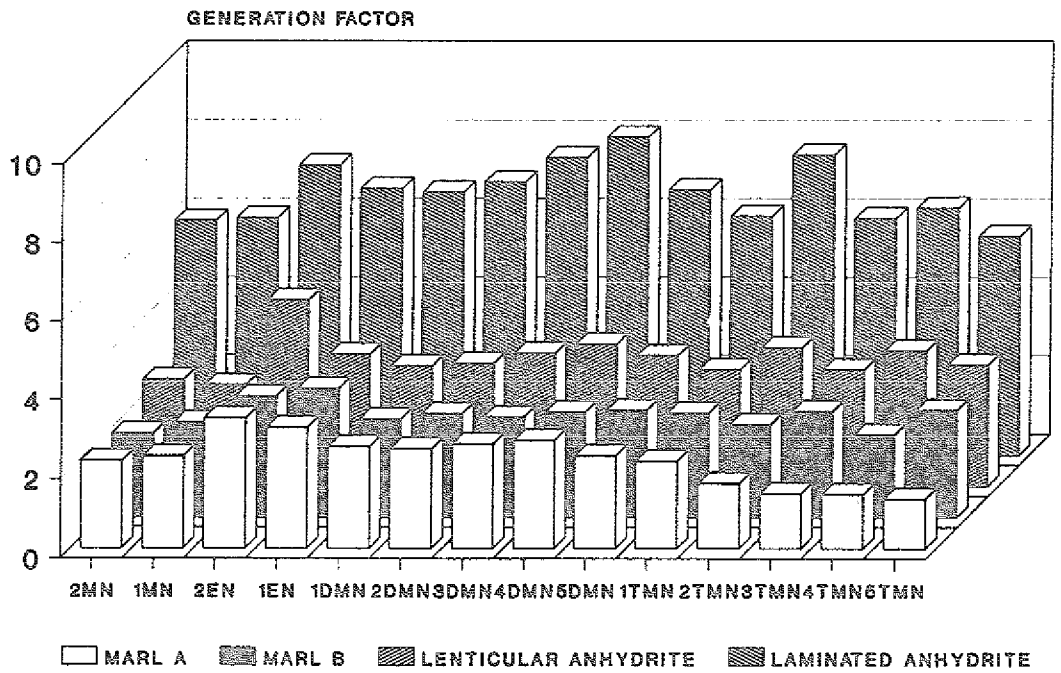

Fig. 82: Generation factors for naphthalenes of the lithofacies of the S unit (for abbreviations see Table 5).

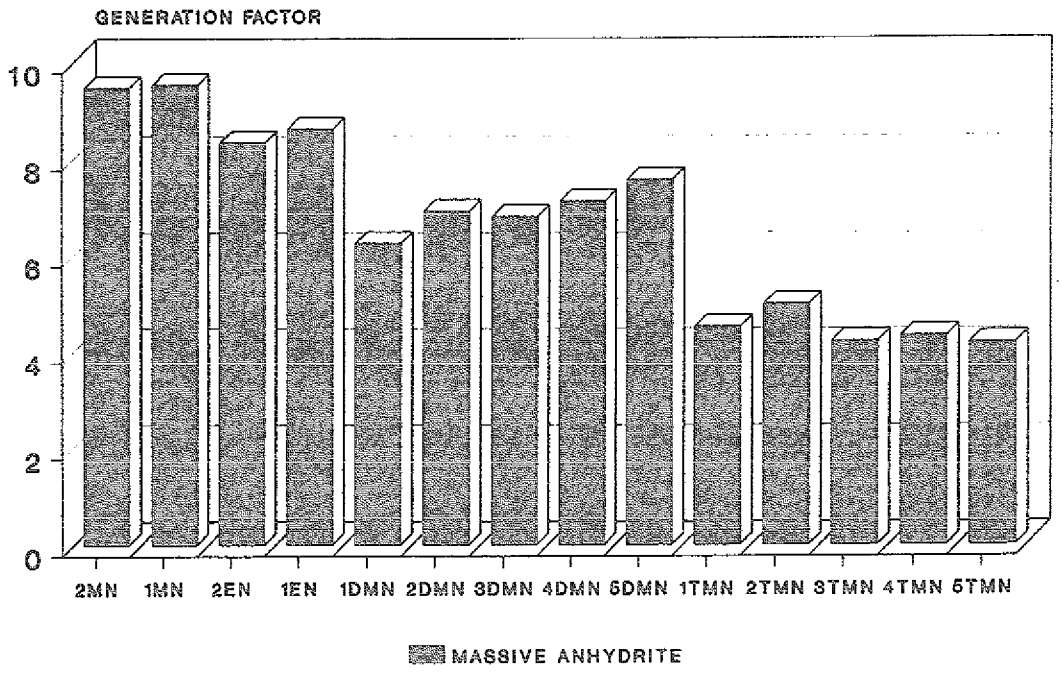

Fig. 83: Generation factors for the naphthalenes of the massive anhydrite lithofacies (for abbreviations see Table 5).

of 2.5 compared to the amounts of n-alkanes present in the samples of the less mature site Amelie II.

The corresponding trend for marls of type B (Fig. 81) that contain organic facies B displays on average higher generation factors than those of organic facies A. In addition, n-alkanes in the C_{15}-C_{20} range formed at a higher rate than n-alkanes in the C_{21+} range in samples of marls of type B.

The trend of relative yield increase for naphthalenes of all sedimentary facies (Fig. 82) indicates that the anhydrite-dominated facies (laminated anhydrite and massive anhydrite) experienced the highest relative yield increases for each naphthalene molecule. Marls of type A, marls of type B, and lenticular anhydrites show rather similar relative yield increases, i.e. by a factor of approximately 3, whereas laminated anhydrites are enriched by a factor of 6. For all of these sedimentary facies, the relative yield increase per individual naphthalene lies in the same order of magnitude. In contrast to these observations are the relative yield increases per naphthalene of the massive anhydrite facies (Fig. 83). Massive anhydrites display distinct differences in yield increase in relationship to the naphthalene groups: methylnaphthalenes are enriched by a factor of approximately 9.5, ethylnaphthalenes by a factor of 8.5,

dimethylnaphthalenes by a factor of 6.5 and trimethylnaphthalenes by a factor of 4.5.

It should also be noted that the relative yield increases of marls of type A and marls of type B, which represent organic facies A and B, respectively, display the same general enrichment patterns (Fig. 82). Marls of type A are only slightly less enriched in the trimethylnaphthalene fraction when compared to marls of type B.

The generation factors for selected n-alkanes of representatives of organic facies A (marls of type A, lenticular anhydrites and laminated anhydrites) vary in a narrow range around 2.5 (Fig. 81). This observation suggests that all lithofacies containing organic facies A have generated n-alkanes to the same relative extent. A different pattern is displayed by marls of type B (organic facies B). In this lithofacies, n-alkanes in the C_{15}-C_{20} range have been more effectively generated than n-alkanes in the C_{21}-C_{29} range. The reason for these differences in generation efficiency are not known, but may be a result of the differences in kerogen or kerogen-equivalent precursor structures. The relative yield increase for both organic facies, however, lies in the same order of magnitude that Radke et al. (1986) observed for saturated hydrocarbons of Type II_B kerogens in the maturity interval between 0.45 and 0.55% R_o. The results indicate that

during this low maturity interval, dominantly n-alkanes of biogenic origin (e.g. C_{15}, C_{17}, etc.) are released from the kerogen or asphaltene structures. The predominant process in the formation of the observed n-alkane distribution patterns appears to be the breaking of carbon-heteroatomic bonds from kerogen, asphaltene and NSO-compound structures.

The naphthalene generation factors show a distinctly different picture (Fig. 82). The relative concentration increase in naphthalenes of lithofacies that are dominated by anhydrite (massive anhydrite, laminated anhydrite) exceed the relative concentration increase of facies that contain significant amounts of clay (marls of type A and B, lenticular anhydrite) by a factor of approximately 3. The naphthalene generation factors of the marl-dominated lithologies lie on average at factor 3, and hence fall in the same range as the generation factors of the n-alkanes of these facies. It can be concluded that n-alkanes as well as naphthalenes have been formed in the same relative amounts in all of these lithologies in the studied maturity interval. Radke et al. (1986) also report generation factors between 2 and 4 for naphthalenes from Type II_B kerogens, however, from a somewhat higher maturity interval (0.45-0.55% R_o). The lithofacies-specific differences in the efficiency of naphthalene generation are difficult to explain and have not been

previously noted. These results are contrary to the observations of Alexander et al. (1982), who demonstrated that naphthalene formation appears to be promoted by clay catalysis of aromatic hydrocarbon exchange reactions.

The uniform formation of individual naphthalene species within the maturity interval from 0.35-0.45% R_o for all lithofacies has implications for the usage of alkylnaphthalene ratios to assess the maturity of the bitumens of the Mulhouse Basin (Radke et al., 1982; 1986, Alexander et al., 1985). All of these ratios rely on the preferential formation of naphthalene isomers with a higher kinetic stability under successively increasing temperatures. The temperature increment from 0.35-0.45% R_o is, however, apparently not sufficient to promote the formation of kinetically more stable isomers in favor of less stable isomers. The alkylnaphthalene ratios stay constant over this maturity interval, which means that the reaction mechanisms needed to form these molecules, whatever their true nature is, appear not to be temperature-controlled.

4.7.4 Hydrocarbon Migration

The yields of the bitumen fractions of the massive anhydrite lithofacies for samples from Amelie II (R_o =

0.35%) and Berrwiller (R_o = 0.45%) are depicted in Fig. 84. It is evident that compound yields decrease from the less mature samples to the more mature samples. The overall decrease results in asphaltene, NSO-compound and aliphatic hydrocarbon yields of samples from Berrwiller that are lower than the ones of samples from the less mature site Amelie II. The aromatic hydrocarbon content, however, increases over the studied maturity interval.

These observations are in marked contrast to the development of the extract yields of the other lithofacies of the S unit, which are characterized by ongoing bitumen and hydrocarbon formation within the maturity interval 0.35-0.45% R_o. Another phenomenon that could only be observed in the massive anhydrite lithofacies is the stepwise decrease of the generation factors of the naphthalenes with increasing carbon number (Fig. 83). These observations raise the questions of how these differences developed and which processes are responsible for the resultant patterns.

4.7.4.1 Bitumen Composition of the Massive Anhydrite Lithofacies

The extract yields of the massive anhydrite lithofacies at Amelie II (111.72 mg/g TOC) is similar to the yields of

the lenticular anhydrite (143.88 mg/g TOC) and laminated anhydrite lithofacies (190.11 mg/g TOC) from the same maturity level (Table 4). The extract composition of all three lithofacies varies by only 1-3% in each bitumen subfraction (Fig. 61). It appears, therefore, that bitumen formation has occurred to a similar extent in each of these lithofacies up to the maturity level of 0.35% R_o.

Another observation shared by the massive anhydrite lithofacies with the laminated and lenticular anhydrite lithofacies is the net loss of asphaltenes and NSO-compounds within the maturity interval from 0.35%-0.45% R_o. As discussed previously (Chapter 4.7.2.2), the net loss of asphaltenes and NSO-compounds in the lenticular and laminated anhydrite facies is most likely the result of the conversion of these compound classes into hydrocarbons via the cleavage of comparatively weak carbon-oxygen, carbon-sulfur, or carbon-nitrogen bonds. It appears likely that at least part of the net loss of the asphaltene and NSO-fractions may be attributed to the same process.

The conversion of asphaltenes and NSO-compounds into hydrocarbons should result in a net increase in the aromatic and aliphatic hydrocarbon fractions in the more mature samples of the massive anhydrite lithofacies. The aromatic hydrocarbon fraction of the massive anhydrites at

Berrwiller follows this trend, even though the amount of newly-formed aromatic hydrocarbons is much lower than would be expected if the complete net loss of asphaltenes and NSO-compounds would have resulted from hydrocarbon formation. The aliphatic hydrocarbons, however, decrease in concentration, contrary to the expected increase by asphaltene/NSO conversion. Therefore, a second process must be involved to explain the observed net result. The decrease in the aliphatic hydrocarbon fraction is most likely a product of bitumen expulsion from samples of the massive anhydrite lithofacies at the more mature site at Berrwiller. Bitumen expulsion is likely to have affected all bitumen subfractions the aliphatic hydrocarbon fraction, the aromatic hydrocarbon fraction, the NSO-compounds and the asphaltenes, since the overall extract yields decrease by more than 50% from Amelie II to Berrwiller. The concentrations of the residual bitumen fractions measured in the more mature samples at Berrwiller reflect, therefore, the combined effects of bitumen formation and bitumen expulsion in the maturity interval from 0.35%-0.45% R_o. The net increase of the aromatic hydrocarbon fraction and the net loss of the aliphatic hydrocarbon fractions may either indicate that aromatic hydrocarbons are formed at a higher rate than aliphatic hydrocarbons in this maturity interval, or that the process of bitumen expulsion was more effective for

the aliphatic hydrocarbon fraction than for the aromatic hydrocarbon fraction, i.e. a fractionation effect.

4.7.4.2 Fractionation of Naphthalenes

In contrast to the decrease in extract and n-alkane yield with increasing maturity, the naphthalene concentrations of the massive anhydrite lithofacies follow the trends of all the other lithofacies and show a marked increase in concentration over the studied maturity interval. The second phenomenon that can be observed in the naphthalenes of the massive anhydrite lithofacies is the evident decrease in the generation factors with increasing carbon number (Fig. 83), which is not displayed by the naphthalenes of any other lithofacies. The generation factor distribution pattern can either stem from preferred generation of naphthalenes with lower carbon number over those with higher carbon number, or must be caused by another mechanism that leads to a carbon-number-specific fractionation. There are three arguments against preferential generation of naphthalenes with lower carbon numbers: 1) Why should a carbon-number-specific generation occur only in one lithofacies and leave the other unaffected? 2) Radke et al. (1986) showed that substantial fractionation, as a consequence of formation of thermally more stable isomers, occurs at much higher

maturities than encountered at Amelie II and Berrwiller. 3) Maturity-induced fractionation is not a carbon number specific process, but depends on the substitution of the alkyl groups on more reactive α or less reactive β positions on the naphthalene nucleus (e.g. Radke, 1987, and references therein). Therefore, it appears unlikely that differences in the generation rate are responsible for the observed generation factor patterns.

If carbon number-specific naphthalene generation is not responsible for the observed generation factor patterns, then other processes must lead to the observed fractionation trend. As demonstrated above, bitumen expulsion from the samples at Berrwiller has most likely taken place in the maturity interval 0.35-0.45% R_o. Hence, one process that may have led to the fractionation of the n-alkane patterns may be bitumen expulsion. The expulsion of naphthalenes from mature shale source rocks as shown by Leythaeuser et al. (1988b) was not associated with a fractionation of the naphthalenes. However, the massive anhydrites of the Mulhouse Basin are not organic-rich source rocks, and hence may follow completely different expulsion mechanisms than shale source rocks.

A process that leads to the fractionation of naphthalenes and has been studied in considerable detail is water washing of hydrocarbons. Hydrocarbons are known to

dissolve in water to varying degrees, depending on hydrocarbon type. Data collected by McAuliffe (1979) and Lafargue and Barker (1988) demonstrate that aromatic hydrocarbons are by far more soluble than aliphatic hydrocarbons. Particularly the n-alkanes with carbon numbers greater than 12 display solubilities of less than 0.01 mg per liter (25°C, McAuliffe, 1979). The naphthalenes, however, are far more soluble than the n-alkanes. Dimethylnaphthalenes, for example, are over 600 times more soluble than n-C_{12} (McAuliffe, 1979). The solubility among members of the naphthalene group also varies considerably. Methylnaphthalenes are approximately 10 times more soluble than dimethylnaphthalenes (McAuliffe, 1979). In general, there appears to be a decrease in solubility from methylnaphthalenes to dimethylnaphthalenes and trimethylnaphthalenes (McAuliffe, 1979; Lafargue and Barker, 1988). Data for ethylnaphthalenes have not been published, however, because solubility appears to decrease with carbon number and molecule size, they are expected to have solubilities that fall between the solubilities of the dimethylnaphthalenes and methylnaphthalenes.

Water washing of a mixture of naphthalenes will, therefore, remove naphthalenes according to their water solubilities. The residual naphthalene mixture remaining in the rock after water washing is expected to show the

effects of fractionation. Methylnaphthalenes will be depleted to the highest degree, followed by ethylnaphthalenes, dimethylnaphthalenes, and trimethylnaphthalenes. This depletion pattern, however, is apparently opposite to the relative stepwise enrichment indicated by the generation factors of the naphthalenes in the maturity interval 0.35-0.45% R_o.

This apparent contradiction can be resolved if the diagenetic evolution of the massive anhydrite lithofacies is reconstructed. As documented in Chapter 3.5, the massive anhydrites were deposited as beds of gypsum (relic pseudomorphs of anhydrite after gypsum can still be recognized). The phase transition from gypsum to anhydrite results in a 39% reduction of the rock volume as water is liberated from the crystal structure of gypsum during burial. The expulsion of this water will result in a fractionation of the naphthalenes present at this time in the rock. Since the phase transition from gypsum to anhydrite has occurred uniformly at Amelie II and Berrwiller, it is to be expected that naphthalene patterns in both areas have been affected. Following the phase transition, the rocks at Amelie II have been buried to 580 m and have continued to generate hydrocarbons, including naphthalenes. The newly-generated naphthalenes will be added to the residual hydrocarbon mixture overprinting the initial depletion pattern. The same

overprint occurs at Berrwiller (1040 m). However, because of the higher degree of maturity at Berrwiller, a larger quantity of naphthalenes is generated after the water washing event, and the depletion caused by water flushing is more and more diluted by the newly-generated hydrocarbons.

If generation factors are constructed, then the naphthalene concentrations of the less mature site Amelie II, which still has a stronger overprint of the water washing event, is compared to Berrwiller, which has a weaker imprint due to the higher admixture by newly generated hydrocarbons. The resultant generation pattern would suggest a preferential generation of methyl-naphthalenes over ethylnaphthalenes, dimethylnaphthalenes and trimethylnaphthalenes, even though this pattern is caused by different degrees of overprinting of an initially water-washed mixture by newly generated naphthalenes.

The fractionation pattern of the naphthalenes documented here indicates clearly that flushing by water resulting from the gypsum/anhydrite phase transition has indeed affected the organic matter of the original sediment. This had previously been suspected by Sonnenfeld (1985) and Warren (1986), who considered water flushing as an

explanation for the low hydrocarbon content of many anhydrite rocks.

It still remains puzzling that this fractionation pattern is only observed in the massive anhydrite lithofacies and not in the lenticular and laminated anhydrite lithofacies. The reason for this observation may lie in the distribution of the organic matter in these lithofacies. In the massive anhydrites, organic matter is randomly distributed throughout the anhydrite matrix. In the laminated and lenticular anhydrite lithofacies, most of the organic matter is concentrated in the marl matrix. Experiments by Burkow et al. (1990) show that naphthalenes can be absorbed on clay minerals, which would tend to protect these hydrocarbon species from being dissolved and flushed out by water washing.

4.8 Summary and Conclusions

The organic matter content of the sediments of the S unit of the Mulhouse Basin is immature. The maturity of the organic matter at site Amelie II corresponds to a vitrinite reflectance level of 0.35%. At sampling site Berrwiller, 0.45% R_o is reached. The composition of the extractable organic matter of the lithofacies of the S unit at all sites is dominated by heterocompounds (NSO-compounds and asphaltenes). Hydrocarbons constitute less than 50% of the soluble organic matter. These extract compositions support the vitrinite reflectance measurements and also point to an immature state of the organic matter. Compared to shale source rocks of the same maturity, the evaporite sediments yield high amounts of extractable organic matter, a phenomenon which is typical for carbonate-evaporite source rocks in many parts of the world (Palacas, 1984).

The comparison of the extractable organic matter from two locations with identical sedimentary facies and presumable initial organic matter content in the form of a mass balance showed that even though the maturity interval is narrow, bitumen formation took place. The mode of bitumen formation, however, was lithofacies specific. Marl sediments, which are in general richer in organic matter than sediments containing considerable amounts of

anhydrite, formed bitumen in a more effective way than their anhydrite-containing counterparts. However, bitumen formation in the marl sediments did not lead to a significant increase in the relative hydrocarbon content of the bitumens. In contrast, anhydrite sediments generated only minor amounts of bitumen in the maturity interval between 0.35% R_o and 0.45% R_o. But the hydrocarbon content of the bitumens increases considerably in the extracts of the more mature samples of these lithofacies: the anhydrite sediments at Berrwiller contain up to 45% hydrocarbons. The differences in the composition of the bitumens can be attributed to different mechanisms of bitumen and hydrocarbon formation. The marl-dominated lithofacies appear to form bitumen by the conversion of kerogen into liquid organic matter. The lenticular and laminated anhydrite facies, however, appear to generate only minor amounts of bitumen via kerogen conversion in the studied maturity interval. The main process that alters the composition of the bitumens of these lithofacies appears to be the conversion of asphaltenes and NSO-compounds into hydrocarbons by cleavage of the weak carbon-oxygen carbon-sulfur, and carbon-nitrogen bonds. The n-alkane and naphthalene patterns generated by either process are identical, which supports the hypothesis that asphaltenes and NSO-compounds can be considered as kerogen-like entities with a similar overall structure.

The migration of bitumen has altered the bitumen concentration and composition of the massive anhydrite lithofacies at Berrwiller. The analysis of the bitumen that remained in the massive anhydrites after "expulsion" showed that aliphatic hydrocarbons were expelled more effectively than aromatic hydrocarbons. Expulsion of NSO-compounds and asphaltenes most likely also took place, but this is difficult to assess, because hydrocarbon formation in the maturity interval 0.35%-0.45% R_o may have taken place via asphaltene/NSO-compound conversion, rather than via kerogen conversion.

The fractionation pattern of the naphthalenes of the massive anhydrite facies appears to be a good indicator for water washing. This fractionation effect is a useful tool to document that the mineral matrix of evaporite sediment has a significant influence on the hydrocarbon content of the sediments at a low maturity range.

5. GENERAL CONCLUSIONS

The sediments of the S unit of the Mulhouse Basin (France) comprise a sequence of organic matter-rich evaporite sediments. The sediments were deposited in a shallow, partially marine-fed, perennial lake that formed in the Oligocene in the rift valley of the Upper Rhine Graben. The sedimentary fill of the lake consists of marl and gypsum (later converted to anhydrite upon burial) and halite beds. The lake conditions were favorable for the accumulation of organic matter. The mass of the organic carbon is concentrated in the marl beds that can reach organic carbon contents up to 7%. The anhydrite and halite beds also contain organic matter in much lower concentrations. The accumulation of organic matter in the marl beds was favored by low sedimentation rates and by excellent preservation conditions, as indicated by the absence of sediment reworking and low pristane/phytane ratios. The accumulation rates of aquatic organic carbon in the marls of the S unit indicate comparatively high paleoproductivity. The most important factor overall in determining the concentration of organic carbon in the sediment of the Mulhouse Basin appears to be total sedimentation rate. Low sedimentation rates correlate with high organic carbon contents. Variation in sedimentation rates is also the cause of the apparent cyclic deposition of organic matter in the S unit.

The organic matter of the sediments of the S unit comes from two sources: The larger mass of the organic matter is aquatic in origin, including algae and probably bacteria. Terrigenous organic matter generally comprises less than 10 vol% of the organic matter content.

The sediment and fossil content of a layer of the sediment were determined by the physical conditions of the lake. Two general lake conditions have been recognized. During meromict (stratified) lake stages, marl deposition took place. When the upper water body was less saline, algae were the dominant organic species. At elevated salinities of the upper water body, alga and bacterial mats developed. Anhydrite and halite beds reflect monomict lake stages with higher salinities and an unstable water column. The only recognizable presence of organisms adapted to these conditions appear to have been salinity-tolerant algae.

It appears, based on the example of the Mulhouse Basin, that shallow evaporitic lakes in rapidly subsiding rift basins are an ideal environment for the formation and preservation of organic matter-rich sediments, which are apt to become hydrocarbon source rocks upon burial and thermal maturation.

The petroleum potential of the evaporite deposits of the Mulhouse Basin is further documented by the fact that substantial amounts of bitumen have been generated in these rocks, even though they have only reached comparatively low maturity levels. In particular the marls of the S unit, which are rich in organic matter, have generated significant amounts of petroleum. It is to be expected that parts of the sediments of the S unit will become petroleum source rocks upon further burial and concordant maturation.

6. APPENDIX

Compilation of the raw data used in the text and figures of the dissertation.

Abbreviations used in the following tables:

Rock-Eval Pyrolysis

PI = Production Index

HI = Hydrogen Index

OI = Oxygen Index

$CaCO_3$ = Carbonate Content

TOC = Total Organic Carbon

HC = Hydrocarbons

Gas Chromatography

C_{15} to C_{29} = n-alkanes with carbon number 15 to 29

PR/PH = Pristane/Phytane ratio

LHCPI = Light Hydrocarbon Preference Index

$(C_{15}+C_{18}+C_{19})/(C_{27}+C_{28}+C_{29})$

Note: Abbreviations used for individual compounds of the naphthalene, phenanthrene and dibenzothiophene groups are listed in Table 5.

AMELIE II

Marls

Sample number	code	depth (m)	TOC (%)	Tmax (°C)	PI	HI (mg HC /g TOC)	OI (mg CO2 /g TOC)	CaCO3 (%)
28251	1	580	2.86	431	0.15	397	168	29.07
28251	2	580	1.61	435	0.18	398	458	42.73
28252	1	580	3.60	431	0.09	456	84	34.57
28252	2	580	1.97	431	0.14	382	184	37.90
28252	3	580	4.59	432	0.09	496	61	30.74
28253		580	2.16	432	0.13	420	276	38.98
28256		580	2.07	431	0.11	361	110	31.82
28257		580	1.80	433	0.13	358	149	39.07
28259	1	580	4.34	434	0.09	492	74	39.48
28259	2	580	3.16	430	0.09	457	59	45.65
28262		580	3.20	427	0.10	407	124	36.90
28266	2	580	4.17	431	0.12	461	132	39.73
28267		580	1.55	439	0.15	388	215	55.73
28268		580	0.85	431	0.21	278	355	38.65
28269		580	1.75	433	0.15	402	218	43.57
28271		580	2.47	432	0.14	439	204	38.73
28272	2	580	1.19	439	0.17	295	331	64.64
28274		580	2.95	428	0.13	405	125	45.32
28276		580	2.49	432	0.15	390	200	42.32
28277		580	3.18	432	0.15	421	117	30.32
28280		580	3.69	426	0.12	393	144	28.32
28281	2	580	3.52	431	0.13	428	185	22.91
28283	1	580	3.07	431	0.11	419	194	35.57
28283	2	580	4.41	431	0.12	450	109	32.32
28284		580	1.49	434	0.24	352	544	36.49
28286		580	2.29	434	0.15	439	207	45.32
28289		580	1.31	436	0.16	298	302	56.56
28291		580	2.01	430	0.18	373	331	42.40
28292		580	1.87	432	0.20	384	319	28.49
28294		580	1.53	433	0.19	331	204	29.82
28296		580	3.33	430	0.11	387	134	33.40
28299		580	4.40	431	0.10	457	71	35.74
28302		580	1.41	434	0.25	300	388	22.57
28304		580	1.34	433	0.19	331	319	23.16
28308		580	1.13	433	0.28	327	581	46.40
28310		580	2.36	435	0.13	436	214	33.15
28312		580	1.20	433	0.17	321	330	26.57
28314		580	1.30	436	0.22	342	487	53.31
28315		580	1.18	433	0.13	351	243	28.07
28318		580	0.83	431	0.21	265	388	22.16
28319		580	0.47	429	0.14	221	447	15.74
28321		580	0.73	431	0.22	266	322	19.99
28324		580	1.12	433	0.17	341	276	30.90
28326		580	1.72	436	0.11	385	147	40.57
28331		580	0.98	433	0.22	340	408	26.16
28332		580	0.93	433	0.23	339	459	26.32
28333		580	0.94	431	0.18	356	385	25.99
28334		580	0.88	432	0.14	305	298	27.82
28337		580	0.89	434	0.23	340	545	29.82
28338		580	1.55	434	0.11	333	290	20.74
28344		580	1.27	436	0.13	303	299	19.58

Table 6: Rock-Eval pyrolysis data for marl samples from the site Amelie II.

UNGERSHEIM

Marls

Sample number	code	depth (m)	TOC (%)	Tmax (°C)	PI	HI (mg HC /g TOC)	OI (mg CO2 /g TOC)	CaCO3 (%)
29525		700	1.73	436	0.09	440	177	36.74
29527		700	2.18	433	0.09	415	138	41.40
29530		700	3.69	426	0.08	537	131	35.82
29531		700	2.58	433	0.09	439	231	42.98
29532	1	700	1.56	434	0.09	369	337	40.48
29533	1	700	2.47	434	0.07	439	166	39.57
29534		700	3.58	431	0.07	577	106	42.98
29535		700	2.81	431	0.07	472	104	41.57
29537		700	3.17	429	0.08	483	90	44.57
29540	1	700	3.05	426	0.10	454	171	49.48
29541		700	2.82	430	0.08	433	266	31.90
29542	1	700	2.82	432	0.09	448	132	31.49
29544	1	700	1.93	435	0.09	433	158	42.90
29544	2	700	2.77	432	0.09	466	117	44.82
29546	1	700	2.11	433	0.08	428	156	48.98
29547	1	700	2.39	434	0.08	491	138	55.56
29549		700	1.78	434	0.11	354	186	41.98
29551		700	1.74	433	0.08	394	152	37.65
29552		700	1.63	436	0.09	350	190	55.89
29554		700	1.52	435	0.07	315	240	28.16
29556		700	1.85	436	0.07	368	158	32.74
29559	1	700	1.33	434	0.11	288	370	42.15
29559	2	700	1.23	434	0.11	246	382	23.32
29561		700	1.53	438	0.09	325	252	27.82
29563		700	1.23	437	0.10	267	340	21.91
29564		700	1.24	437	0.10	326	356	21.91
29565		700	1.14	436	0.10	281	281	24.99
29568		700	0.94	438	0.11	314	400	47.15
29569		700	0.9	431	0.12	252	312	23.24
29571		700	1.34	434	0.09	240	211	25.24
29572		700	0.86	429	0.13	201	398	19.41
29574		700	0.75	432	0.10	236	317	18.49
29577		700	0.99	434	0.10	280	344	26.66

Table 7: Rock-Eval pyrolysis data for marl samples from the site Ungersheim.

BERRWILLER

Marls

Sample number	code	depth (m)	TOC (%)	Tmax (°C)	PI	HI (mg HC /g TOC)	OI (mg CO2 /g TOC)	CaCO3 (%)
29638		1040	1.50	437	0.13	344	138	44.40
29641		1040	2.75	435	0.13	411	105	32.65
29645	1	1040	3.52	436	0.12	457	55	30.90
29646		1040	4.28	433	0.15	461	46	34.15
29647		1040	2.21	435	0.14	346	119	33.40
29648	1	1040	1.92	435	0.13	342	154	41.23
29650	1	1040	2.95	433	0.14	421	54	47.15
29651		1040	3.35	430	0.16	484	41	57.06
29653		1040	3.15	434	0.13	421	54	34.32
29654	1	1040	3.86	430	0.17	427	70	43.48
29655		1040	3.38	435	0.13	422	57	36.57
29657	1	1040	3.35	434	0.17	415	61	29.74
29659		1040	2.07	436	0.17	394	109	58.14
29661		1040	2.17	435	0.17	384	124	46.07
29663		1040	1.88	436	0.16	327	166	32.99
29665		1040	2.03	437	0.17	366	140	43.32
29667		1040	2.67	436	0.18	427	88	36.49
29668		1040	1.68	440	0.12	386	158	54.31
29670		1040	1.64	437	0.15	321	152	49.23
29671		1040	1.71	434	0.17	337	119	30.65
29673		1040	1.68	438	0.14	328	129	29.07
29675		1040	0.98	435	0.19	292	200	30.99
29676		1040	0.85	435	0.18	246	288	24.74
29677		1040	0.79	434	0.17	235	233	23.07

Table 8: Rock-Eval pyrolysis data for marl samples from the site Berrwiller.

Sample number	code	depth (m)	TOC (%)	CaCO3 (%)
AMELIE II				
laminated anhydrite				
28255		580	0.24	7.16
28258		580	0.14	8.83
28264		580	0.22	15.41
28281	1	580	0.55	16.16
massive anhydrite				
28272	1	580	0.15	11.33
28288		580	0.12	7.16
28306		580	0.31	5.25
28325		580	0.19	15.08
lenticular anhydrite				
28266	1	580	1.20	35.74
28278		580	1.84	18.99
28298		580	1.12	32.57
halite				
28317	1	580	0.03	2.00
28317	2	580	0.06	9.66
28320		580	0.25	30.65
28328		580	0.21	1.83
UNGERSHEIM				
laminated anhydrite				
29532	5	700	0.37	20.49
29533	5	700	0.47	13.41
29536		700	0.26	17.08
massive anhydrite				
29538		700	0.26	11.91
29542	5	700	0.2	16.58
29546	5	700	0.15	5.58
29558		700	0.17	1.17
lenticular anhydrite				
29539		700	0.55	15.24
29540	5	700	0.82	30.57
29542	6	700	0.94	24.32
29547	5	700	0.65	22.82
halite				
29573		700	0.01	3.58
29575		700	0.01	0.08
BERRWILLER				
laminated anhydrite				
29639		1040	0.24	2.42
29648	5	1040	0.28	11.58
29652		1040	0.19	21.24
29658		1040	0.78	29.66
massive anhydrite				
29656		1040	0.12	16.66
29660		1040	0.10	6.16
29664		1040	0.08	9.08
29672		1040	0.13	1.75
lenticular anhydrite				
29645	5	1040	0.61	29.32
29650	5	1040	1.78	28.66
29654	5	1040	0.74	37.15
29657	5	1040	0.59	30.82

Table 9: Total organic carbon and carbonate content of anhydrite and halite samples from the sites Amelie II, Ungersheim, and Berrwiller.

Table 10: Organic carbon contents, sedimentation rates and maceral content, and calculated organic accumulation rates of marl samples from site Amelie II.

Sample number	TOC	Sedimentation Rate	Total Organic Carbon Accumulation Rate	Aquatic Organic Carbon Accumulation Rate	Terrigenous Organic Carbon Accumulation Rate	Alginite	Lipto-detrinite	Aquatic Organic Matter	Vitrinite	Inertinite	Terrigenous Organic Matter
	(%)	(cm/1000y)	(g C/m²/year)	(g C/m²/year)	(g C/m²/year)	(vol%)	(vol%)	(vol%)	(vol%)	(vol%)	(vol%)
28252-1	2.10	18.10	10.89	8.38	2.50	52	25	77	19	4	23
28252-3	3.25	7.30	6.75	6.34	0.40	49	45	94	6	0	6
28253	2.16	7.60	4.70	4.09	0.61	52	35	87	13	0	13
28259-1	3.94	9.00	10.05	9.74	0.30	17	80	97	3	0	3
28262	3.20	6.80	6.19	6.01	0.19	62	35	97	3	0	3
28267	1.47	21.40	9.04	8.32	0.72	69	23	92	8	0	8
28268	0.85	16.60	4.07	3.38	0.69	42	41	83	17	0	17
28274	2.95	9.10	7.65	n.d.	n.d.	n.d.	n.d.	n.d.	n.d.	n.d.	n.d.
28280	3.69	10.00	10.47	9.95	0.52	20	75	95	5	0	5
28283	2.90	6.25	5.17	4.96	0.21	53	43	96	4	0	4
28286	1.97	11.80	6.66	6.26	0.40	20	74	94	6	0	6
28291	2.01	10.00	5.76	n.d.	n.d.	n.d.	n.d.	n.d.	n.d.	n.d.	n.d.
28296	3.33	8.20	7.76	n.d.	n.d.	n.d.	n.d.	n.d.	n.d.	n.d.	n.d.
28299	3.20	6.50	5.92	5.68	0.24	36	60	96	4	0	4
28304	1.04	25.00	7.49	n.d.	n.d.	n.d.	n.d.	n.d.	n.d.	n.d.	n.d.
28312	1.20	30.30	10.47	n.d.	n.d.	n.d.	n.d.	n.d.	n.d.	n.d.	n.d.
38314	1.35	19.00	7.38	5.68	1.70	31	46	77	23	0	23
28318	0.89	40.00	10.27	8.22	2.05	80	0	80	20	0	20
28321	0.81	37.50	8.77	6.66	2.98	46	30	76	34	0	34
28333	0.94	36.30	9.84	8.56	1.28	17	70	87	13	0	13
28338	1.55	32.60	14.52	n.d.	n.d.	n.d.	n.d.	n.d.	n.d.	n.d.	n.d.
28344	1.27	35.30	12.90	n.d.	n.d.	n.d.	n.d.	n.d.	n.d.	n.d.	n.d.
27584	1.82	18.20	9.50	n.d.	n.d.	n.d.	n.d.	n.d.	n.d.	n.d.	n.d.
27585	2.59	12.20	9.02	n.d.	n.d.	n.d.	n.d.	n.d.	n.d.	n.d.	n.d.

n.d.: not determined

Table 11: N-alkane content of marl samples from Amelie II.

AMELIE II: MARLS								
Sample #		28259-1	28280	28291	28299	28318	28319	28321
C15	ug/g TOC	593.62	661.99	956.71	624.16	1852.01	1327.64	1030.04
C16	ug/g TOC	745.79	791.57	692.49	692.04	1074.65	503.18	596.15
C17	ug/g TOC	804.98	723.38	939.00	823.65	1860.31	1467.00	1273.79
C18	ug/g TOC	681.59	682.15	677.16	761.25	899.20	625.62	656.92
C19	ug/g TOC	391.91	368.91	360.99	479.21	381.15	307.42	318.85
C20	ug/g TOC	403.85	394.43	423.38	495.04	205.41	155.06	159.03
C21	ug/g TOC	328.00	330.68	370.94	416.85	139.12	103.67	115.19
C22	ug/g TOC	390.97	446.47	523.32	548.00	131.60	82.12	89.44
C23	ug/g TOC	489.42	523.55	481.83	628.12	118.48	78.33	94.89
C24	ug/g TOC	700.68	711.70	629.48	884.24	113.19	63.46	75.31
C25	ug/g TOC	311.18	365.25	450.91	433.31	115.04	72.16	83.30
C26	ug/g TOC	251.62	306.07	479.58	377.48	88.20	41.29	51.56
C27	ug/g TOC	259.37	263.18	354.42	328.99	124.37	78.54	84.21
C28	ug/g TOC	167.99	186.86	299.00	239.19	114.93	49.50	56.07
C29	ug/g TOC	189.65	203.92	323.45	276.40	162.15	108.53	116.61
Sum Alkanes	ug/g TOC	6710.61	6960.10	7962.66	8007.93	7379.81	5063.52	4801.35
LHCPI		3.04	2.71	2.02	2.44	7.82	10.15	8.76
PR/PH		0.22	0.31	0.25	0.29	0.27	0.32	0.35
Pristane	ug/g TOC	748.63	1490.15	1436.67	1046.04	874.34	718.83	789.75
Phytane	ug/g TOC	3414.74	4843.23	5810.05	3615.94	3201.14	2239.70	2266.36
Squalane	ug/g TOC	210.00	117.00	173.00	153.00	149.00	93.00	88.00

Table 12: N-alkane content of anhydrite samples from Amelie II.

AMELIE II: ANHYDRITES										
Sample #		28255	28258	28264	28266	28272	28278	28288	28298	28306
C15	ug/g TOC	276.15	186.52	329.64	660.23	1027.59	429.90	447.42	536.32	752.18
C16	ug/g TOC	302.93	247.06	348.03	604.58	585.30	403.91	150.41	703.69	688.79
C17	ug/g TOC	314.10	279.27	360.78	603.16	744.81	347.09	280.77	650.89	770.40
C18	ug/g TOC	272.42	244.64	341.20	508.84	462.42	311.22	120.18	614.70	450.75
C19	ug/g TOC	147.68	142.56	178.24	267.20	182.91	149.14	44.47	342.97	202.65
C20	ug/g TOC	176.34	175.45	202.70	292.38	185.56	175.75	43.52	380.25	96.81
C21	ug/g TOC	155.61	146.76	157.40	234.15	126.97	149.85	30.51	310.30	65.40
C22	ug/g TOC	212.43	210.33	213.17	297.95	178.96	221.67	42.34	406.36	54.65
C23	ug/g TOC	161.42	182.15	232.91	348.08	147.91	225.64	37.09	460.28	64.06
C24	ug/g TOC	220.96	327.94	371.43	480.50	199.77	361.28	47.55	657.06	59.26
C25	ug/g TOC	178.30	157.00	177.46	244.63	142.49	191.74	33.70	312.57	61.88
C26	ug/g TOC	174.46	192.67	173.61	211.54	150.31	208.40	32.32	284.11	36.10
C27	ug/g TOC	182.91	194.82	155.87	188.82	134.47	151.61	38.59	248.32	58.55
C28	ug/g TOC	129.23	179.35	111.40	135.99	125.49	139.12	29.94	185.11	42.66
C29	ug/g TOC	210.69	166.61	130.51	153.36	149.95	135.70	51.10	203.81	96.89
Sum Alkanes	ug/g TOC	3115.63	3033.10	3484.34	5231.42	4544.90	3602.00	1429.92	6296.75	3501.03
LHCPI		1.40	1.23	2.21	2.88	3.39	1.89	3.72	2.52	7.19
PR/PH		0.24	0.25	0.26	0.28	0.30	0.31	0.40	0.29	0.36
Pristane	ug/g TOC	691.01	251.34	551.99	940.92	916.11	739.29	202.16	943.79	716.47
Phytane	ug/g TOC	2920.33	1017.68	2108.62	3368.53	3028.82	2383.91	505.95	3208.74	1951.74
Squalane	ug/g TOC	45.00	22.00	48.00	80.00	160.00	43.00	50.00	115.00	88.00

Table 13: N-alkane content of marl samples from Berrwiller.

BERRWILLER: MARLS								
Sample #		29651	29654	29655	29659	29675	29676	29677
C15	µg/g TOC	1828.53	1887.97	1829.78	2577.02	2492.50	2053.31	2039.71
C16	µg/g TOC	2247.33	2109.83	1823.52	2162.65	4444.28	2732.04	3480.22
C17	µg/g TOC	1889.63	1767.56	1490.73	1826.17	4132.13	4094.09	3591.57
C18	µg/g TOC	1735.81	1701.78	1393.90	1570.61	3500.36	2757.95	2607.27
C19	µg/g TOC	1133.48	1081.67	891.64	840.92	1195.98	1054.81	1089.49
C20	µg/g TOC	1143.39	1159.63	935.83	936.03	709.13	588.77	639.45
C21	µg/g TOC	1023.08	1081.34	887.17	845.22	342.97	261.56	329.50
C22	µg/g TOC	1278.22	1413.51	1160.59	1172.30	304.04	223.25	312.04
C23	µg/g TOC	1445.31	1576.30	1293.00	1089.23	243.00	209.62	258.59
C24	µg/g TOC	1917.18	2032.54	1667.27	1390.09	247.28	202.93	293.05
C25	µg/g TOC	910.99	1069.80	891.47	946.69	223.21	222.16	250.37
C26	µg/g TOC	785.34	948.60	792.75	1007.54	162.04	180.44	214.36
C27	µg/g TOC	692.35	715.23	612.27	680.52	230.16	202.70	221.80
C28	µg/g TOC	531.25	617.61	511.75	656.70	250.00	184.19	258.82
C29	µg/g TOC	393.07	443.23	382.65	560.01	280.60	265.29	311.69
Sum Alkanes	µg/g TOC	18954.94	19606.60	16564.30	18261.67	18757.68	15233.09	15897.95
LHCPI		2.94	2.56	2.51	2.23	11.60	12.12	9.20
PR/PH		0.27	0.35	0.34	0.33	0.32	0.47	0.37
Pristane	µg/g TOC	1398.32	2121.07	1937.95	2867.09	1776.81	2128.92	1652.12
Phytane	µg/g TOC	5172.73	6160.45	5687.13	8638.34	5530.57	4578.20	4536.66
Squalane	µg/g TOC	346.00	304.00	251.00	283.00	228.00	165.00	184.00

Table 14: N-alkane content of anhydrite samples from Berrwiller.

BERRWILLER: ANHYDRITES										
Sample #		29648	29650	29652	29654	29657	29658	29660	29664	29672
C15	µg/g TOC	869.27	1466.18	591.48	1091.95	1569.35	1695.86	467.04	291.05	309.06
C16	µg/g TOC	1094.27	1786.82	783.29	1195.26	1536.36	1534.08	269.19	190.99	385.93
C17	µg/g TOC	816.52	1481.68	557.12	965.11	1221.34	1242.37	232.22	207.23	246.52
C18	µg/g TOC	745.40	1391.40	533.73	905.09	1098.37	1092.72	188.49	136.74	212.87
C19	µg/g TOC	399.29	907.97	311.27	559.04	601.43	592.67	64.00	56.14	94.92
C20	µg/g TOC	430.16	905.36	346.19	574.14	645.95	664.02	59.78	55.22	57.91
C21	µg/g TOC	375.30	804.22	299.41	512.04	567.58	603.44	51.50	45.10	43.18
C22	µg/g TOC	490.71	991.58	409.01	641.45	799.45	841.53	74.67	65.16	47.12
C23	µg/g TOC	407.44	1112.75	361.59	687.63	772.18	821.21	68.79	67.22	44.48
C24	µg/g TOC	501.97	1481.19	532.60	877.02	1078.75	1173.91	87.56	86.03	50.85
C25	µg/g TOC	368.57	716.97	299.11	455.06	708.44	740.22	62.84	71.96	45.32
C26	µg/g TOC	383.21	617.74	361.11	409.17	802.05	792.66	64.38	68.19	36.18
C27	µg/g TOC	353.84	552.08	308.83	304.99	513.33	529.14	57.23	69.13	42.12
C28	µg/g TOC	292.68	449.57	324.59	265.75	570.11	534.92	49.95	52.00	35.84
C29	µg/g TOC	355.77	339.54	209.97	201.14	367.15	374.94	68.60	79.58	53.05
Sum Alkanes	µg/g TOC	7884.40	15005.04	6229.28	9644.83	12851.82	13233.67	1866.23	1541.74	1705.35
LHCPI		1.96	2.82	1.66	3.15	2.01	2.03	2.76	1.99	4.23
PR/PH		0.28	0.27	0.33	0.36	0.35	0.35	0.46	0.45	0.43
Pristane	µg/g TOC	1061.48	1126.07	389.98	1090.58	1795.37	2099.61	285.63	157.50	552.21
Phytane	µg/g TOC	3734.45	4146.38	1206.23	3032.04	5063.47	6020.86	618.24	348.69	1287.86
Squalane	µg/g TOC	90.00	270.00	49.00	119.00	157.00	162.00	44.00	40.00	87.00

Table 15: Naphthalene content of marl samples from Amelie II and Berrwiller.

AMELIE II: MARLS								
Sample #		28259-1	28280	28291	28299	28318	28319	28321
2-MN	µg/g TOC	93.07	84.98	39.45	56.37	70.18	62.69	109.56
1-MN	µg/g TOC	100.63	90.57	42.80	59.02	63.30	56.46	100.13
2-EN	µg/g TOC	14.95	18.56	9.54	14.81	9.84	13.92	16.71
1-EN	µg/g TOC	18.72	21.25	11.57	16.93	8.21	9.54	14.75
1DMN	µg/g TOC	36.87	42.32	31.77	45.38	24.03	33.17	57.46
2DMN	µg/g TOC	62.62	66.16	47.16	63.48	39.71	45.78	72.22
3DMN	µg/g TOC	37.26	36.94	26.16	36.77	25.93	29.74	45.42
4DMN	µg/g TOC	14.94	15.25	10.75	16.41	11.08	13.03	18.63
5DMN	µg/g TOC	31.22	27.14	18.46	24.64	17.34	18.71	30.66
1TMN	µg/g TOC	23.27	17.92	17.37	28.27	9.57	17.53	19.26
2TMN	µg/g TOC	43.13	32.57	25.53	44.09	17.57	28.53	34.42
3TMN	µg/g TOC	32.89	25.37	22.99	33.99	17.56	23.83	32.54
4TMN	µg/g TOC	20.89	15.15	15.39	23.01	10.13	18.50	20.86
5TMN	µg/g TOC	50.03	31.75	27.18	43.83	23.62	30.45	40.94

BERRWILLER: MARLS								
Sample #		29651	29654	29655	29659	29675	29676	29677
2-MN	µg/g TOC	165.88	241.75	157.99	144.56	139.10	159.09	139.73
1-MN	µg/g TOC	188.02	277.17	179.99	167.63	140.65	153.36	135.88
2-EN	µg/g TOC	63.89	59.87	41.65	65.38	33.72	36.18	40.24
1-EN	µg/g TOC	61.34	75.95	52.45	57.85	32.78	33.27	28.48
1DMN	µg/g TOC	107.49	129.51	91.43	104.11	68.80	72.53	64.97
2DMN	µg/g TOC	160.06	192.09	138.67	165.99	113.25	116.13	104.74
3DMN	µg/g TOC	100.17	116.09	85.23	98.77	66.56	70.38	67.76
4DMN	µg/g TOC	42.73	45.31	36.93	44.15	32.34	32.27	26.70
5DMN	µg/g TOC	62.39	75.71	58.17	63.20	48.38	47.34	43.56
1TMN	µg/g TOC	57.02	42.71	36.17	57.02	32.66	31.11	30.28
2TMN	µg/g TOC	66.91	73.10	57.01	60.66	50.13	49.18	48.01
3TMN	µg/g TOC	39.27	40.34	34.83	44.90	47.70	53.87	55.85
4TMN	µg/g TOC	24.08	24.68	21.74	28.64	26.98	27.23	24.14
5TMN	µg/g TOC	54.25	52.07	40.89	48.55	60.19	68.92	70.87

Table 16: Naphthalene content of anhydrite samples from Amelie II and Berrwiller.

AMELIE II: ANHYDRITES										
Sample #		28255	28258	28264	28266	28272	28278	28288	28298	28306
2-MN	µg/g TOC	32.02	26.20	32.05	64.50	25.14	64.22	35.14	84.64	55.62
1-MN	µg/g TOC	32.19	27.37	32.03	63.66	24.69	68.08	32.08	87.41	54.00
2-EN	µg/g TOC	7.07	7.83	6.48	10.13	5.24	13.04	9.40	15.98	13.12
1-EN	µg/g TOC	6.61	7.72	8.03	14.19	5.38	16.04	7.10	33.32	10.27
1DMN	µg/g TOC	14.54	13.05	16.20	30.47	12.56	32.16	16.79	41.48	27.38
2DMN	µg/g TOC	20.03	19.73	25.34	42.62	17.60	48.78	22.20	63.90	39.79
3DMN	µg/g TOC	10.55	11.47	13.84	23.35	9.48	24.41	12.34	36.04	22.46
4DMN	µg/g TOC	4.45	4.83	5.54	9.22	3.70	10.94	5.52	13.83	9.53
5DMN	µg/g TOC	10.82	10.05	10.75	17.96	7.89	17.28	14.15	25.57	18.56
1TMN	µg/g TOC	7.17	7.81	9.27	14.93	5.80	16.70	8.47	28.52	14.16
2TMN	µg/g TOC	4.11	4.44	5.00	7.40	3.60	10.99	5.05	13.65	7.59
3TMN	µg/g TOC	5.92	5.15	6.61	11.06	4.82	12.58	6.81	18.72	12.51
4TMN	µg/g TOC	3.65	3.51	4.15	7.03	3.36	7.83	4.23	11.22	7.41
5TMN	µg/g TOC	6.99	8.32	8.07	12.76	5.73	15.01	8.64	24.31	15.03

BERRWILLER: ANHYDRITES										
Sample #		29648	29650	29652	29654	29657	29658	29660	29664	29672
2-MN	µg/g TOC	356.76	162.42	280.23	215.55	130.19	145.84	457.95	298.12	529.09
1-MN	µg/g TOC	369.11	174.11	282.65	189.50	134.23	167.86	457.23	276.16	501.91
2-EN	µg/g TOC	76.08	72.14	68.56	63.71	34.42	47.82	78.75	50.05	136.93
1-EN	µg/g TOC	85.82	80.49	78.67	79.84	40.24	50.16	78.93	44.01	103.56
1DMN	µg/g TOC	163.71	98.93	141.61	107.57	81.22	103.03	133.56	79.93	201.55
2DMN	µg/g TOC	256.56	142.16	228.28	161.23	129.50	153.47	200.81	122.64	327.34
3DMN	µg/g TOC	143.08	87.09	145.92	86.54	79.91	88.82	103.62	61.32	190.63
4DMN	µg/g TOC	61.75	35.09	61.03	39.81	34.85	37.70	47.81	30.39	79.64
5DMN	µg/g TOC	106.27	57.02	111.19	67.27	56.05	58.06	91.14	62.45	199.80
1TMN	µg/g TOC	84.89	57.11	77.28	59.44	44.20	49.99	40.74	18.81	86.15
2TMN	µg/g TOC	60.82	31.34	50.34	34.04	30.95	36.16	28.53	8.97	53.29
3TMN	µg/g TOC	66.70	34.37	46.96	36.82	32.13	39.33	30.23	21.86	65.21
4TMN	µg/g TOC	43.13	28.74	30.29	26.09	21.54	26.69	19.60	15.49	39.37
5TMN	µg/g TOC	76.49	47.59	58.31	53.62	38.33	47.73	38.94	23.65	79.09

Table 17: Phenanthrene content of selected marl samples from Amelie II and Berrwiller.

		AMELIE II: MARLS					BERRWILLER: MARLS				
Sample #		28280	28283	28299	28318	28319	29646	29654	29655	29675	29676
PH	µg/g TOC	15.86	17.58	27.19	9.23	21.68	33.53	30.85	21.95	20.80	22.15
3-MPH	µg/g TOC	6.11	6.62	9.93	3.20	8.25	14.29	13.89	9.74	10.21	8.93
2-MPH	µg/g TOC	6.71	6.94	11.42	3.90	10.75	14.89	13.69	9.49	10.93	10.03
9-MPH	µg/g TOC	10.04	10.50	13.49	6.58	11.35	20.35	20.67	14.10	15.41	15.25
1-MPH	µg/g TOC	7.77	8.48	10.93	5.14	8.93	17.41	17.15	11.77	12.52	12.44
1DMPH	µg/g TOC	4.56	5.39	7.46	1.78	3.87	9.08	10.38	8.82	7.35	5.56
2DMPH	µg/g TOC	2.34	3.01	4.22	0.84	2.30	4.29	5.06	5.32	3.63	3.53
3DMPH	µg/g TOC	9.06	9.60	14.24	5.51	10.03	19.13	19.47	12.67	15.01	14.61
4DMPH	µg/g TOC	3.75	5.48	7.80	2.94	6.28	10.66	10.92	12.13	8.83	8.45
5DMPH	µg/g TOC	5.29	5.60	7.27	4.01	5.76	10.89	10.60	8.16	7.24	8.22
6DMPH	µg/g TOC	1.53	1.74	2.71	1.05	1.96	3.87	3.60	5.97	2.82	3.12
7DMPH	µg/g TOC	3.80	5.22	6.58	3.14	3.76	9.70	12.29	9.76	8.65	9.65

Sample #	DBT	4-MDBT	2+3-MDBT	1-MDBT
	µg/g TOC	µg/g TOC	µg/g TOC	µg/g TOC
AMELIE II: MARLS				
28283	26.46	14.81	13.49	25.87
28280	26.92	13.68	11.54	25.53
28299	25.19	16.36	13.97	25.47
28319	14.87	14.69	10.30	12.71
28318	12.15	8.08	5.72	9.85
BERRWILLER: MARLS				
29646	34.14	18.13	20.65	30.76
29654	37.34	29.71	28.20	43.06
29675	39.44	28.92	30.35	42.20
29676	24.41	17.75	14.56	28.01

Table 18: Dibenzothiophene content of selected marl samples from Amelie II and Berrwiller.

Sample #	Extract Yield	Aliphatic Hydrocarbons	Aromatic Hydrocarbons	NSO-Compounds	Asphaltenes
	(mg/g TOC)	(mg/g TOC)	(mg/g TOC)	(mg/g TOC)	(mg/g TOC)
28252-1	152.98	20.29	2.97	78.41	51.31
28252-3	130.93	16.26	1.39	47.56	65.71
28253	110.63	20.54	1.47	44.70	43.93
28259-1	128.96	13.19	1.40	30.17	84.19
28262	106.46	17.00	3.06	26.05	60.35
28267	117.73	29.52	3.09	25.72	59.40
28268	99.87	34.28	5.55	39.76	20.28
28276	185.47	42.66	8.43	70.24	64.14
28280	128.64	13.10	2.86	22.25	90.44
28283	157.79	28.45	3.64	63.03	62.67
28286	147.13	34.69	3.74	62.72	45.98
28289	266.74	21.87	4.71	43.62	196.54
28291	160.26	23.64	2.50	38.61	95.51
28299	249.99	24.09	5.72	40.95	179.23
28314	106.17	25.46	2.92	60.76	17.03
28318	95.36	29.73	4.34	45.37	15.92
28319	120.31	32.93	3.71	66.17	17.49
28321	96.84	25.25	3.15	54.25	14.20
28333	112.99	32.41	2.99	60.57	17.01
29530	172.35	24.94	3.52	60.35	83.54
29531	184.40	9.45	0.83	34.34	139.78
29534	103.59	11.76	1.04	34.63	56.17
29537	126.29	9.57	4.23	31.24	81.25
29540	193.41	18.98	3.27	59.68	111.49
29547	192.28	15.59	4.46	51.93	120.29
29552	107.96	20.51	5.08	54.07	28.30
29559-1	180.48	17.44	22.38	131.51	9.15
29568	175.75	29.89	3.24	112.22	30.40
29569	161.05	25.92	2.31	105.01	27.81
29572	252.87	10.52	1.84	36.02	204.49
29574	115.81	22.74	1.81	68.80	22.48
29577	124.77	21.75	1.77	77.13	24.13
29638	192.55	32.62	6.32	48.05	105.55
29646	223.06	11.64	7.60	22.09	181.72
29651	244.22	24.87	7.73	26.36	185.25
29654	270.14	21.95	4.68	23.11	220.41
29655	223.41	21.33	2.70	20.99	178.39
29659	246.92	30.32	13.82	35.02	167.76
29661	197.01	33.60	13.39	44.70	105.32
29665	160.04	61.08	18.00	54.88	26.09
29668	238.90	27.32	9.40	37.34	164.84
29670	188.47	21.44	6.68	43.38	116.96
29675	236.35	46.09	3.56	86.30	100.40
29676	372.08	31.64	8.93	59.52	271.99
29677	174.68	52.69	9.67	71.39	40.92

Table 19: Extract composition of marl samples from Amelie II, Ungersheim and Berrwiller.

Sample #	Extract Yield	Aliphatic Hydrocarbons	Aromatic Hydrocarbons	NSO-Compounds	Asphaltenes
	(mg/g TOC)	(mg/g TOC)	(mg/g TOC)	(mg/g TOC)	(mg/g TOC)
28255	122.29	23.52	4.14	6.03	88.61
28258	86.10	9.72	6.89	5.85	63.63
28264	118.91	16.87	3.82	8.95	89.27
28266	162.87	25.32	6.14	8.97	122.44
28272	104.44	17.32	5.56	7.34	74.22
28275	161.11	21.77	3.28	16.06	120.00
28278	96.52	12.10	3.31	9.69	71.42
28281	160.76	21.03	6.03	10.10	123.59
28288	73.52	6.11	4.10	4.58	58.73
28293	172.25	21.42	5.72	16.91	128.21
28306	157.18	17.66	2.61	13.72	123.19
28313	181.86	26.78	3.75	21.32	130.01
28317	251.83	47.55	9.68	11.76	182.85
28320	154.72	28.69	3.56	13.91	108.56
28325	123.16	16.11	4.61	10.16	92.28
29532	157.50	13.37	5.55	14.72	123.85
29533	203.62	27.78	4.87	24.20	146.77
29538	163.72	28.41	7.74	16.19	111.38
29536	115.38	9.91	4.29	10.97	90.23
29539	163.99	23.98	7.76	17.66	114.59
29540	146.23	20.36	7.76	13.92	104.19
29542-1	181.04	10.17	8.62	13.99	148.26
29542-2	176.69	19.36	6.32	23.45	127.56
29546	92.89	15.83	4.50	8.18	64.38
29547	209.60	27.65	7.05	31.45	143.45
29558	106.59	9.01	6.18	12.76	78.64
29573	375.22	22.71	11.35	22.76	318.40
29575	288.64	33.91	9.69	12.20	232.84
29639	143.23	42.60	17.87	5.99	76.77
29645	142.83	50.83	21.71	5.76	64.53
29648	143.46	41.03	22.23	7.44	72.76
29650	169.72	28.67	13.44	9.11	118.50
29652	83.40	20.24	16.84	3.45	42.87
29654	116.78	38.46	23.58	5.10	49.64
29656	46.67	8.52	11.14	2.84	24.17
29657	146.85	50.31	25.74	7.65	63.15
29658	151.93	47.03	22.26	11.79	70.84
29660	45.27	15.88	16.11	2.74	10.53
29664	54.92	4.83	7.15	3.81	39.12
29672	70.00	14.83	10.18	5.48	39.51

Table 20: Extract composition of anhydrite and halite samples from Amelie II, Ungersheim and Berrwiller.

7. BIBLIOGRAPHY

Aizenshtat Z., Stoler A., Cohen Y., and Nielsen H. (1983) The geochemical sulphur enrichment of Recent organic matter by polysulfides in the Solar-Lake. In Advances in Organic Geochemistry 1981, (eds. M. Bjorøy et al.), pp. 279-288. John Wiley and Sons, Ltd., Chichester.

Albaiges J. and Torradas J.M. (1974) Significance of the even carbon n-paraffin preference of a Spanish crude oil. Nature 250, 567-568.

Alexander R., Kagi R.I. and Larcher A.V. (1982) Clay catalysis of aromatic hydrogen-exchange reactions. Geochim. Cosmochim. Acta 46, 219-222.

Alexander R., Kagi R.I., Rowland S.J., Sheppard P.N., and Chirila T.V. (1985) The effects of thermal maturity on distributions of dimethylnaphthalenes and trimethylnaphthalenes in some Ancient sediments and petroleums. Geochim. Cosmochim. Acta 49, 385-395.

Anderson R.Y. and Dean W.E. (1988) Lacustrine varve formation through time. Palaeogeogr., Palaeoclimatol., Palaeoecol. 62, 215-235.

Baranyi I., Lippolt H.J., and Todt W. (1976) Kalium-Argon-Altersbestimmungen an tertiären Vulkaniten des Oberrheingrabengebietes: II. Die Alterstraverse vom Hegau nach Lothringen. Oberrhein. Geol., Abh. 25, 41-65.

Barbe A., Grimalt J.O., Pueyo J.J., and Albaiges J. (1990) Characterization of model evaporitic environments through the study of lipid components. In Advances in Organic Geochemistry 1989 (eds. B. Durand and F. Behar) Org. Geochem. 16, 815-828.

Baskin D.K. and Peters K.E. (1992) Early generation characteristics of a sulfur-rich Monterey kerogen. AAPG Bull. 76, 1-13.

Berner R.A. (1980) Early Diagenesis: A Theoretical Approach. Princeton University Press, Princeton, New Jersey.

Berner R.A. (1981) A new geochemical classification of sedimentary environments. J.Sed. Pet. 51, 359-365.

Berner R.A. (1983) Sedimentary pyrite formation: An update. Geochim. Cosmochim. Acta 48, 605-615.

Betts S.H., Sinninghe Damsté J., de Leeuw J.W., and Hofmann P. (1991) Facies determination in a Tertiary evaporitic sequence (Mulhouse Basin, France) with an emphasis on the assessment of palaeosalinity: a molecular organic geochemical approach. In Organic Geochemistry: Advances and Applications in the Natural Environment (ed. D.A.C. Manning), pp. 343-345. Manchester University Press, Manchester.

Bird C.W. and Lynch J.M. (1974) Formation of hydrocarbons by microorganisms. Chem. Soc. Rev. 3, 309-328.

Blanc-Valleron M.M. (1986) Enseignements géologiques tirés de l'étude systématique de la matière organique d'un bassin salifère. Le bassin potassique de Mulhouse (Alsace, France). C.R. Acad. Sc. Paris. 302, Série II, 825-830.

Blanc-Valleron M.M. (1991) Etude sedimentologique des formations saliferes paleogenes du Sud fosse rhenan. Thèse Doc. ès Sci., Strausbourg.

Blanc-Valleron M.M. and Gannat É. (1985) Cartographie de subsurface du Salifère supérieur du bassin potassique de Mulhousse (Oligocène, Alsace). Bull. Soc. Géol. France 1985, t. I, pp. 823-836.

Blanc-Valleron M.M., Foucault A., and Gannat É. (1989) Le contrôle climatique, orbital, et solaire de la sédimentation évaporitique: exemple de la base du Salifère supérieur (Oligocène inférieur) du bassin de Mulhouse (Sud du fossé rhénan, France). C.R.Acad. Sci.,Paris 308, ser. II, 435-411.

Blanc-Valleron M.M., Gely J.P., Schuler M., Dany F., and Ansart M. (1991) La matière organique associée aux évaporites de la base du Sel IV (Oligocène inférieur) du bassin de Mulhouse (Alsace, France). Bull. Soc. géol. France 162, 113-122.

Blumer M., Guillard R.R.L., and Chase T. (1971) Hydrocarbons of marine phytoplankton. Marine Biol. 8, 183-189.

Boon J.J. (1984) Tracing the origin of chemical fossils in microbial mats: biogeochemical investigations of Solar Lake cyanobacterial mats using analytical pyrolysis methods. In Microbial Mats: Stromatolites (eds. Y. Cohen, R.W. Castenholz, and H.O. Halvorson), pp. 313-342. Alan R. Liss, Inc., New York.

Bradley W.H. (1929) The varves and climate of the Green River Epoch. U.S. Geol. Surv. Prof. Pap. 158-E, 87-110.

Brasier M.D. (1980) Microfossils. George Allen and Unwin, London.

Brassell S.C., Wardroper A.M.K., Thomson I.D., Maxwell J.R., and Eglinton G. (1981) Specific acyclic isoprenoids as biological markers of methanogenic bacteria in marine sediments. Nature 291, 693-696.

Brown G., and Brindley G.W. (1980) Crystal Structures of Minerals and their X-Ray Identification. Mineralogical Society, London.

Burkow I.C., Jorgensen E., Meyer T., Rekdal O., and Sydnes L.K. (1990) Experimental simulation of chemical transformations of aromatic compounds in sediments. Org. Geochem. 15, 101-109.

Burnham A.K. and Braun R.L. (1990) Development of a detailed model of petroleum formation, destruction, and expulsion from lacustrine and marine source rocks. In Advances in Organic Geochemistry 1989 (eds. B. Durand and F. Behar) Org. Geochem. 16, 27-39.

Butler G.P., Harris P.M., and Kendall C.G. (1982) Recent evaporites from Abu Dhabi coastal flats. In Depositional and Diagenetic Spectra of Evaporites (eds. C.R. Handford, R.G. Loucks and G.R. Davis), pp. 33-64. SEPM Core Workshop 3. SEPM, Tulsa.

Cardoso J., Brooks P.W., Eglinton G., Goodfellow R., Maxwell J.R., and Philp R.P. (1976) Lipids of recently-deposited algal mats at Laguna Mormona, Baja California. In Environmental Biogeochemistry and Geomicrobiology (ed. J.O. Nriagu), Vol. 1, Ann Arbor Science, Ann Arbor, Michigan.

Carpentier B., Gély J.P., Blanc-Valleron M.M., and Huc A.Y. (1991) Simulation de la sédimentation dans un basssin évaporitique à niveau d'eau sous influence eustatique; application au bassin paléogène de Mulhouse (Alsace, France). Unpublished IFP Report. Institut Français du Pétrole, Rueil-Malmaison, France.

Casas E. and Lowenstein T.K. (1989) Diagenesis of saline pan halite: Comparison of petrographic features of Modern, Quaternary and Permian halites. Jour. Sed. Pet. 59, 724-739.

Cody R.D. and Cody A.M., (1988) Gypsum nucleation and crystal morphology in analog saline terrestrial environments. Jour. Sed. Pet. 58, 247-255.

Cohen Y., Aizenshtat Z., Stoler A., and Jørgensen B.B. (1980) The microbial geochemistry of Solar Lake, Sinai. In Biogeochemistry of Ancient and Modern Environments (eds. P.A. Trudinger and M.R. Walter), pp. 167-172. Springer-Verlag, New York.

Comet P.A. and Eglinton G. (1987) The use of lipids as facies indicators. In Marine Petroleum Source Rocks (eds. J. Brooks, J. and A.J. Fleet), Geol. Soc. Spec. Pub. 26, 99-117.

Connan J., Bouroullec J., Dessot D., and Albrecht P. (1986) The microbial input in carbonate-anhydrite facies of a sabkha paleoenvironment from Guatemala: A molecular approach. Org. Geochem. 10, 29-50.

Cornee A. (1984) Étude préliminaire des bactéries des saumures et des sédiments des salins de Santa Pola (Espagne). Comparaison avec les marais salants de Salin-de-Giraud (Sud de la France). Revista d'Investigacions Geologiques 38/39, 109-122.

Cornee A. (1988) Productivite microbienne, benthique et planctonique, dans les milieux hypersales actuels: une revue. In Evaporites et Hydrocarbures (ed. G. Busson.), Sci. de la Terre 55, 20-41.

Courtot C., Gannat É., and Wendling E. (1972) Le bassin potassique de Mulhouse et ses environs. Étude du Tertiaire. Sci. Géol. Bull. 25, 69-91.

Demaison G.J. and Moore G.T. (1980) Anoxic environments and oil source bed genesis. AAPG Bull. 64, 1179-1209.

Derenne S., Largeau C., Casadevall E., Tegelaar E.W., and de Leeuw J.W. (1988) Relationships between algal coals and resistant cell wall biopolymers of extant algae as revealed by Py-GC-MS. Fuel Process. Tech. 20, 93-101.

Deuser W.G. (1971) Organic-carbon budget of the Black Sea. Deep-Sea Research 18, 995-1004.

Didyk B.M., Simoneit B.R.T., Brassell S.C., and Eglinton G. (1978) Organic geochemical indicators of palaeoenvironmental conditions of sedimentation. Nature 272, 216-222.

Doebl F. (1970) Die tertiären und quartären Sedimente des südlichen Rheingrabens. Intern. Upper Mantle Project, Scient. Report 27, 56-66.

Doebl F. and Teichmüller R. (1979) Zur Geologie und heutigen Geothermik in mittleren Oberrhein Graben. Forschr. Geol. Rheinld. u. West. 27, 1-17.

Edmunds K.L.H. and Eglinton G. (1984) Microbial lipids and carotenoids and their early diagenesis in the solar lake laminated microbial mat sequence. In Microbial Mats: Stromatolites (eds. Y. Cohen, R.W. Castenholz, and H.O. Halvorson), pp. 343-389. Alan R. Liss, Inc., New York.

Elsinger E. and Pevear D. (1988) Clay Minerals. SEPM Short Course Notes No. 22. SEPM, Tulsa.

Espitalié J. (1986) Use of T_{max} as a maturation index for different types of organic matter. Comparison with vitrinite reflectance. In Thermal Modeling in Sedimentary Basins, (ed. J. Burrus), pp. 475-496. 1st IFP Exploration Research Conference, Caracans, France.

Espitalié J., Lapote J.L., Madec M., Leplat P., and Boutefeu A., (1977) Methode rapide de caracterisation des roches mere, de leur potentiel petrolier et de leur degre d'evolution. Rev. Inst. fr. Petrole, Paris 32, 23-42.

Espitalié J., Senga Makadi K., and Trichet J. (1984) Role of matrix during kerogen pyrolysis. Org. Geochem. 6, 365-382.

Eugster H.P. (1980) Geochemistry of evaporitic lacustrine deposits. Amer. Rev. Earth Planet. Sci. 1980 8, 35-63.

Eugster H.P. (1985) Oil shales, evaporites, and ore deposits. Geochim. Cosmochim. Acta 49, 619-635.

Eugster H.P. and Hardie L.A. (1978) Saline lakes. In Geochemistry, Geology, and Physics of Lakes (ed. A. Lerman), pp. 237-293. Springer-Verlag, New York.

Evans R. and Kirkland D.W. (1988) Evaporitic environments as a source of petroleum. In Evaporites and Hydrocarbons (ed. B.C. Schreiber), pp. 256-299. Columbia University Press, New York.

Ferguson J. (1988) Oil generation and migration within marine carbonate sequences -- a review. J. Pet. Geol. 11, 389-402.

Förster B. (1911) Ergebnisse der Untersuchung von Bohrproben aus den seit 1904 im Gange befindlichen, zur Aufsuchung von Steinsalz und Kalisalzen ausgeführten Tiefbohrungen im Tertiär des Oberelsass. Mitt. Geol. Landesanst. Els.-Lothr. 7, 329-524.

Friedman G.M. (1980) Review of depositional environments in evaporite deposits and the role of evaporites in hydrocarbon accumulation. Bull. Cent. Rech. Explor.-Prod. ELF-Aquitaine 4, 589-608.

Friedman G.M. and Krumbein W.E. (1985) Hypersaline Ecosystems: The Gavish Sabkha. Ecological Studies 53. Springer Verlag, Berlin.

Froelich P.N., Klinkhammer G.P., Bender M.L., Luedtke N.A., Heath G.R., Cullen D., Dauphin P., Hammond D., and Hartman B. (1979) Early oxidation of organic matter in pelagic sediments of the eastern equatorial Atlantic: suboxic diagenesis. Geochim. Cosmochim. Acta 43, 1075-1090.

Fu Jiamo, Guoying S., Pingan P., Brassell S.C., Eglinton G., and Jigang J. (1986) Pecularities of salt lake sediments as potential source rocks in China. Org. Geochem. 10, 119-126.

Gelpi E., Schneider H., Mann J., and Oró J. (1970) Hydrocarbons of geochemical significance in microscopic algae. Phytochem. 9, 603-612.

Gely J.P. and Huc A.Y. (1990) Distribution of the organic matter within the Tertiary evaporitic series of the Mulhouse Basin. In Origin and Significance of the Organic Matter in Evaporites (ed. J.P. Gely), First Annual Report 1989 to the European Community. Unpublished IFP Report. Institut Français du Pétrole, Rueil-Malmaison, France.

Gely J.P., Blanc-Valleron M.M., Dany F., Schuler M., and Ausart M. (1990) Characterization of an organic rich evaporitic environment: The lower Oligocene of the Mulhouse Basin (Alsace, France). Submitted to Chemical Geology.

Gerdes G. and Krumbein W.E. (1987) Biolaminated Deposits. Lecture Notes in Earth Sciences 9. Springer-Verlag, Berlin.

Goldhaber M.B. and Kaplan I.R. (1974) The sulfur cycle. In The Sea, (ed. E.D. Goldberg), Vol. 5, pp. 569-655. John Wiley, New York.

Han J. and Calvin M. (1969) Hydrocarbon distribution of algae and bacteria and microbiological activity in sediments. Proc. Nat. Acad. Sci. USA 64, 436-443.

Hardie L.A. (1990) The roles of rifting and hydrothermal $CaCl_2$ brines in the origin of potash evaporites: an hypothesis. Amer. J. Sci. 290, 43-106.

Hardie L.A. and Eugster H.P. (1971) The depositional environment of marine evaporites: a case for shallow clastic accumulation. Sedimentology 16, 187-220.

Hayes J.M. (1983) Geochemical evidence bearing on the origin of aerobiosis, a speculative interpretation. In The Origin and Evolution of Earth's Earliest Biosphere: An Interdisciplinary Study (ed. J.W. Schopf). Princeton University Press, Princeton.

Hillebrand T. and Leythaeuser D. (1991) Reservoir geochemistry of Stockstadt oil-field: Compositional heterogeneities reflecting accumulation history and multiple source input (abstr.). In press, 15th Meeting of the European Association of Organic Geochemists.

Hofmann P. and Leythaeuser D. (1991) Sedimentary facies, organic facies, and hydrocarbon generation in evaporite sediments of the Mulhouse Basin (France). In Origin and Significance of the Organic Matter in Evaporites. Application to the Potash Basin, South of Alsace. Second Annual Report of the European Network of Organic Geochemistry Laboratories (ENOG), 1990, Vol. 3. Institut Français du Pétrole, Rueil-Malmaison, France.

Hollander D.J. and Huc A.J. (1991) Bulk and molecular isotopic analyses of organic matter in the Tertiary, Mulhouse Evaporite Basin (France): Reconstruction of chemical depositional paleoenvironments and the origin of organic compounds. In Origin and Significance of the Organic Matter in Evaporites. Application to the Potash Basin, South of Alsace. Second Annual Report of the European Network of Organic Geochemistry Laboratories (ENOG), 1990, Vol. 4. Institut Français du Pétrole, Rueil-Malmaison, France.

Holzer G., Oro J., and Tornabene T.G. (1979) Gas chromatographic-mass spectrometric analysis of neutral lipids from methanogenic and thermoacidophilic bacteria. J. Chromatogr. 186, 795-809.

Horsfield B. (1984) Pyrolysis studies and petroleum exploration. In Advances in Petroleum Geochemistry, (eds. J.M. Brooks and D.H. Welte), p. 247-298. Academic Press, London.

Horsfield B. and Douglas A.G. (1980) The influence of minerals on the pyrolysis of kerogens. Geochim. Cosmochim. Acta 44, 119-1131.

Hughes W.B. (1984) Use of thiophenic organosulfur compounds in characterizing crude oils derived from carbonate versus siliciclastic sources. In Petroleum Geochemistry and Source Rock Potential of Carbonate Rocks (ed. J.G. Palacas), AAPG Studies in Geology 18, pp. 181-196. American Association of Petroleum Geologists, Tulsa.

Hunt J.M. (1979) Petroleum Geochemistry and Geology. Freemann, San Francisco.

Illies J.H. (1972) The Rhine Graben rift system, plate tectonic and transform faulting. Geophys. Surv. 1, 27-60.

Illies J.H. (1974) Intra-Plattentektonik im Mitteleuropa und der Rheingraben. Oberrhein. Geol. Abh. 23, 1-24.

Illies J.H. and Greiner G. (1978) Rheingraben and the Alpine system. Geol. Soc. Amer. Bull. 89, 770-782.

Javor B. (1989) Hypersaline Environments: Microbiology and Biogeochemistry. Springer-Verlag, Berlin.

Jones, R.W. (1984) Comparison of carbonate and shale source rocks. In Petroleum Geochemistry and Source Rock Potential of Carbonate Rocks (ed. J.G. Palacas), AAPG Studies in Geology 18, pp. 1163-180. American Association of Petroleum Geologists, Tulsa.

Kaplan I.R. and Baedecker M.J. (1970) Biological productivity in the Dead Sea part II -- Evidence for phosphatidyl glycerophosphate lipid in sediment. Israel J. Chem. 8, 529-533.

Keely B.J., Standen G., Eglington G., and Maxwell J.R. (1990) A preliminary examination of the organic geochemistry of seven samples from the Mulhouse Potash Basin. In Origin and Significance of the Organic Matter in Evaporites (ed. J.P. Gely), First Annual Report 1989 to the European Community. Unpublished IFP Report. Institut Français du Pétrole, Rueil-Malmaison, France.

Kelts K. and Hsü K.J. (1978) Freshwater carbonate sedimentation. In Lakes: Chemistry, Geology, Physics (ed. A. Lerman), pp. 295-323. Springer-Verlag, New York.

Kendall, C. G., and Warren, J.K. (1988) Peritidal evaporites and their sedimentary assemblages. In Evaporites and Hydrocarbons (ed. B. C. Schreiber), pp. 66-138. Columbia University Press, New York.

Kenig F. and Huc A.Y. (1990) Incorporation of sulfur into recent organic matter in a carbonate environment (Abu Dhabi, United Arab Emirates). In Geochemistry of Sulfur in Fossil Fuels (eds. W.L. Orr and C.M. White), pp. 170-185. ACS Symposium Series 429. American Chemical Society, Washington, D.C.

Kirkland D.W., and Evans, R. (1981) Source-rock potential of evaporitic environment. AAPG Bull. 65, 181-190.

Kirkland D.W., Bradbury J.P., and Dean W.E. (1983) Source-rock potential of evaporitic environment. AAPG Bull. 65, 181-190.

Kühn R. von and Roth H. (1979) Beiträge zur Kenntnis der Saltzlagerstätte am Oberrhein. Z. Geol. Wiss. 7, 953-966.

Lafargue E. and Barker C. (1988) Effect of water washing on crude oil compositions. AAPG Bull. 72, 263-276.

Largeau C., Casadevall E., Kadouri A., and Metzger P. (1984) Comparative study of immature torbanite and of the extant alga *Botryococcus braunii*. In Advances in Organic Geochemistry 1983 (eds. P.A. Schenck, J.W. de Leeuw, and G.W.M. Lijmbach) Org. Geochem. 6, 327-332.

Largeau C., Derenne S., Casadevall E., Kadouri A., and Sellier N. (1986) Pyrolysis of immature torbanite and of the resistant biopolymer (PRB A) isolated from the extant alga *Botryococcus braunii*. Mechanism for the formation and structure of torbanite. In Advances in Organic Geochemistry 1985 (eds. D. Leythaeuser and J. Rullkötter) Org. Geochem. 10, 1023-1032.

Lewan M.D. (1985) Evaluation of petroleum generation by hydrous pyrolysis experimentation. Phil. Trans. R. Soc. Lond. A 315, 123-134.

Lewan M.D. (1992) Primary oil migration and expulsion as determined by hydrous pyrolysis. Proc. 13th World Petroleum Congress, Buenos Aires, Argentina 1991, in press.

Leythaeuser D. and Schaefer R.G. (1984) Effects of hydrocarbon expulsion from shale source rocks of high maturity in Upper Carboniferous strata of the Ruhr area, Federal Republic of Germany. Org. Geochem. 6, 671-681.

Leythaeuser D., Hagemann H.W., Hollerbach A. and Schaefer R.G. (1980) Hydrocarbon generation in source beds as a function of the type and maturation of their organic matter: a mass balance approach. Proc. 10th World Petroleum Congress 2, 31-41.

Leythaeuser D., Radke M., and Willsch H. (1988b) Geochemical effects of primary migration of petroleum in Kimmeridge source rocks form Brae field area, North Sea. II: Molecular composition of alkylated naphthalenes, phenanthrenes, benzo- and dibenzothiophenes. Geochim. Cosmochim. Acta 52, 2879-2891.

Leythaeuser D., Schaefer R.G., and Radke M. (1988a) Geochemical effects of primary migration of petroleum in Kimmeridge source rocks from Brae field area, North Sea. I: Gross composition of C_{15+}-soluble organic matter and molecular composition of C_{15+}-saturated hydrocarbons. Geochim. Cosmochim. Acta 52, 701-713.

Littke R., Baker D.R., and Leythaeuser D. (1988) Microscopic and sedimentologic evidence for the generation and migration of hydrocarbons in Toarcian source rocks of different maturities. In Advances in Organic Geochemistry 1987 (eds. L. Novelli and L. Mattavelli) Org. Geochem. 13, 549-559.

Loudon G.M. (1988) Organic Chemistry, 2nd ed. Benjamin Cummings, Menlo Park, California.

Louis M. and Tissot B. (1967) Influence de la température et de la pression sur la formation des hydrocarbures dans les argiles à kérogène. In Proc. 7th World Pet. Congr. 2, 47-60.

Lowenstein T.K. and Spencer R.J. (1990) Syndepositional origin of potash evaporites: petrographic and fluid inclusion evidence. Amer. J. Sci. 290, 1-42.

Lowenstein T.K., and Hardie L.A. (1985) Criteria for the recognition of salt-pan evaporites. Sedimentology 32, 627-644.

Mackenzie A.S. and Quigley T.M. (1988) Principles of geochemical prospect appraisal. AAPG Bull. 72, 399-415.

Maikovsky V. (1941) Contribution à l'étude paléontologique et stratigraphique du bassin potassique d'Alsace. Mém. Serv. Carte Géol. Als. Lorr. 6, 1-192.

Martini E. (1973) Nannoplankton-Massenvorkommen in den Mittleren Pechelbronner Schichten (Unter-Oligozän). Oberrhein. Geol. Abh. 22, 1-12.

McAuliffe C.D. (1979) Oil and gas migration: chemical and physical constraints. In Problems of Petroleum Migration (eds. W.H. Roberts and J.R. Cordell J.R.), AAPG Studies in Geology 10, pp. 89-107. American Association of Petroleum Geologists, Tulsa.

Mello M.R., Caglannone P.C., Brassell S.C., and Maxwell J.R. (1988a) Geochemical and biological marker assessment of depositional environments using Brazilian offshore oils. Marine Petrol. Geol. 5, 205-223.

Mello M.R., Telnaes N., Caglianone P.C., Chicarelli M.I., Brassell S.C., and Maxwell J.R. (1988b) Organic geochemical characterization of depositional paleoenvironments of source rocks and oils in Brazilian marginal basins. Org. Geochem. 13, 31-45.

Moore D.M. and Reynolds R.C. (1989) X-Ray Diffraction and the Identification and Analysis of Clay Minerals. Oxford University Press, Oxford.

Muscio G.P.A. (1991) Pyrolyse der makromolekularen organischen Substanz (Kerogene, Asphaltene und Heterokomponenten) einer natürlich gereiften Probenserie des Lias ϵ der Hils-Mulde, NW-Deutschland. Diplomarbeit, Rheinisch-Westfälische Technische Hochschule Aachen.

Neev D. and Emery K.O. (1967) The Dead Sea: Depositional processes and environments of evaporites. Israel Geol. Surv. Bull. 41.

Neugebauer H.J. and Temme P. (1981) Crustal uplift and the propagation of failure zones. Tectonophysics 73, 33-51.

Nip M., de Leeuw J.W., Schenck P.A., Windig W., Meuzelaar H.L.C., and Crelling J.C. (1989) A flash pyrolysis and petrographic study of cutinite from the Indiana paper coal. Geochim. Cosmochim. Acta 53, 671-683.

Nip M., Tegelaar E.W., de Leeuw J.W., Schenck P.A., and Holloway P.J. (1986) A new non-saponifiable highly aliphatic and resistant biopolymer in plant cuticles: evidence from pyrolysis and ^{13}C-NMR analysis of present day and fossil plants. Naturwissenschaften 73, 579-585.

Nissenbaum A., Baedecker M.J., and Kaplan I.R. (1972) Organic geochemistry of Dead Sea sediments. Geochim. Cosmochim. Acta 36, 709-727.

Oró J., Tornabene T.G., Nooner D.W., and Gelpi E. (1967) Aliphatic hydrocarbons and fatty acids of some marine and freshwater microorganisms. J. Bacteriology 93, 1811-1818.

Orr W.L. (1986) Kerogen/asphaltene/sulfur relationships in sulfur rich Monterey oils. In Advances in Organic Geochemistry 1985 (eds. D. Leythaeuser and J. Rullkötter), Org. Geochem. 10, 499-516.

Orr W.L. and Sinninghe Damsté J.S. (1990) Geochemistry of sulfur in petroleum systems. In Geochemistry of Sulfur in Fossil Fuels (eds. W.L. Orr and C.M. White), pp. 2-29. ACS Symposium Series 429, American Chemical Society, Washington, D.C.

Orr W.L. and White C.M. (1990) Preface. In Geochemistry of Sulfur in Fossil Fuels (eds. W.L. Orr and C.M. White), pp. ix-xi. ACS Symposium Series 429. American Chemical Society, Washington, D.C.

Orti Cabo F. and Shearman D.J. (1977) Estructuras y fabricas deposicionales en las evaporitas del miocena superior (Messinense) de San Miguel de Salinas (Alicante, Espana). Instit. Invest. Geolog. Disput. Prov. Univ. Barcelona 32, 5-54.

Orti Cabo F., Pueyo Mur J.J., Geisler-Cussey D., and Dulau N. (1984) Evaporitic sedimentation in the coastal salinas of Santa Pola (Alicante, Spain). Rev. Inv. Geol. 38/39, 169-220.

Palacas J.G. (1983) Carbonate rocks as sources of petroleum: Geological and chemical characteristics and oil-source rock correlations. Proc. 11th World Petroleum Congress 2, 31-43.

Palacas J.G. (1984) Introduction. In Petroleum Geochemistry and Source Rock Potential of Carbonate Rocks (ed. J.G. Palacas), AAPG Studies in Geology 18, p.vii-viii. American Association of Petroleum Geologists, Tulsa.

Palacas J.G. (1988) Characteristics of carbonate source rocks of petroleum. In Petroleum Systems of the United States (ed. L.B. Magoon), U.S. Geol. Surv. Bull. 1870, 20-25.

Palmer S.E. and Zumberge J.E. (1981) Organic geochemistry of upper Miocene evaporite deposits in the Sicilian Basin, Sicily. In Organic Maturation Studies and Fossil Fuel Exploration (ed. J. Brooks), pp. 394-426. Academic Press, London.

Parrish J.T. and Curtis R.L. (1982) Atmospheric circulation, upwelling and organic-rich rocks in the Mesozoic and Cenozoic eras. Palaeogeogr., Palaeoclimatol., Palaeoecol. 40, 31-66.

Pedersen T.F. and Calvert, S.E. (1990) Anoxia vs. productivity: What controls the formation of organic-carbon-rich sediments and sedimentary rocks? AAPG Bull. 74, 454-466.

Pelet R., Béhar F., and Monin J.C. (1986) Resins and asphaltenes in the generation and migration of petroleum. In Advances in Organic Geochemistry 1985 (eds. D. Leythaeuser and J. Rullkötter) Org. Geochem. 10, 481-498.

Perakis N. (1986) Séparation et détection sélective de composés soufrés dans les fractions loudres des pétroles. Géochemie des benzo[b]thiophènes. Ph.D. Dissertation, Univ. of Strasbourg.

Peters K.E. (1986) Guidelines for evaluating petroleum source rock using programmed pyrolysis. AAPG Bull. 70, 318-396.

Pflug R. (1982) Bau und Entwicklung des Oberrheingrabens. Wissenschaftliche Buchgesellschaft, Darmstadt.

Philp R.P. and Lewis C.A. (1987) Organic geochemistry of biomarkers. Amer. Rev. Earth Planet. Sci. 1987 15, 363-395.

Powell T.G. (1984) Some aspects of the hydrocarbon geochemistry of a Middle Devonian barrier-reef complex, Western Canada. In Petroleum Geochemistry and Source Rock Potential of Carbonate Rocks (ed. J.G. Palacas), AAPG Studies in Geology 18, 45-61. American Association of Petroleum Geologists, Tulsa.

Prahl A.K., Springstubbe H., Grumbach K., and Wiermann R. (1985) Studies on sporopollenin biosynthesis: the effect of inhibitors of carotenoid biosynthesis on sporopollenin accumulation. Z. Naturforsch., Sect. C., Biosci. 40, 621-626.

Purser B.H. (1985) Coastal evaporite systems. In Hypersaline Ecosystems: The Gavish Sabkha (eds. G.M. Friedman and W.E. Krumbein), pp. 72-102. Ecological Studies 53. Springer Verlag, Berlin.

Quigley T.M., Mackenzie A.S., and Gray J.R. (1987) Kinetic theory of petroleum generation. In Migration of Hydrocarbons in Sedimentary Basins (ed. B. Doligez), pp. 649-665. Technip, Paris.

Radke M. (1987) Organic geochemistry of aromatic hydrocarbons. In Advances in Petroleum Geochemistry 2, (eds. J.M. Brooks and D.H. Welte), pp. 141-207. Academic Press, London.

Radke M. (1988) Application of aromatic compounds as maturity indicators in source rocks and crude oils. Marine Pet. Geol 5, 224-236.

Radke M., Sittardt H.G., and Welte D.H. (1978) Removal of soluble organic matter from rock samples with a flow-through extraction cell. Anal. Chem. 50, 663-665.

Radke M., Welte D.H., and Willsch H. (1982) Geochemical study on a well in the Western Canadian Basin: relation of the aromatic distribution pattern to maturity of organic matter. Geochim. Cosmochim. Acta 46, 1-10.

Radke M., Welte D.H., and Willsch H. (1986) Maturity parameters based on aromatic hydrocarbons: Influence of the organic matter type. In Advances in Organic Geochemistry 1985 (eds. D. Leythaeuser and J. Rullkötter) Org. Geochem. 10, 51-63.

Radke M., Willsch H., and Welte D.H. (1980) Preparative hydrocarbon group type determination by automated medium pressure liquid chromatography. Anal. Chem. 52, 406-411.

Robert P. (1985) Histoire géothermique et diagenèse organique. Bull. Centres Rech. Explor.-Prod. Elf-Aquitaine Mem. 8. Pau, France

Roll A. (1979) Versuch einer Volumenbilanz des Oberrheintalgrabens und seiner Schultern. Jahrb., Reihe A. 52, 1-82.

Rullkötter J. and Michaelis W. (1990) The strutcure of kerogen and related materials. A review of recent progress and future trends. In Advances in Organic Geochemistry 1989 (eds. B. Durand and F. Béhar) Org. Geochem. 16, 829-852.

Rullkötter J., Littke R., and Schaefer R.G. (1990) Characterization of organic matter in sulfur-rich lacustrine sediments of Miocene Age (Nördlinger Ries, southern Germany). In Geochemistry of Sulfur in Fossil Fuels (eds. W.L. Orr and C.M. White), pp. 149-169. ACS Symposium Series No. 429. American Chemical Society, Washington, D.C.

Rullkötter J., Littke R., Hagedorn-Götz I., and Jankowski B. (1988) Vorläufige Ergebnisse der organisch-geochemischen und organisch-petrographischen Untersuchungen an Kernproben des Messeler Ölschiefers. Cour. Forsch.-Inst. Senckenberg 107, 37-51.

Schaefer R.G., Leythaeuser D., and Weiner B. (1978) Single-step capillary column gas chromatographic method for extraction and analysis of sub-parts per billion (10^9) amounts of hydrocarbons (C_2-C_8) from rock and crude oil samples and its application in petroleum geochemistry. J. Chromatogr. 167, 355-363.

Schidlowski M. (1982) Content and isotopic composition of reduced carbon in sediments. In Mineral Deposits and the Evolution of the Biosphere (eds. H.D. Holland and M. Schidlowski), pp. 103-122. Springer, Berlin.

Schidlowski M., Matzigkeit U., Mook W.G., and Krumbein W.E. (1984) Carbon isotope geochemistry and ^{14}C ages of microbial mats from the Gavish Sabkha and the Solar Lake. In Hypersaline Ecosystems: The Gavish Sabkha (eds. G.M. Friedman and W.E. Krumbein), pp. 381-401. Ecological Studies 53. Springer Verlag, Berlin.

Schreiber B.C. (1986) Arid shore lines and evaporites. In Sedimentary Environments and Facies (ed. H.G. Reading), pp. 189-228. Blackwell Sci. Pub., Oxford.

Schreiber B.C. (1988) Subaqueous evaporite deposition. In Evaporites and Hydrocarbons (ed. B.C. Schreiber), pp. 182-255. Columbia University Press, New York.

Schreiber B.C. and Hsü K.J. (1980) Evaporites. In Developments in Petroleum Geology II (ed. G.D. Hobson), pp. 87-138. Applied Science, London.

Schreiber B.C., Friedman G.H., Decima A., and Schreiber, E. (1976) Depositional environments of Upper Miocene (Messinian) evaporites of the Sicilian Basin. Sedimentology 23, 729 -760.

Schuler M. (1988) Environnements et paléoclimats paléogènes. Palynologie et biostratigraphie de l'Eocène et de l'Oligocène inférieur dans les fossés rhénan et rhodanien et en Hesse. Thèse Doc. ès Sci., Univ. Strasbourg.

Shearman D.J. (1963) Recent anhydrite, gypsum, dolomite and halite from the coastal flats of the Arabian shore of the Persian Gulf. Proc. Geol. Soc. London 1607, 63-65.

Shearman D.J. (1970) Recent halite rock, Baja California, Mexico. Trans. Inst. Min. Metall. 79B, 155-162.

Shearman D.J. (1978) Evaporites of coastal sabkhas. In Marine Evaporites (eds. W.E. Dean and B.C. Schreiber), pp. 6-42. Soc. Econ. Paleont. Miner. Short Course 4. SEPM, Tulsa, Oklahoma.

Shearman D.J. (1985) Syndepositional and late diagenetic alteration of primary gypsum. In Sixth Symposium on Salt (eds. B.C. Schreiber and H.L. Harner), pp. 41-55. Salt Institute, Alexandria, Virginia.

Shiea J., Brassell S.C., and Ward D.M. (1991) Comparative analysis of extractable lipids in hot spring microbial mats and their component photosynthetic bacteria. Org. Geochem. 17, 309-319.

Sinninghe Damsté J.S., D'Engelbronner E.R., Baas M., and de Leeuw J.W. (1990) Molecular organic geochemical characterization of marl samples from the Mulhouse Potash Basin. In Origin and Significance of the Organic Matter in Evaporites. Application to the Potash Basin, South of Alsace. First Annual Report of the European Network of Organic Geochemistry Laboratories (ENOG), 1989, Vol. 2. Institut Français du Pétrole, Rueil-Malmaison, France.

Sinninghe Damsté J.S., Kock-van Dalen A.C., Albrecht P.A., and de Leeuw J.W. (1991) Identification of long-chain 1,2-di-*n*-alkylbenzenes in Amposta crude oil from the Tarragona Basin, Spanish Mediterranean: Implications for the origin and fate of alkylbenzenes. Geochim. Cosmochim. Acta 55, 3677-3683.

Sinninghe Damsté J.S., Kock-van Dalen A.C., de Leeuw J.W., Schenck P.A. Sheng Guoying and Brassell S.C. (1987) The identification of mono-, di-, and tri-methyl 2-methyl-2-(4,8,12-trimethyltridecyl) chromans and their occurrence in the geosphere. Geochim. Cosmochim. Acta 51, 2393-2400.

Sinninghe Damsté J.S., Rijpstra W.I.C., de Leeuw J.W., and Schenck P.A. (1988) Origin of organic sulphur compounds and sulphur-containing high molecular weight substances in sediments and immature crude oils. In Advances in Organic Geochemistry 1987 (eds. L. Novelli and L. Mattavelli), Org. Geochem. 13, 593-606.

Sinninghe Damsté J.S., ten Haven H.L., de Leeuw J.W., and Schenck P.A. (1986) Organic geochemical studies of a Messinian evaporitic basin, northern Apennines (Italy) -- II. Isoprenoid and *n*-alkyl thiophenes and thiolanes. In Advances in Organic Geochemistry 1985 (eds. D. Leythaeuser and J. Rullkötter), Org. Geochem. 10, 791-805.

Sittler C. (1969) The sedimentary trough of the Rhine Graben. Tectonophysics 8, 543-560.

Sittler C. (1972) Le pétrole dans le départment du Haut-Rhin. Bilan d'un siècle et demi de recherches et d'exploitations. Sci. Géol. Bull. 25, 151-161.

Sittler C. (1983) Fossé rhénan: région naturelle et cadre structural, le bloc rhénan aux ères primaire et secondaire, historie et évolution du fossé au Tertiaire, processus tectoniques, volcanisme, structure profonde et origine du fossé rhénan. In Encyclopédie de l'Alsace 5, 3122-3137. Publitotal, Strasbourg.

Sittler C. (1985) Les hydrocarburres d'Alsace dans le contexte historique et géodynamique du fossé rhénan. [The case history of oil occurrence in the Rhine rift valley of Alsace]. Bull. Centres Rech. Explor.-Prod. Elf-Aquitaine 9, 335-371.

Sonnenfeld P. (1984) Brines and Evaporites. Academic Press, Orlando.

Sonnenfeld P. (1985) Evaporites as oil and gas source rocks. Jour. Petrol. Geol. 8, 253-271.

Spencer R.J., Baedecker M.J., Eugster, H.P., Forester R.M., Goldhaber M.B., Jones B.F., Kelts K., McKenzie J., Madsen D.B., Rettig S.L., Rubin M., and Bowser C. (1984) Great Salt Lake, and precursors, Utah: the last 30,000 years. Contrib. Mineral. Petrol. 86, 321-334.

Stach E., Mackowsky M.Th., Teichmüller M., Taylor G.H., Chandra D., and Teichmüller R. (1982) Stach's Textbook of Coal Petrology, 3rd ed. Gebrüder Borntraeger, Berlin.

Stein R. and Littke R. (1990) Organic-carbon-rich sediments and paleoenvironment: Results from Baffin Bay (ODP-Leg 105) and the upwelling area off northwest Africa (ODP-Leg 108). In Deposition of Organic Facies (ed. A.Y. Huc), AAPG Studies in Geology 30, 41-56. American Association of Petroleum Geologists, Tulsa.

Stein R., Littke R., Stax R., and Welte D.H. (1989a) Quantity, provenance, and maturity of organic matter at ODP-Sites 645, 646, and 647: Implications for reconstruction of paleoenvironments in Baffin Bay and Laborador Sea during Cenozoic times. In Proc. Ocean Drilling Program, Scientific Results 105 (eds. S. Srivastava et al.), pp. 185-208. Ocean Drilling Program, College Station, Texas.

Stein R., Rullkötter J., Littke R., Schaefer R.G., and Welte D.H. (1988) Organofacies reconstruction and lipid geochemistry of sediments from the Galicia Margin, Northeast Atlantic (ODP Leg 103). In Proc. Ocean Drilling Program, Scientific Results 103 (eds. G. Boillot et al.), pp. 567-585. Ocean Drilling Program, College Station, Texas.

Stein R., ten Haven H.L., Littke R., Rullkötter J., and Welte D.H. (1989b) Accumulation of marine and terrigenous organic carbon at upwelling-Site 658 and non-upwelling-Sites 657 and 659: Implications for the reconstruction of paleoenvironments in the eastern subtropical Atlantic through late Cenozoic times. In Proc. Ocean Drilling Program, Scientific Results 108 (eds. W. Ruddimann et al.), pp. 361-385. Ocean Drilling Program, College Station, Texas.

Sturmfels E. (1943) Das Kalisalzlager von Buggingen (Südbaden). N. Jb. Miner. Geol. Pal., Abh. 78A, 131-216.

Sweeney J.J., Burnham A.K., and Braun R.L. (1987) A model of hydrocarbon generation from type I kerogen:

application to Unita basin, Utah. AAPG Bull. 71, 967-985.

Tegelaar E.W., de Leeuw J.W., Derenne S., and Largeau C. (1989) A reappraisal of keorgen formation. Geochim. Cosmochim. Acta 53, 3103-3106.

Teichmüller M. (1986) Organic petrology of source rocks, history and state of the art. Advances in Organic Geochemistry 1985, Org. Geochem. 10, 581-599.

ten Haven H.L., de Leeuw J.W., and Schenk P.A. (1985) Organic geochemical studies of a Messinian evaporitic basin, northern Appennines (Italy): Hydrocarbon biological markers for hypersaline environments. Geochim. Cosmochim. Acta 49, 2181-2191.

ten Haven H.L., de Leeuw J.W., Sinninghe Damsté J.S., Schenck P.A., Palmer S.E., and Zumberge J.E. (1988) Application of biological markers in the recognition of palaeohypersaline environments. In Lacustrine Petroleum Source Rocks (eds. A.J. Fleet, K. Kelts, and M.R. Talbot), Geological Society Special Publication 40, 123-130.

ten Haven H.L., Littke R., Rullkötter J., Stein R., and Welte D.H. (1990) Accumulation rates and composition of organic matter in late Cenozoic sediments underlying the active upwelling area off Peru. In Proc. Ocean Drilling Program, Sci. Results 112, (eds. E. Suess, R. von Huene, et al.), pp. 591-605. Ocean Drilling Program, College Station, Texas.

Thompson C.J. (1981) Identification of sulfur compounds in petroleum and alternative fossil fuels. In Organic Sulfur Geochemistry (eds. R.Kh. Freidlina and A.E. Skorova), pp. 189-208. Pergamon Press, Oxford.

Tissot B., Deroo G., and Herbin J.P. (1979) Organic matter in Cretaceous sediments of the North Atlantic: Contribution to sedimentology and paleoceanography. In Deep Drilling Results in the Atlantic Ocean: Continental Margin and Paleoenvironment (eds. M. Talwani, W. Hay, and W.B.R. Ryan), M. Ewing Series 3, 362-374. American Geophysical Union, Washington, D.C.

Tissot B.P. and Welte D.H. (1984) Petroleum Formation and Occurrence, 2nd ed. Springer-Verlag, Berlin.

Tissot B.P., Califet-Debyser Y., Deroo G., and Oudin J.L. (1971) Origin and evolution of hydrocarbons in early Toarcien shales, Paris Basin, France. AAPG Bull. 55, 2177-2193.

Tissot B.P., Durand B., Espitalié J., and Combaz A. (1974) Influence of nature and diagenesis of organic matter in formation of petroleum. AAPG Bull. 58, 499-506.

Tissot B.P., Pelet R., and Ungerer P. (1987) Thermal history of sedimentary basins, maturation indices, and kinetics of oil and gas generation. AAPG Bull. 71, 1445-1446.

Ungerer P. and Pelet R. (1987) Extrapolation of kinetics of oil and gas formation from laboratory experiments to sedimentary basins. Nature 327, 52-54.

Villemin T., Alvarez F., and Angelier J. (1986) The Rhinegraben: extension, subsidence and shoulder uplift. Tectonohpysics 128, 47-59.

Villemin T., Angelier J., and Bergerat F. (1984) Tectonique en extension et subsidence dans le NE de la France. Ann. Soc. Géol. Nord 103, 211-229.

Waples D.W. (1983) Reappraisal of anoxia and organic richness, with emphasis on Cretaceous of North Atlantic. AAPG Bull. 61, 963-978.

Waples D.W., Haug P., and Welte D.H. (1974) Occurrence of a regular C_{25} isoprenoid hydrocarbon in Tertiary sediments representing a lagoonal, saline environment. Geochim. Cosmochim. Acta 38, 381-387.

Warren J.K. (1982) Hydrological setting, occurrence, and significance of gypsum in late Quaternary salt lakes in South Australia. Sedimentology 29, 609-638.

Warren J.K. (1986) Shallow water evaporitic environments and their source rock potential. Jour. Sed. Pet. 56, 442-454.

Warren J.K. (1989) Evaporite Sedimentology: Importance in Hydrocarbon Accumulation. Prentice Hall, Englewood Cliffs, New Jersey.

Welte D. and Waples D.W. (1973) Über die Bevorzugung geradzahliger n-Alkane in Sedimentgesteinen. Naturwissenschaften 60, 516-517.

Whiticar M.J. (1990) Composition of natural gases in evaporites from Alsace. BGR Internal Report. Bundesanstalt für Geowissenschaften und Rohstoffe, Hannover.

Ziegler P.A. (1988) Evolution of the Arctic-North Atlantic and the western Tethys. AAPG Memoir 43.